uOttawa

L'Université canadienne
Canada's university

FACULTÉ DES ÉTUDES SUPÉRIEURES ET POSTOCTORALES

uOttawa

L'Université canadienne
Canada's university

FACULTY OF GRADUATE AND POSDOCTORAL STUDIES

Etienne Poisson
AUTEUR DE LA THÈSE / AUTHOR OF THESIS

M.A.Sc. (Mechanical Engineering)
GRADE / DEGREE

Department of Mechanical Engineering
FACULTÉ, ÉCOLE, DÉPARTEMENT / FACULTY, SCHOOL, DEPARTMENT

Automation of Continuous Composite 2D Braiding Process

TITRE DE LA THÈSE / TITLE OF THESIS

Dr. A. Fahim
DIRECTEUR (DIRECTRICE) DE LA THÈSE / THESIS SUPERVISOR

Dr. M. Munro
CO-DIRECTEUR (CO-DIRECTRICE) DE LA THÈSE / THESIS CO-SUPERVISOR

EXAMINATEURS (EXAMINATRICES) DE LA THÈSE / THESIS EXAMINERS

Dr. W. Hallett

Dr. J. Hayes

Gary W. Slater
Le Doyen de la Faculté des études supérieures et postdoctorales / Dean of the Faculty of Graduate and Postdoctoral Studies

Automation of Continuous Composite 2D Braiding Process

Etienne Poisson

Thesis submitted to the Faculty of Graduate and Postdoctoral Studies
In partial fulfillment of the requirements of
MASTER OF APPLIED SCIENCES

in Mechanical Engineering

Ottawa-Carleton Institute for Mechanical and Aerospace Engineering
University of Ottawa
Ottawa, Canada

April 2009

Your file Votre référence
ISBN: 978-0-494-51652-2
Our file Notre référence
ISBN: 978-0-494-51652-2

Dedicated to all individuals who, due to conflict, culture or ignorance, have not had the chance to learn.

Abstract

This work presents the design of a computer controlled pilot production plant capable of manufacturing hybrid braided/pultruded rod on a continuous basis. The current product design utilizes a high modulus carbon fiber core with a braided over-wrap composed of various materials. Production is accomplished in three phases: core fiber sorting and impregnation, 2D braiding, and resin curing. On-line impregnation of the core strands is accomplished using a pressure-fed impregnation ring. Deposition of the 2D braid is performed by a Maypole braider. Curing of the resin is accomplished using a novel two phase method. An induction heater first increases the temperature of steel wires embedded in the rod core. Next three tunnel ovens provide heat flux to the exterior of the rod. A caterpillar-type puller is used to advance the rod through the process. Prior to this work production was accomplished by manually adjusting machinery operating parameters through controls distributed throughout the production facility. This led to inconsistent quality product. The modifications to production equipment and the development of an automation system which allow one to improve. The modifications to production equipment and the development of an automation system which allow to improve product quality are the main topics of this work.

The automation system is based on a PC equipped with several data acquisition cards. A global controller calculates machine set points based on product specifications and measured production rate. Cascade controllers are tasked to regulate machine operations about these set points. The rotational speed of the braider head and puller are monitored using incremental encoders and are under set point element and integral control. The resin flow rate is estimated from weight measurement of the resin reservoir. To regulate the resin dispensing process a calibration curve is used as a set point elements while disturbances are rejected using integral control. The curing oven temperatures are monitored using thermocouples. The oven temperatures are regulated using gain scheduled PI controllers.

The modification to the production equipment and the development of the automation system allowed for significant improvements in the product quality.

Acknowledgements

I would first like to thank Dr. Munro and Dr. Fahim my thesis supervisors, for their guidance and support throughout my graduate studies which exceeded my expectation.

I would also like to thank the staff of the mechanical engineering machine shop: James for his advice on fabrication and machining which was concise and helpful; Leo for always making time to troubleshoot the numerous electrical problem related to the production line and for assistance in the design and construction of the custom circuits presented in this work; and finally John whose dedication and creative thinking are unsurpassed.

Thank you to Kristina Haase and Steve Recoskie for proof-reading several chapters of this thesis.

A heartfelt thanks to my partner Emilie who has always encouraged and supported me.

Last but not least I would like to express my gratitude to my parents Gisèle and Yves who have always encouraged me to pursue my interest and who have made my education a priority.

Finally I would like to acknowledge the following sources of funding: The University of Ottawa Admission and Excellence Scholarship, The Ontario Graduate Scholarship and soft-funding from Dr. Fahim and Dr. Munro.

Table of Contents

List of Figures

List of Tables

List of Abbreviations

A|G: Acquisition or Generation
ASCII: American Standard Code for Information Interchange
CL: Closed Loop
CPU: Central Processing Unit
CV: Control Volume
DAQ: Data Acquisition Card
DMA: Direct Memory Access
EMI: Electro Magnetic Interference
FRC: Fiber Reinforced Composite
FRP: Fiber Reinforced Polymer
GUI: Graphical User Interface
HMI: Human Machine Interface
HT: Heat Transfer
MIMO: Multi Input Multi Output
OL: Open Loop
PI: Proportional Integral Controller
PID: Proportional Integral and Derivative Controller
SISO: Single Input Single Output
SS: Stainless Steel
TC: Thermocouple

List of Symbols

A	Area, m^2; Current, A
D	Diameter, m; Disturbance, W
E	Error
ER	Expected Ratio
H	Total Enthalpy, J
K_c	Controller Gain
K_i	Integral Gain, 1/sec
K_p	Process Gain
L	Characteristic length, m
Nu	Nusselt number
P	Quantity of interest (generic variable), Power, W
Pr	Prandtl Number
$\dot{Q}$	Flow rate, g/min; Heat transfer rate, W
R	Mandrel diameter, m; Resistance, Ω
Ra	Rayleigh Number
Ra^*	Modified Rayleigh Number
T	Temperature, °C
T_d	Derivative Time, min
T_i	Integral Time, min
U	Total Energy, J
V	Electrical Potential, V
a	State coefficient; Angular acceleration, rad/s^2
b	Input Coefficient
c	Effective thermal capacitance, J/K
f	Frequency, Hz
g	Gravitational Constant, m/s^2
h	Heat transfer Coefficient; Enthalpy per unit weight, J/Kg
k	Thermal conductivity, W/m·K
m	Number of encoder sectors, count/rev; Mass, Kg

n	Counter value, Count
p	Position of encoder, Count
r	Radii, m
s	Laplace Operator
t	Time, second
t_0	Process dead time, sec
u	Process input
z	Heigth, m

Greek Letters

α	Braid angle wrt pulling axis, rad; Pole Thermal diffusivity, m^2/s
ε	Random error; Emissivity
v	Mandrel Speed, m/min; Dynamic viscosity, m^2/s
σ	Stefan-Boltzmann Constant
τ	Process Time constant, sec or min
ω	Angular velocity, rad/min

Subscripts

∞,env	Quantity of surrounding environment
1	Initial State
2	Final State
a	Air mass control volume quantity
a,b	Quantity associated with surface a,b
C	Heating chamber control volume quantity
cond	Quantity associated with conduction
conv	associated with convection
cv	Control volume quantity
E	Element control volume quantity
i	Quantity associated with i^{th} element
in,i	Inlet quantity
k	k^{th} sample
min/max	Minimum/ Maximum of quantity
out,o	Outlet quantity

R	Rod control volume quantity
rad	Quantity associated with radiation
s	Surface quantity
T	Tube control volume quantity

Automation of Continuous Composite 2D Braiding Process

1. Introduction

1.1. Fibre Reinforced Composite Materials

In a broad sense, composites are multiphase materials that are combined on a macroscale in order to obtain the advantageous properties of each phase and/or to obtain a better combination of properties. Fibre reinforced composites (FRC) are composed of a fibre reinforcement and a matrix phase. The fibres may be polymeric, ceramic, metallic or organic. Due to theire high specific strength and modulus, polymeric and ceramic fibres are found in the majority of FRC applications. The most common polymeric fibres are aramid, nylon and ultra high molecular weight polyethylene. Glass and carbon are the more popular ceramic fibres. The matrix phase may be a metal, a polymer or a ceramic. Polymeric matrices are usually preferred when low density is advantageous. Some fibre reinforced polymer (FRP) composites utilize thermoplastic matrices, but thermosetting polymers are more common. Thermosetting resin include polyesters, vinyl ester resins and epoxies.

The nominal length and orientation of fibres have a significant impact on the mechanical properties of FRP material, and therefore, a distinction is made between discontinuous and continuous fibre reinforcements. In discontinuous reinforcement, chopped fibres are usually randomly orientated. This results in isotropic mechanical properties. It is often desirable to obtain anisotropic properties, as the reinforcement material is used more efficiently with respect to the direction of loading. This is commonly achieved using continuous fibres. The work in this thesis is concerned with fibre reinforced polymeric composite materials (FRP)

A number of manufacturing processes for producing continuous fibre composites are commonly in use. The most common are pultrusion and filament winding. A third process which is gaining commercial acceptance is 2D braiding. This process is capable of producing many types of parts at high production rates and is the process of interest in this work.

1.2.2D Braided Composites

The production facility discussed in this work may be used to produce a variety of 2D braided fibre reinforced composite parts. The most common apparatus to produce a tubular braid is the Maypole Braider. As depicted in Figure 1.1, spools of fibre stands loaded on carriers rotate about the machine center on two serpentine paths. The intersection of the paths provides the weaving action to form the braid. The braid angle is controlled by adjusting the ratio between the braider angular velocity (v_r) and the longitudinal feed rate (v_l).

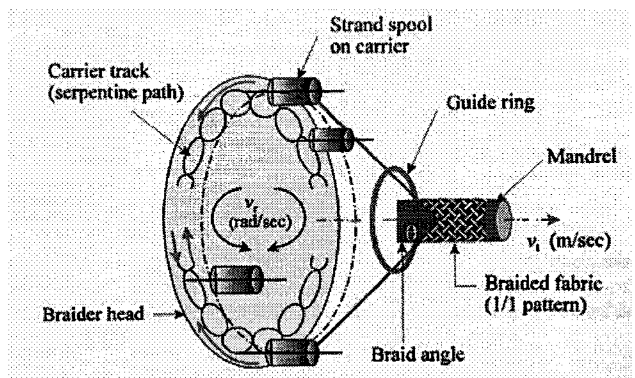

Figure 1.1: Schematic representation of a Maypole 2D braiding apparatus[1].

Depending on the braider strand configuration, the apparatus can produce 2D biaxial (Figures 1.2,1.3 and 1.4) or triaxial (Figure 1.5) braids. Any pliable material in strand form may be braided, including nylon, glass, carbon, aramid, etc. Braiding may be done with or without a mandrel. In the first case, the resulting braid forms a sock (as in Figure 1.2) which can be slipped over various core materials or used flat as tape reinforcement. Mandrels may be of various cross-sectional shapes and sizes. Depending on the final product design the mandrel can be permanent or temporary. Permanent mandrels become an integral part of the final product and can be composed of various materials such as foam, metal or other fibre reinforced materials. Temporary mandrels are removed after resin curing, resulting in a fibre composite shell. As shown in Figure 1.4, 2D braiding with a temporary mandrel allows the formation of hollow braided structures of various shapes with non-constant cross-sections. It is also possible to produce part with an open weave (as in Figure 1.5).

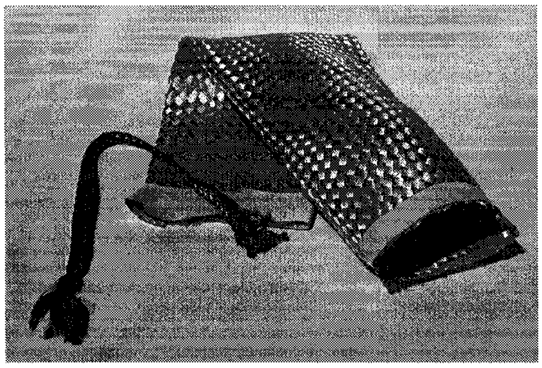

Figure 1.2: A nylon (large) and aramid (small) dry biaxially braided socks.

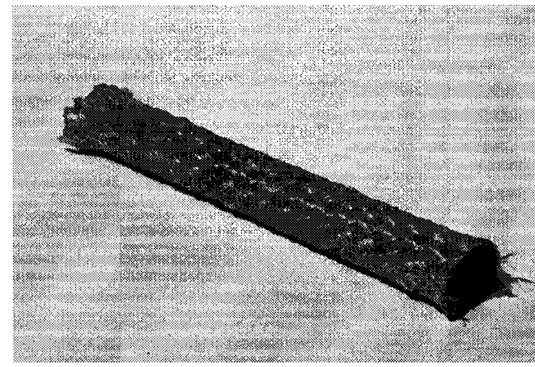

.Figure 1.3: Sample of a 10mm braided rebar in which an aramid 2D braid has been wrapped over a unidirectional carbon fibre

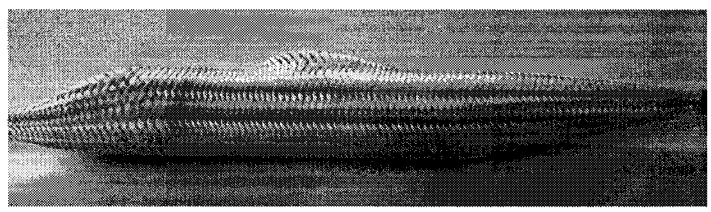

Figure 1.4: Biaxial braid deposited on a variable cross-section mandrel.

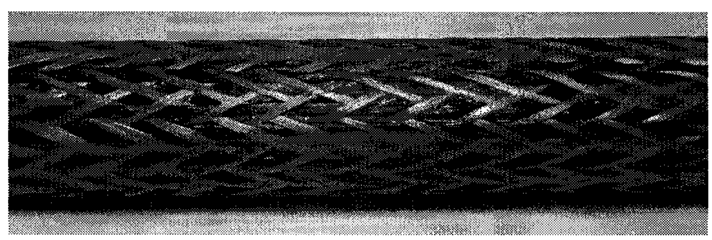

Figure 1.5: Hybrid triaxial open weave 2D braid. Braided fibres are aramid, longitudinal fibres are carbon.

To produce a finished composite part, fibres must be impregnated with a polymeric resin and cured. In 2D braiding impregnation may be accomplished prior to or after the braid formation. The first case is referred to as wet braiding, the second as dry braiding. Dry braiding implies a batch production process where impregnation methods such as the painting of resin and resin transfer molding are commonly used. The most popular method in wet braiding is by use of an impregnation ring.

In both dry and wet braiding curing of the polymer matrix is usually accomplished in an elevated temperature oven or autoclave. Incorporating in-line curing and resin impregnation allows braided products to be manufactured on a continuous basis. For 2D braided thin-walled composites, tunnel ovens or radiant lamps may be used to accomplish continuous curing. Continuous curing of solid fibre composites requires a high heat flux. The major commercial method for in-line curing using external heat flux involves the use of pultrusion dies. In the current pilot production plant, a new method using induction heating of steel wires embedded in a fibre composite core is used. The method allows for fast and controlled curing of thick fibre composite parts. The main advantage of this method is that curing is initiated at the wire locations. Conceptually, this results in less axial cracking compared to the use of a pultrusion die.

1.3.Fibre Reinforced 2D Braided Rebars

Currently, fibre reinforced polymer rods which act as reinforcement in concrete structures are being investigated by the members of the composite manufacturing group at the University of Ottawa. The research is focused on providing an alternative to steel rebars for use in applications where structures are subjected to caustic agents such as sea water or roadway deicing salts. The aim of the research project is to develop an FRP bar with mechanical tensile behaviour similar to steel but that is corrosion resistant. It is a relatively simple matter to match the longitudinal elastic modulus of steel using high modulus carbon fibres in epoxy resin. These fibre composites fail in a brittle fashion at stresses much greater than the yield strength of steel. Unfortunately, they do not exhibit any ductility, a prime requirement for concrete reinforcement. Work completed by Ewen in 2004 at the University of Ottawa explored two nontraditional methods which rely on interfacial shearing to achieve ductility in FRP rebars. A prototype of the product is shown in Figure 1.3. The rod is composed of a central carbon fibre composite core with a biaxially braided aramid overwrap. Specimens for the study were manufactured by batch processing in lengths of 2m due to a limitation in the length of the mandrel drive (shown in Figure 1.6). The validation of the ductility concept would require mechanical testing in large concrete structures (greater than 2m long). This would require a significant quantity of rebars in lengths of at least 5m. In order for production to be logistically feasible the production must be done on a continuous basis at a pilot plant scale. This was the main the driving force for this work.


Figure 1.6: Braiding head and mandrel drive (2004).

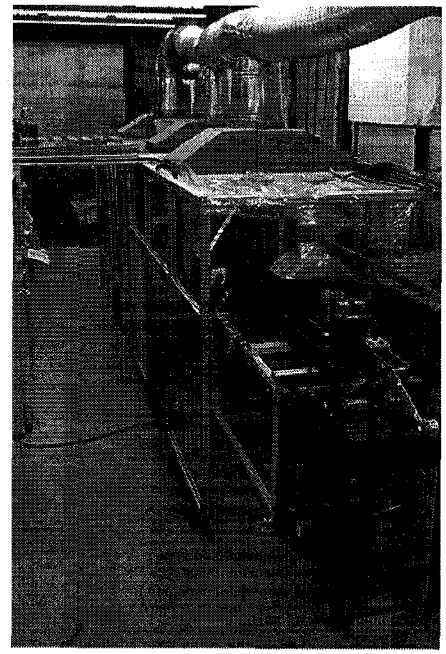
Figure 1.7: Pilot production plant (2008) view from the end of the production line.


Figure 1.8: Pilot production plant (2008) view form the beginning of the production line.

1.4.Past and Current State of Production Equipment

Following research by Ewen, work began [2] to design and construct the necessary facility to produce braided composite rod on a continuous basis. Prior to this, the braiding equipment consisted of the braider head, the mandrel drive and the creel. Several accessories and fixtures for the braiding head and mandrel drive were also available. Although a computer control system had been developed it was not in use and machine operation was manually controlled. The state of the equipment in 2004 is shown in Figure 1.6. The extent of the modifications done since then are apparent in Figures 1.7 and 1.8 which show the current state of the facility.

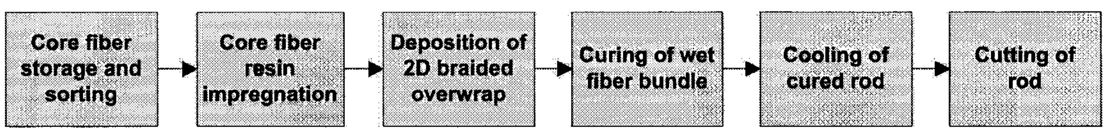

Figure 1.9: General steps for production of hybrid braided/pultruded composite fibre rod.

The manufacturing steps to obtain a specific product are largely dictated by the actual product design. The production steps for both continuous and batch production are similar. To a large extent, the production steps (as depicted in Figure 1.9) were therefore dictated by Ewen through the development of ductile FRP rebars. For batch processing of FRP rebars, the transitions between production steps are sequential and are implied when production personnel begin a new manufacturing step. In the case of continuous processing, all production steps occur simultaneously. The transitions between production steps are driven by the product feed (pulling of rod). From this point of view, the only notable conceptual difference between batch and continuous production is the way in which the product advances through the process. This is not to say that the methods and associated equipment used in each case are similar. Quite to the contrary: for most production steps the methods used for batch processing do not apply to the continuous case. For example, in the study by Ewen, resin impregnation was done by painting resin on the rod surface and curing was accomplished in an elevated temperature oven for several hours. Both of these methods do not apply to continuous pressing. Consequently, new methods and associated equipment were needed for continuous processing.

Work related to the modification and implementation of new processing equipment required for continuous production can be divided in two phases. Phase 1 began in the summer of 2004 and was accomplished by three students under the supervision of Dr. Fahim and Dr. Munro. Phase 2 is discussed in Chapters 3 to 8 of this thesis. The principal work accomplish in phase 1 is summarized below.

- Acquisition of the induction heater, tunnel ovens and two peristaltic pumps. The induction heater and tunnel ovens are used as part of the in-line curing process. The peristaltic pumps are used to supply resin to the process.
- Preliminary tests of the new curing method utilizing an induction heater and tunnel ovens.
- The construction of a ventilated enclosure over most of the production facility. This was necessary in order to contain and exhaust the fumes produced by the curing process.
- The design and fabrication of a puller capable of providing a continuous traction force. This was necessary in order to overcome the maximum production length limitation of the mandrel drive.
- Modification to the creel in order to double its capacity such that a larger core diameter rod could be made.
- Development of a method to impregnate the core fibre. This included testing of various resin bath designs. Ultimately an impregnation ring was developed to accomplish resin impregnation.

Following phase 1 most of the production equipment was in place to accomplish continuous production. Nevertheless, none of the production equipment was equipped with instrumentation. It should be noted that the tunnel oven was equipped with thermocouples and temperature controllers but it was found that these could not adequately regulate the oven temperature. The first production runs which utilized continuous manufacturing occurred in the fall of 2005. For these early production runs, rods with poor quality were produced. This included incomplete or over impregnation, and uncured or burnt sections due to fires. Problems in production were attributed to three main factors,

1. Uncertainty in the required machine parameters to achieve complete and defect-free curing.
2. Functional issues related to key pieces of equipment

3. The lack of instrumentation and an adequate control system.

The nature of continuous production and the available lab space required that curing be accomplished in 2 to 4 minutes. As will be discussed in the next chapter, conventional curing methods do not allow curing of solid composites in this time frame. A new method was devised which provides energy to the core of the rod through a high frequency magnetic field produced by an induction unit. The exterior of the rod is cured using tunnel ovens. As this method had never been used, the appropriate curing parameters, namely, the induction heater power and oven temperature for a given line speed could not be found in the literature. The continuous nature of production coupled with the inability to quickly adjust the oven temperature limited trial and error experimentation which could otherwise be used to obtain a working set of curing parameters. For the current product design, the curing parameters were obtained using computer simulations. The work was performed by John Sandness and is reported in [3]. Details of this work are given in the literature review (section 2.2.5)

Several deficiencies of the production equipment were identified in this work following initial production runs. The design of the fibre handling and sorting system lead to severely damaged fibres. Non-uniform flow around the impregnation ring lead to partial impregnation of the core fibres. The continuous puller lacked sufficient traction force to advance the product through the process.

The lack of instrumentation required manual adjustment from visual observations and operator knowledge. Difficulties in production were compounded by the continuous nature of production. In batch processing, production steps are sequential. In most cases individual operations may be halted or delayed without affecting other operations. This is not the case for continuous production where all production operations must be started and halted simultaneously. Previously, manual machinery controls were located throughout the pilot plant. At the beginning of a production run or in case of malfunction, the actions of several operators needed to be coordinated.

The modifications made to the production equipment, the development of new automation strategies and implementation of a control system are the main topics of this work. An overview of the initial state of the pilot production plant at the beginning of this thesis is shown in Table 1.1.

Table 1.1: Initial state of pilot production line at beginning of thesis

Systems	Phase 1 (2006)
Braiding and Pulling	Braiding and pulling (feed rate) speeds are not monitored.
	A 12V DC motor provide power to the pulling station. The Puller is under-powered, leading to inconsistent feed rates.
Fibre Sorting and Impregnation	Core strand spools are not individually tensioned, leading to entanglement.
	Fibre sorting system inadequately handles core strands, leading to severe fibre damage and incomplete impregnation of fibre strands.
	Dispensing rate of resin is not monitored and controlled
Curing	Two tunnel ovens (total length 1.5m). On/Off control. Temperature not monitored in heating chamber, leading to inadequate temperature control.
	Cooling of rod relies on natural convection with ambient air. Potential puller damage due to hot rod entering the pulling station.
	Oven temperature cannot be decreased rapidly.
Monitoring and Control	No emergency stop system. In case of emergency all equipment must be shut down manually.
	All machinery is manually controlled from operator observations.
	Machine controls are distributed throughout the production plant
	Abnormal operating conditions must be observed by operators.
	No data are available about machinery operation following a production run.

1.5. Objective and Scope

The first objective of this work is the development of an automation system capable of coordinating and regulating production machinery operations. The primary goal of the automation system is to aid researchers to produce fibre composite components at a pilot plant scale with predictable, controllable and consistent quality control. The production system is divided into three sub-systems, namely, 2D braiding and pulling, fibre sorting and impregnation, and resin curing. For each of these sub-systems the behaviour relevant to the production is examined and presented. When required a suitable controller design is investigated and implemented. In all cases, the behaviours of the controllers are presented from actual implementation and not simulation.

This work builds on that accomplished in phase 1 of the project (as described in the previous section). Unless it is judged necessary the methods and equipment developed during this phase are not questioned. Therefore, the second objective of this work is to continue the development of the infrastructure necessary to produce fibre composite rods on a continuous basis. This includes the improvements to the design and implementation of machinery and fixtures. Although at the time of writing the target application is the production of FRP rebars formed by a core of unidirectional carbon fibres with a 2D fibre composite material braided overwrap, the production system is developed to be as versatile as possible. In the hope that it may be used in future projects.

The following should be viewed as a development type work, where relevant engineering knowledge and theories are used to explain and justify the particular design implementation decisions. Since the scope of the project is wide, the development of sophisticated controllers will not be attempted. Instead, an industrial approach is used where a working set of controllers are used to obtain machine behaviour which is satisfactory for the current production needs. The automation system is designed to be easily maintained and upgraded. Therefore, the automation system framework may be used as a basis to implement more sophisticated and application specific control algorithms.

The work on the hardware and software of the control system should be viewed as two of the major contributions of this work.

1.6. Thesis Organization

The organization of the thesis is as follows:

In Chapter 2 the relevant state of the art details relating to the critical manufacturing process steps are given. These are 2D braiding, continuous resin impregnation, and curing of thick cross-section composites. Control strategies for each of the production steps are also surveyed. Chapter 3 will present a description of the proposed continuous 2D braiding process. An overview of the production process equipment is given. Challenges associated with continuous production are highlighted. Finally, the general control approach is presented. Chapters 4 to 6 will present the braiding and pulling, fibre sorting and impregnation, and resin curing systems, respectively. The physical equipment associated with each system are described. The system behaviours are then presented from a control perspective. Next, suitable controller alternatives are presented and evaluated. Chapter 7 will present the hardware and software implementation of the control system. Finally. Chapter 8 presents conclusions for the present work and recommendations regarding further work. The control software code listing is included in the Addendum located on the CD attached to this thesis.

2 Literature Review

In this chapter an overview of the available published literature and other research related to the continuous production of a 2D braided pultruded FRP rod is presented. Prior art related to manufacturing issues for 2D braiding, fibre impregnation and curing of thick composites will first be presented. For each of these topics a short review of the manufacturing-related detail currently in use and other promising techniques will be provided. Next, existing control and automation solutions appropriate for this work will be presented for the 2D braiding, resin dispensing and curing processes.

2.1.Continuous Manufacturing of FRP rods: Related Prior Art and Research

2.1.1.Two Dimensional Composite Braiding

The concept of continuous 2D braiding and coating of the braided product was introduced more than 100 years ago by Healey and Sheppeard [4]. The braid was produced in the downward direction using a maypole braider (Figure 2.1). The process was likely used to produce rope or garment trim. A gravity fed container applied the desired coating. Conceptually, it is similar to the process discussed in this work.

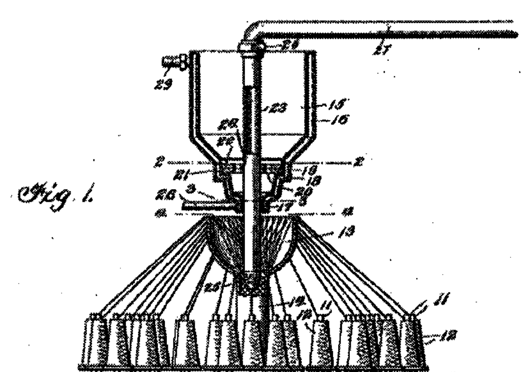

Figure 2.1: Patented apparatus to produce coated braids developed by Healey and Sheppeard [4]

Several general references are available regarding 2D braiding and braided products. The *ASM Handbook (volume 21 Composites p.69-77)*, classifies braiding methods, compares braiding equipment, provide a historical perspective and compares mechanical properties of various braids types. An extensive reference section is also provided. Two widely cited book on the subject are *Braiding and Braiding Technology* by Douglass and *Atkins and Pearce Handbook of Industrial Braiding* by Ko et al. More recently, Freger et al. have written *Braiding Pultrusion Technology for Advanced Structural Composites*. This work is unique as it explores the properties of FRP components with braided layers (external or internal) and an internal pultruded section. The book content is as follows: accepted geometrical models of the braided layers are described and compared to experimental studies, parameters that influence the pultrusion regime are presented, mechanical models are investigated for complex profiles, production processes, common equipment and tooling are described. The details of these general references are given in the Bibliography. For this work the main interest is the control of machine speeds during the manufacturing process.

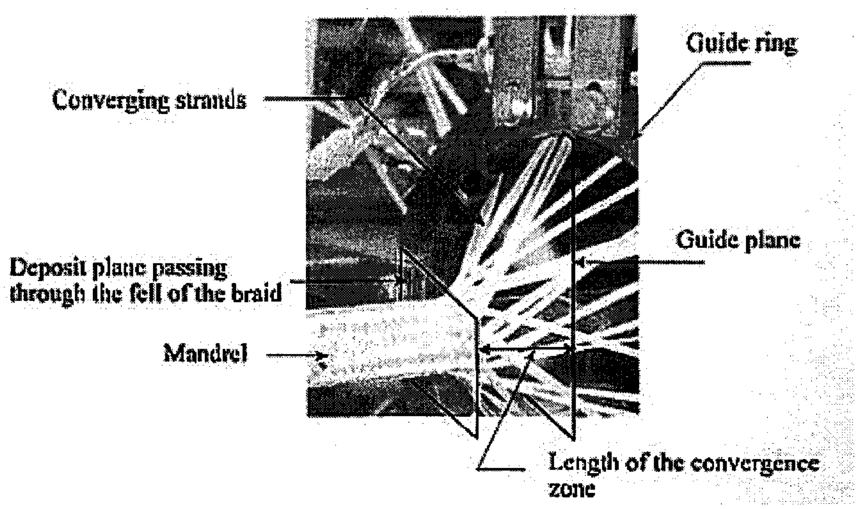

Figure 2.2: Terminology for the region of braiding [1]

As the fibers exit the braiding head they are fed through a guide ring. With reference to Figure 2.2, the intersection between the strands and the guide ring surface forms the guide plane. The deposit plane is located where the strands first contact the mandrel. The convergence zone is the area between both planes. A fundamental problem in the manufacturing of 2D braided structures is the development of models which relate machine parameters (braider angular velocity, mandrel feed rate), the braid formation parameters (Figure 2.2) and the final braid properties such as braid angle and coverage factor. A simple mathematical model which relates the braid angle with braiding machine parameters under a steady state condition for constant diameter mandrels is shown below.

$$\alpha = \tan^{-1}\left(\frac{\omega R}{v}\right) \quad 2.1$$

$where: \alpha = Braid\ angle\ wrt\ the\ braid\ deposition\ axis\ [rad]$
$\omega = Bobbin\ angular\ velocity\ about\ center\ of\ braiding\ head\ [rad/min]$
$R = Mandrel\ Radii\ [m]$
$v = Mandrel\ speed\ [m/min]$

It should be noted that this model was originally proposed for helical filament winding and may be extended to the 2D braiding process by assuming that only one strand is being braided. More specifically, the model assumes that:

i) The yarns are straight in the convergence zone (Figure 2.2). This neglects the interaction and frictional effects between the yarns.

ii) The strand crimp (bending caused by interaction with other yarns) is not incorporated in this models. In short this assumes that the yarns are perfect helices.

iii) There is no strand slippage with respect to the mandrel. This is often referred to as the stick condition which implies that deposited yarns elements remain where they first contacted the mandrel.

Equation 2.1 has been used by others to develop models which extend to non-circular cross-sectional mandrels [5] and non-constant cross-sectional mandrels with varying geometrical centers [6].

A study by Mazzawi [1] showed that assumption I of Equation 2.1 introduced an error (3 to 8°) between the predicted and actual braid angle. The discrepancy is shown in Figure 2.3 for various braiding to pulling speed ratios ($\omega R/v$). It can be seen that when there is no fibre interlacing in the convergence zone (corresponding to *spools ½ empty* curve), the predicted and actual braid angle are very close, but when fibre interlacing occurs (corresponding to *All spools are full* curve), the predicted error increases as the speed ratio increases.

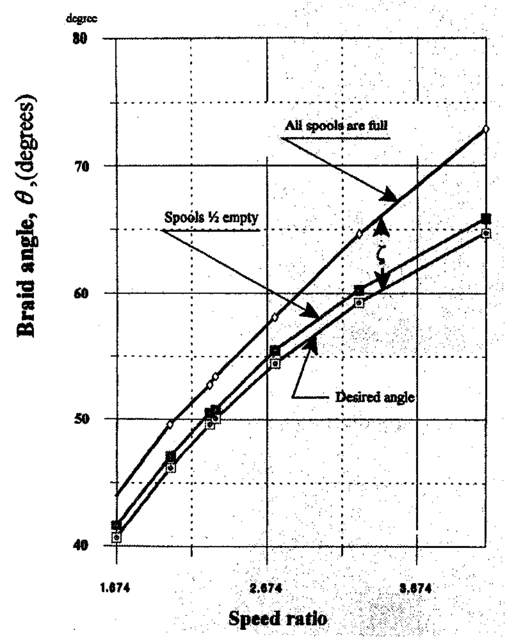

Figure 2.3: Desired and actual steady state braid angle for various speed ratio's ($\omega R/v$)[1].

The transient behavior of the braid formation is also of importance. This is especially true for braiding of non-constant cross-sectional components. In such cases braid formation would be dominated by transient behavior.

2.1.2.Resin Impregnation Methods

Wetting of fibers with the desired quantity of resin is a critical and well studied task for most FRP product manufacturing. In the current context, impregnation must be accomplished on-line and continuously.

For continuous fibers, the most widely used method to wet fibers is the open resin bath approach, where fibers are completely submerged in premixed resin [7]. The method is depicted in Figure 2.4. To ensure complete impregnation, wet fibers travel over and under rollers within the bath. Although this method is simple it is limited to resins with long shelf life and it may be difficult to precisely control the quantity of resin. To obtain high fibre volume fraction dry rollers or orifices may be used to remove excess resin. The frequent handling of the fibre (by roller, guides and/or orifices) increases the risk of fibre damage. This is especially true for brittle fibers such as carbon fibers.

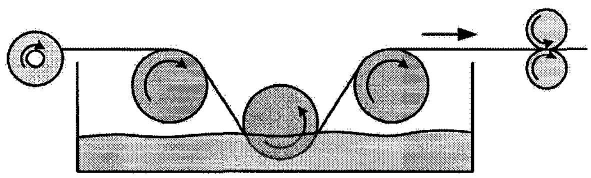

Figure 2.4: Conceptual representation of wetting fibre using an open resin bath.

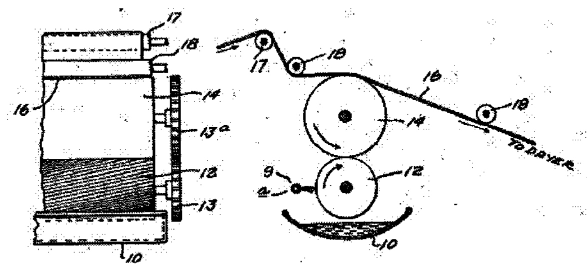

Figure 2.5: Two roller apparatus to wet fabric mats as proposed by Obenshain [8].

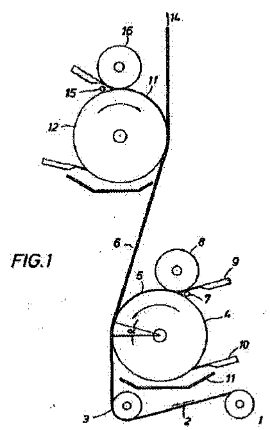

Figure 2.6: Apparatus to apply resin to prepreg material as proposed by Tait et al. [9].

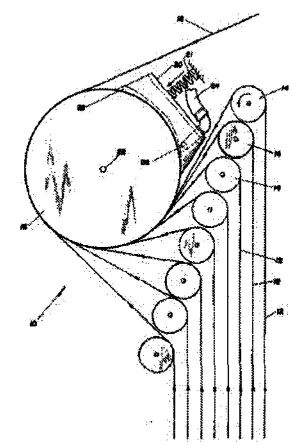

Figure 2.7: Apparatus to apply resin to individual fibre using pressure fed shoe as proposed by Youngkeit [10].

Several methods and apparatuses used to continuously coat papers and fabric with various substances have been documented for almost 100 years. For example, Obenshain [8], proposed a method which utilized two rollers (Figure 2.5). One roller is immersed in the coating substance while the other transfers the coating to the paper or fabric. This method allows little control over coating quantity and can only be used to coat the bottom surface.

Another method utilizes a roller equipped with a doctor blade to improve the accuracy of volume fraction of the resin. The doctor blade is positioned such that the desired coating thickness remains on the roller which is then transferred from the roller to the dry fibre. Recently, the method has been patented by Tait et al. [9] (Figure 2.6). In this case the method is used to apply resin to woven fabric to produce prepreg. Another alternative to the previous approach is the use of a spring-loaded pressure-fed shoe which rests on a rotating roller (Figure 2.7) [10].

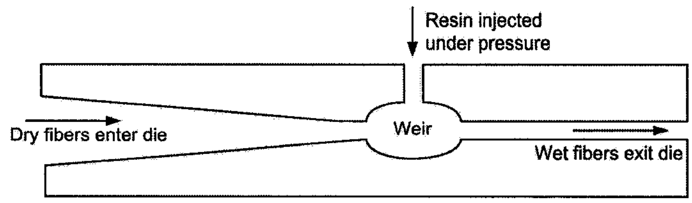

Figure 2.8: Conceptual representation of resin die proposed by Gauchel [11].

Resin injection dies have also been proposed (Figure 2.8). The design of the die is critical in order to obtain thorough impregnation of all yarns. One such design has been proposed by Gauchel [11]. In this design resin is injected under pressure in a long die. It is reported that the injection pressure must be comparable to the pressure provided by the fibre compaction at the exit of the die. To prevent resin from escaping the die, the entrance is long and tapered. The main advantage of this approach is that precise dispensing is possible but the system is considerably more complex than the bath approach as it requires a high pressure delivery system.

Another high pressure approach for continuous impregnation is the use of atomizing nozzles to spray resin on fibers. The method and apparatus is described by Gao [12] for the application of sizing compounds and other aqueous mediums on various fibers. A similar method is used in the production of chopped strand mat. This method has the advantage that minimal contact is required with the fibers during impregnation, minimizing the likelihood of fibre damage. The high velocity and small size of the atomized resin particles also conceivably increase the impregnation speed as resin is forced into the fibre strand. Unfortunately, due to the high viscosity of the resin used in this work, this method would require a high delivery pressure, thus requiring an expensive and mechanically complex pumping system. Over spray would also requirer extensive clean up and could render accurate dispensing difficult.

An automated resin application system for composite braiding was developed by Kruesi et al. [13] under a contract from the US Army. This approach utilizes a "porous" ring. Resin is distributed by an internal plenum to laser drilled passages that lead to the outside of the ring. Fibers are impregnated as they pass over the outside radius of the ring. The resin passages are sized for the highest flow rate and most viscous resin. A system of plugs were designed to accommodate various flow rates and resin viscosities. The ring is supplied with resin and catalyst using two gear pumps driven by numerically controlled servomotors. Mixing is accomplished using a static helically baffled mixing tube. Flow control is performed in an open-loop fashion from a previous calibration. The void content of resin impregnated braids was evaluated using microphotography and reported to be between 1.7 and 3.7%. These values are said to be comparable to manual application of the resin followed by vacuum bagging. Fibre volume fraction between 56.8 to 63.9 % where achieved.

2.1.3.Curing of Composite Parts

As FRP gains acceptance as a viable replacement for traditional engineering materials there is an increased need to produce parts with thicker cross-sections. This poses processing problems, specifically in curing of the polymer matrix. In recent years this problem has been extensively studied and novel curing techniques have been proposed. This section will present a short survey of curing techniques. Limitation of conventional techniques with regards to maximum part thicknesses and processing times are highlighted. Several alternative techniques for curing thick cross-section composite parts are presented.

Some thin fibre composite parts can be cured at room temperature in 5-20 min for polyester and vinyl ester resins and in 8 to 24 hours for epoxy resins. In such cases no external heat is applied and curing is accomplished through exothermic chemical reaction. For higher performance resins, curing is usually accomplished using elevated temperature ovens or autoclaves. Long cure times and residual stresses induced by the curing process limit part thickness which may be produced by the above techniques.

Curing by ultraviolet light is limited to a thickness of approximately 20 mm for fibreglass and considerably less for carbon components due to the limit of penetration of the ultraviolet light. Ultrasonic curing is usually limited to thicknesses comparable to those of the prepreg material (~0.25 to 0.5 mm). Intelligent monitoring and control of manufacturing parameters have reduced typical autoclave curing times from 16 hours to 1.5 hours (for a 25 mm thick flat fibre composite plate) [14].

Pultrusion is currently the most common process for producing constant cross-section FRP components on a continuous basis. Components that are thin (up to 3 mm) can be processed at line speeds of up to 1.5 m/min using conventional resins and up to 1.9 m/ min. using specialty resins. As the thickness of the part increases the line speed decreases. For example, a 19 mm thick section is typically processed at 0.2 m/min. Circular rods have been processed commercially using the pultrusion process with diameters as large as 99 mm; however, the line speed must be very low or very long and expensive curing dies must be used.

For all processes in which the initial heat flux for curing is provided through the outside surface such as in oven curing and pultrusion, internal cracking can occur in thick sections. This is primarily due to the curing and hardening of the outer layer and of the decrease in volume due to chemical shrinkage of the inner layers as they cure. Low temperatures and long cure times or low line speeds have to be used to avoid such defects. Intelligent control may be used to increase the curing rate while limiting the temperature difference (and therefore curing rate) between internal and external sections of a component [15]. Although results are impressive, total cure time remains too long to use in continuous production.

The more promising currently used techniques for the processing of thick (>25 mm) fibre composite components are electron beam and microwave curing. Electron beam curing has an excellent capability for the curing of very thick fibre composite components: a 25 mm diameter rod could be cured at a line speed of 10 m/min based on the energy density reported in the literature for flat plates [16]. However, this has not been proven experimentally. Equipment costs for this capacity are on the order of $3,000,000 for the electron beam curing unit and shielding. Regulation associated with the operation of nuclear devices further increase procurement difficulties of such devices. High frequency microwaves have been used for many years for the curing of thick fibre composite components. Although low cost fixed frequency units are available between $3,000 to $12,000, fixed-frequency microwave curing leads to arcing in carbon fibre composites. To avoid arcing a variable-frequency microwave must be used, typically costing $100,000.

Electron beam curing and microwave curing have the advantage of providing the initial energy for curing uniformly throughout the thickness of a component, and therefore such internal cracks which are likely to occur with conventional curing methods may be avoided with these methods.

One method which as been in use for several years to cure polymeric resin utilizes induction heating. For example, the automotive industry uses induction heating to cure epoxy in order to seam sheet metal panels [17]. A similar process is also commonly used to cure epoxy which encases the rotor and stator armatures of electric motors[18]. Induction heating has also been used by Boeing Co. [19] and Ford Motor Co. [20] to heat a die used to cure a composite preform. A method developed by Kodokian [21] uses magnetic and conductive particles mixed within polymeric resin to produce localized heat when subjected to induction heating. The method is said to cure parts composed of various thicknesses of carbon fibre and resin plates. No literature was found on methods which utilizes induction heating to cure thick cross-section fibre composites parts on a continuous basis.

The ideal curing regime would start the process at the interior of the component and then spread outwards. This would eliminate internal cracking and would conceivably produce a beneficial residual stress due to the continual chemical shrinkage of an outer layer of resin onto an inner layer. As previously mentioned a novel dual curing method involving induction heating of steel wires embedded in the central fibres and heating of the exterior surface of the braided rod using conventional tunnel ovens is used in this work. The initial equipment cost for this method is in the order of $5000. Approximately half of this amount was for the induction unit, the remainder for tunnel ovens. A detailed study of this method was done by Sandness et al. [22]. Experimental studies were conducted to evaluate the resin exothermic curing process and the calorific heat supplied by the induction unit. Analytical models were developed to predict the heating rate of the rod for both the induction and oven stage. A parametric study of the curing process was performed using finite element computer simulation. The cross-sectional temperature and cure fraction are presented for 8 different combinations of feed-rates, induction unit intensity and oven temperatures. The study revealed that full curing of a 24 mm rod could be accomplished in 120 seconds using the proposed method. Experimental curing of a 12 mm rod has been accomplished in 4 minutes.

2.2.Related Control and Automation Solution

2.2.1.Control of Braiding Process

The purpose of a braiding control system is to control the required braider head and mandrel speeds in order to produce the desired braid angle. For simple braided components the task is simplified to determining the appropriate ratio of braiding to mandrel speed. An example of a more complex model-based control has been implemented by Michaeli [23]. In this case, the model allows control of the braid angle or coverage factor based on the mandrel geometry. The model is limited to circular mandrels but core center line eccentricity and angle with respect to the braided axis can be varied. The system utilizes a two tier method. First, a preprocessing (off-line) step verifies the production feasibility of the braided part. This preprocessing step ensures that machine speeds are not exceeded. Furthermore, geometric constraints are verified. For example, it is ensured that the bobbin tensioning system can maintain the braided fibre taught for a given braid angle, mandrel eccentricity and mandrel center line angle. During production the braiding speed is maintained constant. From the mandrel geometry, a model derived from Equation 2.1 is used to calculate the pulling speed.

Another example of model-based control was developed by Potluri [24]. In this case a triaxial braiding machine using a flexible mandrel and controllable pulling direction is first described. Three control strategies are discussed, constant pulling speed, constant braid angle, and constant coverage factor. Experimental resultsf are not given.

For all of the methods discussed above, braid deposition is done under open-loop control. Although braiding head and mandrel speed are individually regulated using closed-loop control, control of the braiding geometry is based on a previously established model and not on-line measurements. As previously discussed, the assumptions made in developing these models make their use limited and errors in the actual braid geometry are observed. The problem is compounded by the transient behavior of the braid formation. For this reason, reports which claim precise control of the braid angle from models should be questioned. This is especially true for mandrels with varying cross-sections in which braid formation may be dominated by transient effects. The ideal system would incorporate on-line measurements of the actual braid geometry on the mandrel or a measurement(s) which allow the estimation of such quantities.

One reported attempt at such a system is discussed by Chiasson [25]. The work involved the development of a computer controlled system for a 36 carrier braiding machine. A sensor (previously developed by Mazzawi [1]) composed of a swing arm connected to a rotary potentiometer allowed one to estimate the angle of the convergence zone. Closed-loop control of the convergence zone angle was achieved using a PD controller. It was hoped that by controlling the convergence zone angle the braiding angle could also be controlled. Unfortunately, difficulties were reported in controlling the location of the deposit plane. This led to fluctuations in the desired braid angle.

The advent of automated vision systems poses interesting possibilities in the area of composite braiding. For example, Lian et al. [26] developed an inspection system for braided preforms. The system is able to measure the braid angle and detect defects in both the preforms and final components. It is reported that the system, based on a 133 MHz computer, is capable of processing images at a rate of 1/3 Hz. A system with increased processing power could conceivably increase the maximum sampling speed by several times, allowing, on-line measurement of the braid angle, deposition plane and mandrel geometry. This would allow a truly intelligent control of the braiding manufacturing process. No literature was found for such a system.

2.2.2. Control of Dispensing Process

Dispensing systems for liquids or slurry fall in two categories, namely batch and continuous. As this work deals with a continuous process, batch dispensing will not be discussed. The task of a continuous dispensing control system is to regulate the quantity of a substance added to the overall process flow. For example, in a chemical process the additive substance could be a pigment which is added to a base material. In the current context, the additive is the resin mixture while the fibres may be thought of as the main flow.

Dispensing control systems have been categorized by Poynton [27] as additive, open-loop and closed-loop. In additive systems no measurements of the process are done.

The pump set point is adjusted based on pump calibration and expected main flow rate. In open loop systems measurements of the main flow are used to adjust the dispensed quantity. For the current application this is equivalent to measuring the pulling speed and adjusting the dispensing rate according to a pre-established calibration. Closed-loop systems employ direct measurement of the dispensing process. In a chemical process, for example, this may be done by measuring the mixed flow PH or by use of a chromatographic analyzer. The dispensing rate is adjusted according to these measurements. For the current application, closed-loop control would require direct measurements of the fibre volume fraction of the impregnated fibre. This cannot be easily achieved. By assuming that all the dispensed resin is fully incorporated and remains in the fibre strands (no dripping) the system can be thought of as a closed-loop system if the resin flow rate is controlled based on the actual pulling speed.

In most dispensing applications a simple feedback controller allows adequate process control. Dispensing pumps, such as the peristaltic pumps used in this work, employ a fixed volume which is periodically filled and discharged. The nature of such devices produces periodic flow and pressure pulses. In most applications this can be tolerated. In applications where flow pulses cannot be tolerated more complex control strategies must be used. For example, Hillerstrom [28] developed a control system with a disturbance model which rejected torque disturbance on the pump motor. The controller provides near constant angular velocity of the rotor. According to the author this is a required condition to minimize flow pulsations.

One state of the art fluid dispensing application described by Moralest [29] is venovenous hemofiltration of infants. This medical procedure involves filtering a patients blood and adding desired constituents following renal failure. Typically, four dispensing pumps must be controlled with dispensing rates between 40 and 100 ml/min. The procedure may last several hours to several weeks in which time changes to the pumping dynamics may occur due to several factors. Due to these changes in pumping dynamics, additive dispensing control based on pump calibration as used for adult patients cannot be used for infants which require more precise dispensing. In order to accurately control dispensing the authors have developed an adaptive control system which continuously adapts an autoregressive model which is in turn used for control purposes. The use of weight measurements of reservoirs is also described as a means to estimate the dispensing flow rate. This method has the advantage that there is no contact between the sterile dispensed fluid and the measurement device. It is reported that this method gives adequate measurement accuracy and is significantly less costly than ultrasonic measurements which are traditionally be used for this application.

2.2.3.Control of Tunnel Oven for Curing

Control of the curing process may be approached in different ways. In most cases the control algorithm considers only the operation of the curing equipment. For these cases, the process control variable may be temperature or heat flux. From the viewpoint of the curing process this method may be regarded as open-loop control, as no measurements of the actual curing process are taken. These methods are analogous to baking, where the oven temperature and bake time is determined a-priori through trial and error experimentation. Determining the curing parameters are often approached in a similar fashion. For more critical applications computer simulations of the curing process may be performed to determined optimal equipment set points. Models of the curing process are often used to devise more complex curing strategies. The goal of such studies is usually to produce uniform curing rates within the part section while decreasing the total curing time. As previously mentioned non-uniform curing can lead to residual stresses and internal cracking of final components. In batch processing an optimal time-varying temperature profile may be used to accomplish uniform curing. For example, Lee et al. [30] developed a time-varying heating profile to produce thick section flywheels while minimizing internal residual stresses. In continuous production the temperature of successive heating zones may be adjusted to obtain similar results. For example, Li et al. [31] report an improvement of 75% in the uniformity of the degree of cure for a pultruded C-section. Optimization of the die temperature profile was done through iterative finite volume simulations.

In general, the most advancd curing controllers consider the curing apparatus, such as the oven, autoclave or die, and the composite component as part of the process to be controlled. This implies that direct temperature measurements of the component must be done during the curing process. In some cases, specifically for large structures, it may be possible to embed thermo-couples in critical sections to monitor cure temperatures. For smaller components this may not be possible due to economic or structural reasons. In this case only the exterior temperature of the component may be monitored. This approach has been used by Parthasarathy et al. [15] to design a controller which minimizes the temperature difference between the interior and exterior of a thick laminate cured using a die. Temperature distribution profiles through the thickness of the laminate weere first obtained by embedding thermo-couples within laminate plies. The data were then used to estimate parameters of a non-linear observer. During production the temperature of the laminate surface is used by the observer to estimate the temperature within the laminate. An inverted model predictive controller is used to obtain the required die temperature. Using this control scheme, the authors report a maximum temperature difference of 6.7°C between the center and exterior of a 48 ply laminate during curing, compared to 25.5°C when the part was process using conventional curing cycle. Although the results are impressive, total cure time remained above 200 minutes.

When applicable, methods which consider both the curing apparatus and component as part of the control process may be advantageous. In such systems it become possible to reject the effect of uncontrolled disturbances which are likely to affect the curing process. For example, the effects of changes in resin reactivity, in fibre or resin quantity or of heat transfer coefficients can be compensated for by the control system. Alternatively, it may be simpler to adequately control factors which may influence the curing process and use an open-loop control approach. This is specifically relevant for continuous processes where temperature measurements of the product are difficult to obtain. In this case the design effort is reduced to providing the curing apparatus with a controller able to track set point commands. For the current project this involves designing a controller for the induction heater and for the multi-zone tunnel ovens. The induction heater unit is equipped with a dedicated control unit. Therefore, set point commands can be tracked without the need for an external controller. The remainder of this section will discuss various controllers used to regulate thermal system and, more specifically, multi-zone ovens.

Control of thermal systems is the one of the most common control tasks. The majority of thermal processes encountered in daily life utilize simple low bandwidth on/off actuators. For this reason, control systems for these applications are usually limited to high gain (i.e. on/off) feedback control systems. This is true for most residential ovens, water heaters, furnaces, etc. For such on/off systems, a compromise must be made between the speed of response and the overshoot to set point changes. If the response is not satisfactory, proportional actuators must be used. This allows regulation through a wide range of controllers. Thermal systems are generally characterized by relatively slow and stable over-damped dynamic responses. Thermal devices will most often demonstrate non-linear behavior over their entire operating range. This is especially true for thermal systems which rely on radiant heat transfer and, to some extent ones that rely on convective heat transfer. However, in most industrial applications, a thermal system will operate about a constant temperature or specific temperature profile. Developing a controller about these operating conditions most often results in adequate process regulation. This is especially true if the speed of the open-loop response is slow compared to the speed of possible disturbances and set point changes. Therefore, most controllers may be adapted to regulate thermal systems.

PID's are the most common controllers used to regulate thermal systems. In industrial settings, controller gains may be tuned by trial and error or by using a tuning strategy. Common tuning strategies include the Ziegler and Nichols ultimate gain or quarter decay methods [32] or the internal model control methods [33]. Often these tuning rules are incorporated in auto tuning PID modules.

The problem of controlling a multi-zone tunnel oven has been addressed by Shinivasan et al. [34] and by Batur et al. [35] in order to produce artificial crystals. The control objective in this work is to maintain a constant temperature gradient within a vertical tunnel furnace. A pole placement approach is used using state feedback. Input (control intensity) / output (temperature) data was first obtained for the purpose of system identification. Next, the parameters of a discrete state space model are identified using least-squared optimization. The resulting state space equations are augmented to include the integral of the tracking error as a state variable. The state feedback coefficients are determined using the discrete linear quadratic regulator. Simulation and experimental results are presented. The resulting control system can be viewed as a state feedback + integral action controller. A major deficiency of this work is that the portions of control action provided by the state feedback part and integral controller are not shown. It is possible that the bulk of the control action is provided by the integral controller. Actuator limits were not considered in the control system design. Therefore considerable overshoot (above 25%) occurs when the system is subjected to a step command. The sensitivity of such a control system to changes in process dynamics are apparent. In one of the experimental studies a crack developed in the heating tube. This caused significant changes in the transient system response compared to simulation results.

3 Overview of Continuous Production of Hybrid Braided/ Pultruded Rods

This chapter will first present the challenges associated with production of fibre composite rods on a continuous basis. Next, a summary of the proposed process to produce braided/pultruded composite rod on a continuous basis is given. The methodologies used for each of the production sub-systems are related to the surveyed literature presented in the previous section. Finally, the global control strategy used to reduce production failures will be presented.

1.1.Production Challenges

In order to produce 2D braided fibre composite rebars several problems needed to be overcome. Figures 3.1 to 3.4 show various specimens of prototype FRP rebars produced from the initial production runs (following Phase 1). Several examples of the interrelationships between production parameters are demonstrated from the collected samples.

The effect of varying the ratio of mandrel speed to braiding speed can be seen in Figure 3.1. Although the braid completely covers the core, the braid angle varies instead of being constant.

During the initial development of the pilot plant, it was common that liquid resin would ignite in the oven chamber. In one instance, this occurred due to improper temperature control of the ovens. In this case, the oven controller indicated a temperature of 225°C while, in fact, the temperature was later verified to be over 500°C. A specimen with a charred exterior is shown in Figure 3.2. The resin on the surface of this specimen was completely oxidized.

An over-impregnated specimen is shown in Figure 3.3. For a given product, the specified fibre volume fraction is only achieved if the correct ratio between resin dispensing rate and mandrel feed rate is maintained.

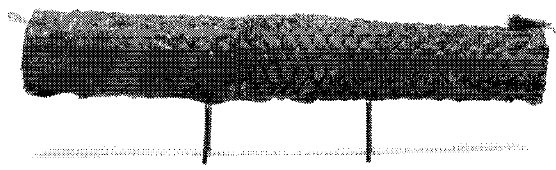

Figure 3.1: FRP rebar prototype sample #1: the braiding angle in not constant due to variation in pulling speed.

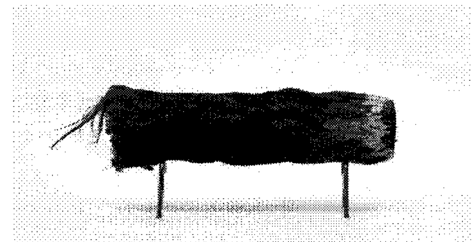

Figure 3.2: FRP rebar prototype sample #2: the resin was completely oxidized.

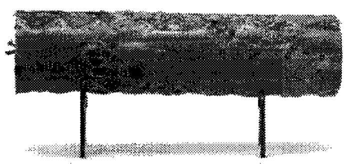

Figure 3.3: FRP rebar prototype sample #3: over-impregnation of the rod can be seen (underside of the rod show).

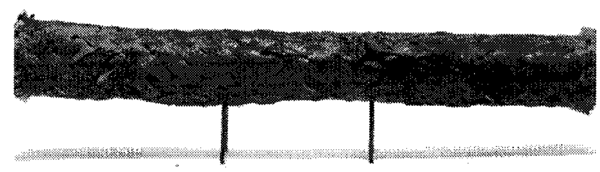

Figure 3.4: FRP rebar prototype sample #4: the sample was crushed by the puller due to incomplete curing of the resin.

Figure 3.4 shows a section of rod which was crushed by the puller belts due to incomplete curing of the resin. This problem likely occurred due to improper temperature control of the ovens at the beginning of a production run. In fact, under-curing of the polymer matrix has been a systematic problem throughout the development of the pilot plant. The problem was mainly due to the slow dynamic responses of the oven system. As a consequence, it was not possible for timely changes in oven temperature to occur. This resulted in the production of several meters of partially-cured rod. The problem is compounded by the inability of the puller to advance a partially cured rod. This is in part due to the compliance of the uncured rod and the lubricating effect caused by the non-rigid resin. The problem is further complicated by the in-line nature of the process as discussed below.

An unexpected decrease in the pulling rate led to several problems in the production line.

- Over-curing of the polymer matrix for rod sections in the induction heater coil would occur. As with the sample shown in Figure 3.2 this resulted in oxidization of the polymer matrix. In this case, oxidization occurs inside of the rod, making damaged sections difficult to identify. Furthermore, a considerable quantity of toxic smoke is produced.
- If the braiding speed was not adjusted accordingly, a decrease in pulling speed affected the braid geometry. This resulted in a variation in the braiding angle as in Figure 3.1.
- If the dispensing rate was not adjusted properly the fibre volume fraction was not as specified. This resulted in over-impregnation of the core strands as in Figure 3.3. Over impregnation may cause other problems later in production. The required heat flux to cure the rod is mainly a function of the resin quantity. If the induction heater power and oven temperature are not increased for over-impregnated sections partial curing is likely to occur. Again, resulting in the inability of the puller to advance the product through the process.

In all the cases presented above, the problems were not in the curing method or production equipment themselves but in the inability of operators to simultaneously control the various machine parameters. A computer-controlled system was therefore seen as indispensable in order to achieve consistent production. The system would be used to regulate individual machinery operation and also to adjust interrelated parameters simultaneously when needed.

The examples given above are extreme cases where production failure was obvious. The goal of the control system and equipment modifications described in this work must eliminate such failures. Furthermore, an increase in overall product quality must be achieved. As previously discussed, this is to allow production of rebars that demonstrate consistent quality control and thus consistent mechanical properties. To achieve these goals several requirements issues where identified.

- The core fibres must not be damaged.
- Core fibres must be fully impregnated before the braid is deposited.
- Precise placement of heating wires within the part section must be achieved.

- The impregnation ratio must be controlled. This implies controlling the resin dispensing rate and the product pulling speed.
- The braiding speed must be measurable and controllable.
- The temperatures of the curing ovens must be monitored and controlled. More specifically, the speed of the closed-loop response must be increased.
- Changes in pulling speed must be reflected in appropriate changes in other production quantities such as braiding speed, dispensing rate and curing parameters.
- The operator(s) must be able to stop production if needed and this without compromising the quality of the product within the production line.
- Machinery controls must be centralized such that they may be controlled and monitored by one operator.

These issues were identified following initial production prior to this work. Subsequent chapters will discuss the challenges associated with resolving each of these key issues. In some cases, redesign of the production equipment was needed, in others a proper instrumentation and control system was required.

1.2. Overview of Pilot Plant Production Line

The overall production line is presented in this section. The manufacturing and control approaches used in the current production line are related to the surveyed literature. As reference material, a photograph taken at the exit end of the pilot production line is shown in Figure 3.5 while a view of the entrance has been previously given in Figure 1.8. It can be seen from these figures that a ventilated enclosure surrounds the majority of the production line. This is to contain and exhaust the fumes produced by the resin curing process.

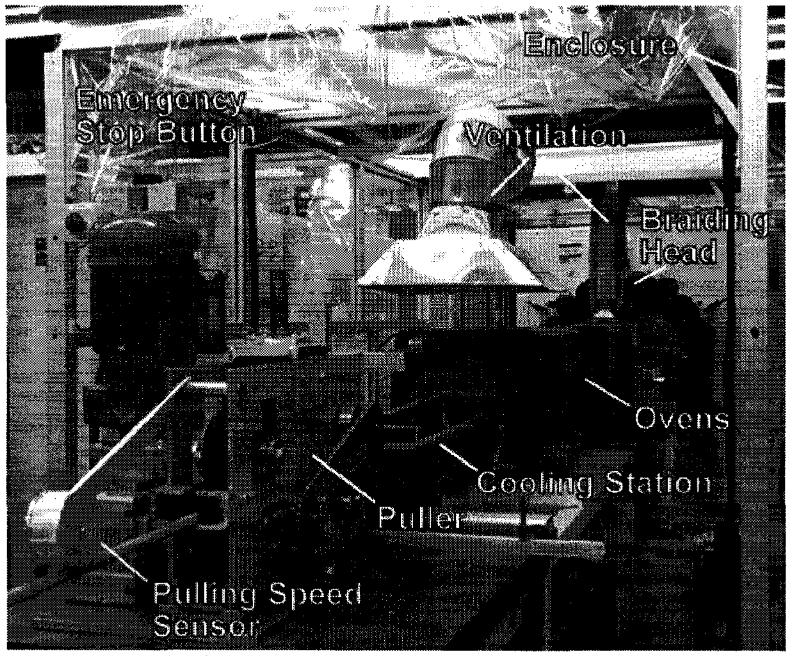

Figure 3.5: Pilot plant, shown are the puller, cooling station, tunnel oven, enclosure and ventilation system.

A schematic of the production equipment is shown in Figure 3.6. The figure depicts the in-line nature of the manufacturing technique described in this work. Raw materials enter at various points in the production line, fibre and resin are combined and transformed on a continuous basis to produce a finished product. Regardless of the exact product design, the production steps and raw material are similar. The core strands are first unwound from their spools and exit the fibre storage frame. Guide eyes and a circular guide plate distribute the fibres in a pressure fed impregnation ring which coats the fibres with resin. A 2D braid is then deposited on the loose core strands. The wrapping effect of the braiding action provides the pressure to form the rod's pultruded core. Curing of the resin is accomplished using an induction heater and a tunnel ovens. Finally the rod is cooled using a water stream. A caterpillar puller provides the product feed for all of these operations. A computer-based control system allows the operators to monitors and adjust machinery parameters. The emergency stop system can be used shutdown all of the production machinery and this independently of the control system.

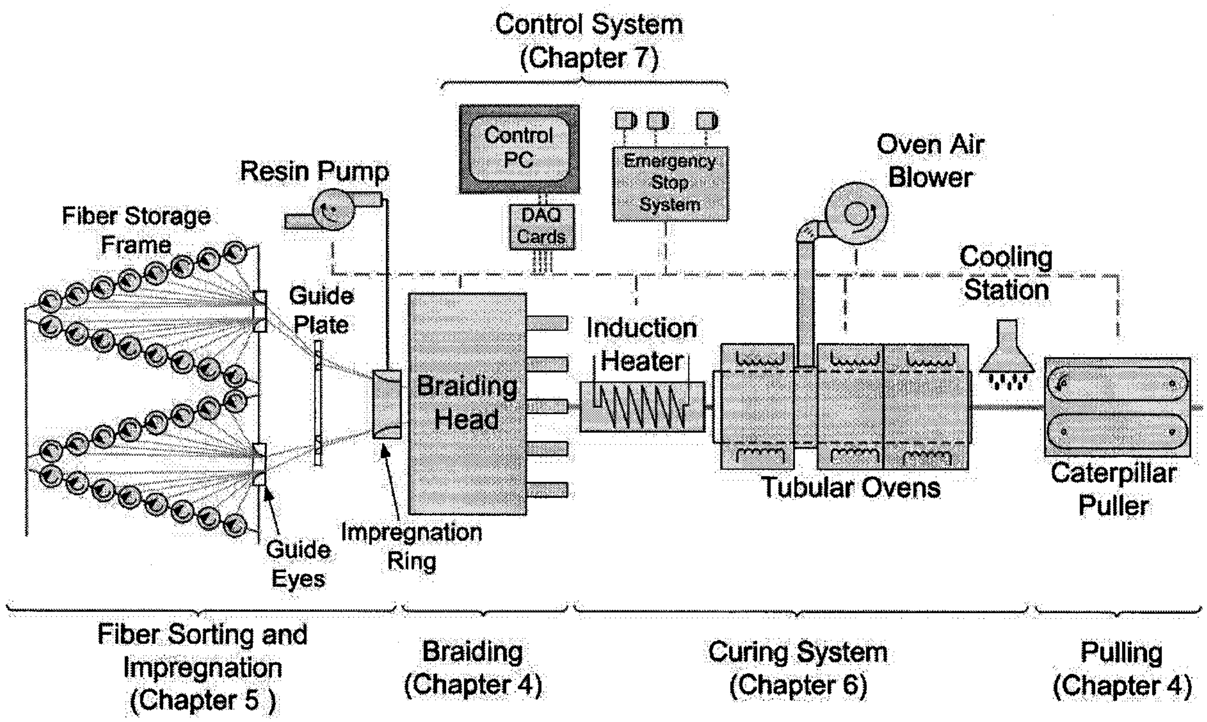

Figure 3.6: Pilot plant equipment overview.

1.3.Manufacturing and Automation Approaches

1.1.1.2D Braiding

Both the braiding and pulling speeds are under closed-loop control using a set point element and an integral trim controller. Two control methodologies are used to achieve the desired braid geometry. The first relies on an operator to manually control the braiding speed for a given mandrel speed. This method is particularly applicable in cases where complete mandrel coverage is desired. In such cases, visual inspection of the rod by the operator can readily confirm that complete coverage of the mandrel is achieved. In fact, this method proves adequate even for non-constant cross-section mandrels [36].

Alternatively, the braid pitch (ratio of braiding to pulling speed) can be specified. In this method the braiding speed is automatically set according to the measured pulling speed. This allows changes in the pulling speed to automatically translate to changes in the braiding speed. Although this control approach is simple compared to approaches discussed in the previous chapter, its use is justified. For the current application, a constant cross-section circular rod is produced. The required braiding and mandrel speeds to produced the desired braid angle remain constant and can be calculated a priori. Furthermore, as continuous production is investigated the transient behaviour of braid deposition is of less concern.

1.1.2. Continuous Product Feed

In order to accomplish continuous production, a puller capable of providing continuous mandrel feed must be utilized. The puller provides the necessary traction force to advance the product through the production line. Two puller configurations, hand-over-hand and caterpillar, are commonly in use for continuous polymeric product feed. A distinction is made between polymer and metal product feed as the forces typically involved in metal manufacturing can be several orders of magnitude greater than for polymer products. Hand-over-hand pullers sequentially pull the product using two linear actuators and product grabs. The main advantage of this configuration is that a greater pulling force is possible compared to the caterpillar configuration but the action of the two actuators and grabs must be coordinated requiring more complex control strategies. The caterpillar puller continuously pull the product using opposing belts placed parallel to the feed axis. This work utilizes a caterpillar puller.

1.1.3. Resin Impregnation and Dispensing Controller

Prior to 2D braiding the core strands must be impregnated with resin. The outer braid is impregnated through contact with the wet core strands. Resin impregnation is accomplished using a pressure-fed steel ring. The apparatus is a simplified version of the one developed by Kruesi et al. [13] for the US Army. A pressure-fed internal channel distributes the resin to an external groove in the interior radius of the ring. Fibres are impregnated by capillary action through contact with the wet inner radius of the ring.

Proper alignment of the fibres with respect to the impregnation ring is essential for correct impregnation. The central core fibres are guided out of the fibre storing rack using a set of polymeric eyes and a circular guide plate equipped with similar polymeric eyes. The plate ensures that the fibres enter the impregnation ring evenly spaced and at the correct angle. Figure 3.7 and 3.8 show the creel, guide plate and impregnation ring.

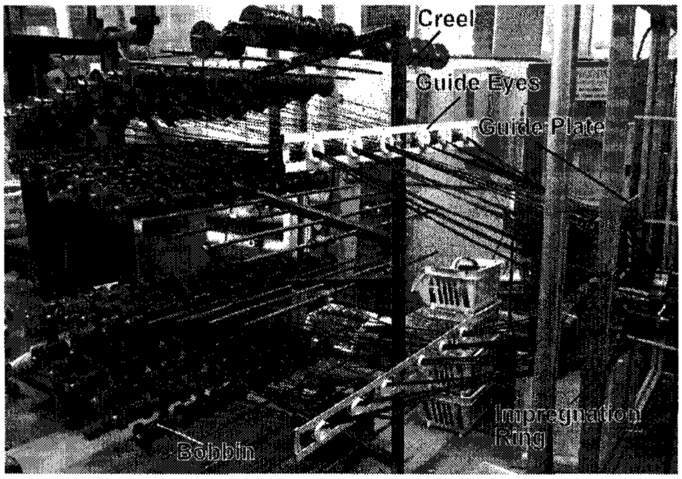

Figure 3.7: Core fibre sorting station, shown are the creel, guide eyes, guide plate and impregnation ring.

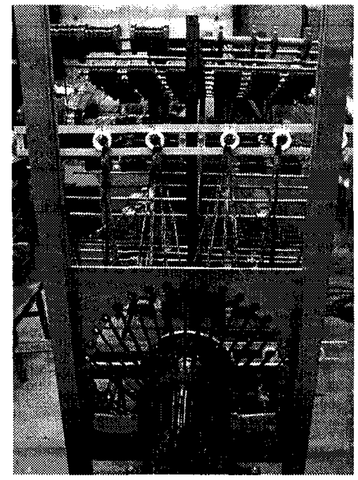

Figure 3.8: Core fibre sorting, detail of the guide plate and impregnation ring.

Peristaltic pumps are used to supply the impregnation ring with resin. A cascade control strategy is used to control the dispensing process. A PID controller is used to regulate the pump rotor speed. The pump rotor speed set point may be adjusted manually. In this case the operator would visually inspect the wet strands and adjust the rotor speed accordingly. This corresponds to manual control. The rotor speed may also be set from a calibration curve. A utility was developed to automatically acquire calibration points (corresponding to flow rate vs. pump rotor speed). Actual flow rates are obtained from a weight balance connected to the control computer. This control strategy corresponds to an additive dispensing system. On-line flow estimates obtained from the weight balance may also be used to provide closed-loop flow rate control. Conceptually, the method is similar to the one used by Moralest [29] for dispensing control in Hemofiltration. The flow rate set point may also be automatically adjusted from pulling speed measurements. This corresponds to specifying the linear dispensing quantity. As previously discussed, combining both closed-loop flow control and automatic adjustment of the flow rate set point corresponds to closed-loop control of the dispensing process.

1.2.Resin Curing

The development of a curing technique capable of quick and controlled initiation of the resin exothermic reaction is critical to the development of the continuous braiding process. Curing of the rod is accomplished using a novel method: an induction heater is used to increase the temperature of steel wires embedded in the fibre core. Next, three tunnel ovens are used to increase the temperature of the exterior of the rod. Selectively placing heating wires withing the rods' core allows for localized heating and, consequently, controlled curing can be achieved. The distribution of the steel wires within a given rod is such that curing proceeds from the inside out. This allows a significant reduction in the likelihood of the development of longitudinal cracks in the finished part. The method allows for fast curing and is suitable for commercial continuous processes. The induction curing method could also be used for curing sections with varying thicknesses. For such sections, internal cracking would typically occur in the thicker regions if the curing does not proceed from the interior to the exterior. This is the case for methods such as oven or pultrusion curing which supply the a heat flux to the exterior. As depicted in Figure 3.9, wires that are heated by induction could be placed in the center of thicker sections. This would cause curing to initiate in these regions. The technique is analogous to metal casting where chills are added to initiate solidification in thick sections.

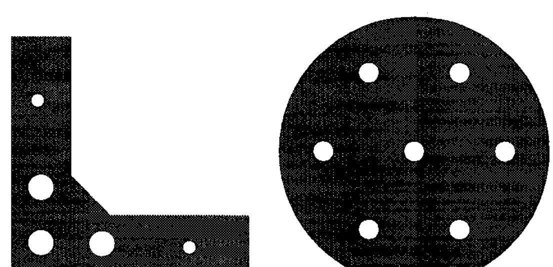

Figure 3.9: Placement of metal wires in L-section and circular rod. Wire placement can be used to initiate curing in specific location.

For this method the curing parameters are the induction heater power and the tunnel oven temperature set points. To some extent the number and distribution of the steel wires may be regarded as a control parameter. Using a computer simulation the proper induction heater and oven set points to produce a fully cured 12 mm circular rod at various line speeds were determined by Sandness [3].

In this work, the controller associated with the curing phase does not explicitly consider the product as part of the controlled process. This is in part due to the difficulty in obtaining relevant feedback of all degrees of cure which may be used to monitor the curing dynamics. The proposed approach assumes that by maintaining the induction heater and oven set point as specified the desired curing dynamics are achieved. Regulation of the tunnel oven temperature is accomplished using gain-scheduled proportional integral controllers.

In the event that an unexpected pause in production is required the oven chamber must be quickly cooled to prevent over curing of the rod section located in the oven stage. The oven system posses a high thermal mass and is well insulated, and therefore the cooling rates of the oven chamber are very long. To increase the cooling rate in such situations, cool air may be forced into the heating chamber using a centrifugal blower. Presently the blower is automatically activated when the production run is paused, at which point its intensity is adjusted from a predetermined set point profile.

1.4. Global Control Strategy

In Section 3.2, the need to automatically adjust machine operation based on the product pulling speed was highlighted. More specifically, it was demonstrated that several production problems could be avoided if the braiding speed, resin dispensing rate and induction heater power were controlled according to the product feed rate. In order to automatically adjust these machine set points, the relationship between pulling speed and other machine operations must be specified.

It was decided to vary the machine set points using a single gain. The gain, specified by the operator, corresponds to the braid pitch (spool rot/m), the linear resin quantity (g/m or ml/m) and the linear energy (Amp/min)) for the braiding, dispensing and induction heating processes, respectively. Representing the relationship between the desired quantities and the feed rate as a zero order process neglects the dynamic behaviour of individual processes. This was judged acceptable as the primary use of the pilot production plant is for continuous steady state production.

Although the braider head transient behaviour is negligible, it was discussed in the previous chapter that a transient behaviour is associated with the braid formation process, therefore such, the proposed control scheme is only valid once the transient braiding period subsides. Detailed knowledge of the transient braid formation process could be used to formulate a model which relates braid formation as a function of pulling speed. Research has shown that several factors influence the braid formation process. For a given braid geometry, some of these factors relate to physical quantities which are not easily measurable. There are therefore doubts as to whether a physical model could be used as an open-loop controller to accurately represent the transient braid formation process. It should also be noted that due to fibre interlacing effects in the braid convergence zone the braid pitch can only be used to estimate the braiding angle.

Adjusting the dispensing process using a single gain results in a control that accurately represents the physical dispensing process. In other words, for a given rod area the desired flow rate will vary linearly with respect to the pulling rate. This assumes that the dispensing process transient behaviour is negligible. A special case arises when the pulling speed drops to zero. In this case the pump would stop rotating but resin flow in the impregnation ring would still be driven by the resin column contained withing the ring (flow is induced due to gravitational forces). This will cause the resin (approximately 20 ml) to slowly drip out of the ring. A solution to this problem would be to reverse the pumping direction when the product speed reaches zero. Unfortunately, this is not possible as the pump rotation cannot be reversed.

The proposed curing process has not previously been exploited and is therefore not ocumented in the literature. Research by Sandness [22] suggests that for a 0.5 in rod an induction setting of 231 amperes would produce the desired curing for a line speed of 0.5 m/min. Induction settings for other feed rates were not explicitly given. Intuitively, a feed rate of zero would require a zero current set point. A linear function can be formulated from these two values. It is reasonable to assumed that for feed rates close to 0.5 m/min satisfactory curing may be achieved by varying the induction current using this linear function. More research is required to obtain better understanding of the required induction heater settings for various feed rates.

A schematic representation of the global control system is shown in (Figure 3.10). The control system utilizes a cascade control strategy. A global controller calculates sub-system set points based on the production parameters specified by the operator and the measured production speed. Cascade controllers are tasked to regulate machine operation about the calculated set points. Alternatively, the global controller can be disabled and machine set points can be directly adjusted by the operator.

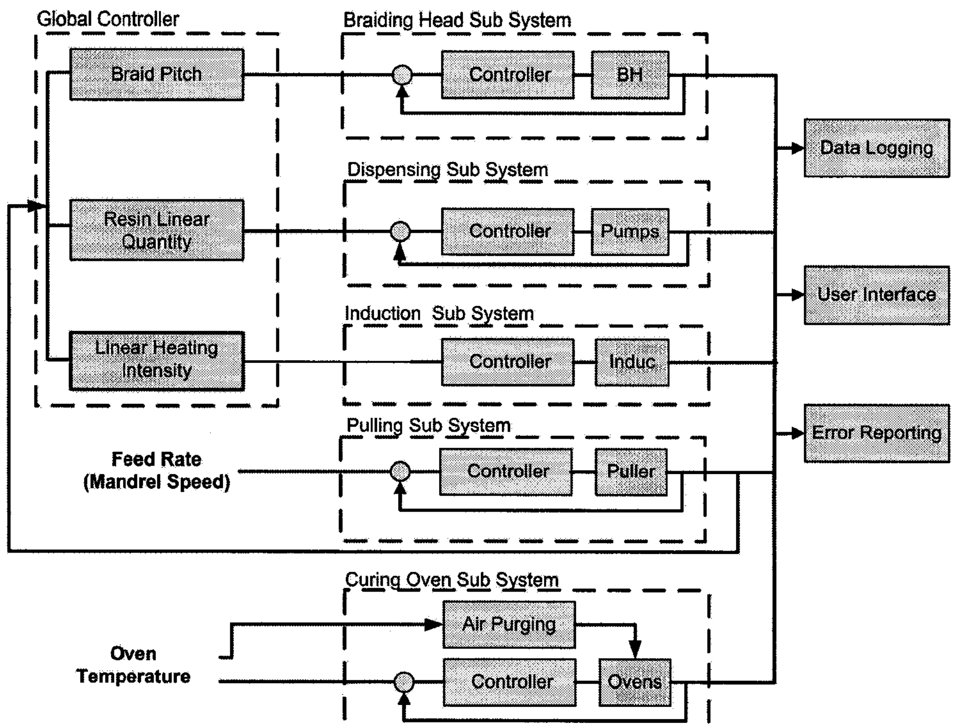

Figure 3.10: Production control strategy.

The following three chapters present the design and development details for the 2D braiding, fibre sorting and impregnation, and curing sub systems of the production line.

4 Development of Braiding System

4.1.Overview

The braiding system is composed of the braiding head (Figures 4.1 and 4.2) and caterpillar puller (Figure 4.3). It was found that both the braiding and pulling processes are dominated by the motor and drive characteristics. More specifically, it is shown that the motor drive limits the motor acceleration. A set point element obtained from open-loop responses and a pure integral controller is used to regulate the process. To prevent overshoot and to control the ramp up speed of both motors, a set point profiler is used. The profiler is designed using a Laplace transfer function and then discretized to construct an infinite impulse filter.

4.2.Physical System

4.2.1.Braider

The braiding head, shown in Figures 4.1 and 4.2, is manufactured by Wilhelm Steeger of Germany. It is equipped with 36 bobbins which are supported by a geared carrier system. The bobbins circulate on two serpentine paths. The intersections of the paths provide the weaving action to form the braid.

Mechanical power for the braider head is produced by two 1 HP synchronous motors. The motors are mechanically coupled which ensures that their rotational speeds are equal. The motors are powered using a single AC Tech Variable speed motor drive. The drive is configured to accept either manual control through a potentiometer or an external control signal (0-10V). Drive enable, motor direction and jog are controlled by connecting specific terminals to ground. Low current relays are used to provide this connection. Other operating parameters such as maximum acceleration, input calibration and driving frequency can be adjusted using trim potentiometers. Breakers with variable tripping current (2.2-3.5A) are connected between the drivers and the braider head motors. The breakers are also equipped with an external interrupt line. Originally, limit switches activated by the retraction of any one of the fibre tensioners were wired to these terminals. Retraction of the tensioner occurs if a braider strand ruptures or a spool empties. The limit switch levers have been removed to disable this functionality.

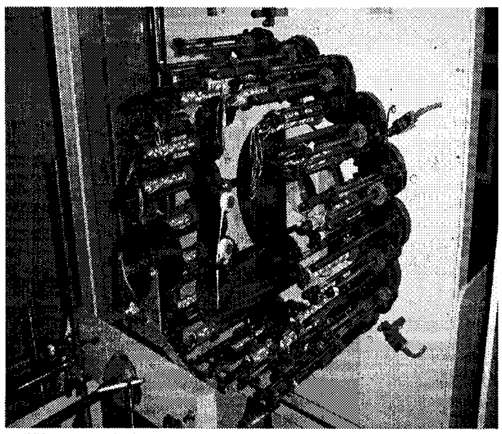

Figure 4.1: Front view of braiding head.

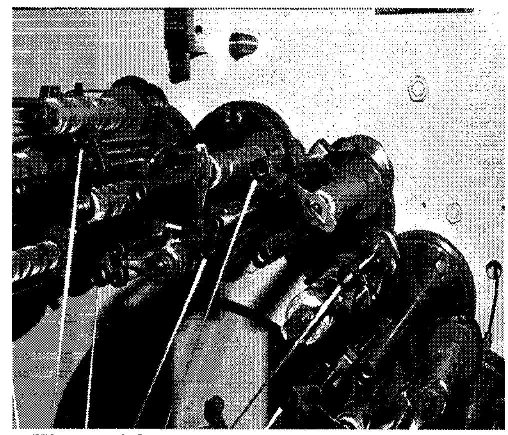

Figure 4.2: Detail view of braiding head bobbins.

An incremental encoder mounted on one of the braiding head motors monitors the braider angular speed. A general purpose counter of the DAQ card is used to estimate the rotational speed of the encoder.

4.2.2.Puller

The caterpillar type puller (Figure 4.3) used in the current production was designed and built in-house during the summer of 2006. A pair of reinforced rubber timing belts are mounted parallel to the pulling direction. The lower belt assembly is fixed while the top belt assembly can move in the vertical direction to accommodate different rod diameters. A force normal to the rod is provided by spring loaded Teflon pads located inside each of the belt assemblies. Mechanical power is supplied by a ¾ HP synchronous motor. The motor speed is varied using a variable frequency motor drive. Two gear boxes, one helical and one worm, reduce the motor speed by a factor of more than 350. This reduction was required to obtain a desired pulling speed between 0.15 and 1.6 m/min. The output of the worm gear box is connected to the lower belt assembly by a flexible jaw coupling. Torque is transferred to the top belt assembly by first reversing the direction of rotation using a pair of spur gears, then by the use of a chain. The chain introduces backlash between the top and lower belt assembly. This problem is apparent at the beginning of production when the puller is first activated or when the puller direction is reversed. For the current continuous production, the latter does not occur during normal operation. This issue should be addressed if precise control of the mandrel position is required. This would occur in applications such as multi-pass braiding or braiding of non-constant cross-section profiles.

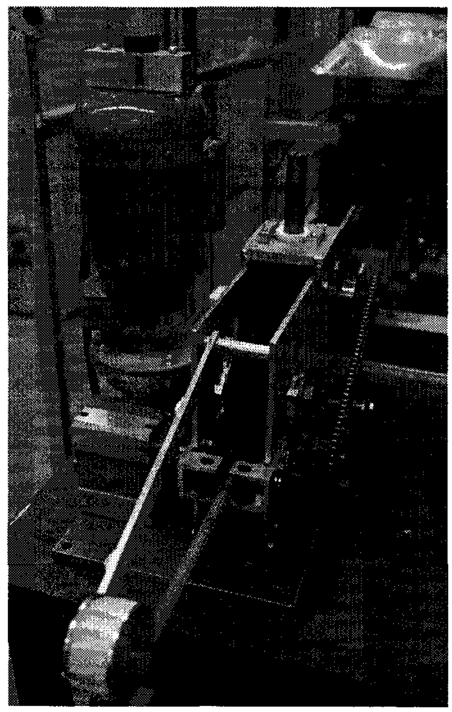

Figure 4.3: Caterpillar puller.

The pulling speed is monitored by two incremental encoders. The first is mounted on the puller motor while the second is connected to a sheave which rests on the pulled rod. The sheave encoder directly monitors the mandrel position. The sensor can be used to detect slip between the puller belt and pulled rod. This may occur in abnormal operating conditions.

The puller must provide sufficient traction force to advance the strands through the process. This force is the result of the braided and creel tow tension. The design of the braider head spool tensioning system renders the individual strand tension discontinuous. Since tension discontinuity will occur randomly for each of the 36 spools the resultant tension will be averaged. As the braid is formed, friction between interlacing yarns will create force discontinuities which affect the overall pulling force. This phenomenon can be observed when manually pulling the strands through the process. The bulk of the pulling force is created by the creel tow tension. This force is due to the spool tensioning system and frictional forces created by strand contact with the guide eyes and the impregnation ring. It will be shown in later sections that both the size of the puller motor and the large gear reduction enables excellent disturbance rejection. In fact, it was observed that the maximum pulling force is function of the maximum friction between the pulled rod and the belt.

4.3.Braiding and Pulling Process Angular Speed Estimation

As previously mentioned the braiding and pulling speeds are monitored using rotary incremental encoders. Incremental encoders were chosen over analog tachometers due to their greater noise immunity. Unlike tachometers which return a signal proportional to their speed, incremental encoders provide positional information. To obtain encoder speed, the encoder position must be differentiated. There are several approaches to obtain velocity estimations from an incremental encoder. The approaches fall in two categories: formal numerical differentiation or pseudo hardware differentiation.

4.3.1.Formal Numerical Differentiation

The formal numerical differentiation approach utilizes a mathematical differentiation algorithm to estimate the velocity from positional measurements. A survey of various numerical differentiation methods is presented by Ram et al. [37]. Formal Numerical differentiation algorithms fall in three categories: difference methods, interpolation methods and regularization. From a control stand point, the numerical difference approach is better suited for servo-control. For pure rotational velocity control, where the position is unbounded, overflow of the hardware counters will occur. Although it is possible to handle overflow using software, the hardware-based approaches are better suited for velocity control and will be used in this work.

4.3.2.Pseudo Hardware Differentiation

In this approach, a hardware counter is continuously incremented by either a clock signal or an incremental encoder pulse and reset by the other, and the result is used as proxy for the speed.

4.3.2.1.Method 1:Incremental Encoder Increments Counter

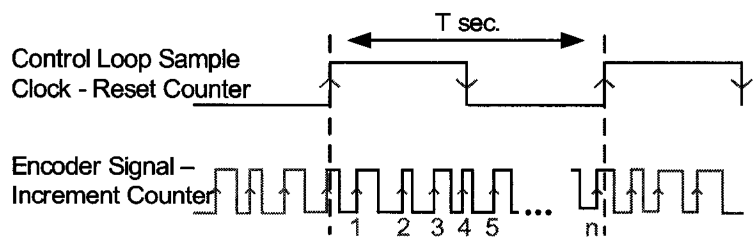

Figure 4.4: Incremental encoder differentiating process, the encoder is used to increment, while the sample clock is used to reset the counter.

For the method in which the incremental encoder increments the counter, (Figure 4.4), a clock periodically resets the counter. In most control systems, the sample clock is used to reset the counter. Before the counter is reset, the value is read and transferred to memory. Multiplying the count by the appropriate constant gives the average velocity of the encoder over the entire sampling period. Mathematically, this method is essentially a two point backward difference and corresponds to the first term of a Taylor series expansion.

$$\frac{\partial p}{\partial t}=\frac{p(t)-p(t-\Delta t)}{\Delta t}+O(t) \quad 4.1$$
$$\text{where}: p=\text{position of encoder}$$
$$\Delta t=\text{differentiating time}$$

The function O(t) is the difference between the estimation and the actual value of the derivative. It corresponds to the higher order terms of the Taylor series expansion. If the differentiating time is small, the discrepancy is also small. Since the counter is reset for each differentiating period, the position at $t-\Delta t$ is always zero. The differentiating time is equal to the sampling period, *T*. The angular velocity estimate in rotations per second becomes:

$$\omega=\frac{n}{Tm} \quad 4.2$$
$$\text{where}: n=\text{counter value}$$
$$m=\#\text{ of encoder sectors}(count/rev)$$

Errors associated with measurement and differentiating time accuracy affect the precision and repeatability of the angular speed estimation. The positional measurement error is equal to ±2 encoder counts. The time is provided by the sampling clock. The current DAQ provides an accuracy of 50 ppm. If the sampling rate is 60 samples/sec, the resulting accuracy is $\pm 8.33e^{-7}$ sec ($1/60 \times 50/10e^{6}$). The error associated with the quantity calculated from several measurements with random error can be calculated using the following formula.

$$\epsilon_P = \pm\sqrt{\left(\frac{\partial P}{\partial q_1}\right)^2 \epsilon_{q1}^2 + \left(\frac{\partial P}{\partial q_2}\right)^2 \epsilon_{q2}^2 + \ldots} \tag{4.3}$$

$$\text{where}: P = \textit{quantity of interest}$$

$$q_i = \textit{measured} \text{ or } \textit{assumed values with associated random error } \epsilon_i$$

Substituting Equation 4.3 into Equation 4.2, the estimation error due to measurement and time difference is given by:

$$\epsilon_\omega = \frac{\pm 1}{T}\sqrt{\frac{1}{m^2}\epsilon_n^2 + \omega^2 \epsilon_m^2} \tag{4.4}$$

$$\text{where}: \epsilon_n = \textit{count error} \quad (\pm 2\, counts)$$

$$\epsilon_T = \textit{Sample clock error} \quad (\pm 8.33\, e^{-7}\, sec)$$

If the encoder speed is very high, the error due to the sample clock inaccuracy will be negligible. Therefore, the error expression becomes:

$$\epsilon_\omega = \pm\frac{2}{Tm} \tag{4.5}$$

The estimation error is a function of the time period and the number of encoder sectors. For example, an encoder with m=500 count/rev and sampling time of 1/60 seconds implies an estimation error, or encoder speed resolution, of ±0.24 rev/sec or ±14.4 rev/min.

Since the estimation error is constant for any speed, the minimum speed which can be measured with this method is error dependent. The maximum measurable speed is bounded by the counter resolution, the number of encoder sectors and the sampling time. For the current DAQ, a counter with 32bit resolution is used.

$$\omega_{max} = \frac{\textit{Counter Resolution}}{\textit{Sampling Time} \times \textit{Num Encoder Sectors}} \tag{4.6}$$

For a 500 sector encoder and a sampling time of 1/60 second the maximum measurable speed is $3.09e^{10}$ rpm !

4.3.2.2.Method 2: Incremental Encoder Resets Counter

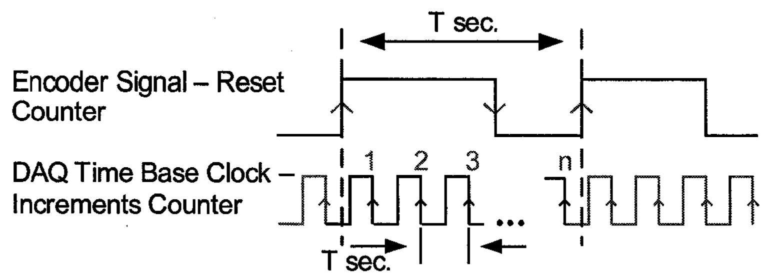

Figure 4.5: Incremental encoder differentiating process, the encoder is used to reset, while the time base is used to increment.

In Method 2, (Figure 4.5), the encoder resets the counter. A clock with a frequency that is several orders of magnitude faster then the encoder maximum frequency (corresponding to maximum speed) is used to increment the hardware counter. The controller clock or DAQ master time base is usually used to increment the counter. This method returns the maximum amount of information from the encoder since a speed estimate is obtained for each encoder pulse. For control purposes, a measurement can be obtained near the end of the sampling period. This is advantageous as it is a closer approximation of the ideal discretization of a continuous system. The encoder speed is the reciprocal of the counter value multiplied by the appropriate constants.

$$\omega = \frac{f}{nm} \qquad 4.7$$
$$where: f = Frequency\ of\ clock\ (Hz)$$

Finding the reciprocal is, in general, more computationally expensive than multiplication and may be difficult on certain hardware platforms. Using the same methodology as used previously, it is possible to find the total error due to the measurement error and time base error as follows:

$$\epsilon_\omega = \pm\omega\sqrt{\frac{1}{f^2}\epsilon_f^2 + \frac{(m\omega)^2}{f^2}\epsilon_n^2 + \frac{1}{m^2}\epsilon_m^2} \qquad 4.8$$
$$where: \epsilon_f = Time\ base\ accuracy\ (1000\ Hz)$$
$$\epsilon_n = Count\ accuracy\ (2\ count)$$
$$\epsilon_m = Encoder\ tolerence\ (count/rev)$$

In the current implementation, the time base frequency is 20 MHz. If the relative accuracy is 50 ppm it results in an absolute accuracy of ±1000 Hz. As with the previous case, the count accuracy is ±2. The encoder tolerance is the mechanical tolerance of the encoder optical chopper. In the previous case, the encoder tolerances and count accuracy were additive error sources. The encoder tolerance could be neglected since the count accuracy (±2) is considerably larger than the encoder tolerance. For this method, the count accuracy is considerably smaller (2 counts of 20 Mhz time base). Therefore, the tolerances of the encoder sectors may have an impact on the accuracy of the estimate. The encoder tolerance is quoted in terms of maximal cycle error and is 5.5 electrical degrees [38]. One electrical degree corresponds to 1/360 angular degree. This corresponds to 0.0153 encoder counts. It should be noted that the present analysis assumes that the cycle error is uniformly distributed where in reality the error is normally distributed. The analysis should therefore be viewed as an approximation.

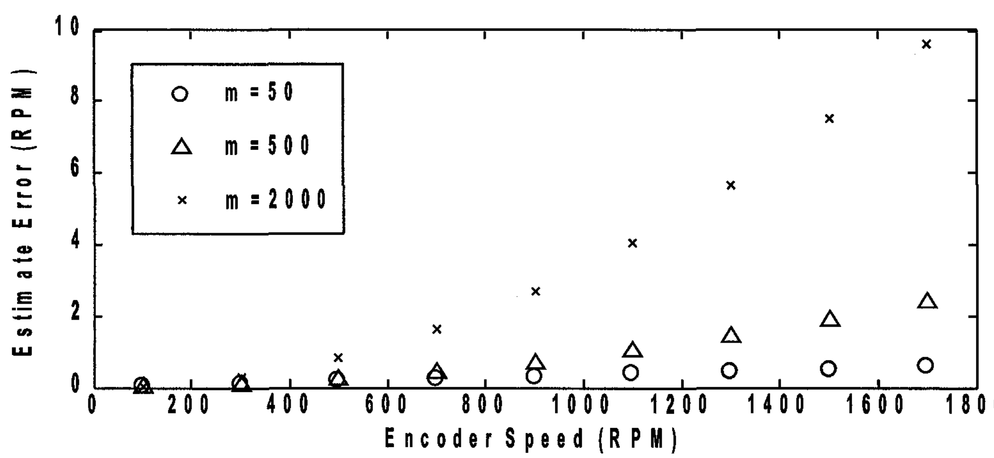

Figure 4.6: Encoder speed estimate error vs. encoder speed for encoders with 50, 500 and 2000 sectors (f=20 MHz).

The estimation error is plotted in Figure 4.6 with respect to encoder speed for encoders with various numbers of sectors. Contrary to the previous method, the estimation error increases as the number of sectors increases. For encoders with 50 and 500 sectors the error is below 0.1%.

Since speed estimates are obtained over a short period (compared to Method 1) this method is considerably more sensitive to process noise. This often requires averaging several measurements to obtain a more consistent estimate. Other problems also arise due to the speed at which the estimates must be transferred from the DAQ to the host memory. For example, a 500 count encoder rotating at 28.33 rev/s (1700 rpm) would generate measurements at a rate of 14.166 KHz. Data must be transferred from the DAQ's on-board memory to the computer RAM at this rate. It was found that the PCI bus could not sustain this throughput for prolonged periods. This causes the control software to report errors which are difficult to handle.

The minimum speed that can be monitored using this method is a function of the clock frequency, the hardware encoder resolution and the number of encoder sectors:

$$\omega_{min1}[RPM]=\frac{Clock\ Frequency}{2^{Counter\ Resolution}\times\ \#\ Encoder\ Sectors}\times 60 \qquad 4.9$$

For example, if the clock frequency is 20 MHz and the counter resolution is 32bit, overflow occurs after 214 seconds. For a 500 sector encoder this translates to a minimum measurable speed of 1.24 revolution/day.

For control applications it is desirable to obtain at least one speed estimate for each sampling period. To obtain an estimate the encoder speed must be a minimum of:

$$\omega_{min2}[RPM]=\frac{2}{\#\ Encoder\ Sectors\times Sampling\ Time}\times 60 \qquad 4.10$$

For example, for a sampling time of 1/60 seconds and a 500 sector encoder, the minimum speed which guaranties that a sample is available for each sampling time is 14.4 rpm.

4.3.3. Choice of Method

The choice of the method better suited for estimating the encoder speed is influenced by several factors, namely, the type of measurements (on-line or off-line), the number of encoder sectors, the encoder minimum and maximum speed and the hardware compatibility with each method.

In general, formal numerical differentiation methods are better suited for off-line estimation. In these cases, the error associated with the differentiation process can be reduced since higher order approximations which utilize non-causal filters may be used. This method is better suited if overflow is guaranteed not to occur. Since the counter is continuously incremented (not reset for each sampling period), the count error is reduced to ±1 count. Potentially, this reduces the speed estimate error by half.

The choice of which pseudo hardware differentiation method to use is mainly a function of the number of encoder sectors. If a high resolution encoder is available, it is preferable to use Method 1. If only low resolution encoders are available, it may be preferable to use Method 2. As previously discussed, the main limitation with the second method is its high sensitivity to process noise due to the short difference time. Inherently, a low count encoder will result in longer differentiating time and thus average process noise.

In the current implementation, Method 1 is used for the braider head, the puller and the pump motor encoders. Formal numerical differentiation is used for the sheave encoder which measures the pulling speed directly. This device and its use are discussed in the next section.

4.4. Direct Measurement of Pulling Speed and Slip Detection

In some cases, the pulling speed reported by the motor encoder may not be representative of the actual pulling speed. As previously discussed, this primarily would occur due to slip between the belt and the product being pulled, but may also occur due to backlash/chatter in the puller drive components.

For continuous production of a braided product, only the pulling velocity is of importance. As such, small amounts of backlash do not hinder production. In cases where the position of the mandrel is required, the puller backlash prevents the use of the motor encoder to determine the mandrel position. In these cases, direct position measurement of the mandrel may prove useful.

In an adverse operation condition, slip between the puller belt and rod may occur. The problem is specifically severe when only partial curing of the composite rod exists. In this case, the uncured resin provides lubrication between the rod and belt. This causes a sudden decrease in the maximum friction force which can be transmitted by the belt to the rod. Slip may also occur in the event that several fibre strands jam in the creel. As was previously discussed in Chapter 2, production parameters such as the braiding speed, resin dispensing rate and induction heater set point are functions of the pulling speed. It is therefore desirable to detect cases where the actual pulling speed differs from the value established by the puller set point. This allows the control system to adjust the other production parameters.

The pulling speed is measured directly using a wheel that rests on the rod as it exists the puller. The sensor is composed of a bar hinged on the puller frame. An aluminum wheel is mounted directly on the shaft of a rotary incremental encoder. The encoder is located at the end of the bar. The weight of the wheel, the low shaft friction torque and the relatively low rod acceleration justify the assumption that negligible slip between the rod and the wheel surface occurs. The braided overwrap creates geometric irregularities on the exterior surface of the rod. It is assumed that the effect of these irregularities on the rod position measurements are negligible. This is justified by noting the relative size of the sensor wheel (6.3 cm) with respect to the surface irregularities (<1 mm).

Inherently, slip will manifest itself as a discrepancy in the expected change in rod position caused by the puller belts as recorded by the puller motor encoder and the actual change in position as recorded by the sheave encoder. It is therefore logical to compare position and not velocity measurements. Since incremental encoders are used, this also eliminates the error that would otherwise be caused by two differentiation processes. During normal operation, the ratio of motor to sheave encoder pulses will remain relatively constant. Comparing the expected and the measured ratio can be used to quantify the amount of slip. Two methods are proposed for quantifying slip and shown below.

$$Slip\ Index\ 1 = \left| \frac{(n_{wheel}/n_{motor}) - EER}{EER} \right| \times 100$$

$$Slip\ Index\ 2 = \left[\frac{(n_{wheel}/n_{motor}) - EER}{EER} \times 10 \right]^2 \qquad 4.11$$

$$\begin{aligned} where: n_{wheel} &= Wheel\ encoder\ count \\ n_{motor} &= Motor\ encoder\ count \\ EER &= Expected\ Encoder\ Ratio\,(n_{wheel}/n_{motor}\ during\ normal\ operation) \end{aligned}$$

For both methods the expected encoder ratio is obtained through experimental calibration. This eliminates the error that would otherwise be associated with physical measurement of the sensor sheave and the puller pulleys. Calibration consists of edge counting the signals from both encoders while several meters of rod is pulled. For the current puller configuration an Expected Encoder Ratio (*EER)* ratio of 0.005142 was obtained.

It is difficult to replicate through experiments the conditions that induce slip as they occur during abnormal operating conditions. To test the methods outlined in this section, a stainless steel rod was advanced by the puller. To induce slip between this rod and puller belts a ViseGrip clamp applying pressure on a friction pad was used to generate a frictional force on the rod. By manually varying the pressure on the clamp handle different levels of slip could be induced. The results of this test are shown in Figure 4.7. For this test no appreciable rod slip is occurring between 0 and 15, 60 and 75, and after 100 seconds. Using the clamp and cloth setup the rod was completely stopped between 15 and 25 seconds, corresponding to a slip index of 100%. Varying degrees of slip where induced between 30 and 60, and between 75 to 100 seconds, corresponding to slip indexes between 10 and 70%.

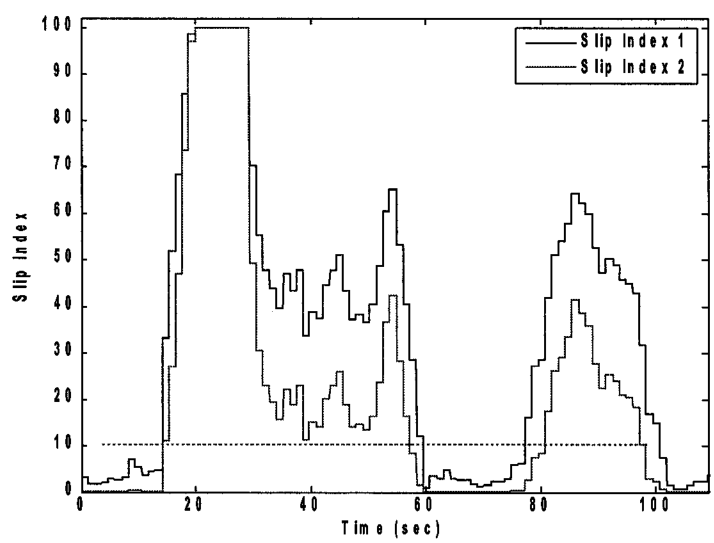

Figure 4.7: Puller rod slip indexes vs time.

Both methods result in a slip ratio of 0 when no slip exist and a value of 100 when the rod is completely stopped and slip is at its maximum. The slip ratio is undefined, if the puller motor is not turning. The values returned by Method 1 have a physical significance whereas the values of Method 2 are difficult to interpret in a physical sense. The main advantage of Method 2 over Method 1 is that it is considerably less sensitive to noise in the encoder measurements. This can be seen in Figure 4.7 where the index values of Method 2 are close to zero, while the values of Method 1 fluctuate between 2 and 7.

As previously stated, it is desirable to detect if slip is occurring such that operators are warned. Regardless of the method used it is desirable to reduce the occurrence of false positives. To reduce the likelihood of false positives, the slip index is first filtered using a running average of six slip measurements (moving window filter of 6). It is found that when a running average is applied to the squared index (Method 2) the resulting slip index value is insensitive to measurement error. This allows the use of a hard threshold limit to detect slip condition. In this case, a slip condition is signaled if the slip index is above the threshold. In the final control system implementation two thresholds are used. The lower threshold condition warns the operator of possible slip. The upper threshold condition alerts the operator that slip is occurring. For example, in Figure 4.7 an upper threshold of 10 is used. The lower threshold (not shown) should be set to approximately 1. Both values may be adjusted by the operator through the interface.

4.5. Braiding and Pulling Process

As previously discussed, both the braiding and pulling processes are powered by synchronous motors driven by variable frequency drives. It will be shown that the process dynamics are dominated by the motor and drive characteristics and not the mechanical systems. The response of the braiding and pulling processes are therefore similar in both open and closed-loop control therefore, both braiding and pulling processes are discussed in this section.

Mechanically, both the puller and braider head may be considered as damped inertial systems. For the puller, the large gear reduction between the motor and pulling mechanisms implies that the bulk of the inertial forces are due to the motor rotor. The moving parts of the braider head have significant mass. It is therefore expected that both the motor rotors and braider head's moving parts contribute to the total mechanical system inertia. Values for the braider head inertia and the damping and braking torques are 5.85 kg/ m^2, 5.79 Nm/rad/sec and 1.976 Nm [1], respectively. Given the braider and puller open-loop response, it will be shown that the process' physical characteristics cannot be used to design a suitable controller.

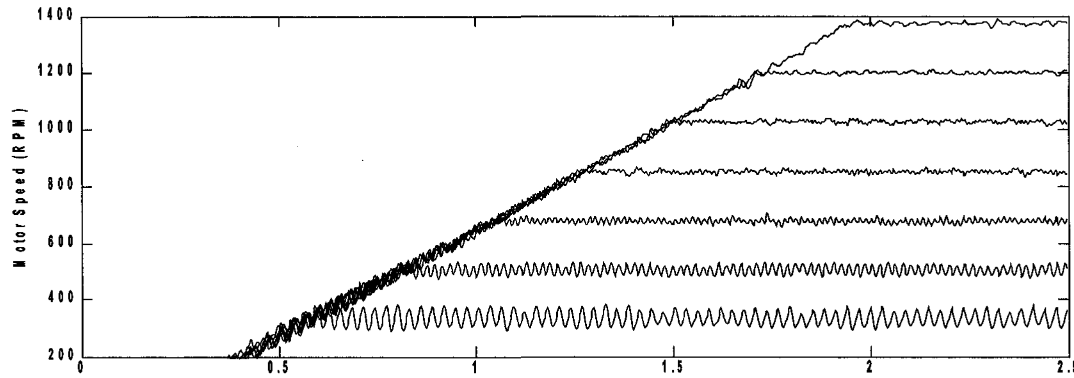

Figure 4.8: Braider head motor speed open-loop response for step commands between 1 and 8 volts. The acceleration is limited by the motor drive.

The open-loop speed response of the braider head and puller are shown in Figures 4.8 and 4.9, respectively. Motor speeds were obtained by differentiating position measurements at a rate of 400 Hz. Oscillations can be observed during both the transient and steady state portion of the response. It is suspected that these oscillations are caused by the motor and drive dynamics and not by measurement or differentiating noise. As the period associated with these fluctuations are short, it is assumed they will not affect the final braiding or pulling speeds.

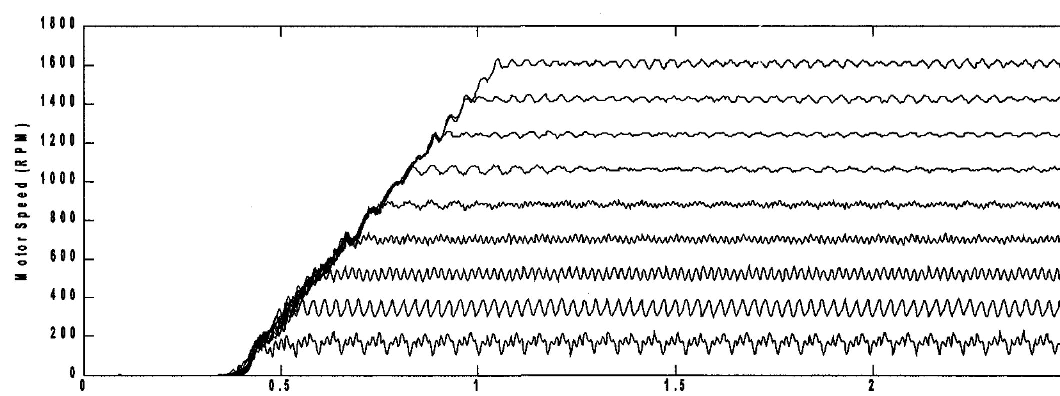

Figure 4.9: Puller motor speed open-loop response for step commands between 1 and 9 volts. The acceleration is limited by the motor drive.

It can be seen that the motor drives limit the motor acceleration. When accelerating synchronous motors, it is desirable to limit the lag between the rotor poles and rotating magnetic poles. It is the interaction between the two sets of poles that generates the motor's torque. If the lag between the poles becomes too large, the system may experience magnetic field slip and become unstable. For this reason, it is common practice to limit the acceleration of the motor. In this case, if the motor is subjected to loads smaller than the maximum torque, all changes in motor velocity occur at the limit set by the motor drive. To verify if the motor acceleration limit occurred for all initial and final set point values, the puller motor speed step responses from non-zero initial conditions were evaluated. Several responses are shown in Figure 4.10. It can be seen that regardless of the initial and final condition, the speed changes occur at a fixed acceleration. It is also interesting to observe that the command delay which was observed for step responses from zero initial condition (as shown in Figure 4.8) is not apparent for step changes which occur from non-zero initial conditions. It should be noted that for clarity, a moving average filter has been applied to the data of Figure 4.10.

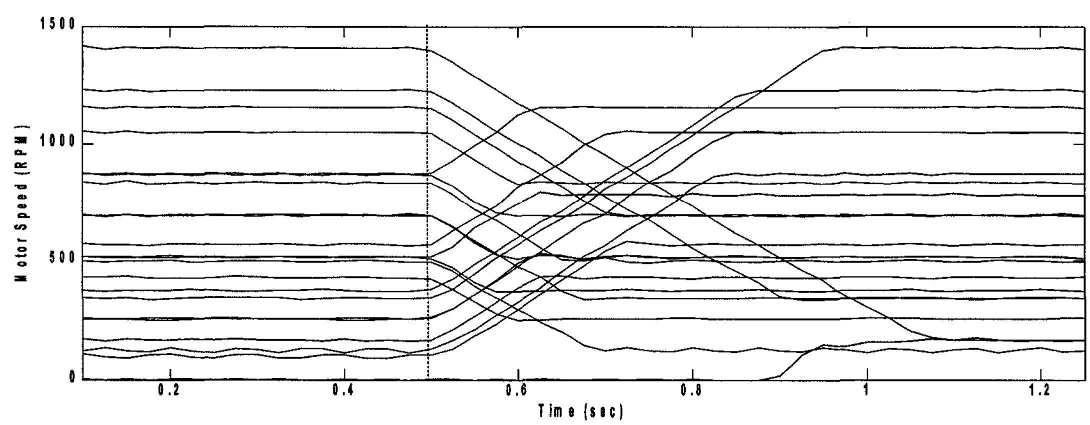

Figure 4.10: Puller step response to random step commands from non zero initial conditions. Step changes occurred at 0.5 sec as depicted by the vertical dotted line.

The relationship between the steady state motor speeds and the control signals are plotted in Figures 4.11 and 4.12 for the braider head and puller, respectively. Motor speed values were obtained by averaging the data between 1.1 and 2 seconds of Figures 4.8 and 4.9. The relationship is seen to be linear and the slope of the curve corresponds to the motor and driver system gains.

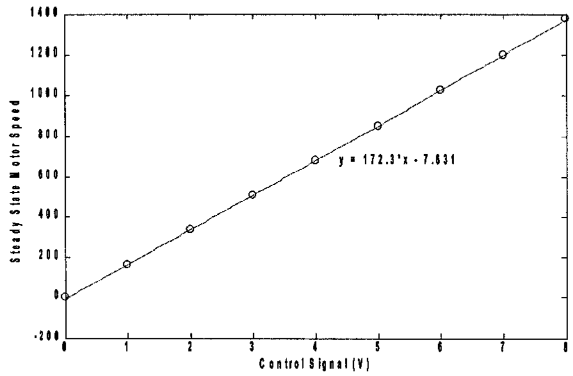

Figure 4.11: Braider Head steady state motor speed vs. control signal.

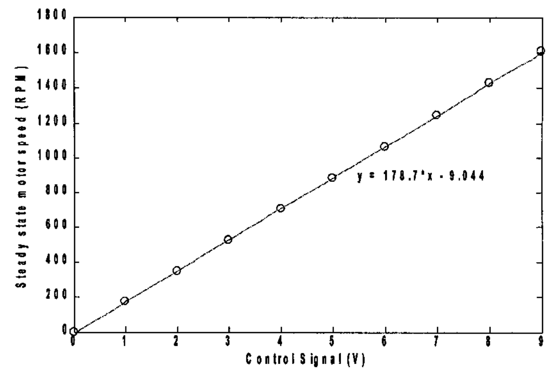

Figure 4.12: Puller steady state motor speed vs. control signal.

It is desirable to express the controlled variables in meaningful quantities. It was chosen to express the braiding speed in spool rotations per minute and the pulling speed in meters per minute. A spool rotation corresponds to the full revolution of a spool about the machine center. The ratio between motor revolution and desired quantities were evaluated. In both cases, the number of motor revolutions were counted using the motors' incremental encoders and a counter on the DAQ card. For the braider head, 30 revolutions of marked spool were counted and used to evaluate the ratio between the motor rotation and the spool rotation. For the puller, the initial and final positions of a pulled rod were used to calculate the ratio of motor rotation to pulling distance. The result of five tests were averaged. The ratios and the motor driver system gains enable the calculation of the overall process gain. The important process characteristics are presented in Tables 4.1 and 4.2 for the braider head and puller system, respectively.

All the system components step responses presented so far were obtained without external applied loads. Step tests were also conducted with constant and discontinuous external loads. In the first case, the load was provided by pulling the central rod fibres. The dead time, maximum acceleration and motor process gain were calculated. No significant changes in these properties were observed between the unloaded and loaded system. A discontinuous load was provided by placing a clamp on a pulled rod ahead of the puller. When the clamp reached the puller frame, the rod suddenly ceased to advance and the maximum load (corresponding to maximum friction force) is experienced by the puller. The data were visually inspected and no change in the velocity could be observed before and after the load discontinuity.

Tests where not performed for the braiding head while a braid was being formed. It is expected that the bulk of the braiding head motor load is due to friction between moving machine components and not the braiding action itself. Given the load response of the puller, it was assumed that the braider head would exhibit a similar disturbance rejection behaviour.

Table 4.1: Important characteristics of the braiding process

Characteristic	Value
Max motor acceleration	752.3 RPM/s
Control Signal / Steady State Motor Speed Gain	0.005804 V/RPM
Motor Encoder Resolution	500 count/rev
Motor Rot : Spool Rot	122:1
Encoder Speed Estimation Error	±0.118 spool RP< ±14.4 RPM
Control Signal (V) / Steady State Braiding Speed (spool rot/ min)	4.757e-4 V/RPM
Dead time from zero speed (IC=0)	0.4 sec
Dead time from non zero speed (IC≠0)	Approx 0 sec

Table 4.2: Important characteristics of the puller process

Characteristic	Value
Max motor acceleration	2345 RPM/s
Control Signal / Steady State Motor Speed Gain	0.005596 V/RPM
Motor Encoder Resolution	500 Count/rot.
Sheave Encoder Resolution	500 Count/rot.
Position Sensor Wheel Diameter	6.3 cm
Gear Box Ratio $1^{st} \times 2^{nd}$ =combined	5.53×60=331.8
Belt Pulley Diameter	0.1016 m
Motor rotation : pulling distance (calculated)	1039.5:1 rot/m
Motor rotation : pulling distance (Measured)	1044.2:1 rot/m
Encoder Speed Estimation Error	±0.014 m/min ±14.4 RPM
Control Signal / Pulling Speed	5.359e-6 (V/m/min)
Dead time from zero speed (IC=0)	0.4 sec
Dead time from non zero speed (IC≠0)	Approx 0 sec

4.6. Controller Design

4.6.1. Overview

In the previous section it was shown that both the braider head and the puller exhibit similar open-loop behaviour. Both processes are characterized by a constant acceleration and steady state speed that is proportional to the command signal.

Although the step response is composed of two linear segments, its transient behaviour cannot be modeled as a linear time invariant system. This makes the use of linear control design, such as pole placement, difficult to apply. Tuning techniques, which rely on 1st or 2nd order models with dead times, cannot be used since the effective open-loop time constant of both processes is not constant. Fortunately, the open-loop system demonstrates excellent transient and steady state properties. Clearly, since the open-loop acceleration of the system is limited, the closed-loop bandwidth cannot be increased. The open-loop bandwidth can therefore be considered optimal. Furthermore, due to its excellent disturbance rejection the open-loop system demonstrates low steady state error, therefore, open-loop control of the braiding and pulling processes may be satisfactory. Nevertheless, it is desirable to provide closed-loop control of the braiding and pulling processes. A feedback controller can compensate for inaccuracy or changes in calibration values. Furthermore, if the loads were to increase, due to an increase in the number of central rod fibres or redesign of the production process, it might be possible that the load disturbances would increase the steady state error.

The proposed controller (Figure 4.13) utilizes a set point element (B) and an integral trim controller (C) to regulate the pulling and braiding speed. To prevent overshoot a set point profilers (D) which provides trajectory generation is used.

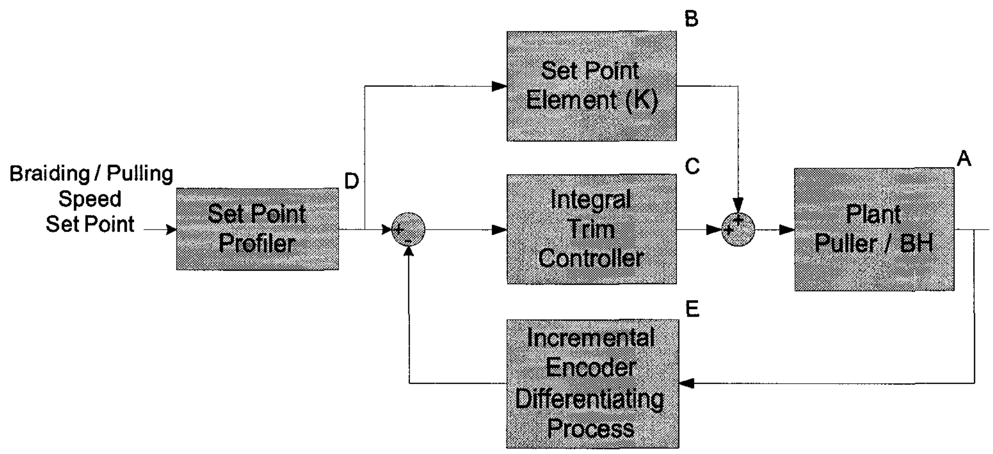

Figure 4.13: Braider head / puller control system schematic. The final controller is composed of a set point profiler, set point element and integral controller.

4.6.2.Controller without set profiler

The open-loop behaviour of the puller and braider head are well conditioned. A set point element consisting of the process gain can archive good set point tracking as long as the maximum rate of change is within the actuator limits, in which case, most of the control action can be provided by the set point element. The addition of pure integral control can be used to increase the steady state accuracy of the process. The step responses, using the set point element and integral controller with gains of 10 and 100, are shown in Figures 4.14 and 4.15.

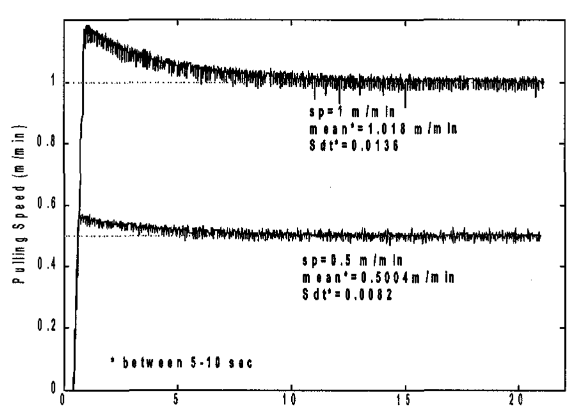

Figure 4.14: Puller step response with integral (*Ki*=10) and set point element.

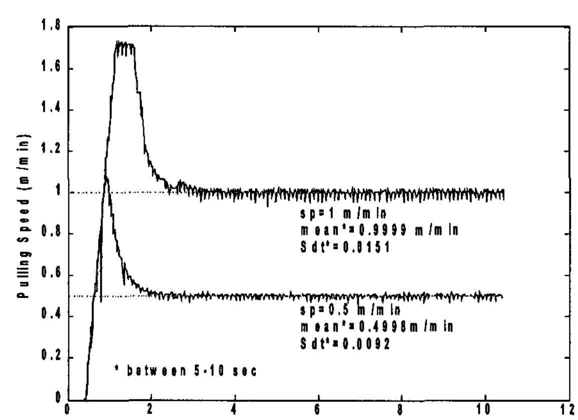

Figure 4.15: Puller step response with integral (*Ki*=100) and set point element.

The mean value is shown for each set point response. It can be seen that the steady state error using the set point element and coupled with the integral controller is very low.

The overshoot observed in Figures 4.14 and 4.15 are due to a gradual increase in the control signal resulting from the integral windup. This is caused by the system rise time and the input delay. This would be less likely to occur if the set point commands were to vary such that the motor acceleration limits were not exceeded.

4.6.3. Controller with Set Point Profiler

The set point profiler generates a series of set point commands for the braider head and puller motor drive. For discrete control systems, the desired set point values may be generated with time domain functions or difference equations. Time domain functions provide greater flexibility in the type of profile that can be produced but are often computationally expensive to execute in real time. Difference equations require fewer computations but require more design effort since the time domain properties must be translated into the discrete domain.

For the present case, a difference equation approach is used to generate a suitable set point profile. Two restrictions are placed on the input profile function. Firstly, the set point function must be such that the maximum actuator acceleration is not exceeded. Secondly, it is desirable that the initial acceleration be zero. Since it is desired to obtain a difference equation, the initial design consists of finding a transfer function that will result in the stated time domain properties. Several transfer functions can produce the desired properties, and were considered, namely two collocated real poles, two distinct real poles and two complex conjugate poles. Although the latter option allows faster step responses, it was found that a closed form solution to relate the pole locations to the maximum acceleration was difficult to obtain. Such a solution can be found for a transfer function with two collocated real poles. The chosen transfer function is given by:

$$\frac{V(s)}{U(s)} = \frac{\alpha^2}{(s+\alpha)^2} \tag{4.12}$$

The pole location that will produce a specific maximum acceleration when *U(s)* is a step input is found as follow:

The inverse Laplace transform of 4.12 is found for: $U(s)=1/s$:

$$V(s)=\frac{\alpha^2}{(s+\alpha)^2}\times\frac{U}{s}$$

$$\begin{aligned} L^{-1}\langle V(s)\rangle &= v(t) \\ &= u[1-(1+at)e^{-\alpha t}] \end{aligned} \qquad 4.13$$

$$where: U=(v_{current}-v_{setPoint})$$

The acceleration and jerk are obtained by differentiating the velocity and acceleration respectively as follows:

$$\begin{aligned} \frac{dv}{dt} &= a(t) \\ &= u\alpha[(1+\alpha t)e^{-\alpha t}-e^{-\alpha t}] \end{aligned} \qquad 4.14$$

$$\begin{aligned} \frac{da}{dt} &= j(t) \\ &= u\alpha^2[2e^{-\alpha t}-(1+\alpha t)e^{-\alpha t}] \end{aligned} \qquad 4.15$$

The time at which the maximum acceleration occurs is found by setting the above function to zero and solving to obtain:

$$\begin{aligned} j(t_{max}) &= 0 \\ t_{max} &= \frac{1}{\alpha} \end{aligned} \qquad 4.16$$

The maximum acceleration is found be substituting the time of max acceleration in the acceleration function to give:

$$\begin{aligned} a_{max} &= a(t=t_{max}) \\ &= u\alpha e^{-1} \end{aligned} \qquad 4.17$$

The pole location that results in a specified maximum acceleration is:

$$\alpha=\frac{a_{max}}{ue^{-1}} \qquad 4.18$$

The original profiler transfer function is expressed in the discrete domain in order to obtained the desired difference equation as follows:

$$G_{profiler}(s)=\frac{\alpha^2}{(s+\alpha)^2}$$

$$G_{profiler}(z)=\frac{\alpha^2(T^2 e^{-aT} z^{-1})}{(1-e^{-aT} z^{-1})} \qquad 4.19$$

where T is the sampling time

From the $G_{profile}(z)$, the difference equation is found as follows:

$$c(k)=a_1 c(k-1)+a_2 c(k-2)+b_1 u(k-1)$$

$$\text{where } a_1=2e^{-\alpha T} \qquad 4.20$$

$$a_2=-e^{-2\alpha T}$$

$$b_1=T^2\alpha^2 e^{-\alpha T}$$

The resulting second order infinite impulse filter is used as the set point profiler. The calculation of the set point involves three floating point multiplications and two additions. This is far less than the number of operations that would be required to evaluate the exponential function if the closed form solution of $G_{profile}(z)$ was to be used.

It can be seen from Equation 4.18 that the desired pole location is a function of the amplitude of the step command. The pole location can be calculated a-priori using the largest step command corresponding to the motor maximum speed. This implies that the process will exhibit a constant effective time constant, regardless of the amplitude of the set point change. Alternatively, the pole locations may be calculated each time a set point change is executed. This involves finding the pole location using the actual amplitude of the set point change and then recalculating the filter constants of Equation 4.20. This methodology allows an optimum settling time for any set point changes. In the current control system, the latter option is implemented.

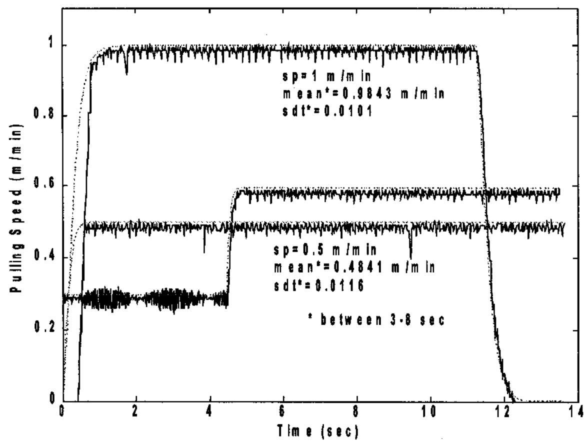

Figure 4.16: Open-loop puller speed step response with set point profiler set to 95% of max acceleration. Integral gain set to *Ki*=0.

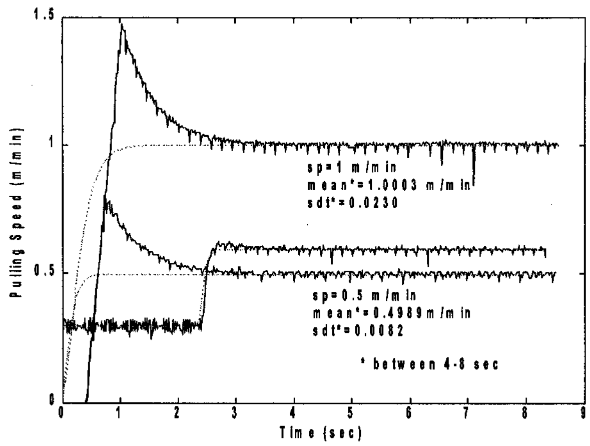

Figure 4.17:Closed-loop puller speed step response with set point profiler set to 95% of max acceleration. Integral gain set to *Ki*=100.

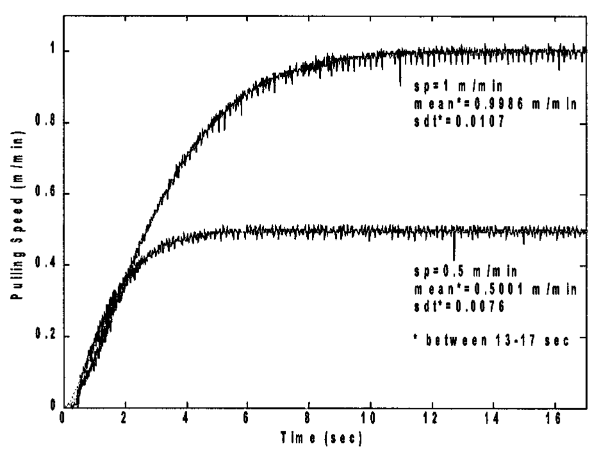

Figure 4.18: Closed-loop puller speed step response with set point profiler set to 10% of max acceleration. Integral gain set to *Ki*=100.

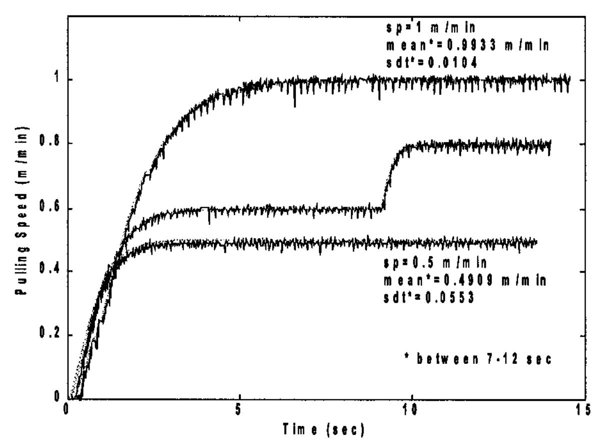

Figure 4.19: Closed-loop puller speed step response with set point profiler set to 20% of max acceleration. Integral gain set to *Ki*=2.

The open-loop response with set point profiler (corresponding to an integral gain of 0) is shown in Figure 4.16. From this figure, it can be noted that the open-loop response demonstrates larger steady state error than the closed-loop response.

In Figure 4.17 it can be seen that the input delay that occurs for set point changes from zero initial speed prevents adequate set point tracking even if the maximum acceleration is not exceeded. From the same figure, it can be observed that when the initial speed is not zero and the input delay is considerably shorter, good set point tracking is achieved.

As shown in Figures 4.18 and 4.19, a simple solution to reduce the overshoot without reducing the feedback gain is to reduce the maximum allowable acceleration. Doing so produces a small initial set point which prevents large integrator windup and thus overshoot. Although perfect set point tracking is not achieved at the beginning of the trajectory, the behaviours are satisfactory.

From a production stand point, slower acceleration at start up is beneficial as it reduces the likelihood of slip between the belt and rod and may prevent strand rupture which may occur due to a suddenly applied load. In general, the use of the set point profiler to regulate the puller and braider head ramp up speed is advantageous. As previously stated, the braiding action is characterized by a transient period. During this period, the braid pattern changes and does not produce the desired braid angle. Allowing fast braider acceleration and slow puller acceleration could conceivably reduce the braid formation transients. This would reduce the waste associated with production start up or a set point change. Although this may be negligible for long production lengths, it would be beneficial for shorter production lengths.

Tuning of the integral gain was done by a trial and error approach. It was found that the system became oscillatory for pulling process gain values larger than 750. From the step response curves in Figures 4.14 to 4.17 it can be observed that increasing the integral gain reduces the steady state error. As the gain is increased, the reduction in steady state error becomes negligible. Noting that a high gain value reduced the stability of the system, it is preferable to keep the gain below 100.

It is suspected that the fluctuations which can be seen about the set point are in fact the oscillations that were observed in the open-loop motor tests (Figure 4.6). Their appearance differs due to the lower sampling rate of the control system. This hypothesis is supported by the appearance of an anti-aliasing pattern of the 0.3 m/min set point of Figure 4.16. Comparing the steady state standard deviation of each set point it can also be observed that fluctuations are consistently larger for the 0.5 m/min set point compared to the 1 m/min set point. This is similar to the behaviour observed from the open-loop tests where the oscillation amplitude decreases as the control signal increases.

It was observed that regardless of the gain value, the standard deviation and thus the fluctuation about the set point are approximately the same. This is not surprising since the oscillations are under sampled for control purposes. Nevertheless, since the fluctuations are very rapid and occur about a central mean it is unlikely that they will affect the pulling process.

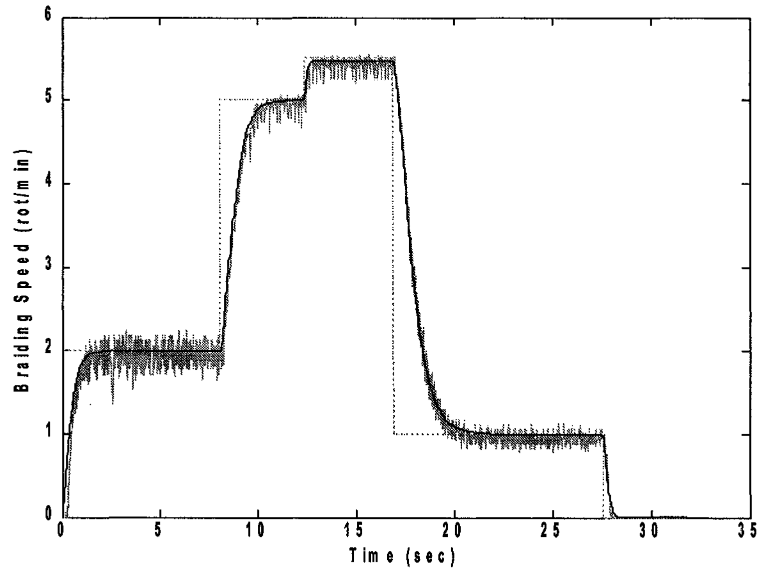

Figure 4.20: Braider head closed-loop response with set point profiler *Ki*=50, Max acceleration is set to 50%.

The closed-loop behaviour of the braiding head is similar to the behaviour of the puller. The response to various step commands with the designed set point profiler is shown in Figure 4.20.

5 Fibre Sorting and Impregnation System

5.1.Overview

Prior to the deposition of the 2D braid, the carbon strands that form the center of the braided product must impregnated with resin (Figure 3.2). These strands are stored on a storage frame. Guide eyes and a guide plate allows the strand to be fed into the impregnation ring. Fibre impregnation is accomplished using a pressure-fed coated steel ring. Resin, supplied by peristaltic pumps, flows through several small holes located in the ring's inner radius. Strands are aligned such that they follow the inner radius and are thus impregnated.

The dispensing process is sensitive to several parameters such as up and down stream pressure, fluid viscosity and tube properties such as diameter, material and compliance. The effect of each of these parameters on the dispensing rate is difficult to evaluate theoretically. For these reasons, calibration curves can be automatically generated using weight measurement of the resin reservoir for later use. These are obtained using a balance connected to the control computer. A feed-forward/feedback controller is used to regulate the dispensing rate during production. On-line flow estimates are obtained from weight measurements of the resin reservoir using a data validation and a robust fitting algorithm.

Prior to this work several production issues related to fibre sorting and resin impregnation limited the quality of the final product. For example, fibre damage was often observed due to inadequate strand management. Furthermore, no means were developed to measure the dispensing rate. Pump operations were manually regulated based on observation of the wet fibre strands. This often resulted in under- or over-impregnation.

5.2. Physical System

5.2.1. Fibre Sorting System

The fibre sorting system is composed of the fibre storage frame, the spool tensioners, guide eyes and the guide plate as shown schematically in Figure 5.1.

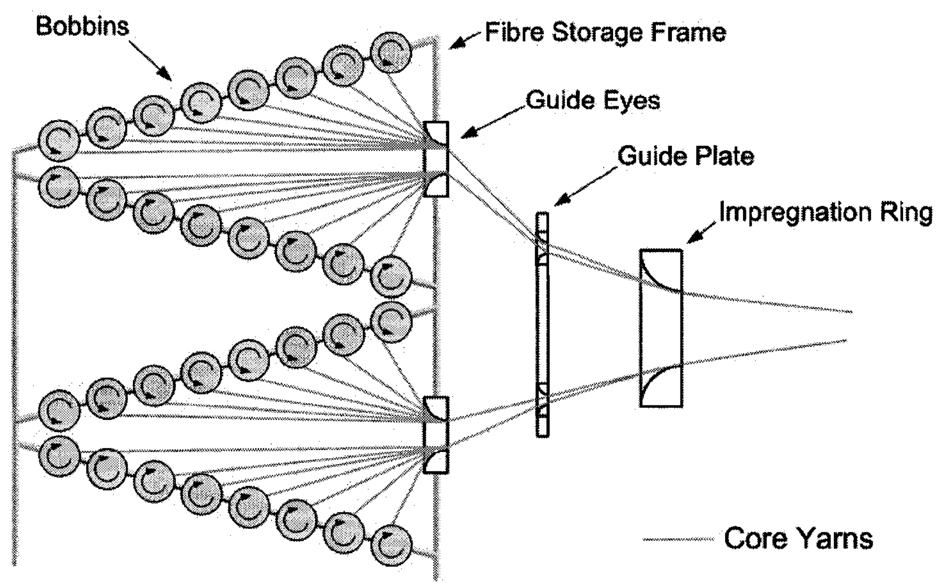

Figure 5.1: Fibre sorting equipment:fibre storage frame, spool, guide eyes, guide plate and impregnation ring .

The goal of the sorting system is to store the central strand spools and to feed the strands into the impregnation ring. In order to be properly impregnated, strands must enter the impregnation ring evenly spaced circumferentially and follow the inner radius of the impregnation ring. Although the parts of the fibre sorting system are mechanically simple their proper functioning is essential for a successful production. The current rod design utilizes high modulus carbon fibres as the central rod material. These fibres are very brittle and subject to severe damage if not handled carefully. Although there are no accepted measurements of brittleness for bulk fibres, it can be assumed that individual fibres fail due to localized bending. For this reason, the maximum strain may be used as an indicator of the brittleness and wear resistance of the fibres. For example, Kevlar 49 (® DuPont), which is used in applications that demand wear resistance and damage tolerance demonstrates a maximum strain of 2.4 % [39]. In contrast, the carbon fibre which is currently in use (TohoTenax G50-500) has a maximum strain of 0.92%[40].

During preliminary testing and initial production it was observed that the existing sorting apparatus caused severe fibre damage. In order to avoid this damage a new sorting system was designed to minimize contact with the fibres. More specifically transverse, fibre to fibre contact is completely eliminated. When contact between the fibres and other materials are necessary, low friction surfaces are used.

Figure 5.2: Damaged (top) and undamaged (bottom) high modulus carbon fibre strands.

An example of damaged and undamaged strands are shown in Figure 5.2. The top strand was damaged by transverse contact with another carbon strand. Similar fibre damage was observed due to rubbing of strands on the creel frame. Frayed strands cause significant problems during production. Loose carbon fibres tend to accumulate in guides and in the impregnation ring causing further fraying and hindering impregnation. Furthermore, air-borne, carbon fibre particles are a health hazard and can cause damage to electronic equipment since they are conductive. In extreme cases, entire strands may rupture, causing entanglement with other strands or spools and necessitating a halt in production. Ultimately, damaged strands affect the final product quality and mechanical properties.

During production, the carbon strands are unwound from the spools and travel through the sorting system and into the impregnation ring. The new spools and storage frame are shown in Figure 5.3. The original and the new frames were designed and fabricated in-house. The original frame had a capacity of 110 spools. As this was not sufficient to produce a rod with a 10 to12 mm fibre core, some spools were double wound. Damage due to fibre to fibre contact was especially severe for these strands. In phase 1 of this project, modifications were made to increase the frame's capacity by extending the creel rods and redesigning the spools to make them shorter in length but with a larger diameter. As part of this work, individual tensioning mechanisms were added for each spool and the frame was configured to better handle the carbon strands.

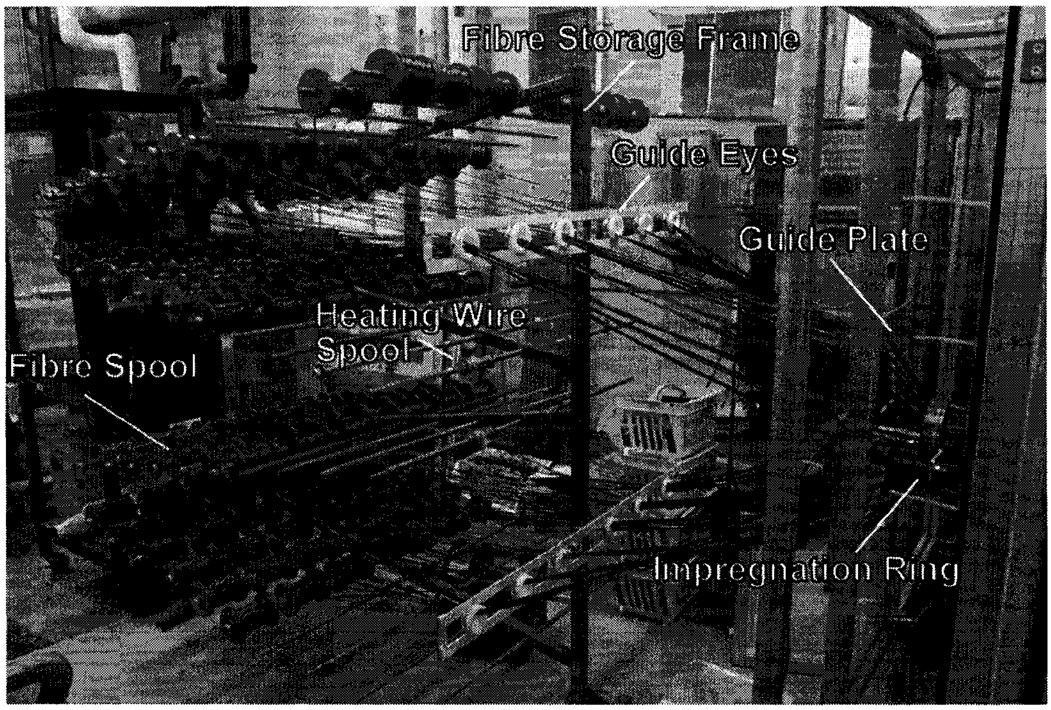

Figure 5.3:Sorting system.

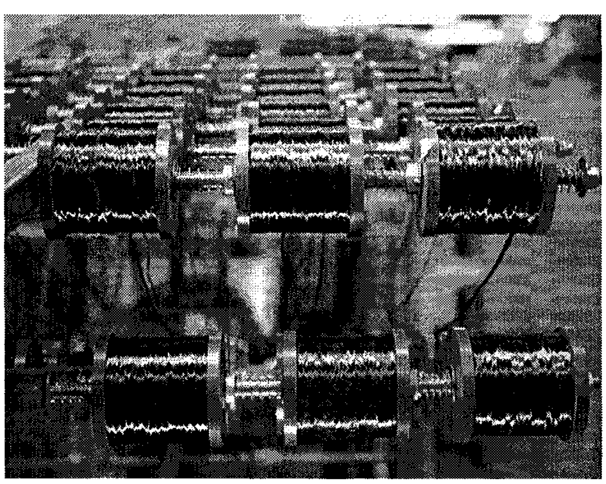

Figure 5.4: Carbon fibre spool and tensioning system.

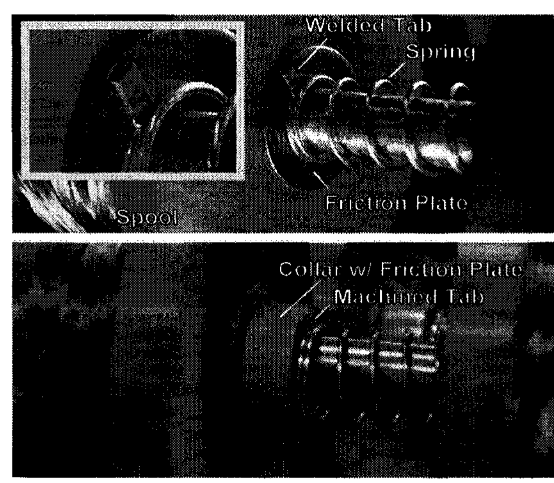

Figure 5.5: Spools, spring and friction plate (top), spring, collar with friction plate (bottom).

Originally the spools were tensioned in groups of two or three. This system was not ideal as it was common to have one strand in a group properly tensioned while the others were not. This led to significant entanglement and consequently damaged fibres.

Furthermore, improperly tensioned strands did not contact the impregnation ring correctly. This led to improper impregnation. Due to the large number of spools, it was important that the new tensioning system be simple to fabricate and assemble. The new tensioning system utilizes coil springs and steel friction disks to generate a frictional torque on the face of each spool (Figure 5.4). A detailed view of the tensioning components is shown in Figure 5.5. Standard flat washers are used as the friction disks. To prevent rotation between the spring and the friction disk, the end of the spring wire rests on a small sheet-metal tab which is welded to the washer. Shaft collars with machined tabs on one side and welded washers on the other are used to isolate each spool from the others in the same group. The shaft collars are fixed to the creel rods using set screws. The parts of the tensioning system are installed in two different configurations which are dependent on the direction of rotation of a spool group.

The resin curing method discussed in this work involves the placement of steel wires in the central core fibres. The curing process is discussed in detail in Chapter 6. The steel wires are stored on the fibre storage frame on small aluminum spools. Presently, six heating wires are fed in the central fibres through eyes of the guide plate. Recommendation relating to the placement of the wires are made in Chapter 8.

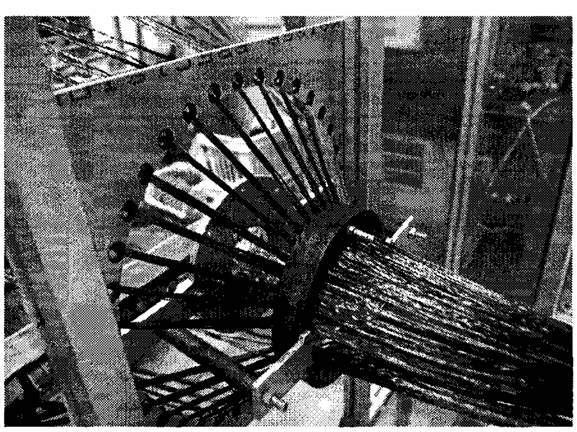

Figure 5.6: Guide plate and impregnation ring.

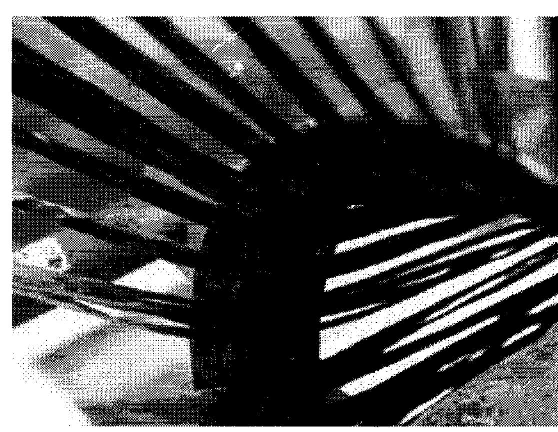

Figure 5.7: Carbon strand as the pass inside the impregnation ring.

Modifications were also made to reduce contact with the strands. Several design options were considered and investigated. The final solution was the addition of guide eyes and a guide plate. As shown in Figure 5.3, two bars support twelve guide eyes. The eyes allow each fibre to exit the fibre storage frame perpendicularly to the spool. This insures that fibres to not rub on the spool wall or frame. Since the fibres are always perpendicular to their respective spools this also guaranties that strands do not cross each other. This significantly reduced the likelihood of fibre damage. As shown in Figure 5.6, the guide plate is equipped with 30 small guide eyes. The eyes distribute the strands evenly around the circumference of the impregnation ring. As shown in Figure 5.7, positioning the impregnation ring at a specific distance from the guide plate insures that the fibres always enter the impregnation ring at the correct angle.

Guide components (eyes, hooks, etc.) specifically designed for handling brittle ceramic fibres are commercially available from several vendors. These components are usually composed of machined and polished steel parts coated with a proprietary ceramic compound. These parts are commonly used in application where line speeds are high. The maximum line speed of the pilot plant is 1.5 m/min. Therefore, the current application does not warrant the use of such products. Qualitative tests were done to evaluate what material would be better suited for the guide eyes. Carbon strands were repetitively rubbed on several stock rounds of aluminum, Teflon®, ABS, and Delrin®. The frictional resistance and fibre abrasion was compared and used as a basis for material selection. Teflon and Delrin were found to be similar in performance. Due to its low hardness, it was felt that Teflon might be more susceptible to wear over time, therefore Delrin was chosen. To obtain low surface roughness, the eyes were machined using high spindle speeds and very low feed rates.

Following the modification described above, no appreciable fibre damage was observed.

5.2.2. Impregnation Ring

The impregnation ring (Figure 5.8 and 5.9) deposits resin on the fibre strands. The impregnated strands form the central rod core of the braided product. The impregnation ring has been designed and fabricated in-house. It consists of a silicone treated steel ring and a flange disk. Resin is fed under pressure and flows through an internal channel machined in the ring. Small holes distributed along the circumference of the ring deliver resin from the inner channel to the exterior radius of the ring. A small groove machined in the interior surface of the ring helps to distribute the resin along its circumference. Impregnation is accomplished by capillary action of the fibres as they contact the wet inner radius of the impregnation ring.

Figure 5.8: Front view of impregnation ring. The fibres are impregnated as they pass over the inner radius.

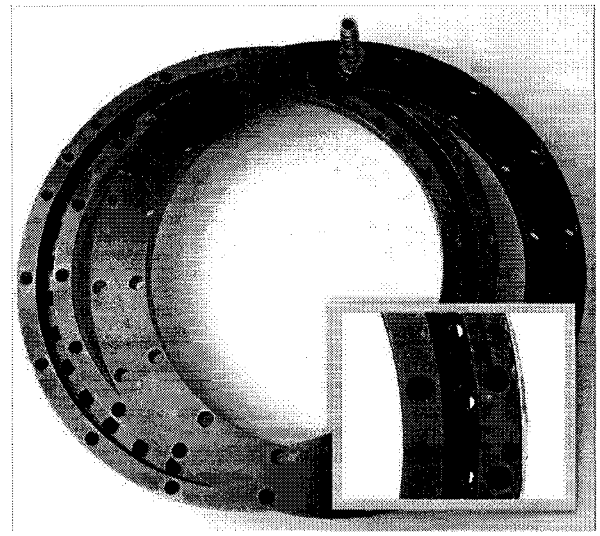

Figure 5.9: Back view of the impregnation ring. The internal plenum and drilled passaged are shown.

Following initial testing of the ring, it was observed that resin flowed considerably more from holes located in the lower half of the ring than the ones located in the top half. This resulted in little or no resin being delivered to the fibres entering the top half of the ring and over-impregnation of the lower fibres. It was realized that the size of the holes between the internal channel and exterior radius, did not allow for sufficient pressure to develop inside the ring so as to fill the entire internal channel. This is attributed to the static head created by the difference in height between the top and bottom of the ring. For the ring to function properly, the flow created by the pressure differential caused by the height difference must be negligible compared to the total desired flow rate. To correct this problem it is necessary for the delivery pressure to be several times that of the pressure differential caused by the liquid column inside the ring. One way to achieve this would have been to drill smaller holes in the impregnation ring. However, there is a practical size limitation of the holes that can be drilled into steel. A more feasible solution is to insert small plastic tubes into drilled holes to reduce the effective hole diameter. Inserting these tubes is a time consuming process which must be repeated prior to each production run. An alternative solution is to place a filter medium between the internal channels and the drilled holes.

Changing the number of filter layers allows for changes in the flow restriction. It was found that cellulose fibre sheet makes a suitable filter medium. The number of filter layers can be adjusted based on the resin viscosity and target flow rate. For the current production, three layers were found to provide adequate flow restriction.

5.2.3. Resin Heating System

As the impregnation ring deposits the resin on the surface of the strands, the capillary effect wicks the resin inside the strand until it is fully impregnated. In this case, the capillary forces are created by the small opening between the individual fibre filaments. The opening creates a discontinuous pressure gradient in the resin. Resin flow occurs until the pressure gradient and surface tension forces are in equilibrium or until the pressure gradient is nullified. The speed of transport in a capillary process is characterized by the ratio of surface tension forces and viscous forces within the resin. This ratio is usually expressed as a dimensionless parameter called the Capillary Number. Large Capillary Numbers lead to higher transport speeds. The surface tension forces are influenced by the nature of the fibre strand which is in turn influenced by several factors, such as the diameters, number , spacing, and surface roughness of the fibre filaments. These properties influence the wettability of a fibre. The viscous forces are a function of the fluid viscosity only.

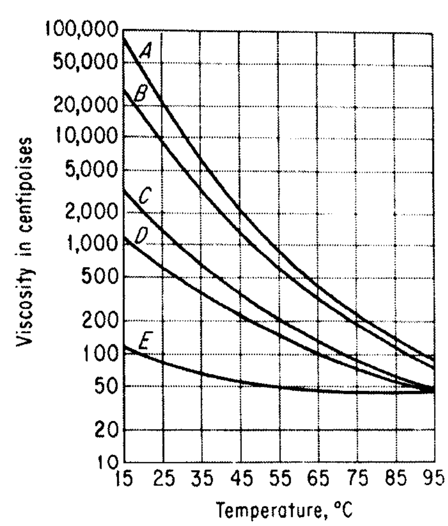

A:Epoxidized phemol-formaldehy novolac

B:DGEBA

C:3,4-epoxy-6-methylcyclohexamethyl-3,4-epoxy-6-methylcyclohexane carboxylate

D: diglycidyl ester of linoleic acid

E: DGE polypropylene glycol

Figure 5.10: Viscosity of various epoxy resins vs. temperature [41].

It is desirable to impregnate the fibre as quickly as possible. The wetability of the strand is difficult to control. The impregnation speed can be increased by decreasing the viscosity of the resin. At room temperature the resin is very viscous (similar to honey). As depicted in Figure 5.10, the viscosity of epoxy resin is reduced exponentially as its temperature increases until it reaches its gel state. By heating the resin, the impregnation speed can be increased considerably. Preheating the resin also has the potential benefit of improving the curing speed.

Several methods were investigated to increase the resin temperature. One method, which appeared simple when first considered, was to construct a simple heat exchanger. Approximately one meter of tubing was immersed in a heated water bath. The tube diameter was chosen such that the resin would circulate in the heat exchanger for several minutes before being fed to the impregnation ring. Unfortunately, it was found that resin would eventually harden on the interior surface of the tube, significantly changing the pumping process dynamics and would eventually completely block the tube. Furthermore several minutes were required for the impregnation ring temperature to reach a steady state temperature. Because of this, it was difficult to evaluate the appropriate filter medium to achieve a distributed flow (as described in the previous section).

A second method, which was considered but not implemented, would be to increase the impregnation ring temperature by means of an electric band heater or similar system. Since the ring is now heating the resin, this method has the advantage of reducing the transient temperature effects as described in the previous method. As with the previous method, it was felt that possible resin hardening could occur in the ring's internal channel. This would eventually create a blockage.

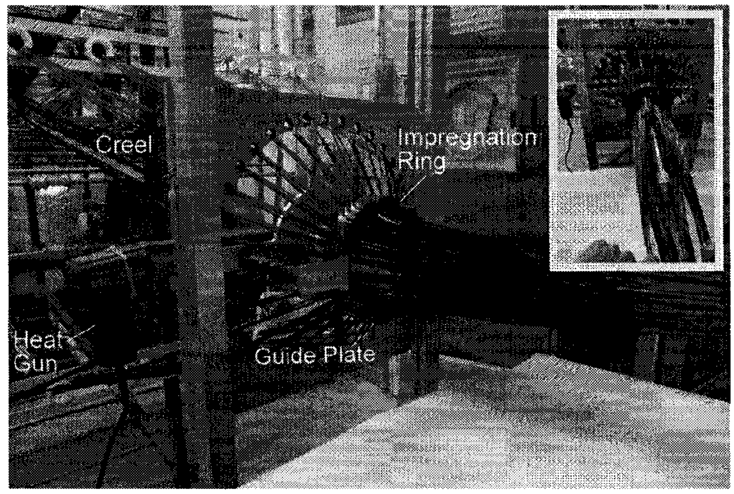

Figure 5.11: Detail of resin heating system. Top insert show the hot air delivery tube.

Figure 5.11 shows the approach that was selected and is currently in use. In this approach a variable power heat gun is used to increase the fibre and resin temperature as they exit the ring and are collected to form a cone. A steel pipe delivers air from the heat gun inside the narrower portion of this cone. The temperature inside the cone is monitored using a thermo-couple, and the heat gun power is set manually to achieve the desired set-po,t temperature. Unlike the previously discussed methods, the resin temperature is not increased through contact with a heated surface. The resin buildup and blockage of internal flow is therefore avoided.

Observation during production runs showed that this method significantly increased the speed of impregnation and allowed for an even resin distribution throughout the rod. Figures 5.12 to 5.14 show three rod cross sections. Figure 5.12 and 5.13 show specimens that were manufactured prior to the impregnation system modifications, while Figure 5.14 shows a specimen that has been manufactured using the improved system. The implementation of the resin heating system significantly reduces the occurrence of non-impregnated occlusions (Figure 5.12), while the addition of the filter medium in the impregnation ring eliminates the undesirable effect of impregnation of only the bottom portion of the rod (Figure 5.13).

Figure 5.12: Rod cross section with voids.

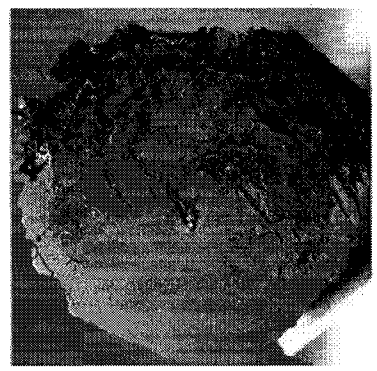

Figure 5.13: Rod cross section which is only half impregnated.

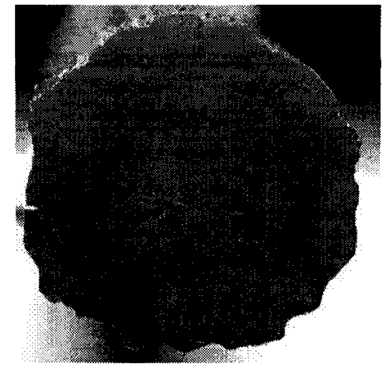

Figure 5.14: Cross Section of fully impregnated rod.

5.2.4.Pumps

Resin is supplied to the impregnation ring using peristaltic pumps. Peristalsis transport relies on successive sinusoidal contraction and expansion along a tubular chamber to convey a fluid or slurry. The phenomenon is extensively studied in biology[42][43][44] due to its importance in the digestive (esophagus, intestines, colon), urinary (ureter) and circulatory systems. The phenomenon can also be exploited for transport of fluid on the microliter scale in MEMS[45]. In an industrial context, peristaltic pumps utilize a flexible tube as the pumping element. In most cases, a rotor with several rollers imparts a successive and periodic compressive action on the tube, while the stiffness of the tube provides the expansion action required for peristalsis transport. As opposed to other common positive displacement pumps, peristaltic pumps do not require shaft seals or valves. For these pumps, only the tube is in contact with the pumped fluid. This has made them very popular in the pharmaceutical, laboratory and food industry. As stated by Pump World magazine [46], acceptance in other industrial sectors has been mainly driven by the advent of new high performance tubing, which can operate at increasingly high temperatures and pressures. In the present project, peristaltic pumps are used due to their ability to pump high viscosity fluids and the ease of cleaning after a production run.

The pumps currently in use are Masterflex Economy Drives (motor, gear box, motor drive) equipped with Masterflex Easy Load II peristaltic heads. The head accepts peristaltic tubing with a diameter range between 4 and 11 mm. The original pump-drive did not allow the use of an external signal to control the rotor speed. Modifications were made to the motor controller to accept control from an external voltage source. In order to isolate the high voltage motor supply system, an input signal and an optical isolator were used. This component renders the control signal to motor speed relationship highly non-linear and inverted (ie. 0V full speed, 10 V off). This problem was addressed in the controller design. When the control software is turned off all analog control lines are at 0V. For the pump, 0V corresponds to the maximum rotor speed. A relay connected to the control system is used to interrupt the pump's 120 V supply when it is not in use.

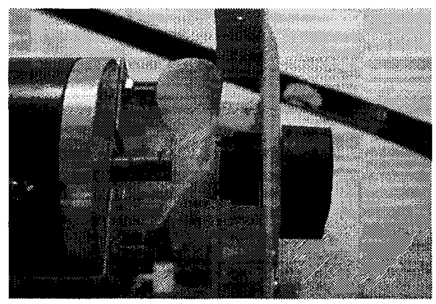

Figure 5.15: Incremental encoder mounted to pump using simple flexible coupling.

A 500 count/rotation incremental encoder is used to monitor the pump motor speed (Figure 5.15). A coupling composed of a plastic disk and roll pins compensates for angular misalignment between the motor and encoder shafts. The pump speed is estimated from encoder measurements using method 1 of pseudo hardware differentiation (section 4.4.4.4). A 500 count encoder is used For a given speed, this increased the encoder count by a factor of 16.5.

5.2.5.Resin Flow Measurement Devices

In order to ensure accurate resin dispensing, measurements of the resin flow supplied to the impregnation ring are required. The dispensing controller utilizes flow measurements in one of two ways, namely off-line and on-line. Off-line measurements are used prior to production to generate a calibration curve of flow rate vs. rotor speed. On-line weight measurements are used during production to estimate the resin flow rate.

Several flow measurement devices were considered. The selection criteria were flow range, accuracy, ease of cleaning, pressure drop and cost. Several devices were not considered due to their inability to handle high viscosity fluids. These include turbines, paddle wheels, and differential pressure flow meters. Several factors such as the crystallization of resin content and temperature changes can affect resin viscosity. Therefore, measurement devices such as variable area rotometers which are sensitive to changes in fluid viscosity were not considered.

The current product design requires a dispensing rate of 60 ml/m at a line speed of 0.5 m/min which results in a nominal flow rate of 30 ml/min. Future product design may require flow rates of up to 120 ml/min at 1.5 m/min. The ideal measurable flow range would therefore be between 20 to 150 ml/min or 24 to 180 g/min (for a resin density of 1.2 g/ml).

The dispensing accuracy (ml/m) is affected by both the pumping process and the pulling process. In chapter 3 it was shown that the measurement accuracy of the pulling process is ±0.014 m/min. For a dispensing rate of 60 ml/m, this leads to a maximum flow rate accuracy of 0.84 ml/min, or 1 g/min. A device with accuracy greater than this value is therefore not required.

The nature of the epoxy warrants a flow measurement device which is easy to clean. Minimizing contact with any surface greatly simplifies post-production cleaning. If cleaning is required, it is important to select a device with materials that are compatible with organic solvents such as acetone.

Given these restriction four flow measurement devices where considered. Those considered included a Coriolis mass flow meter, oval gear flow meter, vertical float and a weight balance.

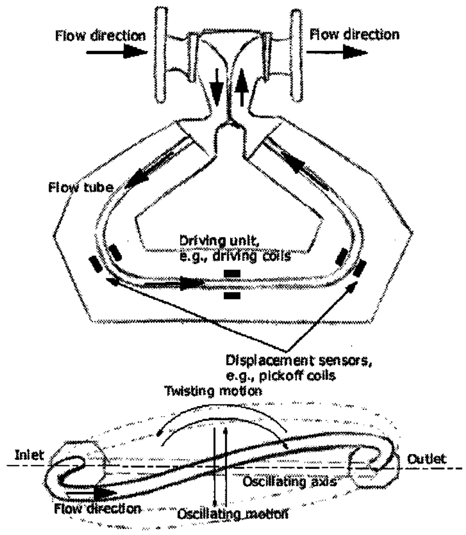

Figure 5.16: Schematic of Coriolis mass flow meter (top view and front view) [47].

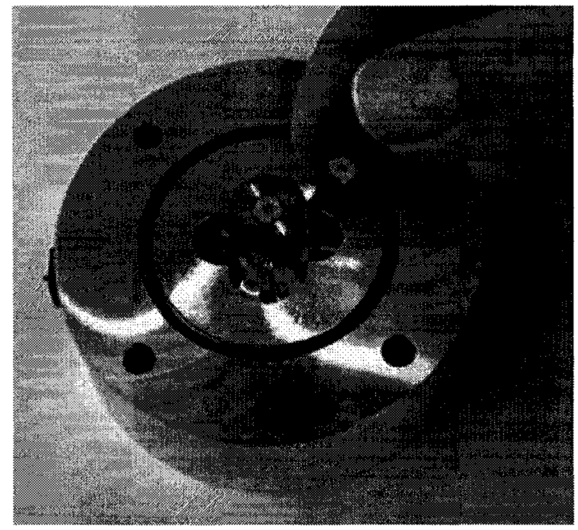

Figure 5.17: Flomec oval gear flow meter [48].

A Coriolis meter (Figure 5.16) utilizes a flexible tube element which is rotated by an electromotive force. As it rotates, the fluid applies Coriolis inertial forces and causes the tube to deflect perpendicularly to the imposed rotation. The magnitude of the deflection is a function of both the fluid velocity and density. From the measured tube deflection, the mass flow rate can be inferred. On the other hand, the operating principal of the gear flow meter (Figure 5.17) is similar to a positive displacement gear pump. As the fluid circulates, the geared rotors are forced to rotate at a speed proportional to the flow rate. Both the Coriolis and geared flow meters are suitable for high viscosity fluids and give a direct measurement of flow rate that is suitable for on-line control. The measurement range can be very low: 6 g/ min and 8 ml/min with a quoted accuracy of ± 0.1% (±0.36g @ 36 g/min) and ± 1% (±0.3 ml @ 30 ml/min) for the readings using Coriolis [49] and gear [50] meter respectively. Both devices could prove difficult to clean. The cost of low-flow Coriolis flow meters ranges between $5000 and $7500 while low-flow gear flow meters range between $750 to $1250. The main advantage of both devices is their short measurement time constant. Flow pulsation created by the pumping action would introduce a considerable amount of process noise in flow measurements. Fast sampling and signal filtering would allow one to obtain adequate measurements, but at the expense of the measurement response. The use of an inlet filter is also recommended for these devices. It was feared that the pressure drop across the filter and measurement device combined with the required supply pressure would be too great for the peristaltic tubing, which has a maximum pressure rating of 30 psig. Tubing with higher maximum pressures is available but it cannot convey very viscous fluids, such as the resin. The peristaltic pump head is limited at a maximum pressure of 80 psig. Following a discussion with the gear flow meter supplier, it was determined that the peristaltic pump could not produce sufficient pressures. For this reason the use of both devices was rejected.

A device capable of measuring the height of the epoxy reservoir was also considered. This device would utilize a float constrained in the vertical direction and a linear displacement sensor such as an LVDT or linear encoder. The maximum resolution of this method would be the function of the cross sectional area of the reservoir and the resolution of the displacement sensor. Decreasing the area of the reservoir would increase the resolution but would also require a larger linear measurement range for a given reservoir capacity. Given a cylindrical reservoir with a diameter of 20 cm and a displacement sensor accuracy of 0.1mm, a maximum volumetric accuracy of 3.1 ml would be achievable. Using a two point difference to estimate the flow rate would require a measurement period of 3.69 minutes to achieve the desired measurement accuracy of 0.84 ml/min. Furthermore, epoxy could easily contaminate the sensor and cleaning of the float would be required.

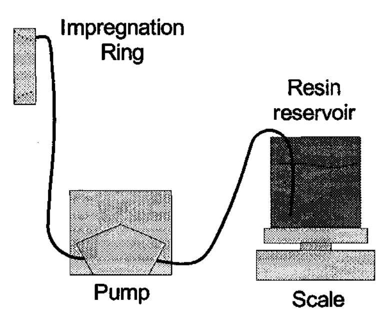

Figure 5.18: Equipment configuration used to estimate resin flow rate.

Successive weight measurement of the resin reservoir to estimate resin flow rate was considered and finally adopted. As depicted in Figure 5.18, the method involves collecting weight measurements at specific time intervals. Numerical differentiation is then used to obtain resin flow rate estimates. Since no part of the scale is in contact with the resin, no supplementary cleaning is required. The equipment cost of this method is also considerably less than the Coriolis and gear flow meters. Scales of this type with features such as computer serial interface, 6 kg capacity and a resolution of 0.1g can be purchased between $200 and $500. Dispensed resin weight and rod displacement measurements provided by the puller sheave sensor can be used to calculate the fibre volume fraction of a product. The weight measurements can also be used to notify the production personnel when resin reservoirs levels are low.

A capacity of 6 kg allows the production of approximately 83 m of rod (assuming 60 ml/m and resin density of 1.2 g/ml). If longer production runs are required resin may be periodically added to the reservoir. In this case, flow estimation would be halted until the new resin is added and the scale reading stabilizes. The differentiating algorithm and associated errors will vary if flow rate estimates are required for calibration purposes or for control purposes. These are discussed in Section 5.4.1.

5.3. Resin Dispensing Process

The mechanical properties of any fibre reinforced composites are greatly affected by the ratio of fibre reinforcement to matrix material. Since the matrix contributes little to the overall strength and modulus of the product when a composite rod is loaded in longitudinal tension, the effect of an incorrect quantity of resin will affect primarily the specific weight. Most importantly, the heat required to cure the rod is proportional to the quantity of resin. Incorrect resin dispensing can lead to under or over-curing of the polymer matrix, therefore it is important to supply the impregnation ring with the correct resin flow rate.

The dispensing process was decoupled into two distinct processes the pump rotor speed process and the pumping process. These are discussed in the following sections. The input and output of the pump rotor speed process are the external control signal and the pump rotor speed respectively. The input and output of the pumping process are the pump rotor speed and flow rate respectively. The resin flow estimating method inherently introduces a time-lag in the dispensing process, and therefore it must be considered as part of the analysis.

5.3.1. Pump Rotor Speed Process

The dynamics of the pump motor and driver must be considered and addressed in the dispensing control system. If the pump rotor speed is not maintained about a constant speed, the dispensing rate will fluctuate.

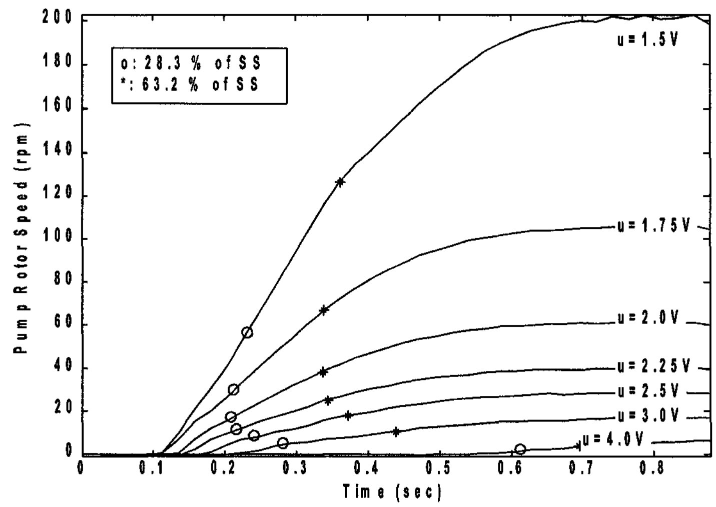

Figure 5.19: Pump rotor speed open-loop response from zero initial condition and no load. The input signal for each step response is shown on the right hand side of each curve. Points corresponding to 28.3 % and 63.2 % of the final values are identified as "o" and "+" respectively.

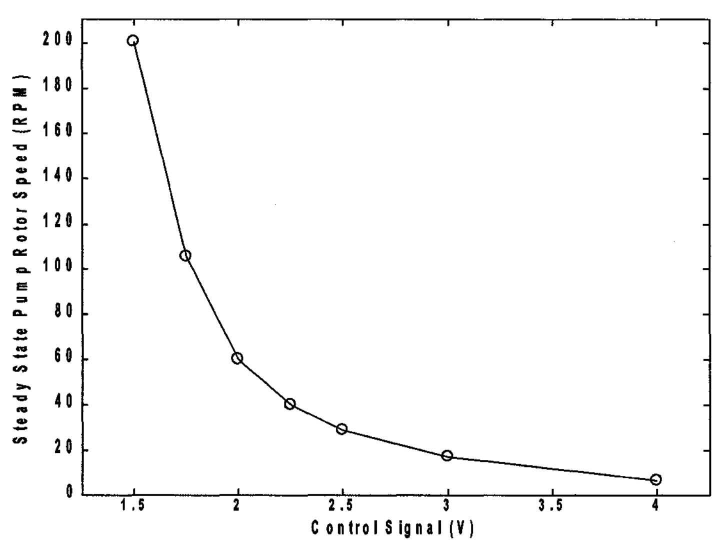

Figure 5.20: Pump rotor speed vs. control signal obtained from steady state values of Figure 5.19.

The responses of the pump rotor system when subjected to different magnitude step changes in the drive input signal are shown in Figure 5.19. The responses are from zero initial rotor speed and with no external loads (ie. no tubing loaded in the pump).

The expected operating range of the pump for the desired flow rate is between 10 and 100 RPM. From Figure 5.19, it can be seen that the system response for this operating range may be approximated using a first order plus dead time model. Such models are characterized by three parameters: the process gain, a time constant, and a lag time. These parameters were obtained for each of the step responses and are shown in Table 5.1. The time constant and dead time were estimated using a two point method. The method was originally proposed by Smith [51] in 1973 and is now a common method cited in numerous texts. Two points corresponding to 28.3 % and 63.2 % of the final value are first identified. The time constant and dead time are estimated as:

$$\tau = 1.5\,(t_{63.2} - t_{28.3})$$
$$t_o = t_{63.2} - \tau \qquad (5.1)$$

$where: \tau = Time\ constant$
$t_o = Dead\ time$
$t_{63.2/28.3} = time\ when\ response\ reaches\ 63.2\ \text{and}\ 28.3\ of\ final\ value$

The actual dead time is extracted directly from rotor speed measurements.

Table 5.1: Pump step response properties from zero initial condition

Control signal (V)	Rotor speed (RPM)	Gain (V/RPM)	2 Point estimated time constant (sec)	Actual dead time (sec)	2 Point estimated dead time (sec)
4	6.28	0.64	0.12272	0.5225	0.57337
3	16.81	0.18	0.20353	0.2275	0.20454
2.5	28.5	0.088	0.19552	0.19	0.17578
2.25	39.84	0.057	0.1894	0.16	0.15358
2	60.69	0.033	0.18956	0.1475	0.14732
1.75	105.3	0.017	0.18951	0.13	0.14987
1.5	200	0.0075	0.19345	0.125	0.16774

Several observations can be made from the data presented in Table 5.1.

- The relationship between the input signal and steady state speed is inverted and highly non-linear. This implies that a single gain cannot characterize the system throughout its operating range. Without a method of linearizing the system gain, a conventional linear controller cannot adequately regulate the process and will likely produce an unstable response. A set point profiler is therefore proposed and presented in a later section.
- For the specified operating range (20 to 100 rpm) the time constant does not significantly vary and is approximately equal to 0.19 seconds.
- Both the actual and estimated lag times are not constant. The lag time appears to be dependent on the magnitude of the input signal. As the input signal decreases so does the lag time. The lag time is an important indicator of the controllability of the system.

During production the pump set point will frequently vary by small step changes. In order to evaluate the system behaviour subjected to such small input steps, tests were conducted from non-zero initial speeds. The system responses for these tests are shown in Figure 5.21.

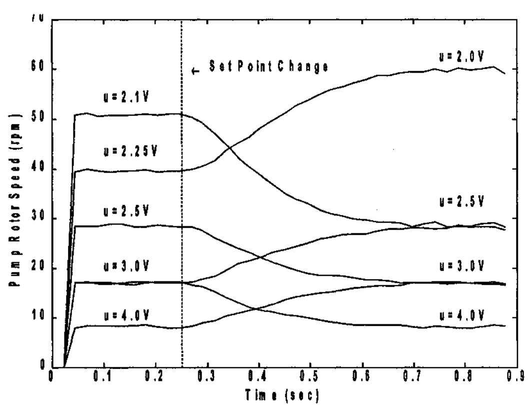

Figure 5.21: Pump rotor speed open-loop response from non zero initial condition and no load.

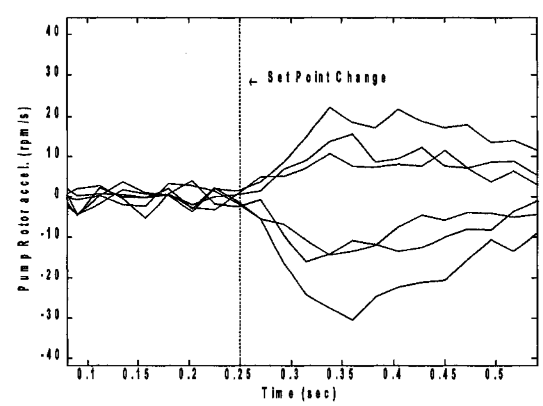

Figure 5.22: Pump rotor estimated acceleration of Figure 5.21.

It can be seen that for non-zero initial conditions, the time constant remains approximately equal to the case of the zero initial condition step response (approx 0.19 sec). The same cannot be said for the lag time. The rotor acceleration obtained via numerical differentiation is shown in Figure 5.22. Although there is a considerable amount of noise in the estimate, a non-zero acceleration (indicating a change in rotor speed) can be seen 0.05

sec after the set point change. This value is considerably shorter than the value reported for zero initial condition tests which where between 0.5 and 0.125 seconds.

The data obtained in this section will allow for the use of various general tuning strategies to determine the gains of the feedback controller. Due to the non-linear process gain, it was also determined that a set point profiler will be required.

5.3.1.Resin Pumping Process

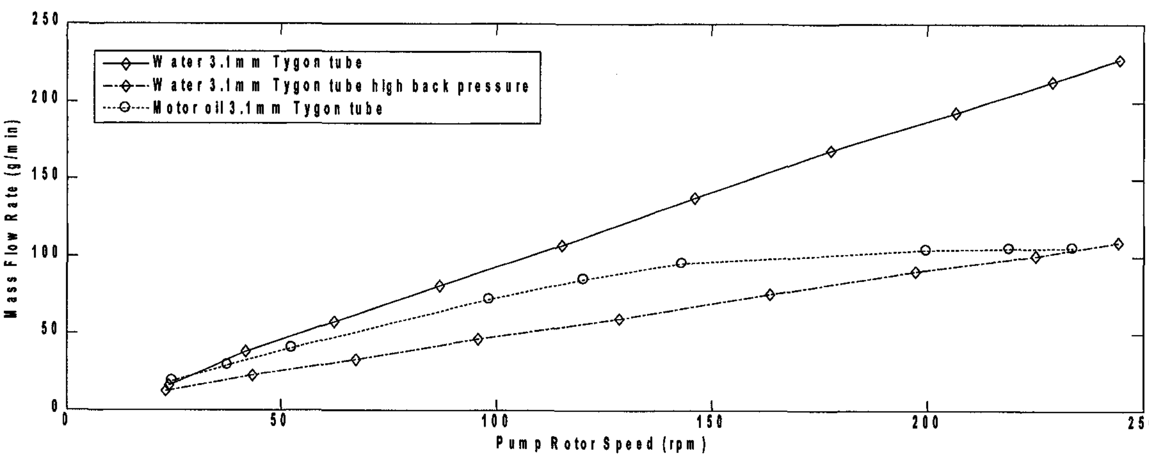

Figure 5.23: Flow rate vs. pump speed of peristaltic pump for water and oil under various flow condition.

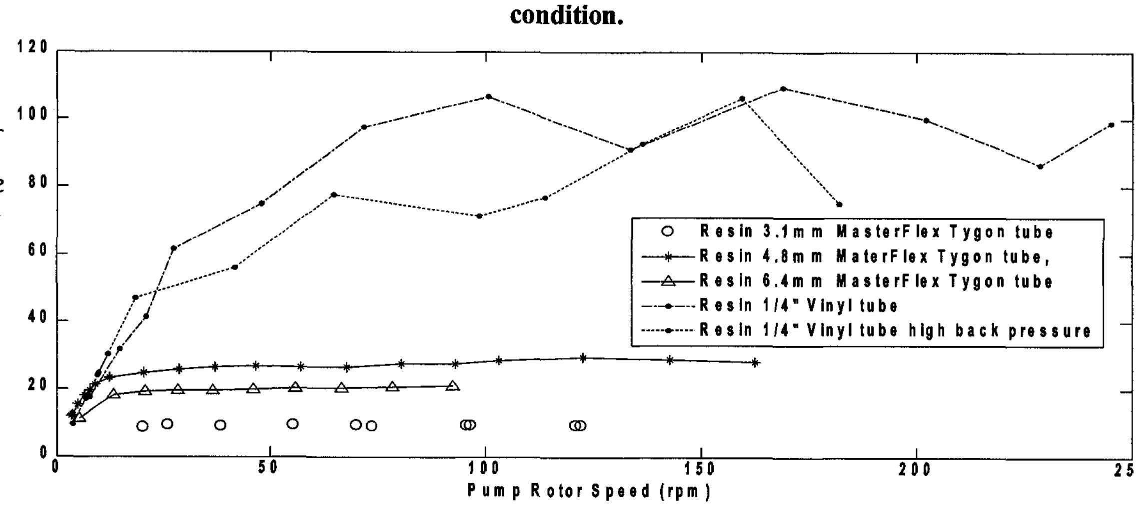

Figure 5.24: Flow rate vs. pump speed of peristaltic pump for resin using various tubing.

The relationship between pump speed and flow rate is affected by several parameters. These include down stream pressures, tubing diameter, tubing type and fluid viscosity. The flow rate versus the pump rotor speed for various flow conditions is shown in Figures 5.23 and 5.24

Flow rate estimates were obtained by differential weight measurements while the pump rotor speed was measured using an optical encoder. A pinch valve was used to increase the delivery pressure. To compare the effects of viscosity, tests were conducted with three fluids; water, oil and resin. Four different types of tubing were used: Masterflex, Tygon, and Lab peristaltic tubes, with internal diameters of 3.1, 4.8 and 6.4 mm, respectively, and a general purpose vinyl tube with an internal diameter of 6.4 mm. Several observations can be made.

- Fluid with a low viscosity (water) causes a linear relationship between rotor speed and flow rate. This is in accordance with published data from several peristaltic pump manufacturers [52][53].
- The flow rate versus pump speed becomes increasingly non-linear as the pumped fluid viscosity increases (Figure 5.24).
- For small tubing and very viscus fluids, flow rate remains constant for any pump speed. (Figure 5.24, Resin 3.1 mm tube).
- The flow rate decreases as the delivery pressure increases.
- The quality of the tubing affects the variability of the pumping process. (ie process noise). Low cost all purpose, tubing produces higher process variability (specifically at high pump speeds) compared to tubing specifically designed for peristaltic pump use.
- It should be noted that the tests presented above were done using partially crystallized resin which is very viscous. In this case, in order to achieve the required flow rate it may be necessary to heat the resin to decrease its viscosity and dissolve the crystallized particles. New uncrystallized resin is conceivably less viscous and does not require heating.

The pumping process is further complicated by variations in the process parameters which may occur during a production run. For example, since carbon strands cover most of the impregnation ring's inner radius, there may be a restriction to resin flow which will cause variations in downstream pressure. Furthermore, for a given resin, viscosity variations may occur due to temperature variations caused by environmental changes or heat generated by the exothermic curing process while in the resin reservoir. The latter complication may be significant if the resin and hardener are premixed and the production runs lasts several hours.

Finally, changes in the tube compliance may occur over long operating periods and can change the pumping behaviour. Literature related to continuous hemo-filtration, reports similar changes in the dynamic behaviour of peristaltic pumps. For example, Schaeffer [54] reports a decrease in the filtration rate for a given pump's angular speed as the downstream resistance to flow increases. Typically, peristaltic pumps are classified as positive displacement pumps. This implies that as the pump speed increases there is a linear increase in the flow rate. From Figure 5.23 it can be seen that this is true for low viscosity fluids and when outlet pressures are relatively low. As the fluid viscosity and outlet pressure increases there are increased non-linearities in the pumping behaviour (Figure 5.24). As reported by Depner et al. [55], this is principally caused by a transient flow reversal at the instant the pump roller ceases to occlude the peristaltic tubing. Increasing the outlet pressure causes an increase in the quantity of fluid conveyed opposite to the flow direction. This reduces the total flow rate. Similarly, a viscous fluid increases the outlet pressure due to an increase in frictional losses in pump tubing. The effect is compounded by a negative inlet pressure caused by highly viscous shear forces in the inlet tubing. For example, when pumping resin it was observed that as the pump speed increases so does the amplitude of the transient flow reversals. This would explain the saturation of flow rate as the rotor speed increases (Figure 5.24, Resin 3.1 mm tube).

The data and observations presented above describes the steady state behaviour of the pumping process. Measuring the dynamic behaviour of the pumping process is not possible since it would require fast flow measurements which are not available. Since the peristaltic pumps are positive displacement devices and the resin may be assumed incompressible, it can be assumed that the dynamic effects of the pumping processes may be neglected. In any case, the control objective is to maintain a constant flow rate, therefore a detailed understanding of the pumping process transient behaviour is not required.

From a control stand-point, the challenges associated with the dispensing process may be grouped into two categories, namely the unknown relationship between pump speed and flow rate, for a given set of operating conditions, and the time dependence of this relationship. The design of the final control system will therefore address both of these issues separately by using a set point profiler and a feedback controller.

5.3.1. Mass Flow Rate Estimate

Both on and off-line flow rate estimates may be obtained using the weight balance. Off-line measurements are made prior to the start of the production run, when dispensing may be started and stopped at will. On-line measurements are used to estimate the dispensing rate during the production run. This section will discuss the errors and parameters of both flow rate estimation methods.

5.3.1.1. Off Line Flow Rate Measurement

As was demonstrated in previous sections, there is a need to obtain flow rate measurements to calibrate the dispensing process prior to the start of a production run. To do so, a two point difference may be used. It is valuable to evaluate the error associated with the flow rate estimate obtained with this method. The methodology is similar to the one used to evaluate the error associated with speed measurements of the pulling and braiding processes. The error of a quantitative measurements derived from several measurements with random error can be found using the equation below.

$$\epsilon_P = \pm\sqrt{\left(\frac{\partial P}{\partial q1}\right)^2 \epsilon_{q1}^2 + \left(\frac{\partial P}{\partial q2}\right)^2 \epsilon_{q2}^2 + \ldots} \qquad 5.2$$

where P is the quantity of interest, and the q_i are measured quantities with associated absolute errors ε_i. If the flow rate is estimated using:

$$\dot{Q} \simeq \frac{m_2 - m_1}{\Delta t} \qquad 5.3$$

then the resulting random error can be found using:

$$\epsilon_Q = \pm\frac{1}{\Delta t}\sqrt{2\epsilon_m^2 + Q^2\epsilon_t^2} \qquad 5.4$$

where Δt is the measurement time with associated error ε_t, Q is the flow rate and ε_w is the error associated with the mass measurements.

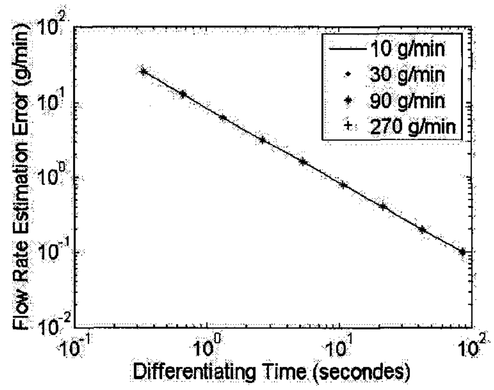

Figure 5.25: Flow rate estimation error vs. differentiating time for various flow rate with measurement accuracy of ±0.1g.

The error versus differentiating time for various flow rates are plotted in Figure 5.25. Since both the difference time error (ε_t)and flow rate (Q) are small compared to the weight measurement error it can be seen that the flow rate does not significantly affect the measurement error. The error associated with the weight measurement is quoted by the scale manufacturer to be ±0.1 g. The figure shows that a differentiating time of approximately 10 seconds will lead to a desired maximum error of less than 1 g/min.

5.3.1.2. Online Mass Flow Rate Estimation

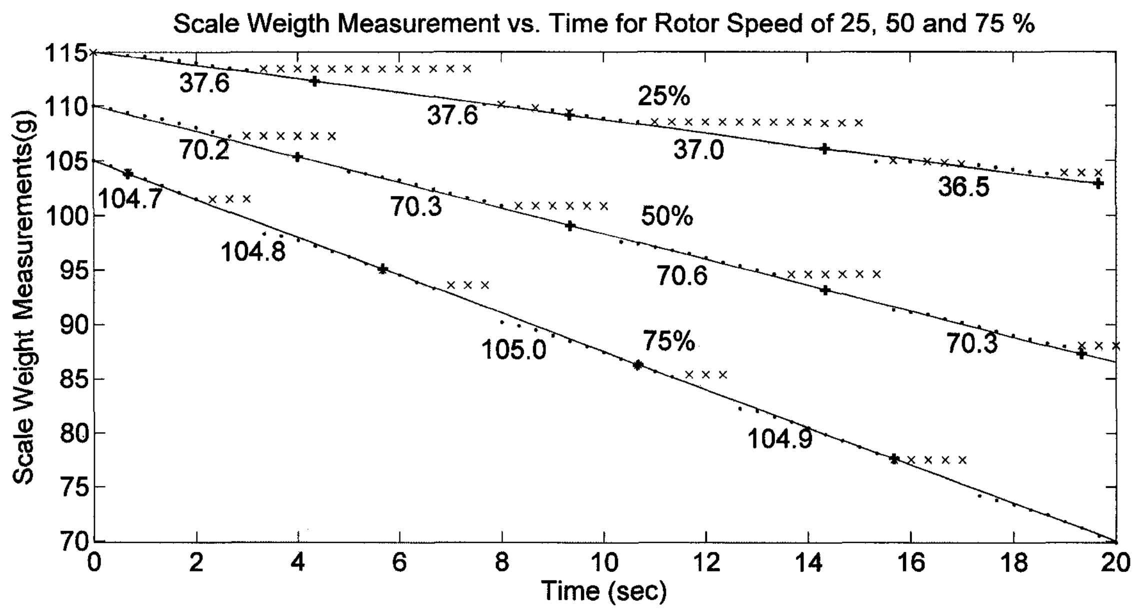

Figure 5.26: Processed weight measurement for rotor speed of 25, 50 and 75% with linear regression used to estimate the flow rate. The model w=Qt+b is fitted to the points "dots" using a least squared algorithm. The "x's" correspond to rejected data. An estimated is obtained after each "+"

As discussed in previous sections, there is a need for on-line measurements of the dispensing flow rate. The weight measurement of a resin reservoir was chosen to estimate the resin flow rate. Unfortunately, the scale output is not what was expected. It can be seen in Figure 5.26 that the weight measurements will decrease as expected and then remain constant for several data points. This behavior is likely attributed to an internal quantization error or a firmware problem of the scale. In Figure 5.26, the "dots" and "x's" represent valid and rejected the weight data points respectively. Observation of the raw data reveals that during this period the fluctuations in weights are at most 0.1g This phenomenon is considerably more significant for lower flow rates. For example, for a flow rate of approximately 37 g/min the ratio of good to bad data points is 3:4. This implies that simple numerical differentiation will not be possible. The desired flow value corresponds to the slope of the weight versus time measurements. In order to evaluate this slope, the model $W=Qt+b$ is fitted to a set of weight versus time data points. When using a simple least squares fitting process the bad data points considerably affect the flow rate estimate. Although a least squares fit is unaffected by random error in the data, it cannot discriminate between bias error such as the one found in the present case. For similar reasons, it is not expected that a Kalman filter could successfully discriminate between good and bad measurements. Two methods are proposed to reduce the effect of corrupted data points on the flow rate estimate. The first is to discriminate between good and bad data points and then perform the fitting process. The second uses a robust fitting process. Finally both data discriminating and a robust fitting may be used together. The result of this combined method is shown in Figure 5.26 with the flow rate values shown under the respective curves.

Given the pattern of invalid data points, weight measurement validation can be done by discriminating invalid measurements based on the difference between two samples. Since the scale sensitivity is 0.1g, it would be expected that valid points would change by at least this value. Therefore any point that remains within 0.1g of the previous point can be considered invalid. As the dispensing flow rate decreases, the expected difference between two successive measurements approaches the sensitivity of the scale. Since the measurement period of the scale is 1/3 of a second, this occurs for flow rates below 18 g/min ($0.1\ g \div 1/3\ sec \times 60$). For low flow rates, it was found that this method worked best if the reject threshold is set to 0 g. This implies that only non-changing measurements are rejected. The results of this data validation method is shown in Figure 5.26, where dots and x's represent valid and rejected data points, respectively.

Several robust curve fitting algorithms can be found in the literature [56]. A popular robust algorithm, called bi-square regression, iteratively estimates the model parameters using a least squares solution. For each iteration, the residue is used to calculate a weighting factor for each data point. When using this algorithm, outliers in the data will iteratively be given lower weighting factors. Consequently, corrupt data will have significantly less effect on the final estimate compared to the data derived from a pure least-squares estimate.

Combining both the data validation and robust fitting method allows for the best estimate to be obtained. By setting the initial weighting factors of the invalid points to zero (as determined by the validation algorithm), corrupt data does not affect the final estimate. This can be seen in Figure 5.26 where the fitted model matches the valid weight data. Combining both methods, would potentially reduce the number of iterations of the fitting algorithm, thus reducing its execution time.

The fitting process is performed on a series of points collected over a fixed sampling time. As the number of points increases it is expected that the measurement noise (variability in flow rate estimate) would decrease. From a control standpoint, the dead time introduced by long sampling times reduces the controllability of the closed-loop system. It is therefore important to select the smallest sampling time that results in an acceptable measurement noise level. To some extent, it is possible to decrease the sampling time while maintaining acceptably low measurement noise. This is done by extending the fitting process to data points from previous sampling periods. In this method, the weighting factors associated with data points of previous periods may be exponentially decreased. To illustrate the extended fitting process consider the data presented in Figure 5.26. The flow rate estimates were obtained using a sampling time of 5 seconds (15 points). The fit is performed on the data of the previous 5 samples. For each previously acquired sample set the weighting factors are multiplied by 0.5. The weighting factors for sample n=0,-1,-2,-3,-4 are therefore 1, 0.5, 0.25, 0.125, 0.0625, respectively. It should be noted that rejected data is still not considered since the weighting factors are initially set to zero by the validation process. Conceptually, the process is similar to applying a low pass filter to the data points. The estimation method requires that three parameters be tuned;

- Ts: the sampling time (number of weight points).
- Np: the number of previous estimated used in the fitting process.
- α:the discounting factor for each passed estimate.

An optimal set of parameters (Ts, Np and α) will depend on the ratio of good and bad points, which has been shown to be dependent on the flow rate. Determining an optimal parameter set is further complicated by the fact that the fitting process is based on heuristic rules. A method to find an optimal set of parameters will not be presented. Instead, general guidelines on how to select the estimation parameters are given.

- It is best to set Ts such that they correspond to the expected period of bad data plus two or three more data points. This ensure that for each sampling period the estimate is updated. Since the number of bad data points is inversely related to flow rate, it is best to set Ts according to the lowest expected flow rate required during a production run.
- Setting Np to a large value allows for all discounted samples to be considered. Np is set such that those samples that contribute more than 5% (weighting factor of 0.05) are used in the fitting process.
- The value of α can be thought of as the filter time constant. Larger values of α lead to an increase in the measurement time constant. For large α, the fitting process is performed on an effectively larger sample, tending to reduce the measurement noise.

For the outlined method there is a compromise between measurement noise and the time constant of the estimation process. Since the goal of the dispensing controller is to obtain high steady-state accuracy and to reject slow varying changes in the process dynamics, preference is given to flow estimation with low variability. It was found experimentally that for flow rates between 25 and 35 g/min, adequate estimates of the flow rate were obtained when the T value was set to four seconds and the α value to 0.5. Through observation, it was determined that three samples were required for the estimate to converge to a steady state value.

The flow rate measurements obtained using the method described above where compared to flow rate estimates obtained by differential weight measurements of a dispensed weight. Test where conducted for several pump speeds over a 1 minute period. The measurements reported by the scale method where averaged and compared to the flow rates obtained from the differential estimates. In all cases, the error between the calculated average and the differential estimate where smaller than 0.5 g/min. The largest error between a differential estimates and an individual measurement (as reported by the scale method) was 2 g/min.

During the final development of the dispensing controller it was observed that an unexpected software error occurred when using the bi-squared algorithm for certain weighted data sets. When the error occurred, the slope of the linear fit was returned as zero.

From the view point of the feedback controller this corresponds to a flow rate of zero. The effect on the system response is equivalent to an impulse disturbance. For large feedback gains, oscillations may be observed for several samples. The issue is currently under review by the vendor. Temporarily, a regular least-squares fitting process is used to estimate the flow rate. If the problem is resolved by the vendor, it is suggested to use the bi-squared algorithm as it leads to estimates with significantly less variability.

5.1.Dispensing Controller

In the previous section, the characteristics of the pump rotor speed and resin pumping process were presented. The capability of the on-line flow measurement methods were also discussed.

It was shown that the pump rotor speed step response can be approximated by a first order plus dead time model. The model displays an exponentially decreasing gain, a fixed time constant and a variable dead time. The pumping process gain curve may vary depending on specific pumping conditions. The relationship will vary and may be linear to exponentially increasing. The time required to obtain a valid flow rate measurement introduces a considerable dead time in the pumping control loop. The design of the proposed dispensing controller will address the above observations.

The pump rotor speed and pumping processes are regulated independently using a cascade control scheme. The inner loop controls the pump rotor speed and accepts set point changes from the mass flow rate controller. A PID is used to regulate the pump rotor process, while a pure integral controller is used for the pumping process. Both processes utilize a set point profiler to compensate for the non-linear gain characteristic. The dispensing controller is depicted in Figure 5.27.

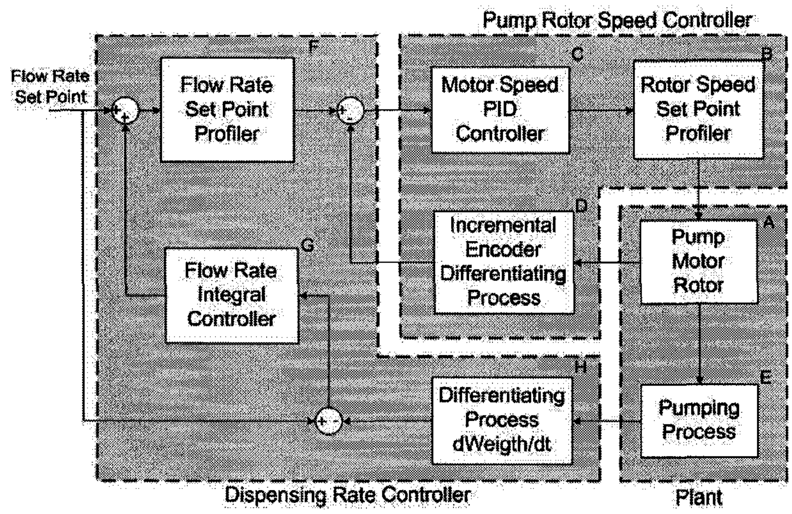

Figure 5.27: Dispensing controller block diagram.

From the dispensing controller diagram (Figure 5.27) it would appear illogical to first differentiate the weight measurement with respect to time and successively integrate the error calculated from this quantity. Alternatively, it would have been possible to forgo the differentiation process and use a ramp reference and proportional feedback control. This method was rejected for several reasons. Firstly, given the pattern of invalid weight measurements, a curve fitting would still have to be performed to extrapolate a valid weight measurement for each sample period. This makes the implementation of both methods similar in complexity. It was thought that an error in the slope estimate would translate into an extrapolated weight measurement with a large error. Furthermore, for pure integral control there is a natural ability to filter noise in the data. This is because the control action is calculated over several samples. The same cannot be said about the proportional action, where a tracking error translates into immediate control action.

5.1.1.Pump rotor speed process controller

5.1.1.1.Pump Rotor Speed Set Point Profiler

The pump speed process gain is linearized using a set point profiler (block B, Figure 5.27). The set point profiler consists of an exponential curve fitted to a measured control signal versus rotor speed points. By placing the set point profiler before the pump, the process gain is made approximately linear. The data points and fit-curve are shown in

Figure 5.28. Three power fit-curves were performed for various rotor speeds (5-10%, 10-30% and 30-100%). It should be noted that previous pump speed data was presented in terms of rotor RPM. Since this measure has no physical significance in terms of the dispensing rate, future rotor speed analysis, as well as the control system implementation will be performed in terms of percent of maximum rotor speed.

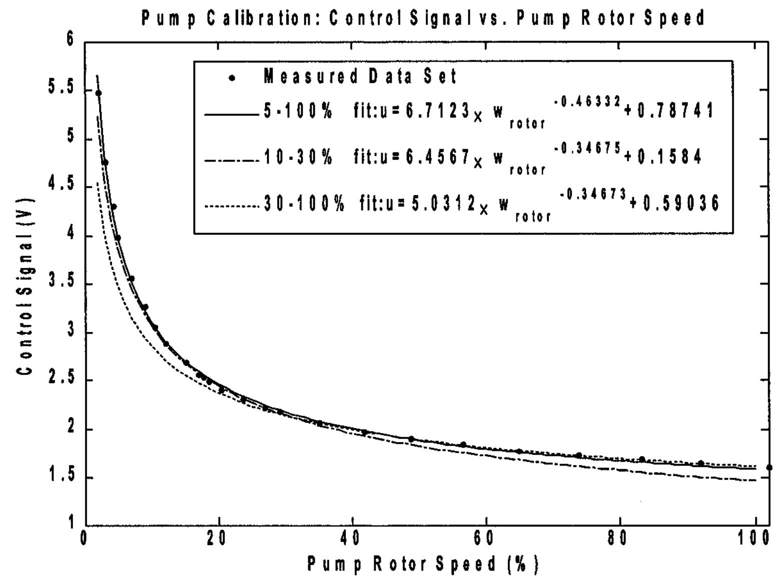

Figure 5.28: Control signal (V) vs. Pump rotor speed (rot/min) with several exponential curve fits used as set point profiler.

To verify their effectiveness, open-loop tests with the fitted curves used as set point elements were performed. Rotor speed measurements were acquired directly in the control program while the control signal was measured using a voltmeter. The results are presented in Figure 5.29.

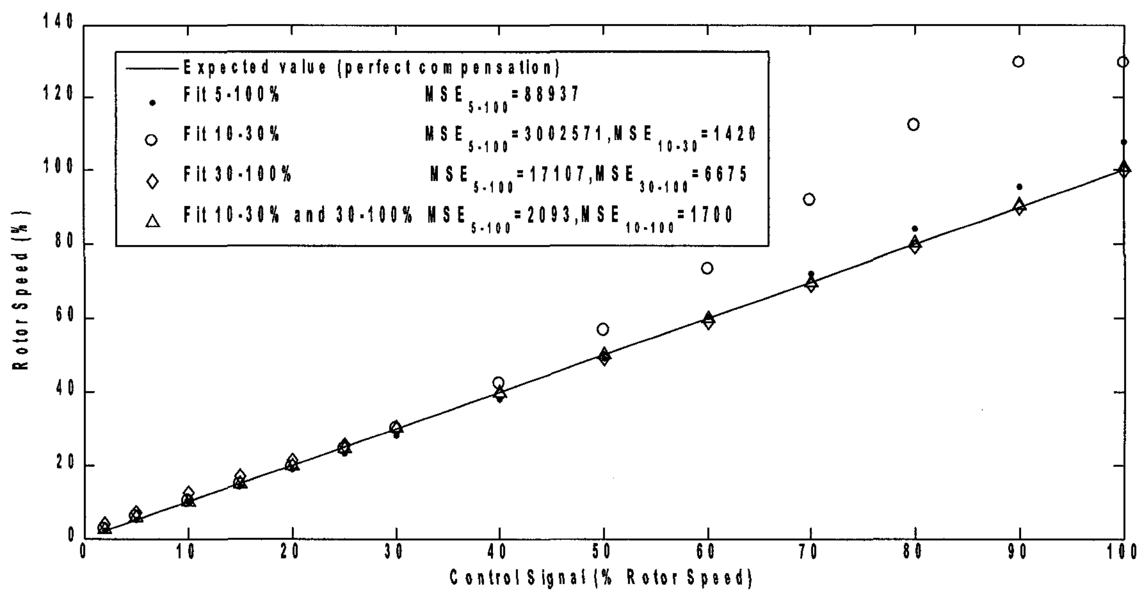

Figure 5.29: Measured rotor speed vs. control signal for various set point profilers. Mean square error shown for entire range and fitted range.

The effectiveness of each fit is evaluated by calculating the mean square error (MSE). The error is taken as the difference between the ideal value (unity gain curve) and the actual measured speed. The MSE for the entire operating range (5-100%) and the fitted range is shown in the legend of Figure 5.29. The predicted error is smaller in the fitted data range since the fitting algorithm aims to reduce this error. The partial fits (10-30% and 30-100%) performed well over the fitted range but perform badly over the entire operating range. It was found that by using both of these partial fit curves, the average error would be reduced considerably compared to using a single fit curve. This is done by switching from one curve to another depending on the desired set point speed. The actual crossover speed was chosen at the intersection point of both curves. This corresponded to 31.2%. Using this method, the MSE was reduced by more than 40 times over the entire range (0 to 100%) and 50 times over the operating range.

The rotor speed step response using the set point profiler is shown in Figure 5.30. For the no load case (i.e. no tube loaded in the pump) the steady state speed is close to the desired value. When the pump load is increased, by loading tubing and a placing a flow restriction on the outlet of the pump, the steady state behaviour changes. It can be observed that the average error between the actual and desired set point increases compared to the unloaded case. This shows that the open-loop system is unable to reject the external disturbances. The use of a feedback controller is therefore warranted and will be discussed in the following section.

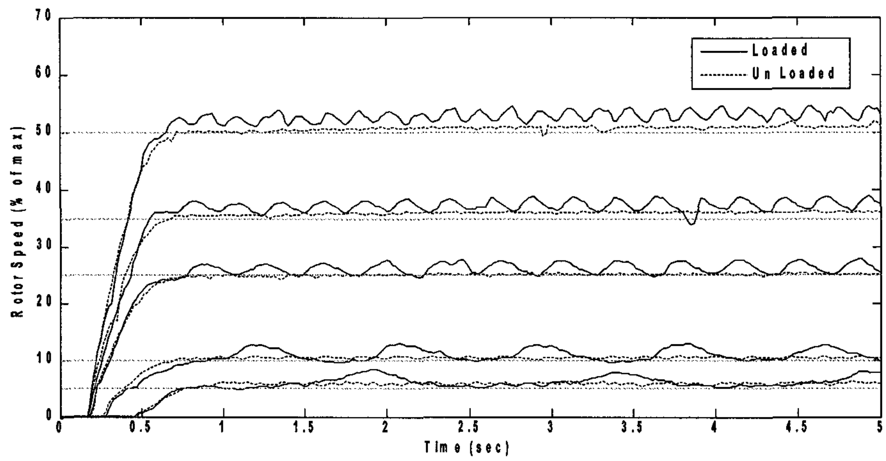

Figure 5.30: Pump rotor open-loop step response with set point profiler.

The oscillations that are observed in the loaded responses are due to the torque fluctuations as each of the four pump rollers compress the peristaltic tubing. In fact, the expected and observed disturbance periods are closely related (Table 5.2). The expected disturbance period is calculated from the average rotor speed between 1.5 and 5 seconds. It should be noted that during the open- loop test presented in Figure 5.30 the maximum rotor speed entry in the control program was inadvertently set to 150 RPM and not 200 RPM as with the rest of this work.

Table 5.2: Calculated and observed pump rotor disturbance periods.

Set Point (%)	Avg. Value (%)	Pump Rotor (RPM)	Expected Disturbance Period (sec.)	Observed disturbance period from Figure 5.30 (sec.)
5	7	11	1.4	1.5
10	11.72	18	0.85	0.86
25	26	39	0.39	0.36
35	37.6	56	0.27	0.25
50	53	79	0.19	0.18

5.1.1.2.Pump Motor Speed PID Controller

A PID feedback controller is used to regulate the pump rotor speed process. Since control is done in a discrete fashion an appropriate sampling time must first be selected. Then the controller design involved determining a set of gains that result in an adequate closed-loop system response.

For under-damped systems, such as the pump rotor process, common practice is to choose a sampling time which results in approximately 10 samples during the system rise time. This results in a sampling frequency of approximately 50 Hz. A sampling frequency of 60 Hz is used in the final controller.

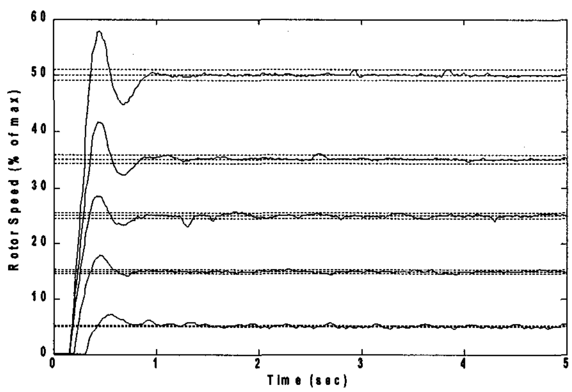

Figure 5.31: Unloaded PID closed-loop pump rotor step response for gains obtained using QD tuning strategy (Kc=1.4, *Ti*=0.0053, *Td*=0.0013).

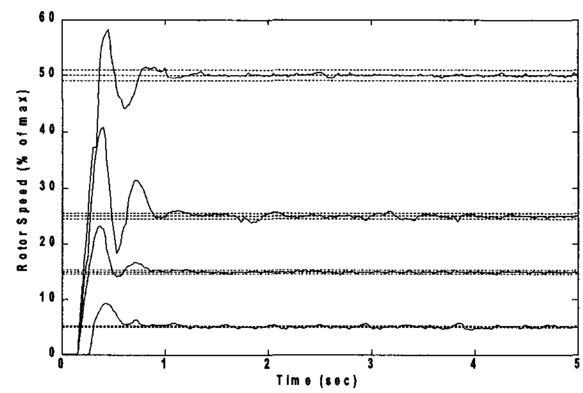

Figure 5.32: Unloaded PID closed-loop pump rotor step response, gains obtained using IMC tuning strategy (*Kc*=2, *Ti*=0.0032, *Td*=0.0003125).

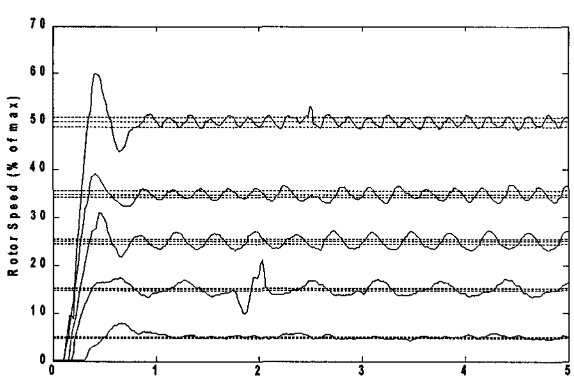

Figure 5.33: Loaded PID closed-loop pump rotor step response for gains obtained using QD tuning strategy (*Kc*=1.4, *Ti*=0.0053, *Td*=0.0013).

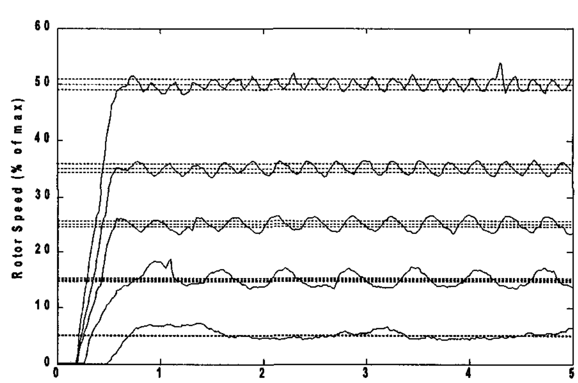

Figure 5.34: Loaded PID closed-loop pump rotor step response, gains obtained using IMC tuning strategy (*Kc=0.5*, *Ti*=0.0032, *Td*=0.0003125).

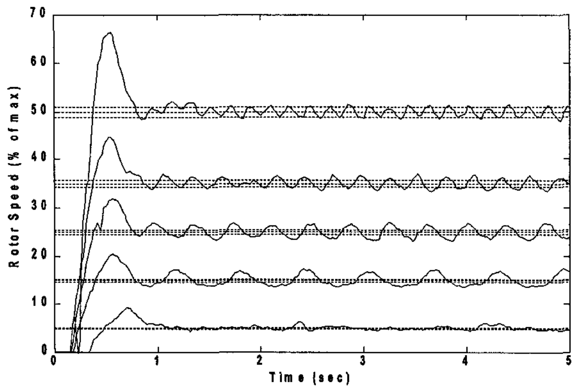

Figure 5.35: Loaded PID closed-loop pump rotor step response, gains obtained using IMC tuning strategy (*Kc=1*, *Ti*=0.0032, *Td*=0.0003125).

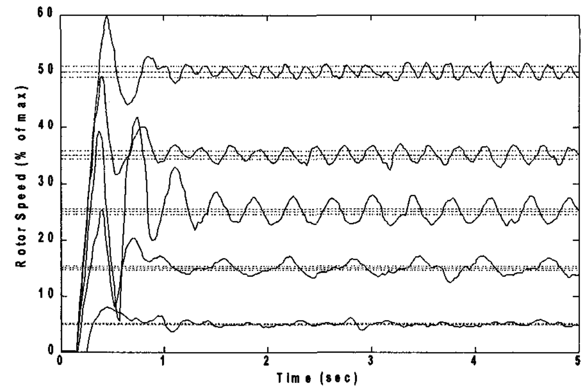

Figure 5.36: Loaded PID closed-loop pump rotor step response, gains obtained using IMC tuning strategy (*Kc=2*, *Ti*=0.0032, *Td*=0.0003125).

Since the pump rotor system response can be approximated by a simple first order plus dead time model, simple PID tunning strategies can be used. The process response with gain sets obtained from two tunning strategies, the quarter decay and the internal model controls, are compared. The quarter decay tuning method (QD) was proposed by Ziegler and Nichols [57] in 1942. The internal model control tuning method (IMC) was first developed by Smith and Corripio [58] under the name "Controller Synthesis". The modern appellation comes from Rivera [33] where a review of various model structures and tunning guidelines are presented. For a first order plus dead time model, the tuning equations are summarized below.

$$
\begin{aligned}
&QD: K_c = \frac{1.2\tau}{Kt_0};\ T_i = 2t_0;\ Td = 0.5t_0 \\
&IMC: K_c\ is\ manually\ adjusted;\ T_i = \tau;\ T_d = \frac{t_0}{2} \\
&where\quad K_p: Process\ gain \\
&\qquad\quad t_0: Process\ dead\ time \\
&\qquad\quad \tau: Process\ time\ contant \\
&\qquad\quad K_c: Proportional\ gain \\
&\qquad\quad T_i: Intergral\ time \\
&\qquad\quad T_d: Derivative\ time
\end{aligned}
\qquad 5.5
$$

The loaded and unloaded rotor speed step responses for the PID controller obtained using the QD tunning strategy are shown in Figures 5.31 and 5.33. The loaded rotor speed step response for proportional gains of 0.5, 1 and 2 are shown in Figures 5.34, 5.35 and 5.36, respectively, while the unloaded response for a proportional gain of 2 is shown in Figure 5.32. In all figures, the dotted horizontal lines correspond to ±2% of the set point value. Several observations can be made from the closed-loop responses depicted in these figures.

All of the resulting closed-loop systems are stable and demonstrate low steady state errors compared to the open-loop response systems. The closed-loop time constants are similar for all gain sets and to the ones observed for the open-loop system response. This indicated that actuator saturation occurred in both the open and closed transient portion of the step response. As the controller gain is increased, the closed-loop response demonstrated a larger overshoot.

As with the open-loop case there are sustained oscillations when the pump is subjected to an external load. This is observed by comparing the unloaded responses (Figures 5.31 and 5.32) with the loaded responses (Figures 5.33 to 5.36). As the rotor speed increases, the effect of the cyclic load disturbance can be seen for all gain sets. It is suspected that the open-loop dead time associated with the pump motor drive prevents the process from reacting to the controller commands. This statement is supported by observing the response shown in Figures 5.33 and 5.35 for 5% set points. In these cases, the disturbance period is long compared to the dead time. The closed-loop system response shows little effect on the disturbance, which can be seen for the same set point in the open-loop system response (Figure 5.30).

Up to an optimal gain value (between K=0.5 and 1), increasing the controller gain seems to decrease the amplitude of the steady state oscillations. Above this value, the amplitude increases up to a point where the system is unstable (experimentally found to be approximately K=4 for the IMC gain set).

Since the rotor speed oscillations occur about a central mean, the effect on the pumping process will be averaged over several disturbance cycles. It is therefore unexpected that the rotor speed fluctuations would hinder the dispensing process. The final gain set of $K_c=0.5, T_i=0.0013\,min, T_d=0.00032\,min$ obtained using the IMC method is used. As depicted in Figure 5.34, this gain set results in a CL system which demonstrates low overshoot, low steady state error and attenuates some of the oscillation caused by the load disturbances.

5.1.2.Pumping Process Controller

5.1.2.1.Flow Rate Set Point Profiler (Pump calibration)

As was previously demonstrated, the flow rate versus pump rotor speed relationship is affected by several parameters. It is a common industrial practice to use a pump calibration to ensure the desired dispensing quantity. In fact, several commercially available dispensing pumps include calibration utilities or even built-in balances to streamline the calibration process.

The calibration procedure consists of acquiring several mass flow rate versus pump rotor speed data sets within the expected operating range of the pump. A polynomial function is then fitted to the data and used as a set point profiler. The relationship corresponds to the reciprocal of the curves shown in Figures 5.23 and 5.24. Flow rate estimates are obtained using a two point difference while the rotor speed measurements are obtained using the external encoder. Since the calibration procedure should be performed prior to each production run, the dispensing calibration process is automated. The implementation of this system is discussed in chapter 6.

The dispensing process open-loop behaviour with a step disturbance at sample 30 is shown in Figure 5.37. It can be seen that when the system is undisturbed the estimated flow rate is closed to the desired dispensing rate. The average flow rate is approximately 31 g/min with variability of approximately 2 g/min. This is higher that the required error of 1 g/min as stated in the previous section (p.96). It should be noted that the variability in measurements are considerably smaller when using the bi-square fitted process. When the system is subjected to a step disturbance, corresponding to an increase in delivery pressure, the dispensing rate decreases significantly. The design of a feedback controller is therefore warranted.

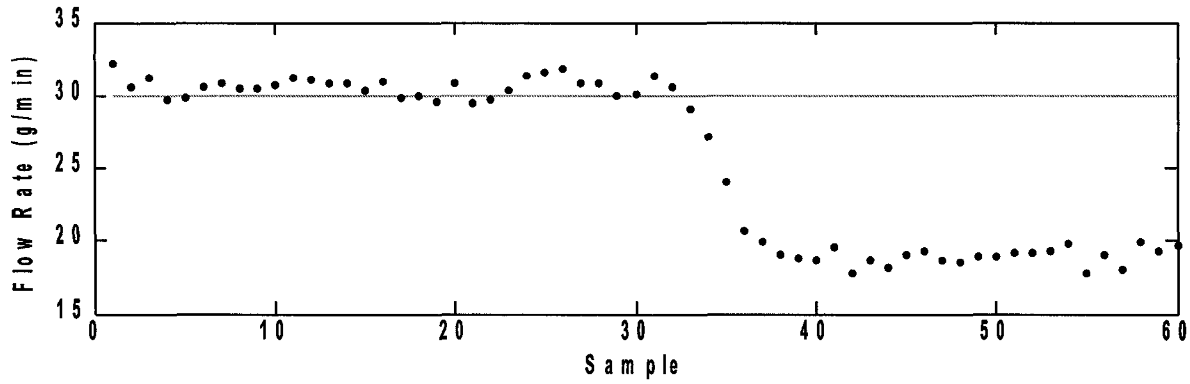

Figure 5.37: Open-loop flow control with step disturbance at sample 30

5.1.2.2.Flow Rate Integral Controller

The pump calibration when used as a set point profiler allows for open-loop control of the pumping process. In order to compensate for changes in the pumping process and to reject disturbances which may occur during a production run, a closed-loop controller is desirable.

The flow rate estimation process introduces a dead time of approximately 5 seconds in the closed-loop flow control system, therefore the system is only designed to reject constant or slowly varying disturbances (as described in Section 5.3.1.). For such disturbances the closed-loop dead time does not significantly hinder the control of the dispensing process.

Corripio [58] suggests that for processes where the dead time is considerably longer than the dominant process time constant, pure integral control should be used. In this case the discrete integral controller becomes:

$$\begin{aligned} & C_k = C_{k-1} + K_i E_k \\ & \textit{where}: C_{k/k-1} = \textit{control action at sample } k \text{ and } k-1 \\ & \qquad K_i = \textit{Intergral Gain} \\ & \qquad E_k = \textit{Error at sample } k \end{aligned} \tag{5.6}$$

The same author suggests that K_i be tuned using the following formula:

$$K_i = \frac{1-q}{K[1+N(1-q)]}$$
$$\begin{aligned} &where: q = an\ adjustable\ parameter\ (0 \text{ to } 1) \\ &\quad K_p = Process\ Gain \\ &\quad N = t_o / Sampling\ Time \\ &\quad t_o = Total\ system\ dead\ time\ (s) \end{aligned} \qquad 5.7$$

As determined in the previous sections, the dead time introduced by the measurement t_o is approximately 5 sec. The rotor process sampling time is T=1/60 sec. Since a set point element is used in the dispensing process, the system gain from the perspective of the feedback controller is equal to K=1. Setting q to 0 leads to an integral gain of K_i= 0.00332. It was observed that the closed-loop system response was considerably under-damped, and therefore, several minutes were required for an error in dispensing rate to be corrected. In this case, the above tuning rule results in a overly conservative gain.

Using the gain obtained from the above tuning rule as a stating point, an adequate gain was obtained through trial and error testing. It was first determined that for the current measurement parameters the dispensing process remained stable when disturbed if the gain was below 0.75. The dispensing system closed-loop response for gains of 0.1, 0.5 and 0.25 are shown in Figures 5.38, 5.39 and 5.40 respectively. In these figures, the top plots show the estimated dispensing rate versus sample count while the bottom plots show the pump rotor speed versus sample count. The sampling time is 4 seconds. In all cases the closed-loop system was first allowed to reach steady-state operation. Next, the pump delivery pressure was increased by constricting the outlet tube using a pinch valve. The effect of this step disturbance can be seen. It should be noted that the amplitudes of the disturbances in terms of the tube occlusion or increase in delivery pressure are not necessarily equal. This is due to the design of the pinch valve, which does not allow repeatable adjustments. The amplitude of each disturbance can be qualitatively evaluated by observing the pump rotor speed once the disturbance has been completely rejected. For example, the test performed for K_i=0.5 (Figure 5.39) showed a greater disturbance than the test for K_i=0.1 (Figure 5.38). It should also be noted that step disturbances of large magnitudes such as the ones used in these tests are not expected to occur during normal production. Therefore, the present tests should be regarded as a demonstration of the robustness of the control system, its ability to reject disturbances and to maintain low steady state error.

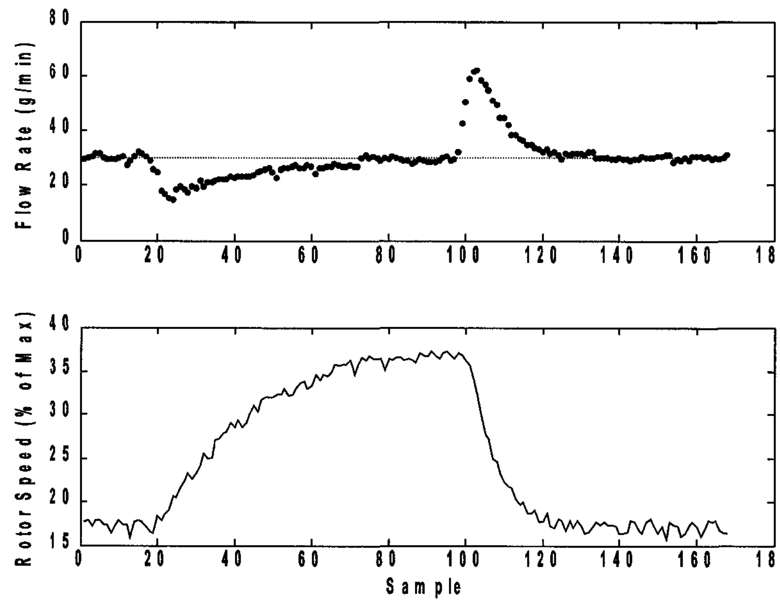

Figure 5.38: Closed-loop flow control *Ki*=0.1 with step disturbance between sample 20 and 100. (T_{sample}=4 sec).

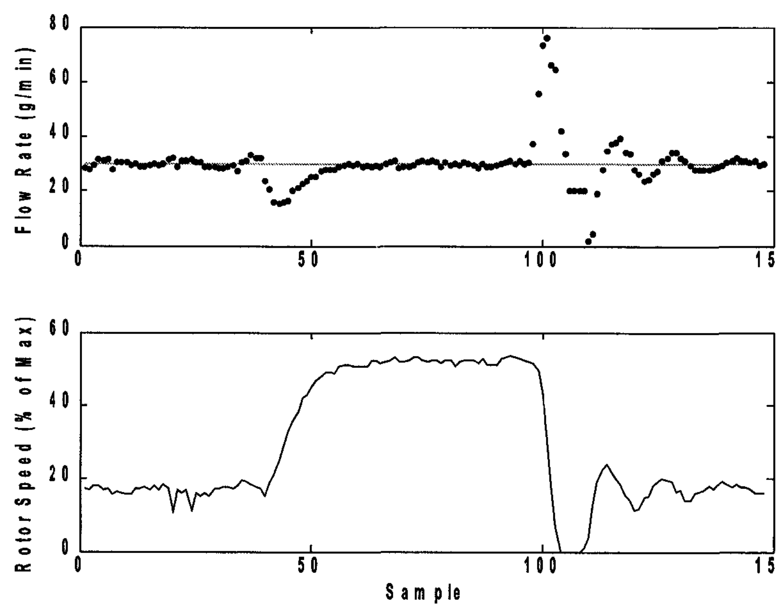

Figure 5.39: Closed-loop flow control *Ki*=0.5 with step disturbance between sample 40 and 100. (T_{sample}=4 sec).

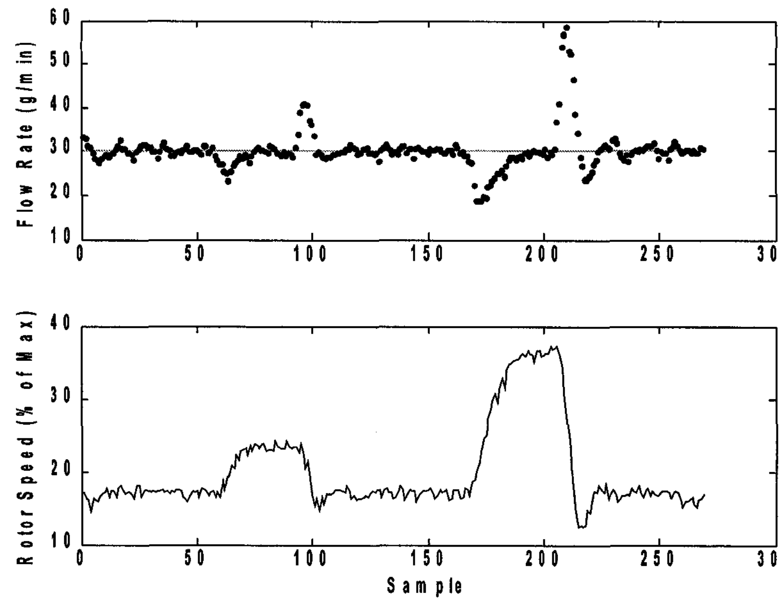

Figure 5.40: Closed-loop flow control *Ki*=0.25 with step disturbance between sample 55 and 100 and between sample 170 and 210. (T_{sample}=4 sec).

Several observations can be made from the dispensing system responses presented in Figures 5.38, 5.39 and 5.40;

- The dispensing control system is capable of rejecting step disturbances of large amplitudes.
- As expected, large integral gains lead to faster settling times than smaller gains. The settling time for K_i=0.1 , 0.25 and 0.5 are approximately 4, 1.6 and 0.67 minutes, respectively.
- In all cases there is an overshoot in the dispensing rate when the original operating conditions are restored. The magnitude of this overshoot is proportional to the amplitude of the original disturbance.
- For K_i=0.5 (Figure 5.39) and K_i=0.25 (Figure 5.40), there are visible oscillations in the dispensing rate when the original operating conditions are restored.

In deciding on the feedback gain of the dispensing controller there is a compromise between the system settling time after a disturbance occurs and the desired stability margins of the system. In the final control system, implementation of the integral gain may be adjusted by the user. The values are limited to K_i=0.5 and set to a default value of 0.2.

6 Curing System

6.1. Overview

In order for curing to begin the resin temperature must be elevated to at least 80° C. The speed of the resin exothermic curing reaction can be increased by providing a sustained heat flux to the uncured impregnated fibers. As previously discussed, rapid curing of the exterior layer can produce internal cracks due to chemical shrinkage of the internal resin. Furthermore, the maximum temperature, and consequently the maximum external heat flux supplied by ovens is limited by the flash point of the resin (approximately 251° C [59]). The use of tunnel ovens as the only heat input therefore is limited to rods of small diameters and becomes impractical for larger diameter components. The proposed curing method is one that involves two stages, namely an induction heating system followed by conventional heating in tunnel ovens.

In the first stage, an induction heater elevates the temperature of steel wires embedded in the central fibres. The wires heat the surrounding resin and start the exothermic reaction in the resin at these locations. However, the time required to cure the entire rod using induction heating alone is too long for the existing setup of the pilot plant.

In the second stage of the curing method, three tunnel ovens provide the necessary heat flux to cure the exterior of the rod. The three ovens are divided into seven controllable zones. The multi-zone configuration allows the oven temperature to match the internal temperature profile due to the resin exothermic reaction.

The curing of the composite rods has proved to be the most challenging part of production. During preliminary production runs many problems were directly caused by oven temperatures and temperature fluctuations that are not compatible with those required to achieved full curing. The problem is compounded by long time lags in set-point changes of the oven temperatures. This resulted in either a partially cured rod or severely oxidized ones, and in some cases spontaneous ignition of the resin. In all cases, failure of the entire production run occurred. As previously discussed, partial curing often results in the inability of the pulling station to advance the product through the process.

In order to obtain reasonable optimal set point values for the induction heater and oven temperature, an analytical and computer finite element model of the curing process was developed by Sandness [3]. The author suggests that production of the 12 mm FRP rebar be performed at 0.5 m/min with an induction heater set point of 231 amps and oven temperatures set points of 200° C.

The induction heater is equipped with a built in controller. Set point commands can therefore be issued directly from the control computer. The temperature of the heating chamber is measured using a wire supported thermo-couple assembly. A gain scheduled PI controller is used to maintain the oven temperature at the desired set point. An air purging system which forces cool air into the oven has been implemented. The air purging system can decrease the oven temperature quickly in the event that production must be unexpectedly halted. Conceivably, the system could prevent over curing of rod section located in the oven state during pauses in production.

6.2.Physical System

6.2.1.Induction Heater

Induction heating is used in many continuous industrial processes. Examples include the heat treatment of steel chains, and the joining of discontinuous wire segments to produce continuous lengths. During induction, alternating current circulates in a copper work coil which produces a magnetic field. When a metallic part is inserted into the work coil movement of electrical current is induced by the magnetic field. Heating occurs due to two energy dissipation mechanisms, namely losses due to Joule heating and losses due to magnetic hysteresis. Joule losses are due to internal resistance to the current in the heated component. Power is dissipated at a rate of I^2R, where I is the current circulating in the part and R is the resistivity of the metal. Magnetic hysteresis energy dissipation occurs as a result of rapid magnetization and demagnetization of the work piece. As the magnetic field changes direction so does the flow of current within the work piece. Energy is released when the metallic dipoles are forced to rotate in opposite directions due to the change in current direction. The release of energy is a function of the area contained within the hysteresis loop of the metal flux density vs. field strength curve (B-H curve). Non-magnetic metals rely on Joule heating only. It should also be noted that above the Curie temperature magnetic materials become paramagnetic (weakly magnetic) and as such would rely only on Joule heating.

Work piece heating is a function of the current circulating in the work coil and the induction unit operating frequency. The current may be adjusted during operation. This is not the case for the operating frequency, which is a function of the inductance/capacitance resonator circuit. The capacitance of the circuit is provided by an adjustable capacitor (hard wired) while inductance is provided by the work coil itself. The coil design is therefore critical in order to achieve controlled and efficient heating. Guidelines regarding coil design can be obtained from the induction unit manufacturer [60]. To prevent an increase in coil temperature, cooling water circulates within the work coil and through an external heat exchanger

The induction heater currently in use is a 2 kW unit manufactured by Ameritherm. Operating properties can be adjusted manually via the power supply front panel, by external voltage (0-10V) or current source (2mA-20mA). Terminals are also provided to start, stop and to provide emergency stop interruption. Three output terminals indicate the operational state of the unit, namely ready, heating and fault.

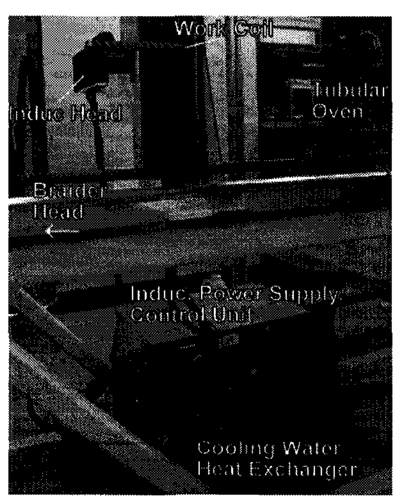

Figure 6.1: Induction station: induction head, work coil, power supply/control unit and cooling water heat exchanger are shown.

6.2.2.Ovens

6.2.2.1.General specifications

Three tunnel ovens divided into seven controllable zones are used in the current production line. Heat is generated by electric resistance nickel chromium heating coils. The coils for each zone are embedded in two semi-circular ceramic blocks. The heating coils and ceramic block form the heating elements. The elements are surrounded by insulation and a steel shroud. The heating chamber is the volume inside each oven zones where the product is heated. The ovens are shown in their closed and open configurations in Figures 6.2 and 6.3 The main specifications for each oven and their respective zones are listed in Table 6.5.

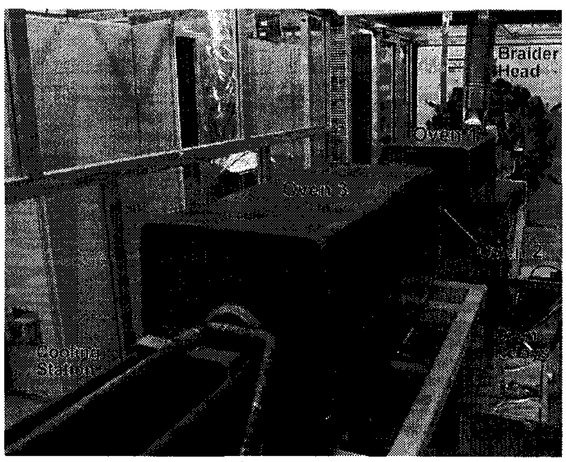

Figure 6.2: Oven curing station.

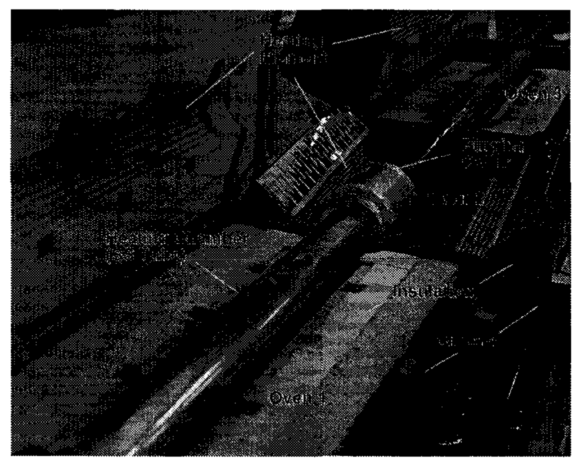

Figure 6.3: Curing ovens with stainless steel tube and purging collar.

During normal production a small quantity of resin will normally drip from the uncured rod. To contain this excess resin and prevent it from coming in direct contact with the heating elements, a thin-walled tube has been placed along the length of the ovens. The tube is hand rolled from a 26 gage, 304 stainless steel. A series of spot welds, deposited by TIG welding, joins the seam. The inside of the tube forms a heating chamber 7 cm in diameter and 2.1 m in length. It should be noted that the usable diameter of the tube is reduced to 4.7 cm due to the purging shroud located between the first and second ovens. To ease cleaning after production a removable drip pan is also installed within the tube.

Table 6.1: Tunnel oven specifications

Oven	Manufacture	Electrical Service	Zone #	Heater length (m)	Heater Resistance (Ω @25°C)	Current (A)	Power (kW)
1	Lindberg	220 V 30A	1	0.25	43.4	5.5	1.1
			2	0.5	21.9	10.9	2.2
			3	0.25	43.4	5.5	1.1
2	Satec System	3× 110V 15A	4	0.18	13.1	9.2	1.1
			5	0.18	13.1	9.2	1.1
			6	0.18	13.1	9.2	1.1
3	Lindberg	2× 110V 15A	7	1	2×16.2	2×14.8	2×0.89

6.2.2.2. Oven Power Control

Electrical power to the oven elements is controlled using solid state relays. The relays are located in a ventilated enclosure. Electrical power is provided by one 220V 30A service (oven 1) and five 120V 15A services (ovens 2 and 3). Each service is fused to protect the equipment in case of a malfunction. The oven relays, fuse and associated electrical connections are located in the oven relay enclosures shown in Figure 6.4.

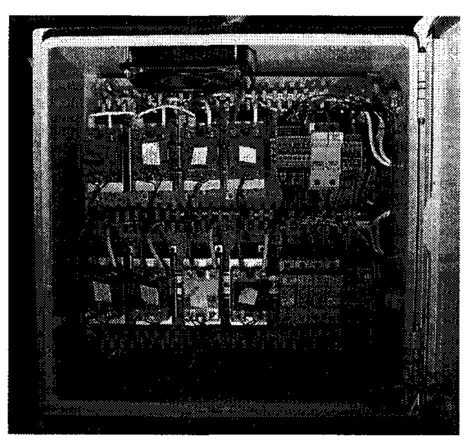

Figure 6.4: Oven relay enclosure.

Simple thermal system temperature control is often regulated using high gain proportional control (ie ON/OFF control). When more sophisticated regulation is warranted, a method to vary the heating intensity must be implemented. A common approach for electrical resistance heaters is to used pulse width modulation (PWM) of the heater electrical supply. In PWM a signal generator supplies a square wave of fixed frequency to an electrical switching device. The duty cycle of the square wave is varied to achieve the desired device output. For a given application, the base frequency of the PWM signal is chosen such that it is much smaller than the smallest time constant of the device. From a physical view point, PWM relies on a system of internal dynamics (capacitance, inertia, inductance...) to integrate the input energy and generate a constant output. The choice of the PWM base frequency is therefore device-dependent and will vary from several kHz for motor control to Hz for slower systems.

Omron solid state relays (model G3NA-220B) are used as the electrical switching devices for the oven system (Figure 6.4). The switching speed of these relays are quoted in terms of the minimum operating time and the maximum release time. For a DC input with 60 Hz AC loads, both the operating time and release time are 0.93 ms [61]. This implies a minimum switching speed of 1.86 ms. From a reliability stand point it is desirable to keep the minimum switching speed well above this value. Furthermore, the exact release time will vary as a function of the phase angle of the electrical load. The value must therefore be viewed as a source of random error in controlling the duty cycle. As the shortest allowable switching time is increased this error becomes negligible. Given the statements made above, the duty cycle has been discretized in 100 incremental values, with a base frequency of 0.1 Hz, a duty cycle of 1% and 99% result in a switching time of 100 ms. The implementation details of the PWM signal generation by the DAQ card is given in chapter 7.

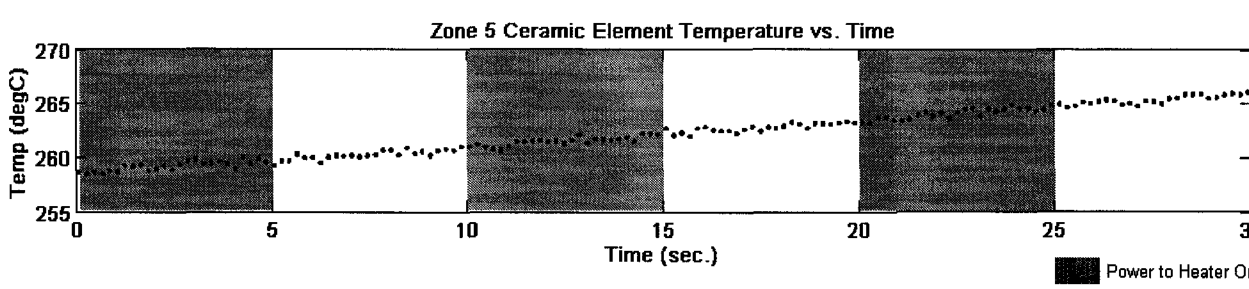

Figure 6.5: Element temperature vs. time with heating duty cycle of 50%.

Tests reveal that no appreciable temperature fluctuation of the ceramic heater occurs throughout the PWM cycle. This can be seen in Figure 6.5 where the temperature of the ceramic element is shown for a heating duty cycle of 50%. A thermo-couple with a small junction (32 wire gage) is used in this test. This reduces the time lag associated with the temperature measurements. The gray area indicates when the ceramic element is powered. It appears that there is no apparent correlation between the state of the heating element and the measured temperature. This is not surprising as the dominant open-loop time constant for this zone is on the order of 60 min. A PWM base frequency of 0.1 Hz corresponds to one six hundredth of this time constant.

6.2.2.3. Thermo couples and Signal Conditioner

Thermo-couples are used to monitor the oven temperature. Traditionally, for this type of oven, thermowells located directly in the ceramic heaters are used for temperature control purposes. The addition of the stainless steel tube in the oven creates a temperature difference between the ceramic heater and the heating zone. It is therefore required to monitor the temperature inside the tube directly. An attempt was made to measure the temperature inside the tube by inserting thermo-couples through the elements and small holes drilled in the heating tube. However, this method proved unreliable as heat generated by the ceramic heater travels through the thermo-couple leads and heats the measurement junctions thus giving false measurements.

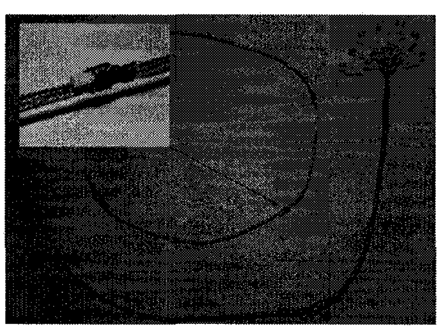

Figure 6.6: Wire mounted oven thermo-couples.

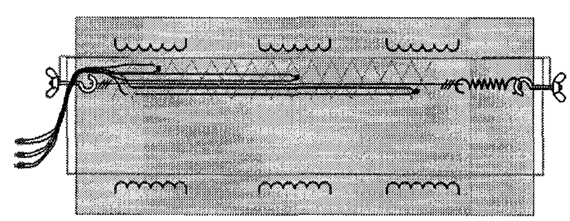

Figure 6.7: Schematic of oven thermo-couple arrangement.

To obtain reliable temperature measurements the thermo-couples are mounted on a taut steel wire inside the oven tube. A helical spring is used to compensate for any thermal expansion of the steel wire. As can be seen in Figure 6.6, the measuring junctions are maintained in position using double bore ceramic tubes that are fastened with annealed steel wire. The thermo-couple leads are covered with a braided cooper braid. The braid serves two functions, firstly, it protects the leads from mechanical and thermal damage, and secondly, it provides electromagnetic shielding. This proved a significant advantage due to the close proximity of the induction heater to the oven stage.

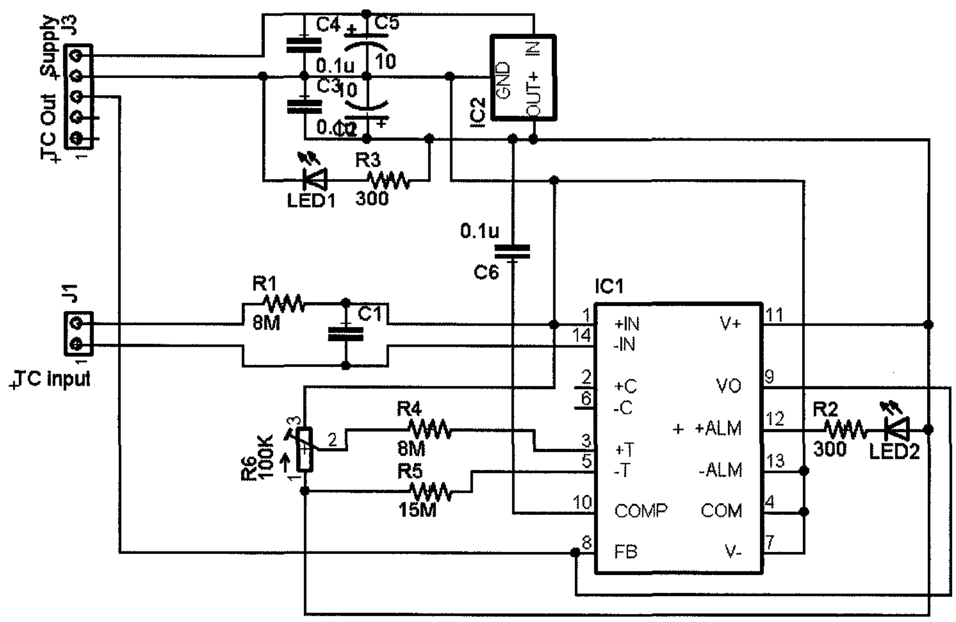

Figure 6.8: Schematic of oven thermo-couple signal conditioner PCB (one channel).

Thermo-couples produce a voltage proportional to the difference between the measurement junction temperature and a reference junction. Traditionally, a second thermo-couple submersed in an ice bath is used as the reference junction. Modern integrated circuits equipped with built-in temperature sensors eliminate the need of such reference thermo-couples. The nominal outputs of the thermo-couples are 41 μV/°C (Type K). Since small amounts of noise result in low signal to noise ratios, the transmission length at these levels must be kept short. For this reason, amplification of the thermo-couple signal is performed close to the ovens. To perform the functions described above a signal conditioning module was designed. The circuit diagram for one channel of this module is shown in Figure 6.8. The major components of the circuits are the Analog Device AD595 IC's which amplify the thermo-couple signal and provide an output which is linearly proportional to the thermo-couple temperature. Additional components are shown on the circuit schematic which allows for thermo-couple calibration, provides warning in case of an open input, ands add low-pass filtering of the thermo-couple input. The input filter R_1C_1 reduces the input bandwidth to approximately 5 Hz. The amplifier bandwidth is also limited by capacitor C_6 to approximately 100 Hz. The circuit supply is also filtered and the voltage regulated from 24V to 12V. This reduces the noise on the supply lines. To further reduce the effect of noise, a grounded, shielded cable connects the thermo-couple signal conditioning module and the DAQ cards. Finally, a bypass capacitor connects the amplified positive signal and ground leads. The bypass capacitors are inserted in the DAQ terminal block junctions.

6.2.2.4.Air injection system

The air purging system provides heat removal from the oven heating chamber. As previously mentioned, this is important due to the long time constant associated with the natural cooling of the heating chamber.

Low pressure air is provided by a 12 cm centrifugal blower powered by a DC motor. The speed of the blower motor is regulated by an external controller using tachometer feedback. The controller accepts a voltage command to externally control the motor speed.

Purging air is delivered to the oven tube using a galvanized conduit (Figure 6.9) and then injected in the heating chamber through two rectangular ports cut in the oven tube (Figure 6.12). A purging collar distributes the air evenly to each port. Braided glass ropes are used to form a seal between the purging collar and the oven tube (Figure 6.11). A tunnel shroud is placed inside the oven tube to prevent cool air from being blown directly on the product (Figure 6.12).

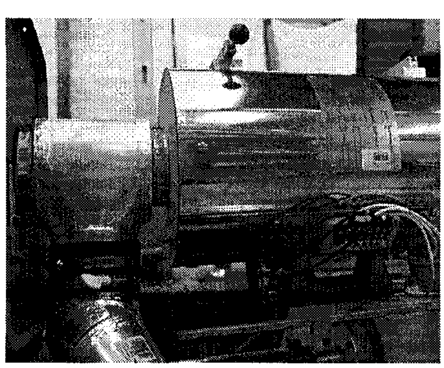

Figure 6.9: Detailed view of the purging collar located between the first and second ovens.

Figure 6.10: Detailed view of purging collar.

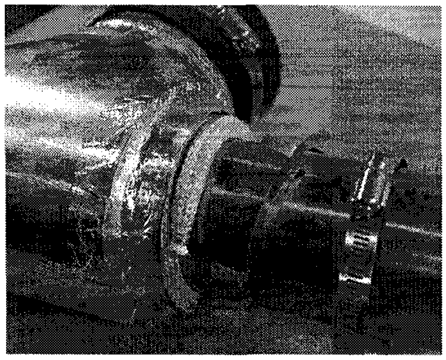

Figure 6.11: Detail of fibre glass seals around oven tube.

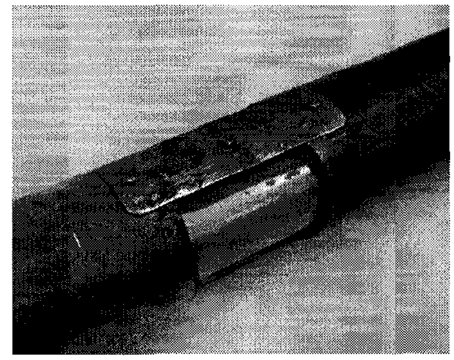

Figure 6.12: Detail of purging port in oven tube. The inner shroud prevents direct coolling of product.

6.2.3.Cooling Station

When the product exits the last curing oven its surface temperature can exceed 200°C. Damage to the puller belts can occur if the rod is not cooled before entering the pulling station. Since the distance between the oven mouth and pulling station is limited by lab space, sufficient cooling would not occur due to natural convection between the air and rod alone. Cooling using forced convection is therefore required. Cooling using air or water was considered. For a system of similar complexity, water cooling will enable a much higher heat flux than air cooling. This can be demonstrated by considering the relationship that governs a heat flux between external flows and cylinders:

$$h = Nu_d \frac{k}{D} \qquad 6.1$$

In the relation above, h is the heat flux, Nu_d is the Nusselt number, k is the flow thermal conductivity and D is the cylinder diameter. Several empirical relationships have been developed for calculating the Nusselt number for the given condition [62]. Using the Churchill relation [63], Nusselt numbers are found to be approximately 30 and 475 for air and water, respectively. Assuming a flow temperature of 25°C, a cylinder diameter of 0.1 m and flow rates of 10 and 1 m/s for air and water respectively, the thermal conductivity of air and water at room temperature is 26×10^{-3} and 613×10^{-3} W/mK respectively. This leads to a heat flux of 0.78 and 291W/m^{2}K for air and water respectively. Although only approximations, these results demonstrate that forced convection using water leads to considerably higher cooling rates.

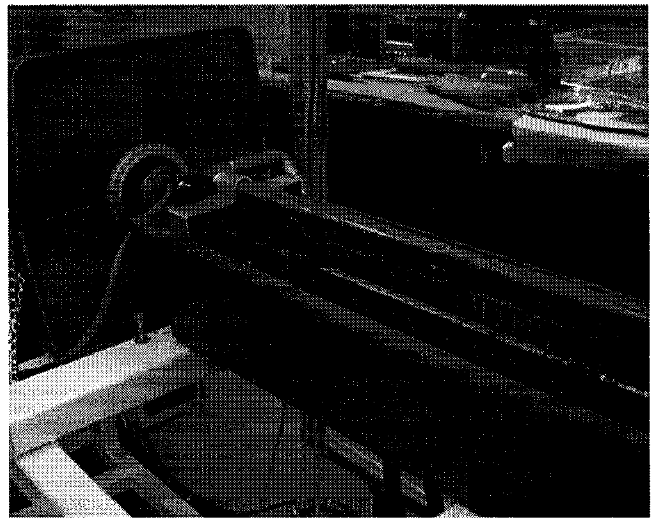

Figure 6.13: Product cooling station.

As shown in Figure 6.13, the cooling station consists of a copper pipe placed above and parallel to the rod. Holes drilled in the pipe allow water to flow onto the hot rod. The hole diameters are progressively increased from the inlet to provide uniform flow along the length of the tube. Used water is collected and returned to the building's drain. The water flow rate is adjusted manually using a gate valve.

The sudden cooling of the exterior of the rod creates a large temperature gradient in the rod. The effect of these temperature gradients should be investigated. More specifically it should be determined if residual stress are created by rapid cooling of the rod. If analytical theory indicates that residual stress occurs, experimental studies (computer simulation or mechanical testing) should be performed to evaluate these effects on the mechanical properties of the rod.

6.3.Electromagnetic Noise Consideration

Electromagnetic interference (EMI) such as the interference created by a hair dryer on television reception is a common phenomenon. Although EMI problems can cause annoying inconveniences in daily life, their effects can be crippling to industrial systems. Standard practices were followed to mitigate the effects of EMI throughout the pilot production plant; this includes the use of high quality shielded cables, analog low pass filtering of signals, metallic enclosures and spatial separation of components. Digital filtering and data averaging are also used.

Of all the equipment in use in the production line, the oven thermo-couples are the most vulnerable to EMI. To mitigate EMI within the thermo-couples, several counter-measures are used. These include covering the thermo-couple leads with a grounded braided copper sleeve and filtering the thermo-couple signal using the signal conditioning module. These were discussed in Section 6.2.2.3.

To identify radiation sources, and the effectiveness of counter-measures, an antenna composed of a pair of twisted wires was connected to an oscilloscope. Using this method, the main EMI generators were identified to be the control computer clock, the braider and puller variable frequency motor drivers, and the induction heater. It should also be noted that the Colonel-By basement (where the tests are performed) is an electrically noisy environment. It is suspected that EM noise may originate from an older HVAC system, fluorescent lights, or nearby lab activities. While investigating EMI problems it is found that the lab's main electrical panel is not grounded using dedicated grounding wires. Instead the steel electrical conduit is used as a grounding line. As most EMI counter measures rely on a proper grounding path, this likely compounds the EMI problems.

Of all the devices used in the production line, it is found that the induction heater generates the most EMI. This is not surprising as the induction unit is essentially a radio frequency magnetic field generator. Interference is identified using the antenna and oscilloscope method, and is seen to emanate from two areas, namely from the heating coil itself and from the external control terminals.

6.3.1. Induction Unit EMI

It was found that the interference generated from the heating coil could be significantly reduced by the addition of a Faraday cage around it. A Faraday cage is a closed chamber made of a conducting material that when placed in an electric field, generates a current which rearranges the charge distribution on the surface of the enclosure. Current continues to flow until the charge distribution on the surface of the enclosure results in electrical equilibrium. The result is a cancellation of the electric field inside the cage. If the field generator is placed inside the cage a similar behaviour is observed. Faraday cages do not block the static magnetic field, however, rapidly changing magnetic fields (such as in the induction heater) generate an electric field. Canceling the electric field also cancels the magnetic field. Examples of Faraday cages can be found in cell phones, microwave ovens and anti-static bags.

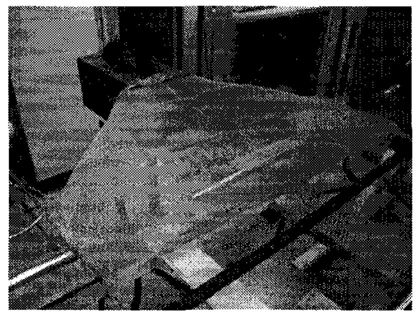

Figure 6.14: Prototype Faraday cage for the induction work coil.

As shown in Figure 6.14, a Faraday cage constructed of steel wire mesh was installed to completely enclose the work coil. Figures 6.15 and 6.16 show the measured voltage due to radiation from the unshielded and shielded work coil. The antenna and oscilloscope method was used to evaluate the effectiveness of the Faraday cage. In both cases, the antenna was placed parallel to the coil at a distance of approximately 10 cm. It can be seen that for the given case, the Faraday cage reduces the emitted radiation by approximately 29 dB.

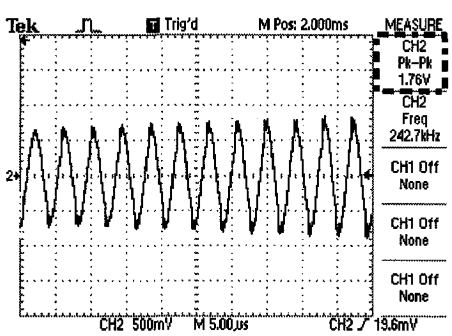

Figure 6.15: Measured voltage vs. time due to emitted radiation by induction work coil without Faraday cage.

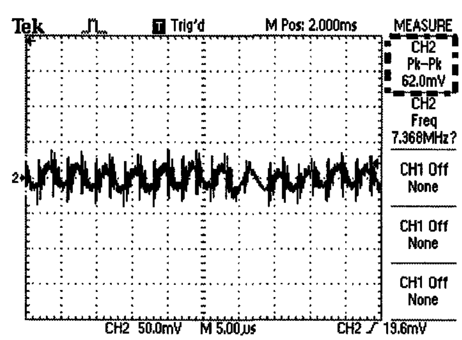

Figure 6.16: Measured voltage vs. time due to emitted radiation by induction work coil enclosed in Faraday cage.

6.3.2. Induction Unit Control Terminal EMI

The induction unit power output is controlled using an analogue voltage signal (0-10V) and two normally open connections (start/stop, emergency stop). It was found that a significant amount of noise emanated from these input terminals. Tests revealed that, once connected, the induction unit control wires became noise generators. When the control cable was routed in the control cabinet significant noise was observed on all analog and digital lines. Grounding the shield of the control cables does not significantly reduce the EM emissions. The use of a low pass RC (resistance/capacitance) filter on the control lines also has an insignificant impact in noise reduction. This is not surprising, since at radio frequencies the impedance of most capacitors is close to zero. The addition of a low pass LRC (inductance/resistive/capacitive) filter to the control lines reduced the generated noise level to acceptable values. Two unshielded wires wound around a toroidal ferrite bead (approximately 10 turns) provides the necessary inductance. A schematic of the circuit is shown in Figure 6.17.

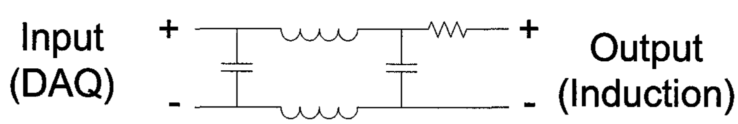

Figure 6.17: Schematic of induction heater line filter (one channel shown).

6.3.3. Counter Measure Validation

The effectiveness of the induction noise countermeasures were evaluated by measuring the standard deviation of analog voltage measurements. The results are shown in Table 6.2. Tests are performed by connecting a constant voltage source (9V battery) to one of the computer data acquisition analog input channels. All other connections to the terminal block were removed. Measurement samples were gathered at a sampling frequency of 100 Hz and the standard deviation was calculated every second.

Table 6.2: Measured standard deviation of analog input for different RF interference counter measures

Induction Heater State	Counter Measures	Standard Deviation on analog measurement
OFF	None Base line	1.1 mV
ON at 200A	None	105.1 mV
ON at 200A	Line filter only	2.2 mV
ON at 200A	Faraday cage only	43.2 mV
ON at 200A	Line filter and Faraday cage	1.3 mV

The line filters had the greatest effect in reducing the measurement noise. Since the noise reduction of the Faraday cage was minimal, it is currently not implemented. When both counter-measures are used the noise in analog measurements is reduced to a level close to the base-line measurement.

6.4. Curing Oven System Modeling

6.4.1. Overview

The control approach used for the resin curing process involves controlling the temperature of the heating chamber of a tunnel oven. This section will present the dynamic response of these ovens. A lumped parameter model was developed from basic principles and assumptions. Developing a model serves two purposes: Firstly, it allows for the exploration of the physical phenomena which affect the curing process within the oven stage. Secondly, it provides insight into the design of a satisfactory control system. In the present case the response of the resin curing process is not directly controlled. Instead, it is assumed that, if the correct oven temperature distribution is maintained, full curing will occur. The implication of this assumption will be discussed at the end of this section. As was shown in previous sections, the ovens are composed of several different materials. From a modeling point of view, the geometry and the construction of the ovens are relatively complex. Building a model from physical properties would prove difficult. The modeling approach will therefore focus on developing a model with identifiable parameters.

A schematic of the curing ovens system is shown in Figure 6.18. The sectional views of the ovens are depicted in Figure 6.19.

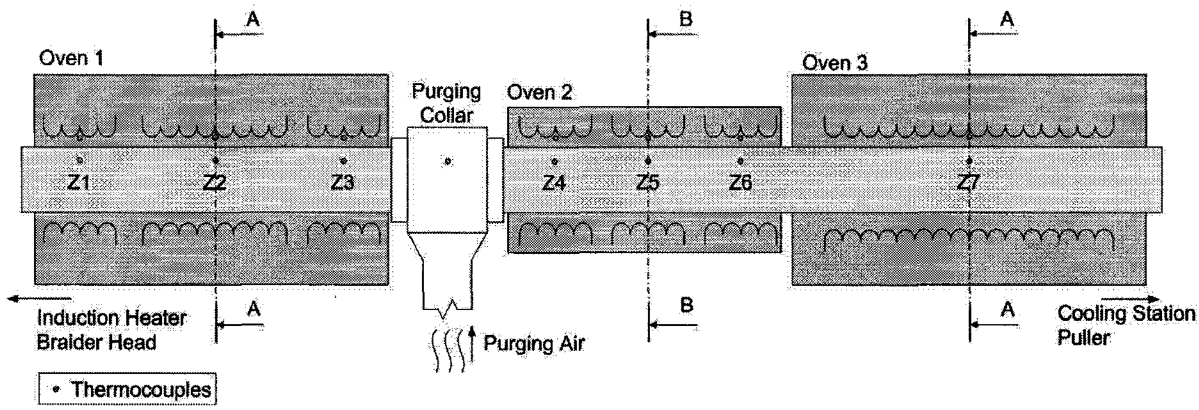

Figure 6.18: Schematic of curing oven system. Section views are shown in Figure 6.19.

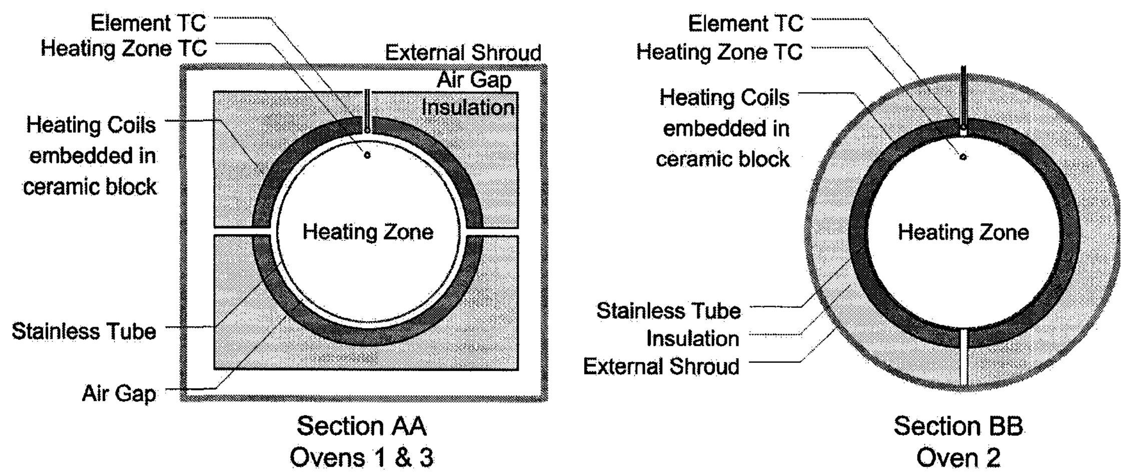

Figure 6.19: Sectional view of the curing ovens.

Ovens 1 & 3 are manufacturer by Lindberg. Oven 1 is divided into three zones, whereas oven 3 is a single-zone oven. The construction of oven 1 and 3 are identical with the exception that the heating coils of oven 1 are covered with a refractory material as opposed to the exposed coils of oven 3. Oven 2 is divided in three zones and is manufactured by Santec Systems. This oven is smaller in size and is cylindrical. For all ovens, heat is produced from coiled nickel chromium wires. The wires are embedded in semi-circular ceramic blocks. For ovens 1 and 3 one of the blocks is located above and below each heating chamber. For these ovens, an air gap of approximately 15 mm separates the interior surface of the heating elements and the outside of the heating tube. For oven 2, the blocks are located on each side of the heating tube and there are no appreciable air gaps between the element and the tube. For this oven, the ceramic block is in direct contact with the heating tube. For all ovens, the stainless steel heating chamber is surrounded by the heating blocks, which are in turn surrounded by insulation. The insulation of ovens 1 and 3 is composed of a rectangular box surrounded on all sides by a 40 mm thick air gap and external steel shroud. The insulation of oven 2 is cylindrical with the shroud directly covering the insulation without an air gap.

6.4.2. Preliminary Assessment of System Behaviour

To better understand the relationship between the oven power (process input) and heating chamber temperatures (process output) open-loop step tests were conducted for each zone. In each case only one element was activated and three step commands were issued. One such response, for zone 5, is shown in Figure 6.20. Several observations can be made from this figure. One is that the open-loop response is under-damped. This is expected as physical thermal systems have no second-order states. The dominant time constant for this zone is in the order of 60 minutes. This is attributed to the high thermal capacitance of the ceramic which encases the heating wires. Heat transfer occurs primarily from the heating element to the heating chamber. Heat transfer also occurs between heating chambers. This is not surprising, as each chamber shares a boundary.

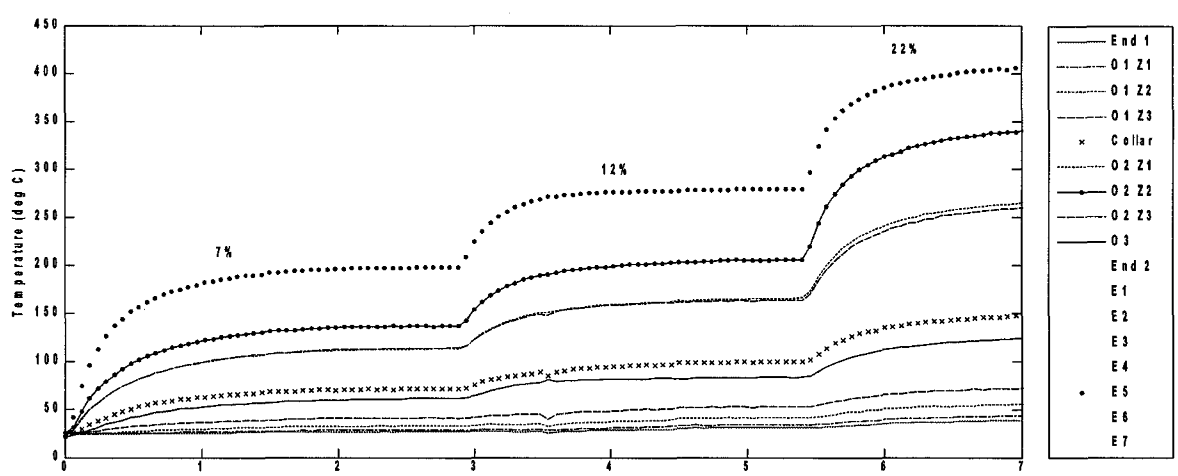

Figure 6.20: Heating zone and element temperature vs time for three step commands of zone #5 (O=Oven, Z=Zone, E=Element, End1=mouth of oven). Legends without symbols are not plotted.

For each of these responses, parameters of a first order transfer function are estimated by least square fitting. One estimate is obtained for each step command. Three gains and three time constants are therefore obtained for each zone response. These parameters are listed in Table 6.3. The transfer function input corresponds to the element duty cycle, and the output to the corresponding heating chamber temperature.

$$cT(s)s + kT(s) = bU(s) \qquad 6.2$$

Rearranging gives,

$$\frac{T(s)}{U(s)} = \frac{b/k}{c/k\,s+1} \qquad 6.3$$

In this context, c is the effective thermal capacitance, k is the thermal energy losses to the environment and b is the input coefficient. Collecting coefficients of Equation 6.3,

$$\frac{T(s)}{U(s)} = \frac{K_p}{\tau s+1} \qquad 6.4$$

the transfer function coefficients are simplified into two parameters, the gain (K_p) and time constant (τ). This function is analogous to a first-order RC filter. In this context, the gain represents the ability of the heating elements to change the heating chamber temperature given the thermal losses. The time constant indicates the responsiveness of the system from the perspective of each heating chamber.

Table 6.3: First order process model properties for oven heating chambers

Oven/ Zone	**Open-loop Command (u)**			**Process Gain (K_p)**				**Time Constant (τ)**			
	Step 1	***Step2***	***Step3***	***Step1***	***Step2***	***Step3***	***AVG***	***Step1***	***Step2***	***Step3***	***AVG***
O1/Z1	10	20	30	12.6	10.2	9.16	10.65	6917	5733	3879	5509
O1/Z2	10	20	30	18.4	17.9	16.3	16.3	8882	9174	7003	8353
O1/Z3	10	20	30	11.5	10.5	9.61	10.54	8234	9873	4729	7612
O2/Z4	7	12	22	18.5	16.6	14.9	16.67	3917	4348	3193	3819
O2/Z5	7	12	22	19.6	17.1	15.5	17.4	4798	4129	3699	4208
O2/Z6	7	12	22	17.7	15.9	13.7	15.77	3924	5109	2749	3927
O3/Z7	10	20	30	8.18	6.87	6.42	7.16	6031	6204	6346	6193

It will be shown in following sections that coupling between zones renders single input and single output (SISO) modeling invalid when more than one zone is energized. The results shown above apply to a specific initial condition, i.e. when a single element is energized. In essence, this approach models the behaviour of the entire oven system but from the perceptive of a specific zone. Although the results do not apply for the cases when more than one element is energized, several observations about the dynamic behaviour of individual zones can be made from these experimental results.

- For all zones, the steady state gain decreases as the heating chamber temperature increases. This result may be attributed to two factors. The first is that the heat output from the heaters decreases as the temperature increases. As the heating coil temperature increases so does it's resistance. As the supplied voltage is constant this leads to a decreases in electrical losses. A second factor, may be that heat loss increases as the oven system temperatures increases.
- The central zones (Z2 and Z5) of ovens 1 and 2 have higher gains than the zones located at the ends of the ovens. This is attributed to the higher heat loss (k) which would occur at the outer ends of each oven.
- The results for oven 2 have the highest average gain of all three ovens. Oven 2 is located in the center of the heating chamber. It is logical to assume that less heat loss will occur through the outer ends of the oven due to the higher thermal resistance from the long heating tube located on each side of this oven. In contrast with ovens 1 and 3, there is only a very small air gap between the elements and the heating tube. This would lead to a significant increase in heat flow through conduction compared with the two other ovens.
- The results for oven 3 have the lowest gain out of the three ovens. Ovens 1 and 3 are of similar construction. As shown in Table 6.1, the power of oven 3 is approximately half of the total power of oven 1. It is interesting to note that the gain of oven 3 is approximately half of the average gains of oven 1.
- Although it is not true for all cases, the trend in the time constants indicate that as the oven temperature increases the time constants decrease. As with the process gains, this may be attributed to an increase in heat flow as the temperature increases.
- The time constants of oven 2 are the smallest. Physically, this oven is smaller. Since the materials used in the construction of all of the ovens is similar, it is logical to assume that the smaller oven will have a lower total thermal

capacitance compared to larger ovens. The time constants of oven 1 and 2 differ by 46%. In contrast, the average time constant of ovens 1 and 3 differ by only 13%.

- The average time constants of the central zones (Z2 and Z4) are higher than the time constants of end zones. Again, this may be attributed to the lower thermal losses of central zones in comparison to end zones. Physically, central zones have more effective thermal inertia as they must heat surrounding zones before the system reaches a steady state.

6.4.1. Definition of Control Volumes

The temperature within the heating chamber will vary continuously along the length of the heating chamber. From a modeling point of view, the geometry of the ovens is fairly complex. The development of a distributed parameter model would require significant effort which is outside the scope of this work. Instead, a lumped parameter approach is used to model the oven process. For modeling and control purposes it is therefore assumed that the temperature within a heating chamber is uniform. The temperature of the oven system components (heating wire, ceramic block, stainless steel tube, air, insulation, steel shroud) will affect the dynamic response of the oven. From a practical perspective, it is not necessary to include all of the oven components in a system model.

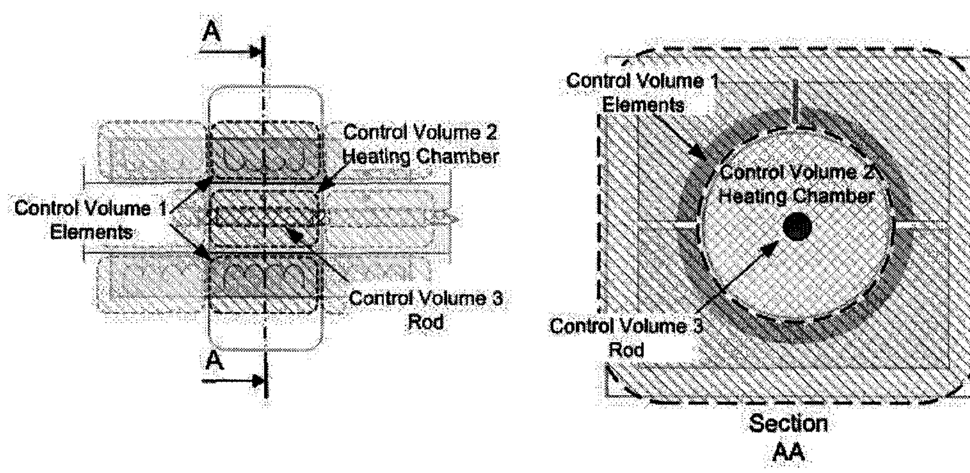

Figure 6.21: Curing process control volumes used in lumped capacitance model.

It seems logical that each zone is considered individually as three separate control volumes (CV), namely the elements, the heating chamber and the rod CV. These CVs are depicted in Figure 6.21. The elements CV includes the heating wire, the ceramic blocks, the insulation and the external shroud. The heating chamber CV includes the heating tube and the air within the tube. The rod CV is spatially fixed and includes the section of the product located within each zone. As previously mentioned, this work will not explicitly control the dynamics of the rod (curing process). Nevertheless, in order to understand the system as a whole, the energy balance of the rod is calculated below.

6.4.2. Energy Balance

The energy balance for each control volume is expressed using first principles as follows:

$$\begin{aligned}&\dot{Q}_{cv}+\sum \dot{m}_{\text{in}}(h_{\text{in}}+V_{\text{in}}^2/2+gz_{\text{in}})\\&\quad=W_{cv}+\sum m_{\text{out}}(h_{\text{out}}+V_{\text{out}}^2/2+gz_{\text{out}})\\&\quad+\left[\frac{m_2(u_2+V_2^2/2+gz_2)-m_1(u_1+V_1^2/2+gz_1)}{\Delta t}\right]\end{aligned} \tag{6.5}$$

For all of the control volumes the variations in kinetic and potential energy are negligible. Furthermore no external work is performed, therefore $W_{CV}=0$. Each control volume contains components made out of different materials; therefore it is convenient to express the energy balance in terms of total enthalpy and internal energy.

$$\dot{Q}_{cv}+H_{\text{in}}=H_{\text{out}}+\left[\frac{U_2-U_1}{\Delta t}\right] \tag{6.6}$$

The materials contained within the element CV are solid, and therefore, no mass enters or leaves the CV. The energy balance for the element CV is therefore represented by the following equation:

$$\dot{Q}_E=\left[\frac{(U_{\text{E2}}-U_{\text{E1}})}{\Delta t}\right] \tag{6.7}$$

The heating chamber CV. shares an open boundary with adjacent heating chambers and with the environment (in the case of zone 1 and 7). Air is therefore free to flow in and out of the heating chamber.

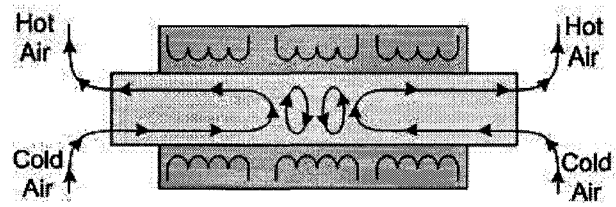

Figure 6.22: Hypothetical oven chamber flow induced by natural convection.

In the presence of a temperature gradient between heating chambers, an air flow is induced by natural convection. A hypothetical flow regime for a simplified version of the curing oven is shown in Figure 6.22. As depicted in the figure, warm air rises in the oven chamber and exits from the top section of the tube. This draws cool air from the environment to enter into the lower section of the tube. Due to a change in the refractve index of the warm air this phenomenon can be observed. It is also suspected that the flow is more pronounced for the heating chambers located at the end of the chamber. This is supported through experimental observation. When the same heat input is provided to the oven zones, the central heating chamber temperature always exceeds the end heating chamber temperatures. There is no practical way of measuring the flow through the heating chamber boundary. The ability to predict the flow from physical principles is limited by the lack of instrumentation needed in order to obtain the spatial temperature distribution in the heating chamber. In fact, even if an applicable model were available to predict the flow, it is doubtful that it could yield results which could be useful in a control context. Given the inability to measure or predict the air mass flux for each heating chamber the effect of mass flow between heating chambers is treated as an unknown disturbance. The heating chamber energy balance becomes:

$$\dot{Q}_C = \frac{U_{C2} - U_{C1}}{\Delta t} + D_{airExchange} \qquad 6.8$$

In both cases the subscripts 1 and 2 refer to the initial state and the final states after time Δt, respectively. The variation of internal energy may be approximated using $U_2 - U_1 = C \Delta T$. This amalgamates the mass and the specific heat of all substances contained withing the control volume. In this case air in the heating chamber CV is treated as a perfect gas. Since the air pressures and temperatures are low this is a valid assumption. The energy balance for the element and heating chamber CVs are then calculated as follows:

$$\dot{Q}_E = c_E \frac{\Delta T_E}{\Delta t} \qquad 6.9$$

$$\dot{Q}_C = c_C \frac{\Delta T_C}{\Delta t} + D_{airExchange} \qquad 6.10$$

If $\Delta t \rightarrow 0$, a first order ordinary differential equation is obtained.

$$\dot{Q}_E = c_E \frac{dT_E}{dt} \qquad 6.11$$

$$\dot{Q}_C = c_C \frac{dT_C}{dt} + D_{airExchange} \qquad 6.12$$

The relationship of Equations 6.11 and 6.12 state that the temperature of a CV is a function of the CV thermal capacitance and the heat flow to and from the CV. The form of the equation is consistent with the response results presented in Figure 6.20.

A similar derivation is performed for the rod CV. In this case, mass is continuously entering and leaving the CV. The internal energy of the rod within the CV may also fluctuate. Therefore the energy balance for the rod becomes:

$$\dot{Q}_R = H_{Rout} - H_{Rin} + c_R \frac{dT}{dt} \qquad 6.13$$

6.4.3. Heat Transfer

Heat flow between control volumes is assumed to occur through a combination of conduction, convection and radiation. For the heater CV, heat is also produced by resistive losses in the heating wire. This energy is externally supplied and is therefore included in the heat flow term. In the case of the rod CV, heat may be consumed or produced by the resin curing chemical reaction. This chemical reaction energy is included in the rod CV heat flow term as follows:

$$\dot{Q}_{CVheater} = P_{\text{in}} + \dot{Q}_{cond} + \dot{Q}_{conv} + \dot{Q}_{rad} \qquad 6.14$$

$$\dot{Q}_{CVHeatingChamber} = \dot{Q}_{cond} + \dot{Q}_{conv} + \dot{Q}_{rad} \qquad 6.15$$

$$\dot{Q}_{CVRod} = \dot{Q}_{resin} + \dot{Q}_{cond} + \dot{Q}_{conv} + \dot{Q}_{rad} \qquad 6.16$$

The following three sections will present the governing equations for each type of heat transfer. Heat flow between the element and heating chamber CVs occurs between the semi-circular elements and the heating tube. Similarly, heat flow between the heating chamber and rod CVs occur between cylindrical bodies. Therefore, specific attention is given to the case of heat transfer between two concentric cylinders.

6.4.3.1. Conduction Heat Transfer

Heat transfer by conduction occurs through energetic transfer at the molecular level. Energy transport occurs through kinetic interaction between molecules of a high energy state to molecules of lower energy states. On a macroscopic level heat transfer by conduction is governed by Fourier's law;

$$Q'' = -k \nabla T \qquad 6.17$$

In this case Q'' is the heat flux per unit area, k is the thermal conductivity, and ∇T is the three dimensional temperature field. For one dimensional heat flow the equation is often written in terms of thermal resistance.

$$Q'' = \frac{T_a - T_b}{r''_{cond}} \qquad 6.18$$

The thermal resistance, r''_{cond}, is a function of the geometry and material properties of the body, where T_a and T_b are the respective temperatures of point A and B where heat flow is occuring. In the case of conduction through a cylindrical body the thermal resistance is:

$$r'_{condCyl} = \frac{\ln(r_o/r_i)}{2\pi k} \qquad 6.19$$

where r_o and r_i are the exterior and interior radii receptively, of the cylindrical body and k is the thermal conductivity. The resulting heat flow per unit length of cylinder is given by:

$$Q'_{condCyl} = \frac{2\pi k}{\ln(r_o/r_i)}(T_o - T_i) \qquad 6.20$$

6.4.3.2. Convection Heat Transfer

Heat transfer by convection occurs by bulk, or macroscopic, motion of a fluid. The phenomenon occurs when a temperature difference exists between a fluid and a surface. Convection is categorized according to the nature of the flow. Forced convection occurs when the flow is caused by an external source such as a fan, pump, or atmospheric winds. In contrast, the flow in natural convection occurs due to buoyancy forces which arise from variations in fluid density due to temperature gradients within the fluid. For the present case no external flow is provided. The remainder of this analysis will therefore consider the effects of natural convection. It should be noted that the effects of forced convection due to purging air will be discussed in section 6.5. The governing equation for convection heat transfer is termed Newton's Law of Cooling.

$$Q''_{conv} = h_{conv}(T_s - T_\infty) \qquad 6.21$$

where h_{conv} is the convection coefficient and, T_s and T_∞ are the surface and free stream temperatures, respectively. The convection coefficient is affected by several factors such as geometry, the stream velocity and temperature, and the surface temperature, etc. Although there are some analytical solutions to simple convection problems, most convection problems are solved using empirical models or computer simulations. In the case of an empirical solution, each model is applied to a particular geometry and is valid over a specific range of parameters. An empirical model of this type was developed by Raithby and Hollands [64] for natural convection of concentric cylinders. In this case, the heat transfer per unit length of cylinder is given by:

$$Q'_{ConvCyl} = \frac{2\pi k_{eff}}{\ln(D_o/D_i)}(T_i - T_o) \qquad 6.22$$

The relationship predicts the increase in heat transfer due to the effects of natural convection. The effective thermal conductivity, k_{eff} is gaged such that a stationary fluid should have to transfer the same amount of heat as the moving fluid. The suggested correlation for k_{eff} is expressed as follows:

$$\frac{k_{eff}}{k} = 0.386\left(\frac{Pr}{0.861 + Pr}\right)^{0.25}(Ra_c^*)^{0.25} \qquad 6.23$$

where Pr is the Prandtl number and Ra_c^* is the modified Rayleigh number which is related to the standard Rayleigh number by:

$$Ra_c^* = \frac{[\ln(D_o/D_i)]^4}{L^3(D_i^{-3/5} + D_o^{-3/5})^5} Ra_L \qquad 6.24$$

The standard Rayleigh number is the ratio between buoyancy and viscous forces and is given by.

$$Ra_L = \frac{g\beta(T_i - T_o)L^3}{\nu\alpha} \qquad 6.25$$

where g is the gravitational constant, β for a perfect gas is $min(1/T_s, 1/T_\infty)$, L is the characteristic length $(r_o - r_i)$, ν is the stream kinematic viscosity and α is the stream thermal diffusivity.

6.4.3.3. Radiation Heat Transfer

Most matter, be it solid, gas or liquids emits radiative energy. The energy of a radiation field is transported by electromagnetic waves. The radiation heat transfer between a surface and a much larger surrounding is expressed per unit area as follows:

$$Q''_{rad} = \epsilon\sigma(T_s^4 - T_{sur}^4) \qquad 6.26$$

The expression assumes that the surface at temperature T_s^4 is for a gray body and that the surrounding is a black body at temperature T_{sur}^4. A black body is a surface which demonstrates perfect absorption and emission according to the Stefan-Boltzmann spectral distribution. For a gray body it is assumed that the surface emissivity and absorptivity are equal and do not vary with wavelength. The scaling factor ϵ is the surface emissivity while σ is the Stefan-Boltzmann constant. When radiation heat transfer occurs between two enclosed surfaces of similar sizes the geometry of the problem must be considered. For an infinitely long concentric cylinder composed of gray diffuse surfaces the heat flow per unit length is given by:

$$Q'_{radCyl} = \frac{\sigma 2\pi r_1(T^4{}_1 - T^4{}_2)}{\frac{1}{\epsilon_1} + \frac{1-\epsilon_2}{\epsilon_2}\left(\frac{r_1}{r_2}\right)} \qquad 6.27$$

In this case the subscripts 1 and 2 refer to the small and large cylinders, respectively. In the present analysis the effect of radiation from the air located in the CVs is neglected. In the case of diatomic gases such as O_2 and N_2, this is justified since the gas does not emit radiation and is transparent to incident radiation. Polyatomic gases such as CO_2 and H_2O which are present in air emit radiation. The emissivities of these gases are proportional to the partial gas pressure times the beam length (characteristic distance between surfaces). In the present case these values are in the order of 0.008 and 0.001 for water vapor and CO_2, respectively. This translates to emissivities in the order of 0.02 and 0.006 for the water vapor and CO_2, respectively. Therefore, due to the small beam length and low concentration of the principle polar gases contained in air, neglecting the volumetric radiation of the air is justifiable.

6.4.3.4. Comparison of Heat Transfer Modes

In previous sections, equations were presented which estimate the heat flow between two concentric cylinders by conduction (Equation 6.20), natural convection (Equations 6.22 to 6.25) and radiation (Equation 6.27). In this section, these equations are used to predict the contribution of each type of heat transfer mode which occurs between the element and heating chamber CVs.

Sample calculations were performed for the heat flow between the heating element (element CV) and the stainless steel heating tube (heating chamber CV). The example was carried out according to the geometry and material of oven 1 (Figure 6.19). For this oven, the elements' heating coils are covered with a refractory material. There is a cylindrical air gap between the surface of the elements and heating tube. The heat flow was considered to be under a steady-state condition and was calculated for several temperature combinations. In all cases the temperature difference between the element surface and the tube surface is assumed to be 100° C. This value is consistent with element and heating chamber temperatures as observed from the oven responses such as the ones presented in Figure 6.20. Relevant data for the calculations are presented in Table 6.4. The results are presented graphically in Figure 6.23.

Table 6.4: Data for heat flow estimate between element and heating tube of oven 1

Properties	Values	Unit
r_i / r_o	0.07 / 0.10	m
T_i / T_o	400/500, 500/600, 600/700, 700/800	K
k_{air} [a]	37.3, 43.9, 49.7, 54.9	$10^3 (W/m{\cdot}K)$
α_{air} [a]	32.39, 45.57, 60.21, 76.37	$10^6 (m^2/s)$
ν_{air} [a]	47.2,66.7,87.3,109	$10^6 (m^2/s)$
Pr_{air} [a]	0.686,0.683,0.69,0.702	-
ϵ_i (Stainless Steel)	0.28 (New/Clean) to 0.9 (Highly oxidized) [65]	-
ϵ_o (Refractory)	0.8 to 1.0 [65]	-

[a] Properties taken at mean temperature $T_m = (T_i + T_o)/2$

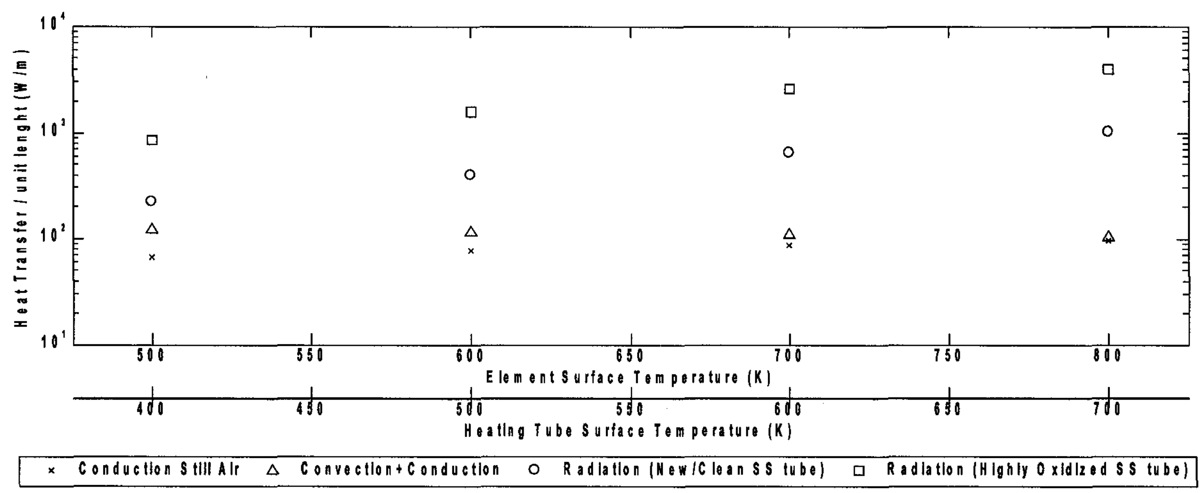

Figure 6.23: Heat flow through conduction, convection and radiation between the element and heating tube for various temperatures for oven 1.

The results indicate that the contribution of natural convection becomes negligible as the temperature increases and that the bulk of the heat flow occurs through radiation. The thickness of the chromium oxide layer on the stainless steel is dependent on the service temperature, the duration of time at the elevated temperature, and the number of elevated temperature cycles. The variation in the quantity of surface oxides will affect the emissivity properties of the surface. A comparison was made for two extreme cases; one corresponding to a tube of new stainless steel material and the other to a highly oxidized stainless steel. In these cases the range in emissivity is between 0.24 for a new (shiny tube) and 0.9 for an oxidized tube. For less extreme cases, emissivity values can fall in this range depending on the degree of oxidization of the surface. As the heating tube is in service, changes in the surface color and specularity are observed. If under normal operating temperatures the oxide formation stabilizes, it is reasonable to assume that after a break-in period the emissivity value will also remain constant. Regardless of the exact emissivity properties of the heating tube it is assumed that the majority of heat flow between the element and heating chamber CVs occurs through radiation.

6.4.3.5. Electrical Heat Input

The power provided by the electrical heaters is a function of the heating wire resistance R and the supply voltage V. As previously discussed PWM is used to vary the element power over each sampling time. The heater power is given by:

$$P_{\mathrm{in}}=V^2/R_{heater}\times DC \qquad 6.28$$

where DC is the duty cycle

When PWM is used to control the power, it is common to maintain the supply voltage is constant. As the heating wire temperature increases so does its resistance. To verify the effect of this non-linearity an ammeter was used to monitor the element current. In one experiment, the coil was energized from room temperature until a red glow was visible. No appreciable changes in the heating coil current was observed. This result is supported by literature which state that the nominal temperature coefficient of resistance for 80% Ni/ 20 % Cr heating wire is 0.00011 Ω/Ω/°C [66]. This translates to an increase in wire resistance of 5.5% over a 500° C range. It can therefore be assumed that over the operating temperature of the ovens, the effects of increased heating wire resistance can be ignored. This is especially true given other sources of process non-linearity (such as radiative heat transfer). The heater power becomes a function of the duty cycle only and may be expressed as:

$$P_{\mathrm{in}}=b\times Duty\ Cycle=bu \qquad 6.29$$

where b is the input coefficient.

6.4.3.6.Heat Transfer Paths

Based on the oven system construction, and observation of the process responses such as the ones presented in Figure 6.20, the formulation of the following hypotheses involving principle heat transfer paths between CVs are made:

- Heat loss to the environment occurs from the element and heating chamber CVs located at the ends of the heating chamber (corresponding to zone 1 and 7). To some extent heat may also be lost to the environment through the zones adjacent to the purging collar (corresponding to zones 3 and 4).
- Heat in the heating chamber CVs are primarily gained through heat flow from associated elements.
- Heat flow occurs between adjacent zones. As previously discussed, mass flow is likely to occur due to natural convection.

The observations outlined above are schematically represented in the form of a thermal resistive diagram shown in Figure 6.24. In the next section hypotheses relating to principle heat transfer paths are used to build a linear, time-invariant model of the oven system.

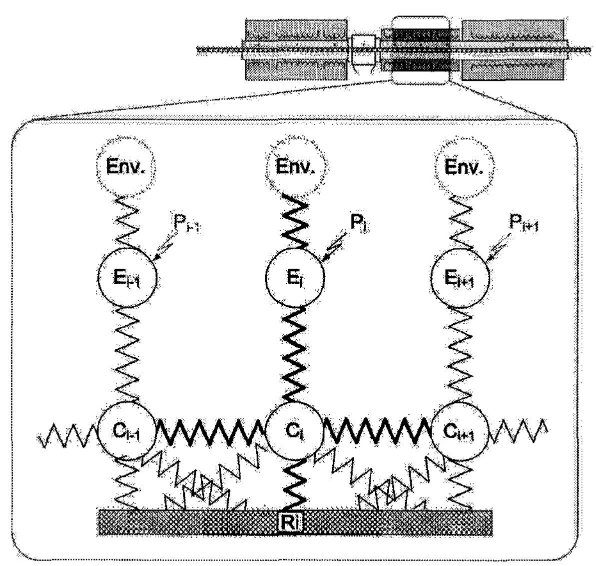

Figure 6.24: Thermal resistivity model of tunnel oven. heating element and heating chamber considered as control volumes.

6.4.1.Linear Time Invariant Model

In previous sections, the governing equations for a lumped parameter thermal model were applied to the curing oven system. This modeling approach led to an energy balance being performed for each element, heating chamber and rod CVs. A first order differential equation was obtained for each of these control volumes. The equation predicts that the dynamic behaviour of each of the CVs is a function of the heat flow through the CV boundaries and the respective heat capacitance of each control volume. The equations relating to heat transfer by conduction, natural convection, and radiation between two concentric cylinders are presented. An illustrative example using these equations shows that the bulk of the heat flow between the element and heating chamber CVs occurs through radiation. Although it is not demonstrated, it is also believed that the same statement is true for the heat flow between the heating chamber and rod CVs.

For convenience, the relevant equations are repeated below.

Equation 6.11 (p.147): $\dot{Q}_E = c_E \frac{dT_E}{dt}$

Equation 6.12 (p.147): $\dot{Q}_C = c_C \frac{dT_C}{dt} + D_{airExchange}$

Equation 6.14 (p.147): $\dot{Q}_E = P_{in} + \dot{Q}_{cond} + \dot{Q}_{conv} + \dot{Q}_{rad}$

Equation 6.16 (p.147): $\dot{Q}_C = \dot{Q}_{cond} + \dot{Q}_{conv} + \dot{Q}_{rad}$

Equation 6.29 (p.153): $P_{in} = bu$

Equation 6.18 (p.148): $Q''_{cond} = k_{cond}(T_a - T_b)$

Equation 6.21 (p.149): $Q''_{conv} = h_{conv}(T_a - T_b)$

Equation 6.26 (p.150): $Q''_{rad} = \epsilon\sigma(T_a^4 - T_b^4)$

For Equations 6.18, 6.21 and 6.26 the nomenclature of the temperatures are changed to make them more general. In this case the subscripts a and b refer to the appropriate surface temperatures between which the heat flow takes place. For example, in the case of the heat flow between the element and the heating chamber CVs, T_a would refer to the surface temperature of the heating element while T_b would refer to the temperature of the heating tube. At this point it becomes apparent that the number of parameters exceeds the number of instrumentation values. As previously stated, thermo-couples are used to monitor the temperatures of the air of each heating chamber. Thermo-couples also monitor the temperature of the heating element. In both cases, the thermo-couples do not explicitly monitor the temperatures of the surfaces. For modeling purposes it is therefore assumed that a correlation exists between the measured temperatures (heating chamber and element) and the actual surface temperatures.

Since one of the goals of this work is to construct a linear system model, another problem must be discussed regarding this particular modeling approach. Heat transfer by radiation is non-linear with respect to temperature. In fact, as shown by Equation 6.26, the phenomenon varies by the fourth power of the surface temperatures. It is suggested by Incropera and DeWitt [67] that the radiation heat flow can be linearized by assuming that:

$$h_{rad}=\epsilon\sigma(T_a+T_b)(T_a^2+T_b^2) \qquad 6.30$$

This simplification will only be valid about a specific operation point. About this point, the total radiative heat flow may be expressed as follows:

$$Q_{rad}=h_r(T_a-T_b) \qquad 6.31$$

Linearization allows for the combination of all heat transfer modes into one term. The heat flow term for the element (Equation 6.14) and its heating chamber CVs (Equation 6.16) can now be expressed as follows:

$$\dot{Q}_E=b_i u_i+k_{a\Leftrightarrow b}(T_a-T_b) \qquad 6.32$$

$$\dot{Q}_Z=k_{a\Leftrightarrow b}(T_a-T_b) \qquad 6.33$$

where $k_{a\Leftrightarrow b}$, represent the heat transfer coefficient between surface *a* and *b*.

From the thermal resistivity diagram presented in Figure 6.24, the element energy balance (Equation 6.11), and the linearized element heat flow term (Equation 6.32), the following equation is obtained for each element CV:

$$c_{Ei}\frac{dT_{Ei}}{dt}=b_i u_i-k_{Ei\Leftrightarrow Ci}(T_{Ei}-T_{Ci})-k_{Ei\Leftrightarrow env}(T_{Ei}-T_{env}) \qquad 6.34$$

Similarly, using Equation 6.12 and 6.35 the following is obtained for each heating chamber CV:

$$\begin{aligned}c_{Ci}\frac{dT_{Ci}}{dt}=&k_{Ei\Leftrightarrow Ci}(T_{Ei}-T_{Ci})-k_{Ci\Leftrightarrow Ci-1}(T_{Ci}-T_{Ci-1})-k_{Ci\Leftrightarrow Ci+1}(T_{Ci}-T_{Ci+1})\\&-k_{Ci\Leftrightarrow Ri}(T_{Ci}+T_{Ri})-k_{Ci\Leftrightarrow Ri-1}(T_{Ci}+T_{Ri-1})-k_{Ci\Leftrightarrow Ri+1}(T_{Ci}+T_{Ri+1})\\&+D_{airExchange}\end{aligned} \qquad 6.36$$

As previously discussed the states of the rod CV are not controlled. The heat flow between the heating chamber and rod CVs is therefore considered as an unknown disturbance. Grouping the terms which relate to heat flow to and from the rod CV result in the following expression:

$$Di=-k_{Ei\Leftrightarrow Ri}(T_{Ci}+T_{Ri})-k_{Ci\Leftrightarrow Ri-1}(T_{Ci}+T_{Ri-1})-k_{Ci\Leftrightarrow Ri+1}(T_{Ci}+T_{Ri+1}) \qquad 6.37$$

where D_i, is the disturbance caused by the rod in each oven section. Furthermore, it is reasonable to assume that the intensity of natural convection between adjacent heating chambers will correlate to the difference in temperature between the chambers. The effect of the air exchange disturbance ($D_{airExchange}$) is therefore included in the heat flow term which occurs between adjacent chambers.

Equation 6.36 then becomes:

$$c_{Ci}\frac{dT_{Ci}}{dt}=k_{Ei\Leftrightarrow Ci}(T_{Ei}-T_{Ci})-k_{Ci\Leftrightarrow Ci-1}(T_{Ci}-T_{Ci-1})-k_{Ci\Leftrightarrow Ci+1}(T_{Ci}-T_{Ci+1})+D_i \qquad 6.38$$

Equations 6.36 and 1 are expressed in matrix form as follows:

$$\dot{\bar{T}}=A\bar{T}+B\bar{U}+\bar{D}+K_{env}T_{env} \qquad 6.39$$

The resulting matrix equation has 14 states (7 heating chambers + 7 elements). The thermal capacitance and heat flow coefficients are amalgamated in the state transition matrix, A. Matrix B is the input matrix, $\bar{U}$ is the input vector and D is a time-dependent vector and is a function of the disturbance caused by the rod. The term $K_{env}T_{env}$ is composed of extraneous variables which represent a part of the effects of the heat lost to the environment. If T_{env} is assumed constant, the term becomes part of the initial condition of the problem and may be neglected in the controller design

It is interesting to note that Equation 6.39 is essentially a MIMO version of the first order SISO transfer function presented in Equation 6.2 (p.142). It becomes clear from Equations 6.34 and 6.38 why several decoupled SISO transfer functions cannot be used to model the oven system. Doing so would neglect the coupling between state variables. This is equivalent to saying that the state transition matrix (A) of Equation 6.39 is diagonal, which, as can be seen it is not.

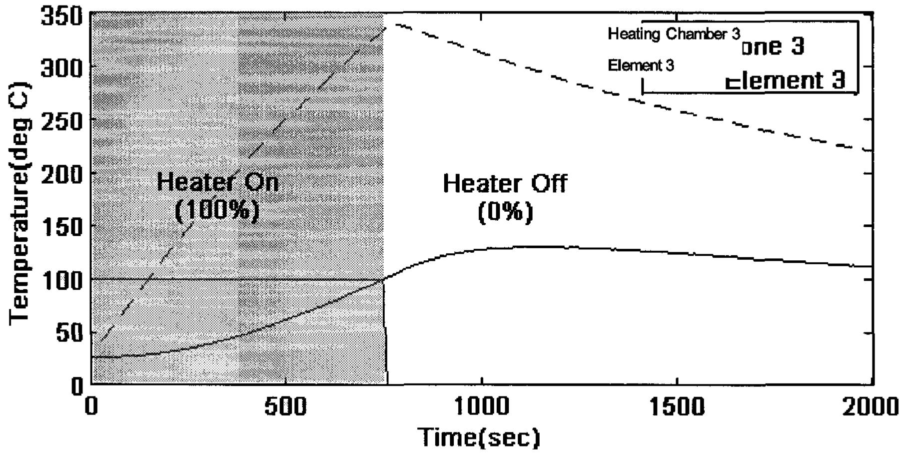

Figure 6.25: Response of zone 3 for step change in command. Temperature continues to increase after the heater is turned off.

The response presented in Figure 6.25 is obtained by energizing element 3 at 100% for 10 minutes. The element is then turned off and the heating chamber and elements are allowed to cool. For the proposed model, it is expected that as the element is de-energized its temperature will immediately start to decrease. In this case, the temperature of the element (heating wire and refractory material) continues to increase for approximately 30 seconds after the element is de-energized. This indicates that the placement of the thermo-couple is such that it does not represents the average temperature of the mass included in the element CV. From a modeling point of view, this indicates that the system states cannot be tracked solely from the current input. Alternatively, the integral of the input may be included in the energy balance. This quantity corresponds to the total energy supplied to the system. For simplicity, the disturbance and environmental loss terms of Equation 6.39 are ignored. The simplified system equation becomes:

$$\dot{\bar{T}}=A\bar{T}+B\bar{U}+C\int\bar{U} \qquad 6.40$$

For the SISO case, the above equation is simplified to:

$$\dot{T}=aT+bu+c\int u \qquad 6.41$$

Taking the Laplace transform of Equation 6.41, gives:

$$T(s)s=aT(s)+bU(s)+c\frac{U(s)}{s} \qquad 6.42$$

Rearranging results in the following:

$$\frac{T(s)}{U(s)}=\frac{bs+c}{s(s-a)} \qquad 6.43$$

The resulting transfer function has one integrator, one real pole and one real zero. The same derivation from Equation 6.39 (ignoring D and $K_{env}T_{env}$) leads to a transfer function with one real pole as follows:

$$\frac{T(s)}{U(s)}=\frac{b}{s-a} \qquad 6.44$$

In order to evaluate which transfer function best represents the heating chamber and element responses, the parameters of Equations 6.44 and 6.43 are fitted using Matlab to the data presented in Figure 6.25. The results of these and other fits are presented in Table 6.5.

Table 6.5: Loss function value for various process model fits for oven temperature responses of Figure 6.41

Input	*Output*	#	*TF Form*	*Loss Function Value*
Element Power (%)	Element Temp (°C)	TF1	$\frac{k}{(s-a)}$	5.4
		TF2	$\frac{bs+c}{s(s-a)}$	2.7
		TF3	$\frac{k}{(s-a_1)(s-a_2)}$	47.5
		TF4	$\frac{bs+c}{(s-a_1)(s-a_2)}$	4.9
Element Temp (°C)	Heating Chamber Temp (°C)	TF5	$\frac{k}{(s-a)}$	2.5
		TF6	$\frac{bs+c}{(s-a)}$	1.8
		TF7	$\frac{bs+c}{(s-a_1)(s-a_2)}$	1.7
Element Power (%)	Heating Chamber Temp (°C)	TF8	$\frac{k}{(s-a_1)(s-a_2)}$	1.5
		TF9	$\frac{bs+c}{(s-a_1)(s-a_2)}$	0.96

The loss function is the sample mean squared between the estimate the actual value.

It is used here as an indicator of the goodness of fit.

Loss functions of 5.4 and 2.7 were obtained for TF1 (Equation 6.44) and TF2 (Equation 6.43), respectively. This leads to the belief that including the integral of the input into the system of equations results in more accurate modeling of the system behaviour. Fitting the same data to a transfer function TF3 (equation not shown) results in a loss function of 47.5. This indicates that the element temperature response is not of second order with respect to the heater input.

It is interesting to note that the relationship between the element temperature response and the power input can be well modeled (TF1 and TF2) by a first order transfer function. This demonstrates that the dynamic characteristics of the heating chamber CV have a weak influence on the dynamic response of the element CV. In contrast, the heating chamber temperature response is a minimum of second order with respect to the heater input (TF8 and TF9). This indicates that the dynamic characteristics of the element CV have a strong influence on the dynamic response of the heating chamber CV.

According to the final energy balance for the heating chamber CV (Equation 6.34) the heating chamber temperature is not directly affected by the element input. If the heat transfer to adjacent heating chambers and the disturbance term are both neglected, Equation 6.34 becomes:

$$c_{Ci}\frac{dT_{Ci}}{dt}=k_{Ei\Leftrightarrow Ci}(T_{Ei}-T_{Ci}) \qquad 6.45$$

From this equation a first order single pole transfer function between the heating chamber and element temperatures could be obtained. Fitting parameters of the transfer function results in a lost function value of 2.5 (TF5). To some extent this validates the derivation of the linear time invariant model presented previously. Including a zero to TF5 leads to a decrease of 30% in the loss function value (TF6). Again, this would seem to indicate that the heating chamber temperature response is a function of the present but also of past inputs.

It is interesting to note that directly relating the heater input and heating chamber temperatures results in the smallest loss functions (1.5 and 0.96 for TF8 and TF9, respectively). This indicates that the energy state of the oven system is well represented by the heating chamber temperatures. For control purposes, measuring the element temperature may not be necessary. Again, it can be seen from the loss function value that including a real zero when representing the oven process (TF2,4,6,7,9) increases the accuracy in the model predictions.

In developing the linearized model, the heating element command signal bounds (actuator limits) were not taken into consideration. The command signal upper bound corresponds to 100%, whereas the lower bound corresponds to 0%. The heating elements cannot be used to actively remove energy from the system. This implies that the closed-loop response during heating may be modified through a control action, while the dynamic response while cooling cannot. In other words, the closed-loop response is equivalent to the initial condition response during cooling, and this is regardless of the control strategy. The open loop time constants obtained for the SISO cases are between 50 and 130 minutes. In some situations these open-loop time constants are much too long. This is the case when it is desired to obtain a working set of curing temperatures through trial and error testing. In order to increase the speed of the cooling response, heat must be actively removed from the system. As previously described (Section 6.2.2.4.), this is accomplished by injecting room-temperature air into the heating chamber using a centrifugal blower as discussed in the following section.

6.5. Oven System modeling with Forced Cooling

6.5.1. Preliminary Assessment of System Behaviour

As discussed in Section 6.2.2.4. room temperature air is forced into the heating chamber through the purging collar located between ovens 1 and 2 to provide cooling. A forced cooling response is shown in Figure 6.26. The responses are divided by a dashed vertical line according to the state of the inputs. The first segment (0 and 100 sec.) corresponds to steady state temperatures. The second and fourth segments demonstrate the effect of forced cooling using different blower intensities. The third segment shows the system behaviour after the air flow is turned off. The last segment corresponds to the next heating cycle.

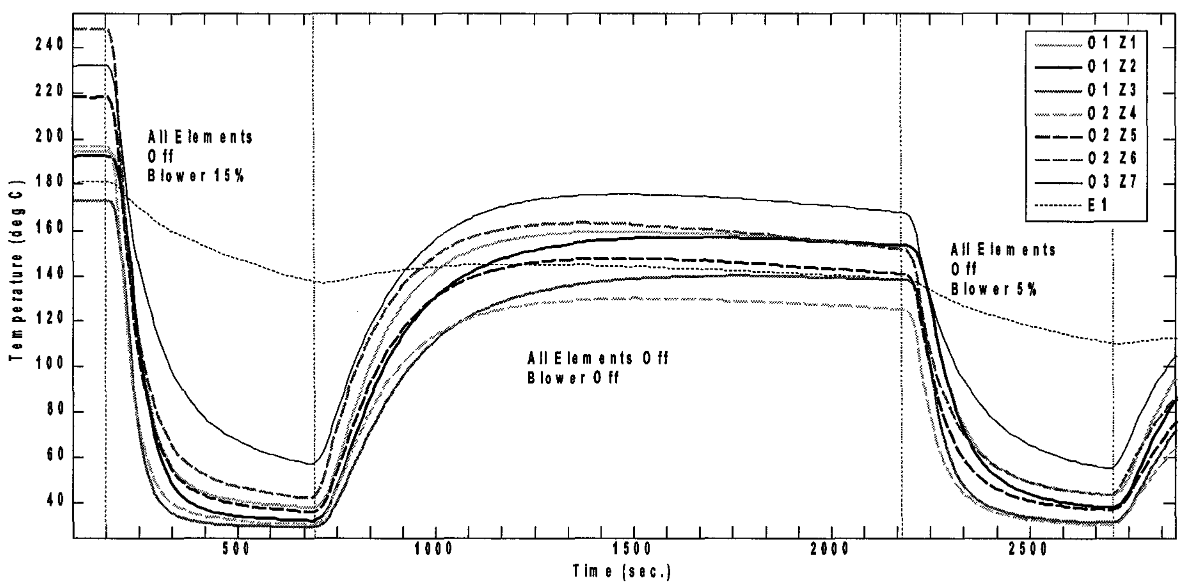

Figure 6.26: Oven temperatures with forced and natural cooling.

The response curves presented in Figure 6.26 illustrate several important characteristics of the system when active cooling is in use. Several observations can be concluded from this figure:

- The purging system removes heat from the entire oven system. As previously stated, the bulk of the thermal energy of the oven system is stored in the ceramic heating elements. Removing heat from the heating chamber also cools the elements. This is observed for both forced cooling segments where the temperature of element 1 decreases significantly faster than under natural cooling (latter half of segment 3). It is interesting to note that once the purging of air is complete the element temperature rises by a few degrees. This is indicative of the element thermo-couple not completely representing the energy state of the element.

- Cooling is more pronounced for the zone located near the purging collar and becomes progressively less pronounced for zones located further from the purging collar. This is reflected in both the cooling rate and the final temperature of each zone. This can be observed for both of the forced cooling segments for zones 3,4,2,5,1,6 and 7 which are progressively further from the purging collar.
- The temperature prior to cooling influences the final zone temperature. This statement is supported by the final temperatures of zones 2, 5 and 3, 4. In both cooling segments, the zone with the highest final temperature corresponds to the zone with the highest initial temperature.
- The speed of the cooling response associated with forced cooling is significantly higher than the ones associated with natural cooling. This is observed from the second and third segments where the lowest settling times are 200 and 500 seconds, respectively. In contrast, the settling time for natural cooling is in the order several hours.
- The system demonstrates nonlinear behaviour between the zone temperatures (output) and the air intensity (input). This is apparent when considering that two inputs that differ by 10% (of full scale) result in settling times which differ by 150%.

From the observations outlined above, it appears that the purging air system is capable of significantly increasing the cooling rate compared to natural cooling alone. From initial observations the system demonstrates a more complex behaviour in comparison to the case without forced cooling. In fact, it appears that the system demonstrates a nonlinear dynamic response. In the following sections, a lumped parameter model is developed to gain insight into the behaviour of the oven system with purging air. The analysis begins by choosing appropriate control volumes.

6.5.1. Control Volumes

For the oven system without active cooling, the heating tube and air are considered to be a part of the same CV (heating chamber). This was based on the assumption that the energy states of the air and of the heating tube could be modeled as one. In the present case, the energy state of the air will, to some extent, depend on the temperature of the heating tube, but will be greatly affected by the air flow condition. Similarly, the energy state of the heating tube will depend on the air flow conditions but will also be affected by the heat flow from the element. Therefore, a mismatch between both energy states exists. Consequently, the air and the heating tube must be treated in different CVs. The proposed CVs used to model the oven system with active cooling are depicted in Figure 6.27.

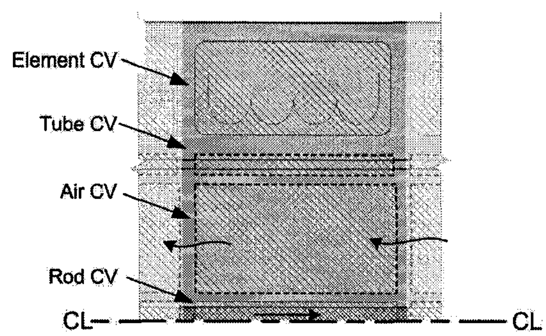

Figure 6.27: Oven control volume with purging air.

The element and rod CVs, and their energy balance formulations remain the same. The tube CV includes the heating tube only while the air CV includes the air contained within each zone.

6.5.2. Energy Balance

The energy balance for the tube CV is

$$\dot{Q}_T = c_T \frac{dT_T}{dt} \qquad 6.46$$

The air CV is spatially fixed. From first principle, the energy balance for the air CV is given by:

$$\dot{Q}_z + \dot{m}_i h_i = \dot{m}_o h_o + \frac{dU}{dt} \qquad 6.47$$

where the terms $\dot{m}_i h_i$ and $\dot{m}_o h_o$ represent the energy entering and leaving through a mass flux across the CV boundaries. The air CV is essentially open to the environment; it is therefore reasonable to assume that $\dot{m}_i = \dot{m}_e$. Considering the air as an ideal gas allows one to assume that:

$$h_o - h_i = C_p (T_o - T_i) \qquad 6.48$$

and that,

$$\frac{dU}{dt} = C_v m_a \frac{dT_a}{dt} . \qquad 6.49$$

The air flow rate is modulated by varying the speed of the blower. If the resistance to air flow (caused by the system ductwork back pressure) and the inlet conditions remain constant, it can be assumed that the mass flow rate is a function of the blower speed only. Combining these assumptions, the air CV energy balance can be calculated as follows:

$$\begin{aligned} & C_a \frac{dT_a}{dt} = \dot{Q}_a + \dot{m}_a (u_{blower}) C_p (T_{ao} - T_{ai}) \\ & where : T_{ao}, T_{ai} = Air\ CV\ outlet, inlet\ temperatures \\ & C_a = C_v m_a \end{aligned} \qquad 6.50$$

It is important to note that unless either the mass flow or the outlet/inlet temperature difference is assumed constant the equation cannot be linearized. Both of these quantities cannot be assumed constant as the mass flow rate is a system input while the outlet and inlet temperatures are directly linked to the model output.

6.5.3. Heat Transfer

It was shown earlier that without forced cooling the heat flows between the chosen CVs are primarily transferred through radiation. For the forced cooling case, the effect of forced convection cannot be ignored. Conclusions based on the oven system construction and observations of the process responses allow for the formulation of the model based on the principle of heat flow paths between CVs. These models are represented schematically using a thermal resistivity diagram (Figure 6.28) and are described below.

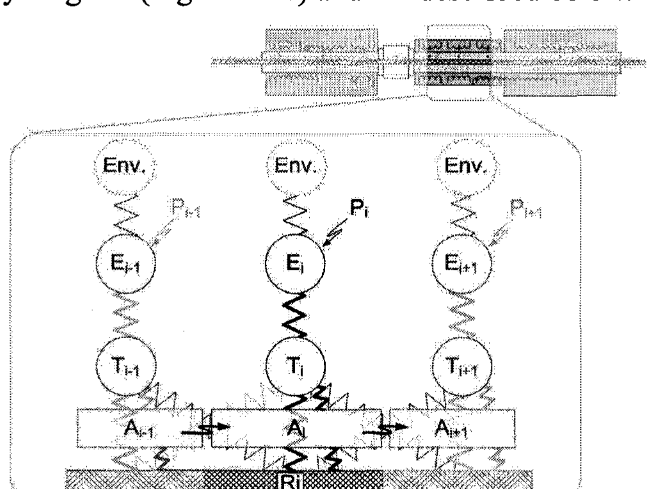

Figure 6.28: Thermal resistivity diagram for oven system with purging air. Thick lines depict principle flow paths.

- Since no purging air circulates in the region between the element and heating tube, the heat flow between the element and tube CVs is due to the same mechanism as described for the element and heating zone CVs (Section 6.4.3.). It is believed that the majority of the heat flow between these CVs is through radiant heat transfer.
- Heat loss to the environment is believed to occur via radiation and natural convection. As air travels in the heating chamber it absorbs energy from the tube and rod CVs and conveys it to the environment. The amount of energy which is expelled by forced cooling is significantly higher than heat losses which occur due to natural cooling. This is apparent when observing the time constant associated with the zone temperature response with and without forced cooling.
- As cooling air begins to flow, hot air contained within the chamber is replaced by cooler air. Heat transfer between the cool moving air and the tube surfaces occurs through forced convection. This decreases the heating tube temperature, which in turn significantly decreases the radiative heat flow between the heating tube and the rod.
- Heat transfer between the rod and the air will also occur through forced convection. This may heat or cool the rod depending on the relative temperatures of the air and of the rod.

From these observations and from the developed model it becomes apparent that the required instrumentation is not available to fully quantify the oven system in the presence of cooling air. More specifically, the instrumentation capable of measuring the surface temperatures of the heating tube is not available. As a significant portion of the heat flow is provided by radiant heat transfer, the temperature of the oven tube is required to evaluate and ultimately regulate the relative quantity of heat flow to the rod. It is also noted that the air temperature must also be measured. This quantity, in combination with the air speed, gives a measure of the heat flow which occurs through forced convection.

6.1. Curing oven controller design

6.1.1. Control Objective

When elevated temperature ovens are employed to batch cure fibre reinforced polymer composites either a constant temperature or a constant flux heating profile is typically used. The two profiles are sown in Figures 6.29 and 6.30 respectively.

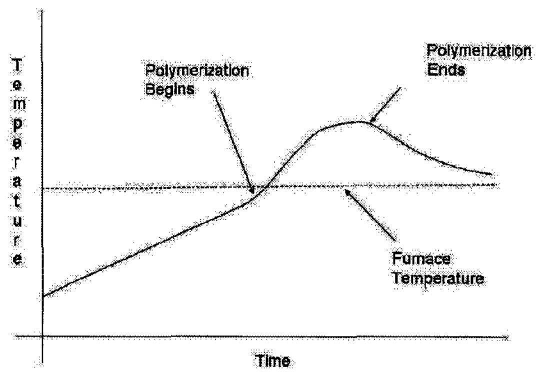

Figure 6.29: Resin curing in constant temperature oven ([3] p.43).

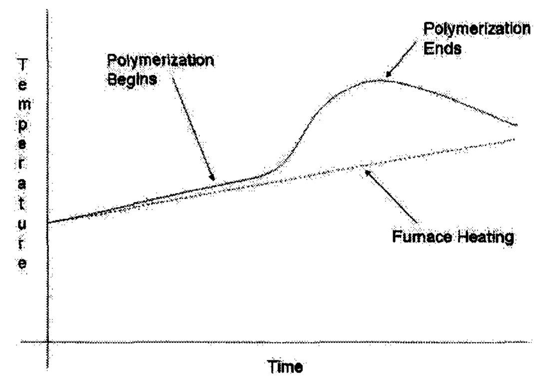

Figure 6.30: Resin curing in constant heat flux oven ([3] p.42).

The first and simplest method involves maintaining the heating chamber at a constant temperature. This method provides a large heat flux at the beginning of the heating phase which progressively decreases as the product temperature reaches the heating chamber temperature. In the second method, the heating chamber temperature continuously increases with respect to time. Conceptually, if the temperature difference between the heating chamber and product is maintained constant, this method is capable of providing a constant heat flux to the product. To a large extent the product design (type of resin, fibre, size) dictates which method to use. For the current product (FRP rebars), studies by Sandness [3] were conducted for constant temperature curing.

For continuous processes, it is possible to obtain the same heating pattern as previously described by varying individual zone temperatures. For the first method all zones are maintained at equal temperatures. In the second case, individual zone temperatures are set such that the desired temperature gradient with respect to time is achieved. To some extent, the continuous case offers more flexibility in setting the desired temperatures gradient. The open-loop oven temperature responses presented in Figure 6.20 show that a temperature gradient of 1° C/cm within the oven chamber is physically attainable. This spatial temperature gradient results in a rate of 50° C/min for a rod moving at line speeds of 0.5 m/min. For most ovens used in batch processing this gradient would be difficult to attain.

Regardless of which temperature distribution is desired in the tunnel oven chamber, the control objective may be divided in two phases, namely, the preheating and the operational phases. The task of the controller in the preheating phase is to bring the zone temperatures to their desired set point as fast as possible. As this phase occurs prior to production it is not important. In the operational phase the task of the controller is to regulate the zone temperatures about a constant set point. In chapter two, it was stated that some production problems had been attributed to partial curing of the wet strands. In fact this was a result of disturbances which affected the oven temperature at the beginning of the production run. The sources of this disturbance are attributed to one of two masses moving though the oven chamber. These are a stainless steel pull tube and the wet fibre strand.

At the beginning of each production run a stainless steel tube (*OD=12mm, ID=8.8 mm*) is used to advance the central carbon strands through the process. The central fibres are fastened at one end of the tube (near the impregnation ring) while the opposing end is inserted in the puller. As the cool tube travels in the oven it absorbs heat and causes a decrease in zone temperatures. The magnitude of this disturbance is equal to $E_{tube}=160\,\Delta T$ J °C/m, where ΔT is the increase in tube temperature from room temperature. For example, if the rod temperature were to increase by 100° C as it travels through the entire oven chamber, this would translate to a disturbance of approximately 16 KJ.

The second disturbance is created by the partially cured rod itself. Whether this disturbance is positive (energy is given to oven) or negative (energy removed from oven) will depend on the nature of the curing process. Results of computer simulation performed by Sandness [3] provide insight into the magnitude of this disturbance. The result of such a simulation is shown in Figure 6.31. The figure illustrates the temperature distribution through the rod cross-section as it advances through the induction unit (10, 20 and 30 second curves) and ovens (45 to 120 seconds curves). It can be seen that as the rod enters the oven its exterior temperature is approximately 110°C (45 seconds curve at 12 mm) It is therefore expected that the disturbance in the first zones will be negative. When the rod enters the last oven zones (120 seconds curve Figure 6.31.) it is possible that its exterior temperature is greater than the heating chamber. This would correspond to a positive disturbance. It should also be noted that for the current production, parameters such as rod diameter, fibre volume fraction, production rate, and induction heater power remain constant. Therefore the magnitude of the disturbance caused by the rod traveling through the oven stage will also remain constant.

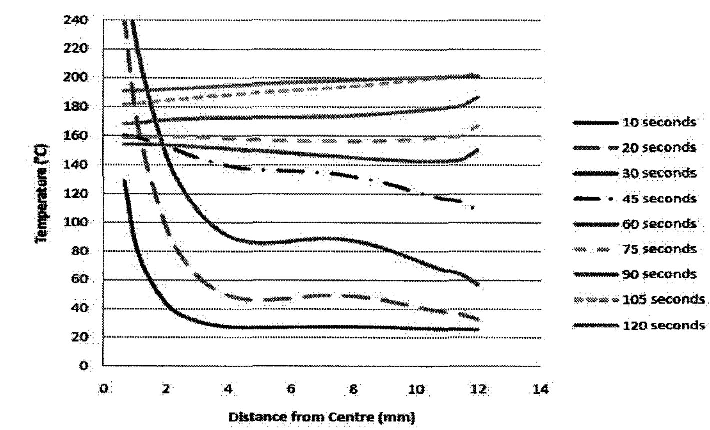

Figure 6.29 - Temperature Cross-Section profile for Sim 3 (231 Amps, 200 °C)

Figure 6.31: Simulated temperature through cross section of 22mm rod using inducting heating at 231 amps and oven temperature of 200° C for line speed of 0.5m/min.(Sandness p.94 [3]).

To some extent the heat storage capacity of the ceramic heaters provides good open-loop disturbance rejection. The actual response when disturbed is mainly effected by the closed-loop dynamics. Therefore, the design of the oven controller will first be presented. Experiments will show the effect of disturbances under closed-loop control.

6.1.2.Oven Controller: Natural Cooling

In previous sections it was shown that the oven system with natural cooling has a slow dynamic response. A model derived from basic physical principles showed that the dynamic behaviour of each zone could be described by two first order differential equations. One is associated with the heating element, the other with the heating tube and air volume contained in each zone. It was also shown that each zone is coupled to its neighbors through heat transfer. It was further shown through experimental observation that the derived model structure coincided well with the observed system behaviour but that the prediction accuracy could be improved if the integral of the heater input was added to the system model. This was attributed to the inability to accurately track the energy stored in each control volume from temperature measurements.

This section investigates the oven system response under closed-loop PI control. The design of the controller is reduced to determining the proportional and integral gains for each zones. In Table 6.3, the behaviour between the zone inputs and temperatures was characterized using a first order transfer function. From the derived MIMO model and from further experimental observation it is clear that the relationship is of second order. All methods proposed in the literature for tuning the PI gains of SISO transfer function do not take into account coupling between zones. It was further judged that the identification of parameters for a higher order TF would not necessarily provided a better basis for tuning. Therefore, the parameters presented in Table 6.3 are used to obtain an initial gain set. In some cases the gains are then refined through experimental observation.

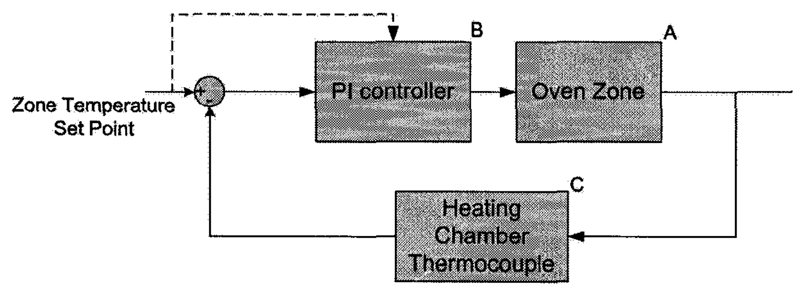

Figure 6.32: Schematic of the oven control system. The dotted line represents gain scheduling based on the set point value.

A standard structure with the controller placed in the feed forward path is used for the oven control system (Figure 6.32). A listing of the gains used for each of the responses presented in this section is included in Table 6.6. It should be noted that while performing a test on the oven system, the element of zone 2 was inadvertently energized at full power for several hours. This cause the temperature in this zone to exceed 1100°C thus damaging the ceramic element. Attempts to replace the element were not successful, and therefore, the remainder of this work zone 2 is unheated.

The oven response presented in Figure 6.33 is obtained using the internal model control (IMC) tuning rule. This tuning rule was used in chapter 5 to tune the pump rotor speed PID controller.

Ovens 1 and 3 demonstrated slower closed-loop response compared to oven 2.

Ovens 1 and 3 did not demonstrate any over shoot while oven 2 demonstrated an overshoot close to 20%. The settling time for oven 3 is significant.

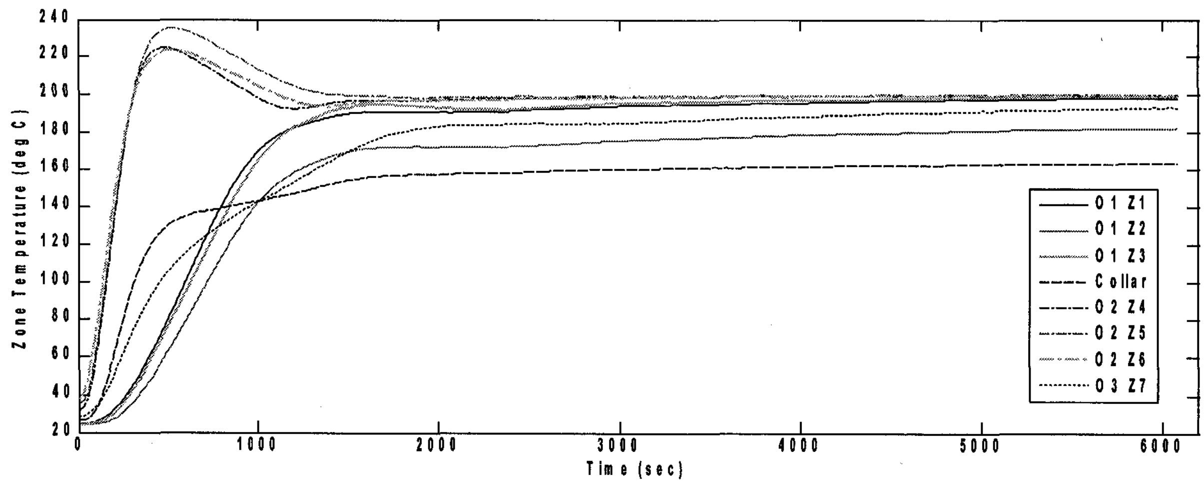

Figure 6.33: Oven closed-loop response using PI controller tuned with IMC rules (gain set #1). All zone set points are 200°C.

The response of Figure 6.33 illustrates the duality involved in choosing the integral gain. If the gain is too large, integral windup occurs which results in overshoot. If the gain is too small, the settling time, disturbance rejection properties and steady state errors are not acceptable. For the braider head and puller motor control these issues were resolved by using a set point profiler. In this case, the main motivation for the use of this method was to prevent actuator saturation. For the oven system, actuator saturation allows significantly faster responses compared to limiting actuation. If actuator saturation is permitted, the design of a set point profiler is considerably more complicated as it involves considering nonlinear dynamics.

To obtain low overshoot and good steady state properties a PI gain scheduled controller is proposed. Two gain schedules are used. Gain switching occurs when the error reaches a fix percentage of the zone set point (15%). For this method, one gain set is used to bring the system close to the desired response. For this gain set, the integral gain is set to zero. As such no integral windup can occur. The second gain set, which includes an integral term, is used to regulate the oven temperature about the desired set point. This control strategy decouples the initial heating which occurs prior to the production run and the steady state control which occurs during production.

Different tuning techniques are used for each schedule. For the first schedule, the proportional gain is obtained analytically by pole placement (assuming a first order process model). The closed-loop transfer function for a first order process model with proportional control is given by:

$$\frac{T(s)}{U(s)}=\frac{K_p K_c}{T_p s+1+K_p K_c} \qquad 6.51$$

where K_c is the controller gain, K_p and T_p are the first order process model parameters as shown in Table 6.3. Setting the denominator of Equation 6.51to zero and solving it for the controller gain gives:

$$K_c=\frac{-sT_p-1}{K_p} \qquad 6.52$$

where s is now the desired closed-loop pole.

The second gain schedule is obtained using the IMC tuning rule (Section 5.1.3.5). The integral time is therefore set to the process time constant. For the IMC tunning rule the proportional gain is obtained by trial and error. The initial proportional gain is obtained using the same poles placement method as described for the first gain schedule.

Table 6.6: Listing of Oven PI gains

Gain set	K_{c1}	$T_{i1}(min)$	K_{c2}	$T_{i2}\,(min)$
#1	1 / 1 /1 0.57 / 0.57 / 0.57 1	74 / 55 67 39 / 54 / 36 161	NA	NA
#2	1 / 0.53 / 0.70 0.21 / 0.22 / 0.21 0.85	NA	2.19 / 2.32 / 3.06 1.02 / 1.07 / 1.05 3.83	69 / 104 / 95 48 / 53 / 49 76
#3	2.0 / 0.53 / 0.70 0.21 / 0.22 / 0.21 3.4	NA	2.19 / 2.32 / 3.06 1.02 / 1.07 / 1.05 3.83	69 / 104 / 95 48 / 53 / 49 76

System responses for the controller and the tuning rule presented in Table 6.6 are shown in Figures 6.34,6.35 and 6.36. For all these responses, the zone settling times are comparable to the ones obtained using the standard PI controller (Figure 6.33) but the overshoots are smaller. The responses shown in Figure 6.34 were obtained using gain set #2. Although the responses of zones 4 to 6 are satisfactory, zones 1 and 7 never reach the second gain schedule. To correct this problem the proportional gains of zones 1 and 7 are increased by a factor of two and four, respectively.

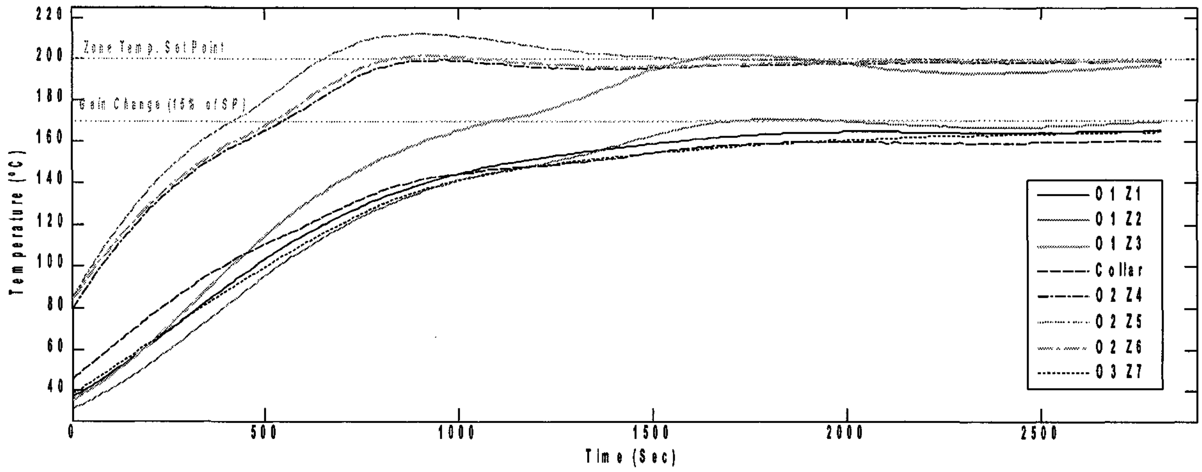

Figure 6.34: Oven closed-loop response using gain scheduled PI controller for gain set #2.

As can be seen in Figure 6.35, with the increased proportional gain all zones reached the second schedule. It is interesting to note that zones 3 to 6 demonstrate similar transient response throughout the first schedule. This validates the pole placement approach. Since the closed-loop pole of zone 1 is chosen as double that of other zones, its initial transient response is faster, but it is slower in the second schedule where the gain is not increased. Although it is set four times that of other zones, the response of zone 7 is the slowest. As can be seen in the lower plot of Figure 6.35, this is attributed to a saturation in the heater command.

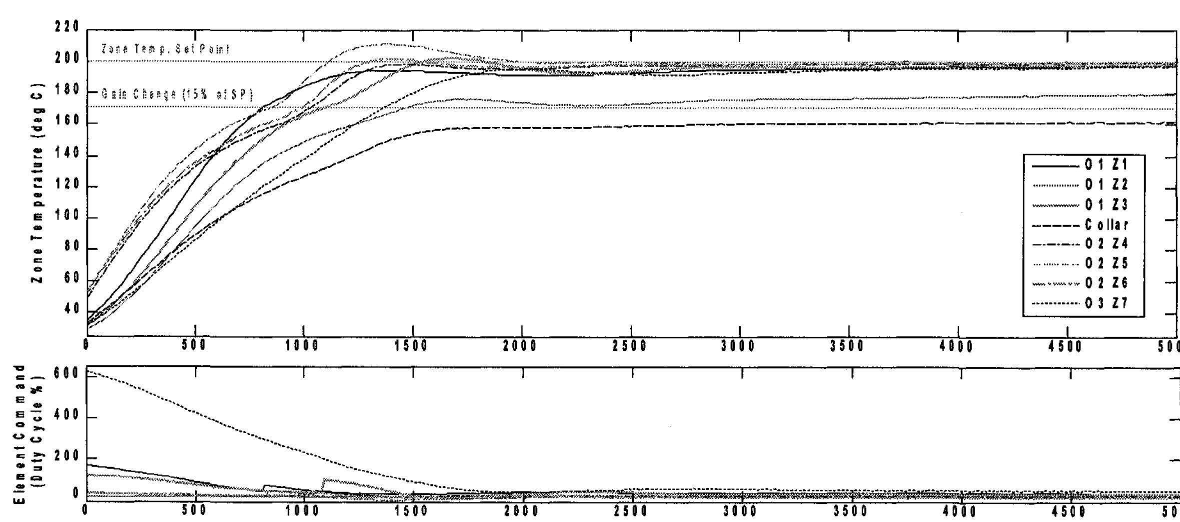

Figure 6.35: Oven closed-loop response using gain scheduled PI controller for gain set #3 (top plot shows temperature vs. time, bottom plot shown control signal vs. time).

The responses presented in Figure 6.36 are obtained using the same gain set as in Figure 6.35. For this response the zone temperature set points are chosen such that a decreasing temperature gradient occurs along the oven chamber. The effect of coupling between zones can be seen from the responses of zones 4, 5, and 6. At approximately 800 seconds the temperature of zone 4 increases rapidly due to a change in schedule. This causes a temperature increase in zone 5, which has undergone an overshoot. All zones eventually reach their desired set point but only after approximately 45 minutes. In the preheating phase (prior to production) this is not a concern but in the event of disturbances such coupling could be problematic.

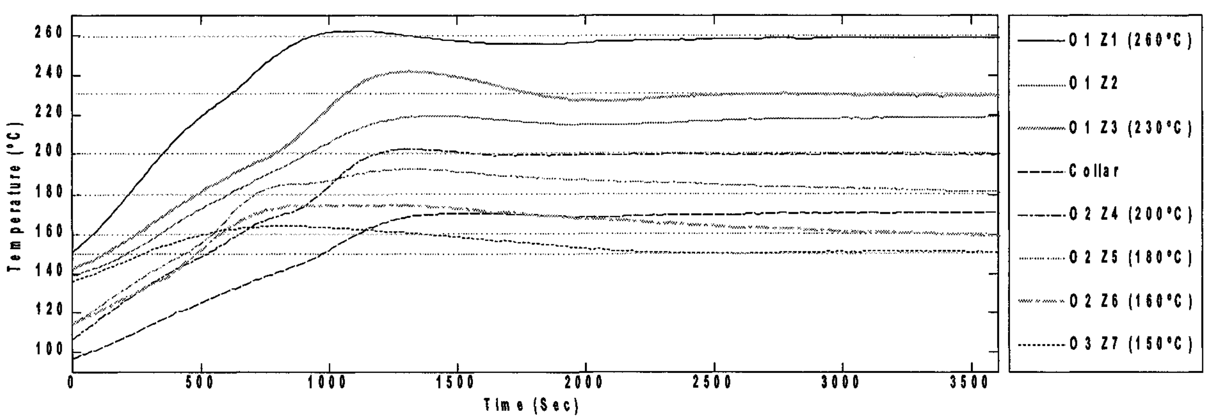

Figure 6.36: Oven closed-loop response using gain scheduled PI controller for gain set #3 for decreasing temperature set points.

Experiments were conducted to evaluate the effect of a disturbance under closed-loop control. In the first experiment (Figures 6.37) the oven chamber temperature was uniformly controlled. In the second (Figure 6.38), the controller maintained a temperature gradient through the oven chamber. In both experiments the puller tube (same tube which is used to advance the fibre through the process at the beginning of production) was placed along the length of the entire heating chamber. The total magnitude of this disturbance is approximately 28 KJ/m (assuming T_i=20° C and T_f=200° C). For this disturbance, heating chamber temperatures decrease by 2 to 12° C. The effect of the disturbance lasts several minutes, but lower than desired temperatures are only observed for 8 minutes as the controller corrects for the disturbance. This can be confirmed from the overshoot in the temperature traces

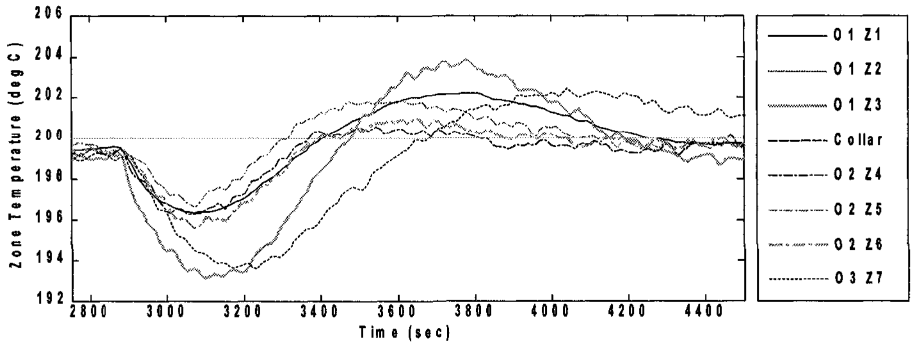

Figure 6.37: Effect of a disturbance under gain schedule PI (gain set #3) created by placing the cool puller tube in the oven chamber when zones are at equal temperatures.

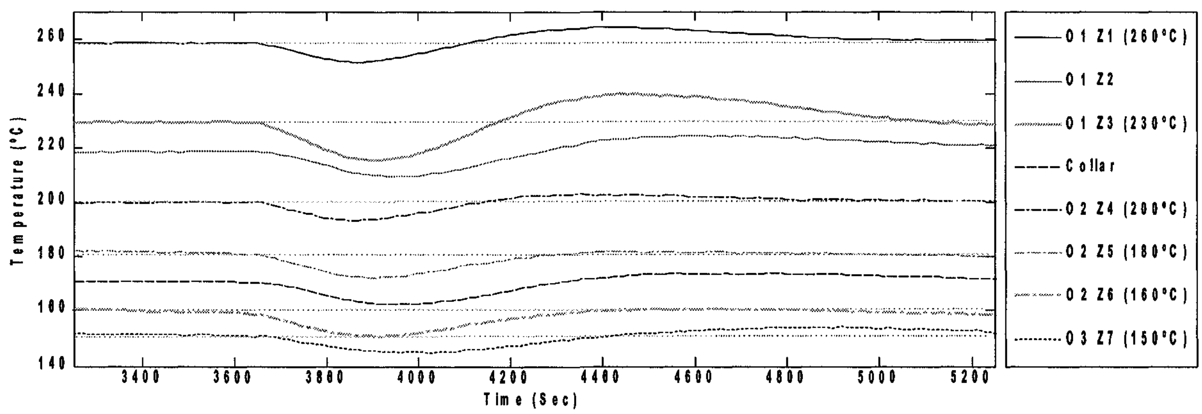

Figure 6.38: Effect of a disturbance under gain schedule PI (gain set #3) created by placing a cool puller tube in the oven chamber when a temperature a gradient is imposed on the zone temperatures.

As previously stated in Section 6.1.1., such a disturbance is likely to occur at the beginning of production. A simple solution to mitigate its effects would be to initially set the zone temperatures such that as the disturbance takes effect and the oven chamber decreases, the desired production temperatures are achieved. At that point the oven zone set points would be lowered to their desired production values. It is difficult to replicate the exact disturbance which occurs at the beginning of a production run, and therefore the correct preheating temperature with respect to the desired production temperature will be refined from the behaviour observed at the beginning of each production run. From the result of experiments presented in Figures 6.37 and 6.38, it would appear that setting the initial zone temperatures 5 to 20°C above the production temperature would result in good disturbance cancellation.

Under normal production, disturbances affecting the oven temperatures are not expected to occur. This is because factors which could disturb the oven system such as resin content and feed rate are regulated using closed-loop control. Nevertheless, if an unexpected disturbance would occur and it was judged that under- or over-curing would result, the appropriate course of action would be to decrease the production rate (mandrel speed) such that the equivalent heat flux could be transferred to the rod by the ovens. As the disturbance subsides the production rate could progressively be increased. These operations are greatly simplified by the automatic adjustment of other production parameters such as the resin dispensing rate, braiding speed, and the induction heater power.

6.2. Thermo-couple Time Response

Throughout the development of the oven control system it was assumed that the time lags associated with the oven's thermo-couples where negligible compared to the dynamic characteristic of the oven system. It was later observed that this is not the case. In one experiment, the thermo-couples were removed form the oven chamber, while the oven chamber temperature was increased to 157°C. Two thermo-couples where then placed in the hot oven chamber. One thermo-couple TC1 was located in the center of oven 3 while the other TC2 was place closer to the mouth of the oven where the temperature was lower. The thermo-couple's response is shown in Figure 6.39. It can be seen that the settling time is approximately 600 and 700 seconds for TC1 and TC2 respectively. This indicates that the speed of response associated with the oven thermo-couples are of the same order of magnitude as the ones associated with the oven closed-loop response.

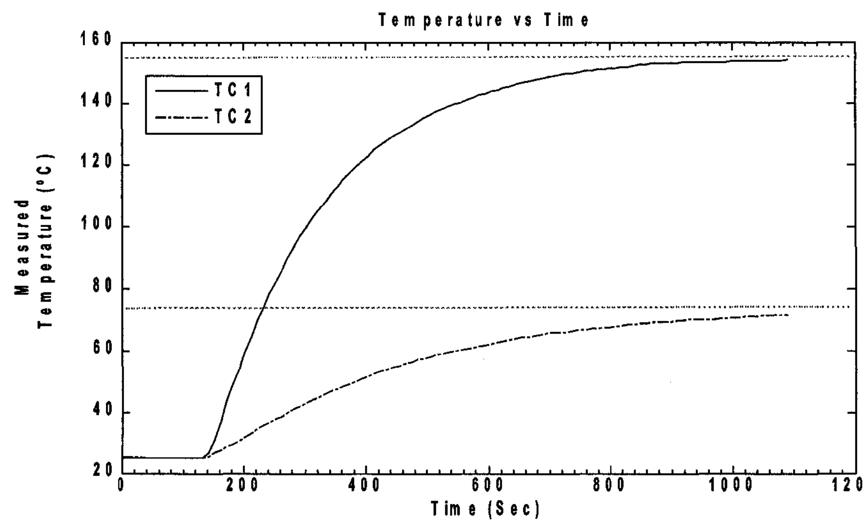

Figure 6.39: Oven thermo-couple step response.

It is believed that the slower than expected response of the thermo-couples are attributed to the thermal mass created by the addition of the ceramic tube close to the measurement junction (section 6.3.4.6). As the measurement junction is heated, heat is transferred to the ceramic tube through thermal conduction by the thermo-couple leads. Until the ceramic tube reaches the oven chamber transient measurements are reported by the thermo-couples.

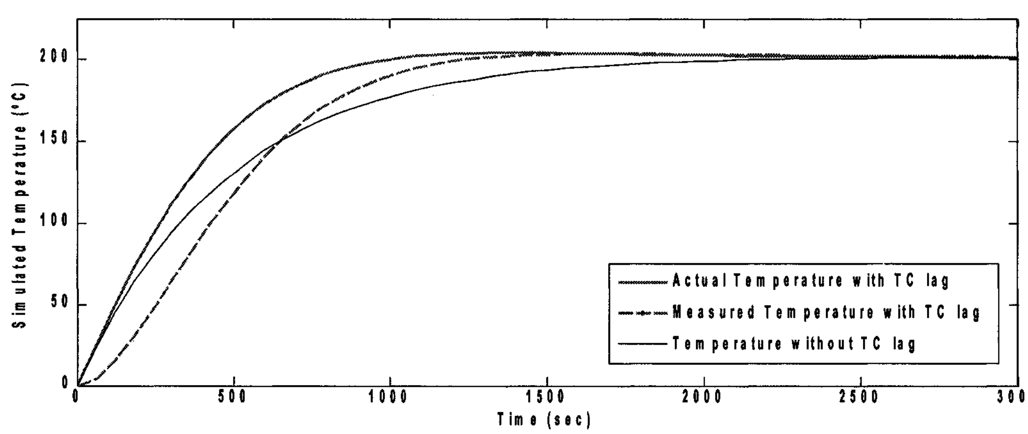

Figure 6.40:Simulation showing the effect of oven thermo-couple lag.

To evaluate the effect of the thermo-couple measurement lag on the closed-loop system, a computer simulation was developed. The oven and thermo-couples were modeled using a first order transfer function while the PI controller was modelled using a continuous integrator. The results of the simulation for zone 5 as shown in Figure 6.40. In this simulation, the gain and time constant for the oven and thermo-couple transfer functions were K_p=16 / τ=3800 (zone #5, Figure 6.39) and K_p=1 / τ=150, respectively. The controller proportional gain and integral time were K_c=0.5 / T_i=3360 (gain set #, zone #5) respectively. The simulation is performed for zone 5 which experimentally was shown to have the fastest response. The effect of the thermo-couple time lag is visible from this simulation. It is first observed that for a given gain set, the oven response with a thermo-couple time lag (Actual temperature with thermo-couple lag) is faster than the response with no time lag (Temperature without thermo-couples lag). The simulation shows that the error between the actual and measured temperature is significant in the transient portion (0 to 1500s.) of the response but become progressively smaller as a steady state regime is established. As the operation of the oven system is principally under steady state conditions, the thermo-couple lag is not expected to adversely affect the production. Nevertheless, this situation is not ideal and several related recommendations are made in Section 8.3.5. From the simulation presented in Figure 6.40, the result of some of the experiments presented in this chapter are revisited:

- The oven open-loop response presented in Figure 6.20 (p.141) is likely unaffected by the thermo-couple time lag. In this case, the oven response time constants where reported to be between 3800 to more than 8000 seconds.
- The open-loop response presented in Figure 6.41 and subsequent analysis relating to measurement of the zone temperatures did not consider the effect of thermo-couple lag. For the heater response, the thermo-couple lag does not apply as a thermo-couple with no ceramic tube was used to measure the heater temperature.
- A difference between the measured temperatures and the actual heating chamber temperatures exist for the transient portion of the closed-loop responses (Figures 6.33 to 6.38). As shown in the simulation, the discrepancy between the actual and measured temperatures are greatest when fast temperature variations are occurring. Therefore, responses associated with disturbance experiments are expected to have the largest discrepancy between the actual and measured temperatures. This implies that although the measured temperature fluctuations were at a maximum of 10°C, the actual temperature fluctuation is likely larger. Similarly, any measured overshoot will be smaller than the actual overshoot.

In light of these observations it also becomes apparent that the current temperature measurement method may not be suitable when forced cooling of the oven chamber is used. To confirm this suspicion an experiment was conducted to evaluate the range of response obtained when the oven thermo-couples are subjected to forced cooling (Figure 6.30).

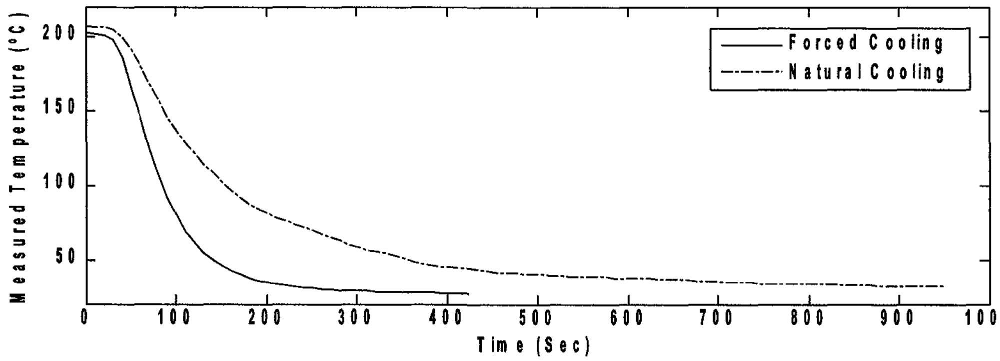

Figure 6.41: Cooling of oven thermo-couple through forced and natural convection.

In this experiment one of the oven thermo-couples was removed from the oven chamber. This thermo-couple assembly (Section 6.2.2.3.) was heated for several minutes using a heat gun. After the temperature of the assembly reach steady state, the assembly was inserted quickly into the oven chamber. Two such experiments where conducted and their result are shown in Figure 6.41. In the first experiment, labeled "Forced Cooling" in the figure, the oven blower was set to 50 %. In the second, labeled "Natural Cooling", the oven blower was turned off. The setting times for the forced and natural cooling are approximately 200 and 700 seconds respectively. These values correspond to a dominant time constants of 50 and 175 respectively. In comparison, the dominant time constants which were observed for the open-loop forced cooling responses, shown in Figure 6.26, were as short as 100 seconds. It can therefore be said that the current measurement method is unable to measure the actual oven response in the presence of purging air. For this reason the use of the purging system as a controllable input will not be investigated. Nevertheless, the use of the air purging system to quickly decrease the oven temperature is investigated in the next section. Recommendations relating to the air purging system are made in section 8.3.5.

6.3. Oven control with forced cooling

During production it may become necessary to stop the production line to resolve any number of unexpected problems. The objective of the purging system is to force a rapid decrease of the oven temperature such that over-curing of the rod section located in the oven stage does not occur during pauses in production. In the current implementation, the forced cooling system can operate in two modes, manually, and in open-loop. In manual mode, the blower set point is adjusted by the operator via a numeric field of the control software. The open-loop mode is activated via a command button. Once activated the oven PI controllers are disabled and the heater commands are maintained at their current levels. A set point profiler is used to adjust the blower intensity. When first activated, the blower intensity is set to 100%. The intensity is then progressively decreased (at a rate of 5% for each 10 second sample period) until it reaches a final intensity (currently 25%). At any time, the blower intensity can be manually overwritten.

It should first be noted that the forced cooling responses presented previously where obtained with the purging collar located between ovens 1 and 2. The response presented in this section is obtained with the purging collar located at the mouth of oven 3. The collar was moved such that a decreasing temperature gradient is achieved along the oven chamber (as depicted in Figure 6.10). The forced cooling response in open-loop mode is presented in Figure 6.42. It can be seen that in the first minute after the activation of the purging system the measured zone temperatures decrease by approximately 100°C. Due to the thermo-couple time lag the actual cooling rate is likely higher. After 300 seconds, it can be seen that the oven temperatures begin to stabilize. Again, due to the thermo-couple time lag, this likely occurs sooner. When the cooling system is deactivated (4950 sec.) the measured zone temperatures increase back to their original temperatures in approximately 400 seconds at which point production may be restarted. Overshoots in temperature between 8 and 12% are observed. This behaviour is likely to be beneficial as it will contribute to mitigate the effects of the disturbance created by the cool rod entering the oven chamber (as discussed in section 6.1.1.).

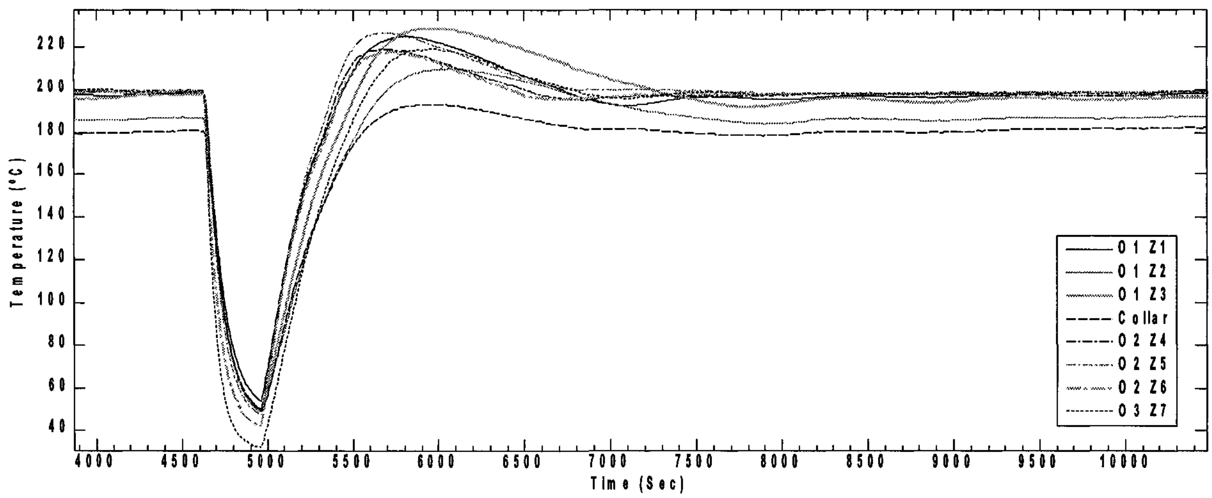

Figure 6.42: Oven forced cooling response. Cooling is activated at 4600 sec. and deactivated at 4950 sec.

The forced cooling system presented in this section allows one to quickly decrease the oven chamber temperature. The system will likely minimize the adverse effect of pauses in production on the product. Nevertheless, the oven system with forced cooling is not optimally controlled. It is believed that significant improvements could be achieved with adequate temperature measurements and through the development of more sophisticated control strategies. Recommendations regarding the oven system are given in Chapter 8.

7 Development of the Pilot Production Plant Automation System

This chapter describes the implementation of the automation system for the pilot plant. Both the hardware and software implementation are discussed. The features implemented in the current control software, limitations of the development environment and the operating system are highlighted in this chapter. The goal of this chapter is to provide sufficient information regarding the implementation of the automation system such that others may develop it further. The section is not meant as a full engineering report on the implementation of the automation system as this may be too lengthy.

7.1.System Overview

The functional diagram for the automation system is shown in Figure 7.4. The systems are divided according to the production machinery, namely the braiding and pulling, the dispensing, and the curing systems. Two more systems are also included: the emergency stop and computer control systems. Details regarding control and monitoring hardware specific to the braiding and pulling, dispensing, and curing systems were presented in Chapters 4, 5 and 6, respectively.

At the heart of the automation system is a personal computer equipped with three National Instrument multifunction data acquisition cards (DAQ). Machinery is monitored and controlled via analog and binary signals (identified by arrow heads in Figure 7.4). All signals with the exception of the resin weight which communicates using the computer serial port, are acquired and generated using the DAQ cards.

Several components of the automation hardware are housed in a ventilated steel enclosure (Figure 7.1). These components are mounted on steel tracks. Wires within the enclosures are organized using a modular channel system. An inside view of the enclosure is shown in Figures 7.3 and 7.4. Captions have been provided for ease of identification.

The control software was developed using National Instrument LabWindows development environment. Under LabWindows, programs were compiled using an ANSI C compiler. The functionalities offered by LabWindows are similar to those provided by the more popular LabView. While LabView provides a graphical development environmental, LabWindows provides a textual programing environment. The data acquisition cards functionalities are accessed using the supplied *DAQmx* drivers.

A graphical user interface was developed for the control software and allows the user to monitor and adjust machinery operation. The control system screen, keyboard and mouse are located on the door of the control enclosure (Figure 7.1). The control enclosure is located adjacent to the braider head.

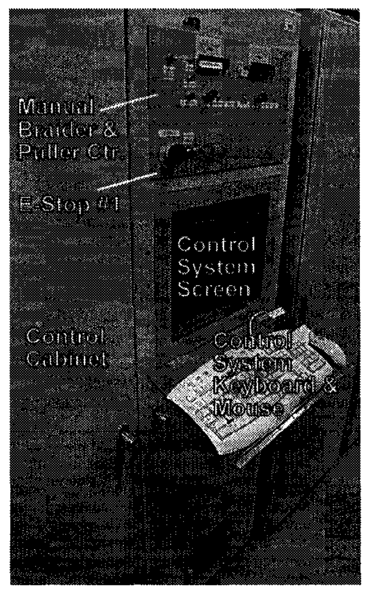

Figure 7.1: Exterior view of the control enclosure, manual braider & puller controls, screen and keyboard and mouse shown.

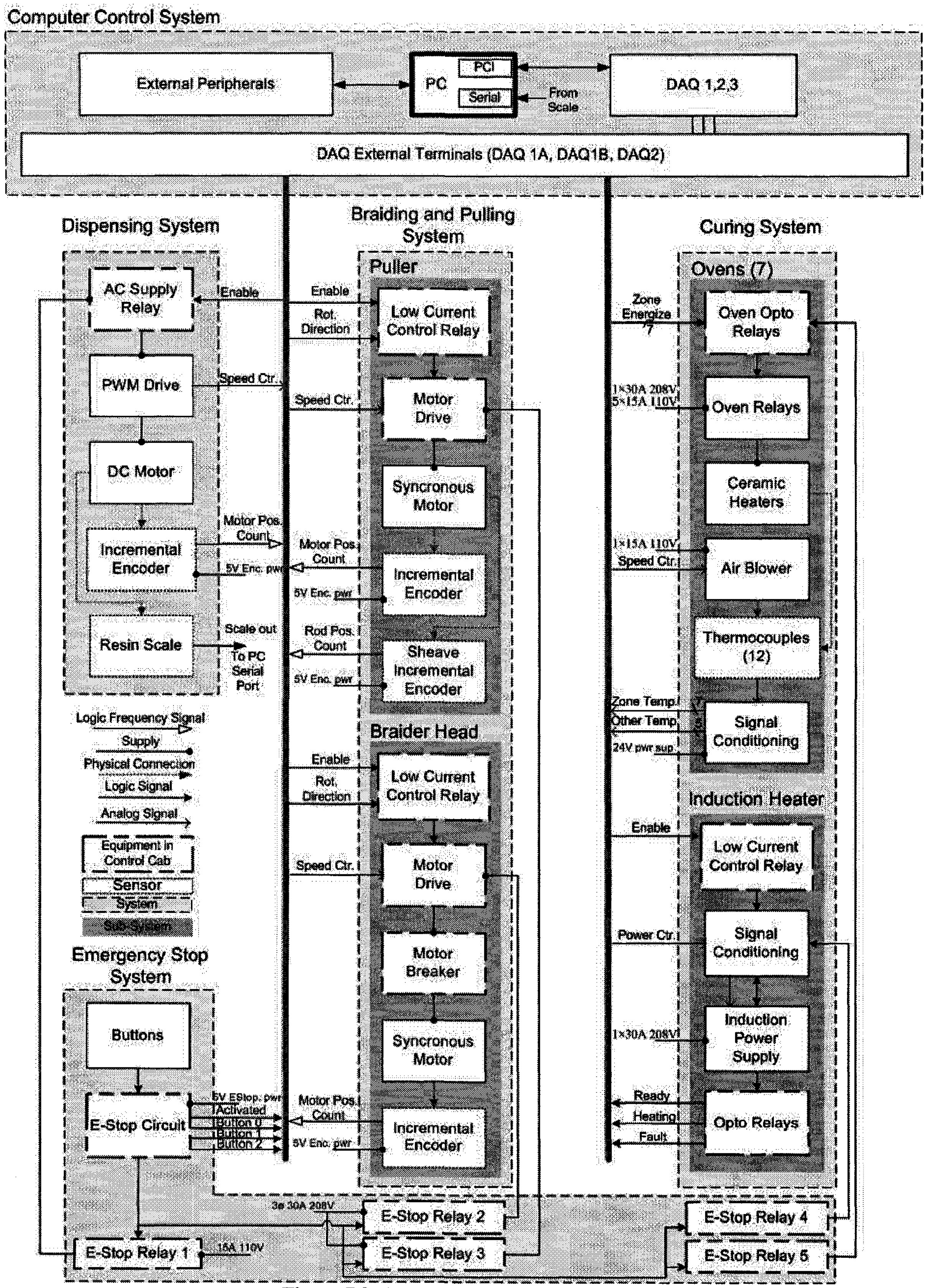

Figure 7.2: Automation system schematic.

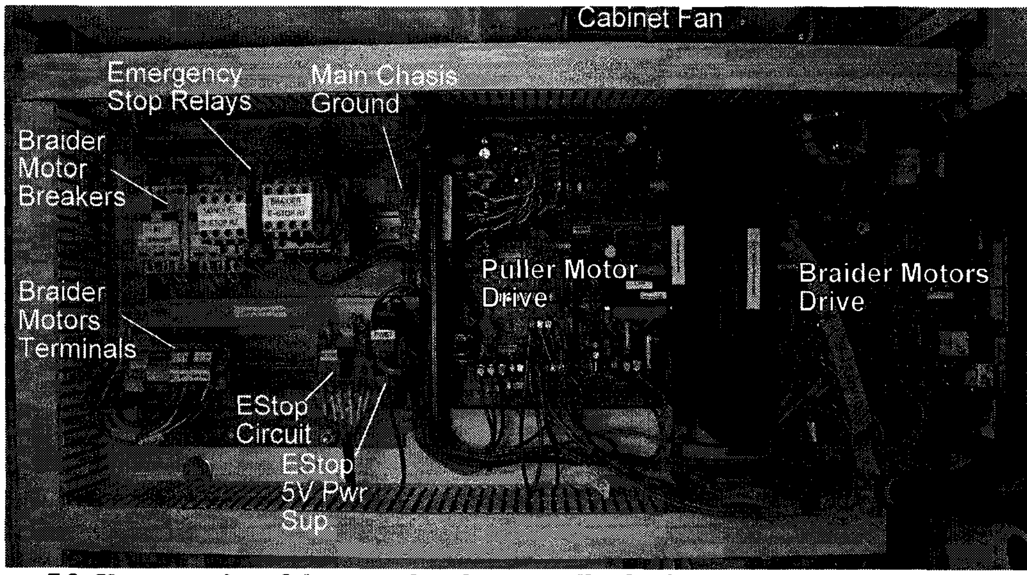

Figure 7.3: Upper portion of the control enclosure: puller, braider and emergency stop components shown.

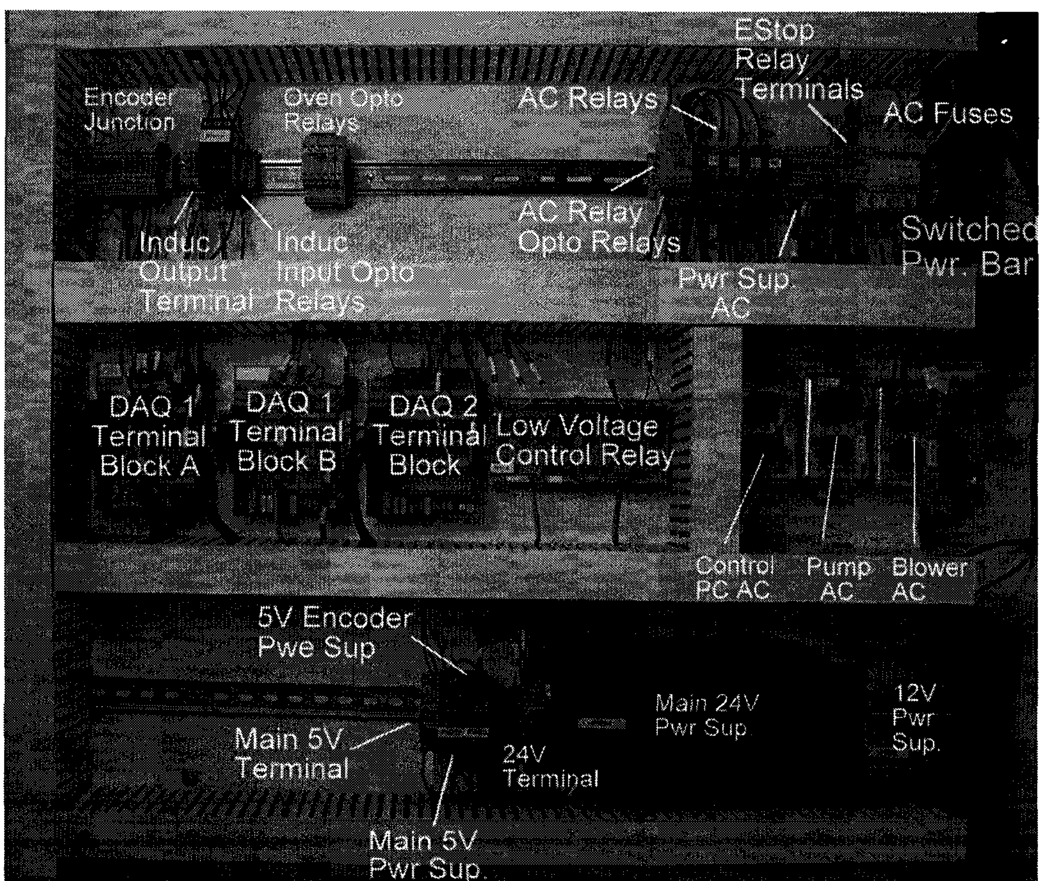

Figure 7.4: Lower portion of the control enclosure: external junctions, AC distribution, DAQ terminal blocks, Low current relays and power supplies shown.

7.2.Automation System: Hardware

This section will present details relating to the emergency stop system and the computer control system. Details regarding control and monitoring hardware specific to the braiding and pulling, dispensing, and curing systems were presented in Chapters 4, 5 and 6 respectively.

7.2.1.Emergency Stop System

The emergency stop system allows one to shut power to all of the production machinery, independently of the main automation system. As depicted in Figure 7.5, six normally closed switches are located around the production enclosure. Each switch is wired to a custom designed printed circuit board. The circuit diagram is shown in Figure 7.6. The board is located in the control enclosure (Figure 7.3, labeled "Estop Circuit"). The board utilizes the enable out pin of a 4 bit encoder to open or close a small reed relay which in turn open or close the main power relays.

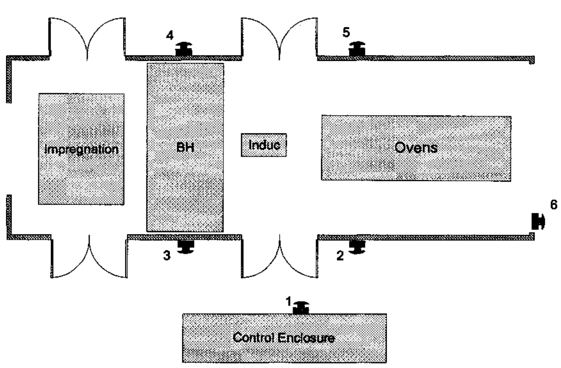

Figure 7.5: Emergency stop button locations.

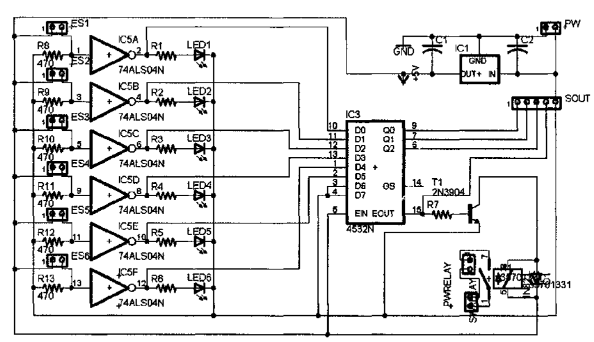

Figure 7.6: Emergency stop PCB circuit diagram.

In the event of an emergency stop condition, the electrical supply to the pump, braider and puller motor drives are interrupted by the emergency stop relays (Figure 7.3, labeled "Emergency Stop Relays"). The induction heater is also disabled by mean of external connections to a built-in relay. The ovens are disabled using opto-relays which interrupt the control signal to the main control relays. The opto-relays are shown in Figure 7.4 and are labeled "oven opto-relays". It should be noted that in this figure the opto relay components have not yet been wired. The emergency stop circuit output lines allows the control software to detect emergency stop conditions and to decode which button has been activated. When an emergency stop button is pressed during production, a dialog box allows the user the option of stopping or resuming production.

7.2.2. Computer Control System

Three data acquisition cards are used in the current control system. These are National Instrument multipurpose DAQ card model 6252M, 6215M and 6323E. These cards are referred to as DAQ 1, 2 and 3, respectively. Communication between the DAQ cards and the computer is done via the PCI bus. External signal connections to the DAQs are done via terminal blocks (shown on Figure 7.4 and labeled "DAQ1 Terminal Block A ", "DAQ1 Terminal Block B "and "DAQ2 Terminal Block"). DAQ 3 presently has no terminal block. Each card may be used to generate and acquire analog and digital signals. In the current application, analog input channels are used to acquire oven temperature measurements while analog outputs are used to control the braider, puller, pump, and induction heater. Digital outputs are used to enable all devices. They are also used to control the direction of the braider and puller and to activate the oven relays. Digital input lines are used to report the state of the induction heater and of the emergency stop system. Each card is also equipped with 2 multipurpose counters. In the current system the counters are used in conjunction with rotary encoders to estimate the speed of the braider, puller and pump motors. A fourth counter and encoder is used to track the position of the rod as it advances through the process.

The National Instrument DAQ driver *DAQmx* provides a wealth of configuration options which allows one to perform a variety of signal measurements and signal generations. For simple measurement scenarios, examples supplied by the manufacture may be modified to produce the desired program. For the system design in this work, considerable time and effort was required to find the correct configuration options to obtain the desired results. Under *DAQmx*, DAQ operations are divided into software constructs called *tasks*. To perform signal acquisition or generation the following general steps must be followed.

1. **Create a task.** Creates a task object.
2. **Add physical channels to the task.** These may include several channels of the same type. For example, a task may contain several analog inputs or outputs. A task may only contain one counter channel.
3. **Configure the measurement type.** The type of measurements available will depend on the type of channels and the capability of the specific DAQ. For example, analog input channels may be configured to measure acceleration, temperature, etc. In this case the appropriate conversion between voltage and the physical quantity is automatically done by *DAQmx*.
4. **Configure the timing.** The type, source, frequency and number of samples to acquire must be specified. Timing is discussed below.
5. **Start the task.** A command must be given to start the task. This reserves physical resources. The task is started with a trigger. This is discussed below.
6. **Write or read data.** Function call transfers data to or from the DAQ and host computer memory. Depending on the timing configuration data may be written or read once or at fixed intervals.
7. **Stop the task.** Stop signal generation or acquisition
8. **Clear the task.** Release physical resources associated with a task.

For all signal acquisitions and generation tasks, a timing source, start trigger and number of samples must be specified. The start trigger signals the DAQ hardware to begin a specific acquisition or generation operation. The timing source signals the DAQ hardware when to measure or generate a signal. The trigger and timing specified in the program code are converted to physical signals by the DAQ processor. The number of samples specified in the program is used by the host computer and the DAQ for communication purposes. For example, in an analog acquisition operation the timing signal would activate an analog hold circuit and generate an interrupt that would in turn trigger the analog to digital conversion process. When the specified number of samples have been acquired, the DAQ transfers the data to the host computer memory.

Most acquisition or generation operation may be configured with one of two types of triggers, software or hardware. Software triggers are done in the program by calling a start or stop function. Hardware triggers use a specified digital signal to trigger a specific operation. Alternatively, it is possible to configure the DAQ such that a trigger is automatically generated in the first instance of a timing signal. This is referred to as "automatic start".

Five types of timing instructions are available: on demand, finite, continuous, one sample and implicit instructions. The type of timing affects the trigger and number of sample options. On-demand timing instructs the DAQ to acquire or generate a signal. In this case, only software triggers may be used. The timing source and number of samples may be set arbitrarily. In finite operations a specified number of samples are acquired or generated according to a specified timing source and number of samples. For finite operation a hardware start trigger may be used. In continuous operation instructions, samples are acquired or generated according to a specified timing source until a software stop command is issued. One sample is a specific type of continuous operation instructions where the number of samples must be one. One sample timing is usually used in control loop applications. Finally, implicit timing instructions are used in cases where the timing information is implicitly contained in the measured signal. For example, implicit timing is used for pulse width measurement using hardware counters. In this case, a sample corresponds to one cycle of the measured pulse train.

The NI DAQ offer several timing sources. Independent analog input and output clocks are available on each DAQ card. The clock frequencies may be set to any value up to 1 kHz. While analog inputs and analog outputs may have distinct timing sources all analogue inputs and all analog outputs of a given DAQ must share the same timing source. This is due to the physical configuration of the hold circuitries which share a common sampling line. Timing signals may be share between DAQ's through the RTSI bus. The bus consists of a ribbon cable which connects the DAQ's and allow them to share up to 8 digital signals. In the current application the analog output clock of DAQ1 is share using RTSI_1 and used to time analog output operations of DAQ2. The same sample clock is also used for the braider, puller and pump counters used for digital differentiation. The analog output operations are configured as One Sample with Automatic start triggers.

The oven system uses a different timing source. The oven's PWM command signals are generated using timed digital lines. The PWM period of 10 seconds with 100 discretized duty cycle values is used. A software function generates a boolean array with the appropriate values. For example, an array corresponding to a duty cycle of 50% would contain 50 "1" followed by 50 "0". In order to generate a signal with 100 discretized step and base periods of 10 seconds a sampling clock with a frequency of 10 Hz is required. Contrary to the analog input and output lines, the digital output lines do not have a dedicated sample clock. A suitable signal is therefore generated using counter 1 of DAQ3. The counter output is routed to RTSI_3. It is also necessary to synchronize the end of the PWM command signal and the analog measurements used to read the oven thermocouple outputs. To ensure that the PWM signal and the thermo-couple measurements are synchronized, an additional timed digital line is used. By writing a "1" at the last position of the associated boolean array the line may be used to synchronize both command signal and measurements.

The use of proper timing sources is critical in order to obtain a deterministic control system. The main challenge in designing the control system under the current platform (ei personal computer running Windows XP) is the ability to synchronize the sampling loop (acquisition and generation) and the software loops which execute the control algorithms. This issue demanded considerable design effort and is discussed in Section 7.3.3.

This section was intended as a brief overview of the functionally and usage of the DAQ card. For more information regarding the configuration options, functionality and usage of the National Instrument cards used in this project the reader should consult the manufacture's web site (www.ni.com) and perform a search using the appropriate card model number. Further information regarding implementation details can be found in the code listing located in the Addendum CD included with this thesis.

7.1.Automation System: Software

This section describes the automation software of the pilot production plant. The organization of the graphical user interface along with specific software functionality are described. Limitation of the current development environment are highlighted. Specific implementation issues such as the program structure, real time consideration and timing are discussed.

7.1.1.Development Environment

LabWindows uses an ANCI C compiler to generate executable programs. This version of C was developed in 1989 and does not provide some of newer functionalities of modern C compilers such as C99[68][69]. Nevertheless, LabWindows provides several libraries which provide high level functionality with minimal code development. The functions included in these libraries provide the same functionality as the function blocks of LabView. These include access to data acquisition hardware, mathematical functions and network communication. Furthermore, several packages provide abstraction to application program interfaces (API) and access to Windows Standard Development Kit (SDK) functions. Development of multithread applications, access to standard dialogs and external peripherals are therefore greatly simplified. LabWindow can also create professional looking graphical interfaces. Several specialize command and display widgets are provided. These include buttons, sliders, graphs, stripcharts etc. Newer version of LabWindows can also compile programs as dynamic linked libraries (DLL). This allows software to be executed on a real time platforms such as a PXI controller or a personal computer running a real time operating system.

7.1.2. Overview of Software Structure

The automation software is developed using a multithread architecture. Thread resources are allocated in the "Start" callback and released by the "Stop" callback. The code contained in each thread is cyclically executed. Code execution is regulated using various mechanisms. This is extensively discussed in the following section. The thread description along with their execution rates and execution control mechanisms are given in Table 7.1.

Table 7.1: Automation Software Thread and Description

Thread	Thread Functional Diagram	Description	Execution Rate (sec)	Execution Control Mechanisms
Display	Figure 7.7 p.198	Updates the graphic user interface.	0.5-10 (user defined)	Software timed
Fast Control	Figure 7.8 p.199	Execute control algorithms for the braider, puller and pump rotor. Log data associated with these devices.	1/60	Hardware based interrupt from analog output sample clock
Oven Control	Figure 7.9 p.200	Execute the control algorithm and log data for tubular ovens.	10	Hardware based interrupt from analog input operation
Resin Scale	Figure 7.10 p.201	Read data from scale, estimates dispensing rate and adjust pump set points	4	Software timed
Digital Input	Figure 7.11 p.202	Read DAQ digital input buffer and transfer to variables	1	Software timed

The automation software code is divided in several modules; each contains several functions. This design approach is used to group functions that provide similar functionality. The result is a program with improved code readability and maintainability. A description of each module is given in Table 7.2.

Table 7.2: Program modules and description

Module	Description
CBC.c	Contain the program main, execution control code and GUI callback functions. Thread functions are located in this module.
Data.c	Contains all shared variable declarations. Data.h contains several constants associated with each device
IO.c	Functions related to signal measurement and generation. Initialization function: create measurement or signal generation task, reserve physical resources, configure timing and specifies DAQ buffer size. Read or write: issue a command to transfer data between the DAQ and PC. Clear functions: Release physical resources related to a device.
Control.c	Function that perform machinery control can be found in this module. See section YY for more details
Keyboard Control.c	Contains function that allow the user to use the keyboard to control machinery operation. See YY for a discussion of this functionality.
Log.c	Contains functions that save machine operation data to text files. Create functions: creates a text file and inserts the appropriate header. Log functions: places the relevant data in the file input stream. Close functions: saves the file and releases the stream
Util.c	General utility functions can be found in this module. These include mathematical routines, file naming utility, etc.
Resin Scale.c	This module contains function to acquire data from the resin scale serial stream. Circular buffer data structure initialization and read functions allow data acquired from the serial port to be stored. Function that decode the serial stream and return relevant data are also included.

The Data.c module contains declaration of all variables that are shared between modules. The "extern" identifier is used to make the variables global (seen by all program code). Declaring variables as global allows the division of functions in different modules without incurring the additional overhead associated with passing or referencing variables between functions. Since variables may be used by several threads, care must be taken when performing "write" operations. In most cases, several threads will read a variable but only one thread will write to a variable. This ensures that variable are not corrupted by two simultaneous "write" operations. It should be noted that variables which are only used in a specific module or function are declared locally.

7.1.3.Real Time and Timing Consideration

The basic assumptions in designing a discrete control system are that the sampling time is known and constant. Although the latter is not an essential criterion, assuming a constant sampling time simplifies the control system design and greatly reduces the complexity of the control algorithm. Therefore, control systems are usually designed under this assumption unless other factors warrant a variable sampling periods. Whether the system employs a fixed or variable sampling time, the sampling period must be known a-priori since the magnitude of the control action will depend on the time to the next control action. Uncertainty in the sampling period or jitter is present in any control system. If the jitter is below a permissible value, the control system is said to be deterministic.

Jitter will manifest itself as a disturbance of the system under control. Its effect is a function of the system states and the control vector. If the jitter is small, the magnitude of disturbances is negligible and may not be detectable. For a nondeterministic system where an entire sampling period may be missed these disturbances can affect the system considerably. If stability margins are small, excessive oscillation may occur or the system may become unstable. Therefore, the controller gains (PID) or desired closed loop poles (state space controller) must be selected appropriately.

Since Windows XP is not a real time operating system, techniques such as the use of multithread code execution and hardware timing of the control loop allow one to achieve near deterministic behaviour. Nevertheless, known and constant sampling times cannot be guaranteed. To understand this statement, the principle and use of multithread code execution and hardware timing of the control loop are presented.

7.1.3.1.Multithread Paradigm

The basic operating principle of all modern operating systems is the ability to simultaneously (from the user's perspective) execute several programs. In such paradigms, program code is divided into threads. Each thread requires some computational time (code execution by CPU) and the use of shared resources, such as memory or peripheral access. The goal of the operating system is to manage the execution of all threads in order to maximize the execution speeds of all the programs. When a thread requests access to a shared resources its execution is halted until the resource becomes available. During this time other threads are executed. Switching from one thread to another when a particular thread is idle maximizes the use of the CPU and, consequently, maximizes the execution speeds of all programs currently in execution.

For the present control software, the use of a multithread code execution is advantageous since considerable use of peripheral resources is required. For example, a typical iteration of a control loop will consist of data transfer between the DAQ and the memory (read external signal), some computation (control algorithm) and data transfer between memory and DAQ (writing control signal). Furthermore, if logging is enabled, data must also be written to a file input stream. Operations which require interaction with the user interfaces (displaying data or acquiring user input) require considerable CPU time. Executing the control code in one thread and the display update code in another allows the latter to be executed while the control code waits for data from the DAQ. This increases the execution efficiency compared to a single thread program.

Unfortunately, Windows XP provides limited control over thread execution. In contrast, a real time operating system provides mechanisms which enable the developer to specify thread scheduling. It should also be noted that a number of unrelated threads must remain active during the control software execution. These threads are automatically scheduled by the window kernel and may retard the control software execution.

From a control stand point, another advantage of multiple threads is the ability to execute specific code segments using different timing sources. For example, updating the display is timed using a software timer and is done every 1 to 5 seconds. The control algorithms associated with motor speed regulation must be updated considerably more frequently, at a rate of 60Hz. The use of appropriate timing sources to regulate thread execution is critical to proper execution of the control software.

7.1.3.2.Thread and DAQ Timing

Thread execution may be regulated using either software-based timing or hardware interrupts.

Software timing corresponds to halting the execution of a thread for a specified amount of time. A timer internal to the operating system is used to reactivate the thread after the specified delay. This type of thread timing allows for a greater flexibility in loop times as the operating system uses independent timers for each thread. The disadvantage of this method (for non-real time operating system) is that deterministic thread execution and timing of external event cannot be achieved. In the present context, acquisition and generation of external signals is requested by the operating system. The control software is therefore unable to ascertain the exact time when a signal is aquired or generated. This method is therefore preferred for operations where deterministic behaviour is not necessary. In the current implementation, user interface updates, control of the dispensing process (Figure 7.10) and acquisition of digital signals (Figure 7.11) are done using software-base timed loops.

Regulating thread execution using hardware interrupt requires that hardware timing be used. Synchronization between the acquisition or generation operation of the DAQ and of the control algorithms must be ensured. National Instrument provides two mechanisms to implement hardware and program execution synchronization.

The first utilizes the DAQ read instructions. Each time a DAQ read command is issued the thread is halted until all the requested data have been collected. This only occurs after a transition of the sample clock. The acquisition clock can therefore be used to regulate code execution. This method is used for the oven control thread. In this case the analog read instruction provides timing for the control algorithm.

The second method utilizes a command which explicitly waits until the next sample clock of a specified task occur. In the current implementation this method is used in the fast control thread which executes the braider, puller and pump motor regulation algorithms.

Non-deterministic behaviour occurs when the execution of the control software cannot keep up with the hardware timed DAQ operations. This is not a problem for the oven control thread since the control period is 10 seconds. The problem is observed for the fast control thread which executes the control algorithm for the braider, puller, pump rotor. DAQmx provides a means to detect when a missed sample occurs during the wait for next sample clock instruction. This proved useful to qualitatively evaluate how missed samples could be reduced. It was found that missed samples could be significantly reduced by decreasing the display update rate, by increasing the scheduling priority of the fast control thread and decreasing the priority of the display update thread. Manually closing an unrelated process had no appreciable effect on the missed sample rate nor did increasing the process priority in Windows Task manager. Presently, the missed sample rate for the fast control thread is between 5 and 10 sample per second. As previously stated, the effect of missed samples on the control processes is reduced by the use of PID algorithms that utilize continuous approximations for the integral and derivative term. It was found that the missed sample did not significantly hinder the control processes. Recommendations regarding this issue is given in Chapter 8.

7.1.4. Program Functional Diagram

The program functional diagrams for each thread are shown in this section. The diagram shows the main program structure. In most cases individual blocks refer to a function. For implementation details of each function a code listing is included in the addendum which can be found on the CD which accompanies this thesis.

7.1.4.1.Display Thread

The display thread updates the graphical user interface. The update rate is defined by the user. The display update may also be suppressed by the user. The graphical user interface is divided into several tabs. Only the displayed tab is updated. Semaphores are used to signal when new data is available to be displayed. The semaphores are implemented using flags which are cleared by the display thread and set by the threads which generate the data.

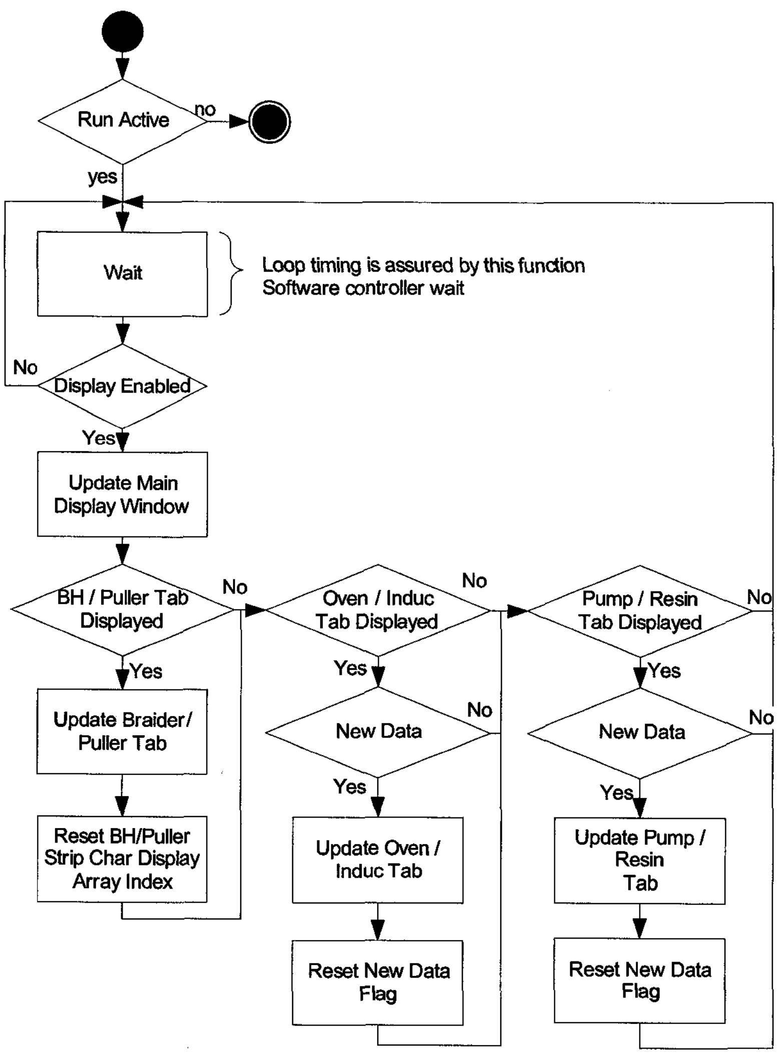

Figure 7.7: Display thread function flow chart.

7.1.4.2.Fast Control Thread

The fast control thread executes the control algorithms for the puller, braider head and pump rotor. Data logging of measurements, set points, and control signals associated these devices is also handled by this thread.

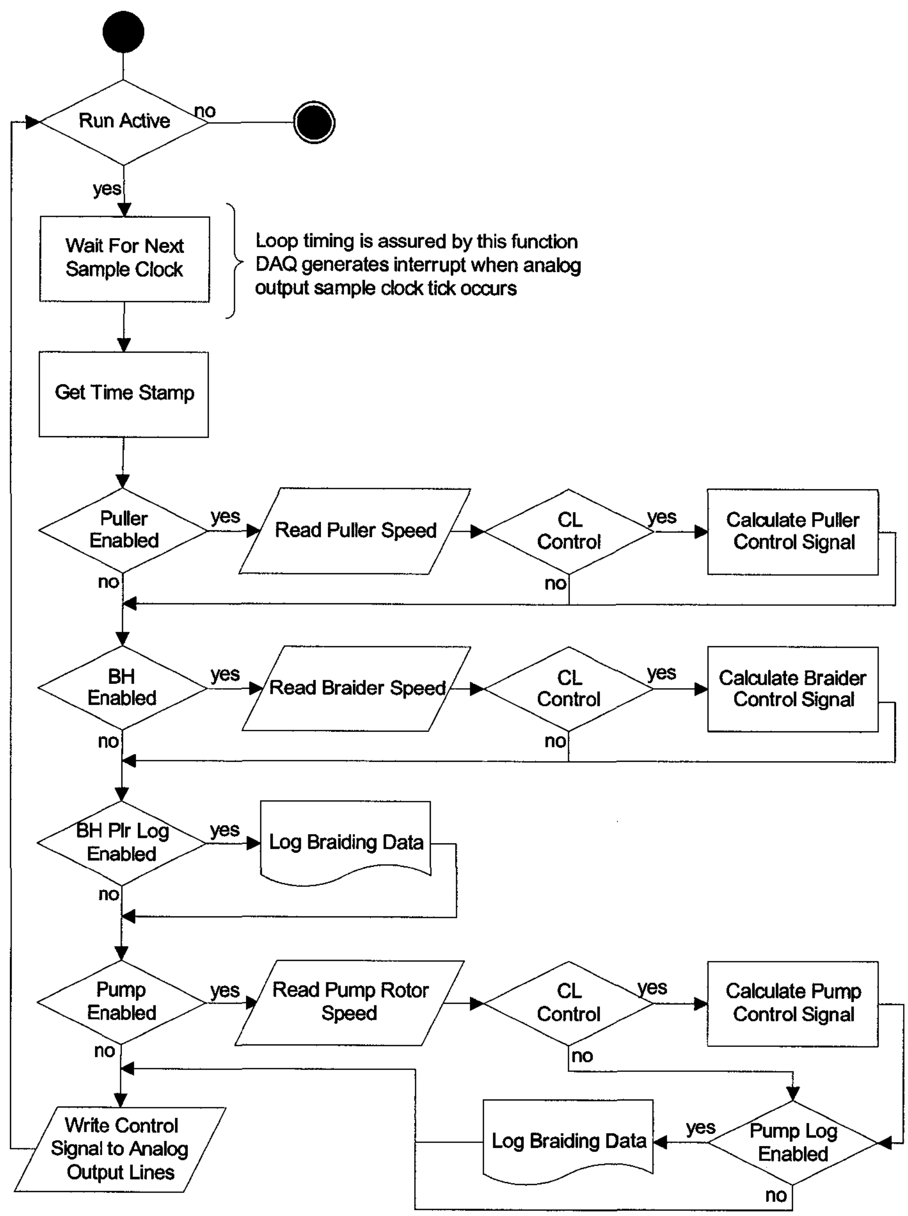

Figure 7.8: Fast control thread function flow chart.

7.1.4.3.Oven Control Thread

The oven control thread executes the control algorithm to regulate the tube oven temperature. Data logging of the oven temperature is also done by this thread.

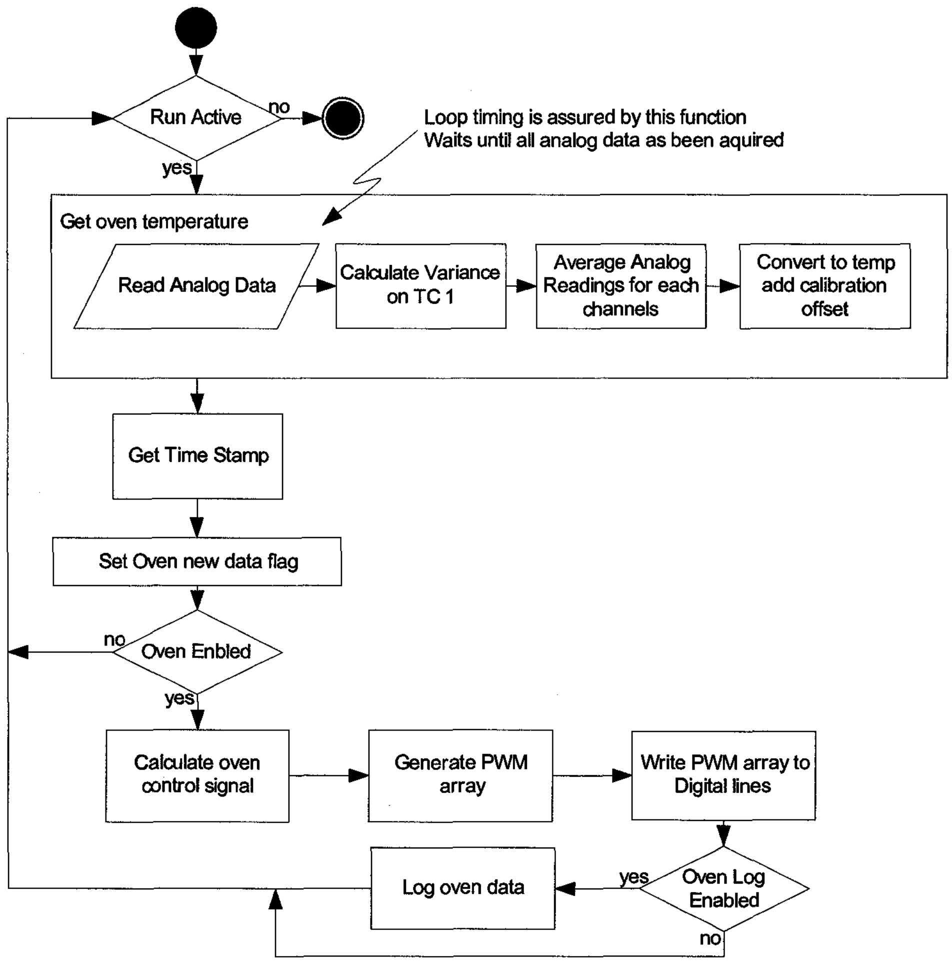

Figure 7.9: Oven control thread function flow chart.

7.1.4.4.Resin Scale Thread

The resin scale thread reads weight measurement data loaded in the serial queue, estimates the dispensing flow rate and adjusted the resin pump set point.

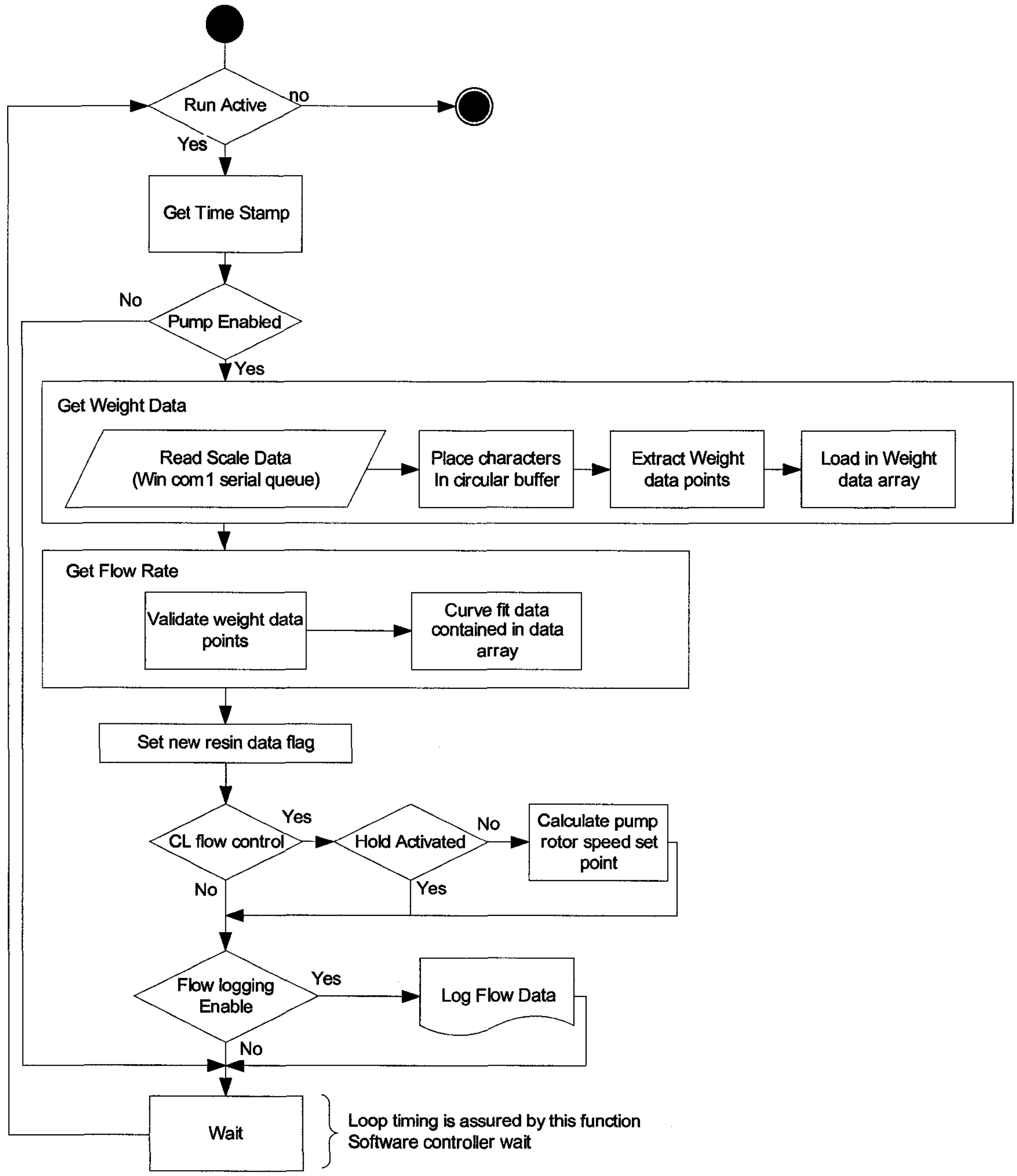

Figure 7.10: Resin scale thread function flow chart.

7.1.4.5.Digital Input Thread

The digital input thread polls the digital lines and update the state of the software variables. The digital input lines are used to report the status of the induction heater and the emergency stop system.

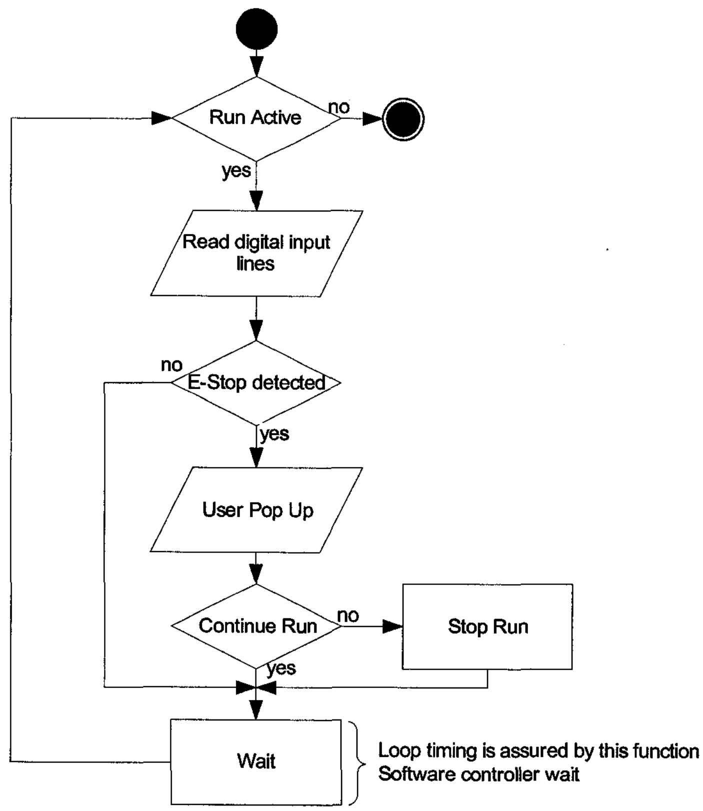

Figure 7.11: Digital input thread function flow chart.

7.1.5.GUI Interface and Software Features

7.1.5.1.Automation Software Screen Shots

Iteration with the automation software is done via a graphical user interface. Toggles, buttons, check boxes, combination boxes and numeric fields allow the user to change machine control options. Numeric fields, LED widgets and various graphs present machine data to the user. Machine controls are organized on four panels. General control and information are located on the right hand side of the interface window.

Machine controls are divided onto three tabbed panels; braiding and pulling, oven and induction, and resin dispensing. The panels are contained within a tab widget on the right hand side of the screen. Screen shots of the automation software for each of the tabs are shown in Figures 7.12,7.13 and 7.14. A screen showing the automatic pump calibration utility is shown in Figure 7.15. This utility is used to automatically generate calibration points.

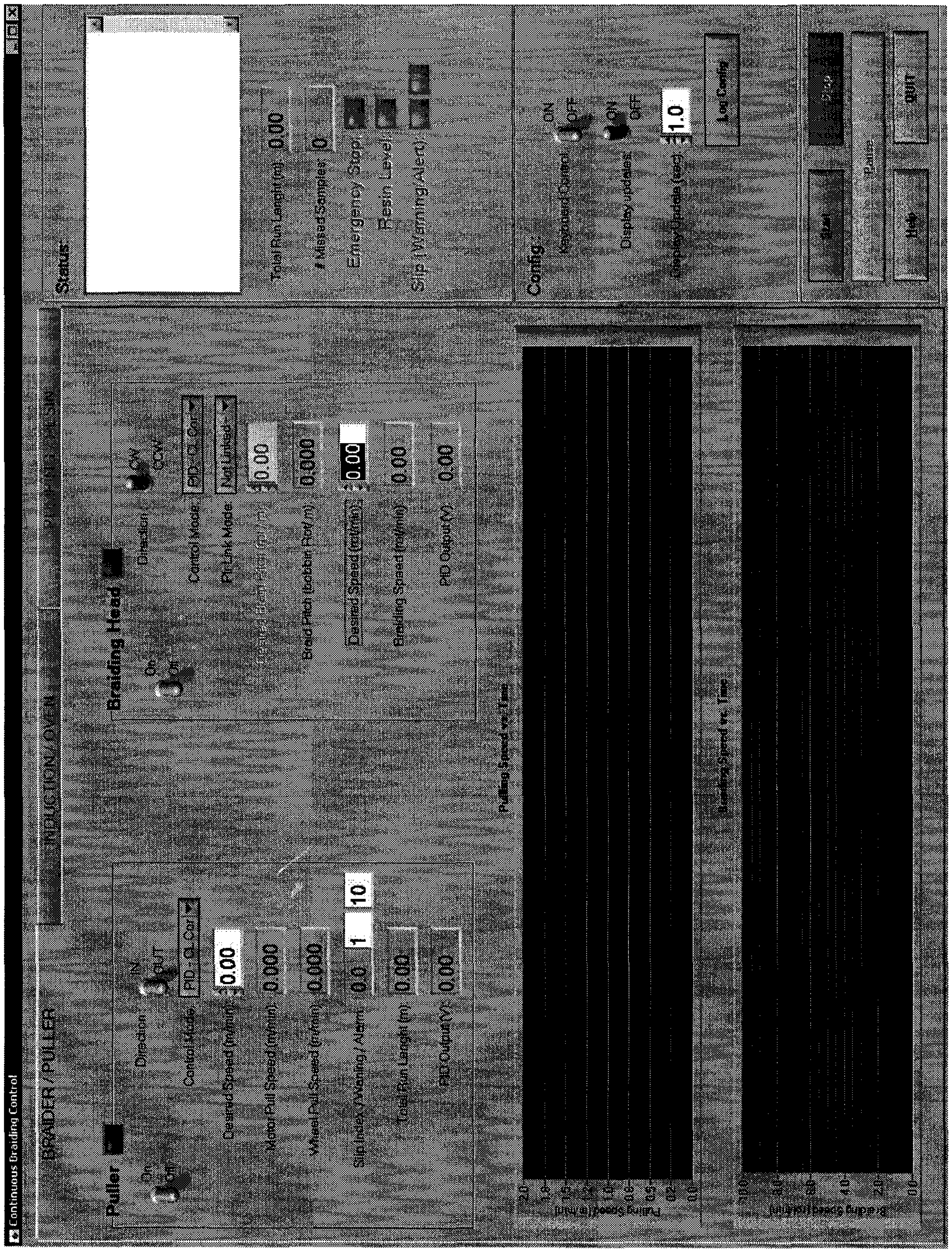

Figure 7.12: Screen shot of the Braider / Puller tab.

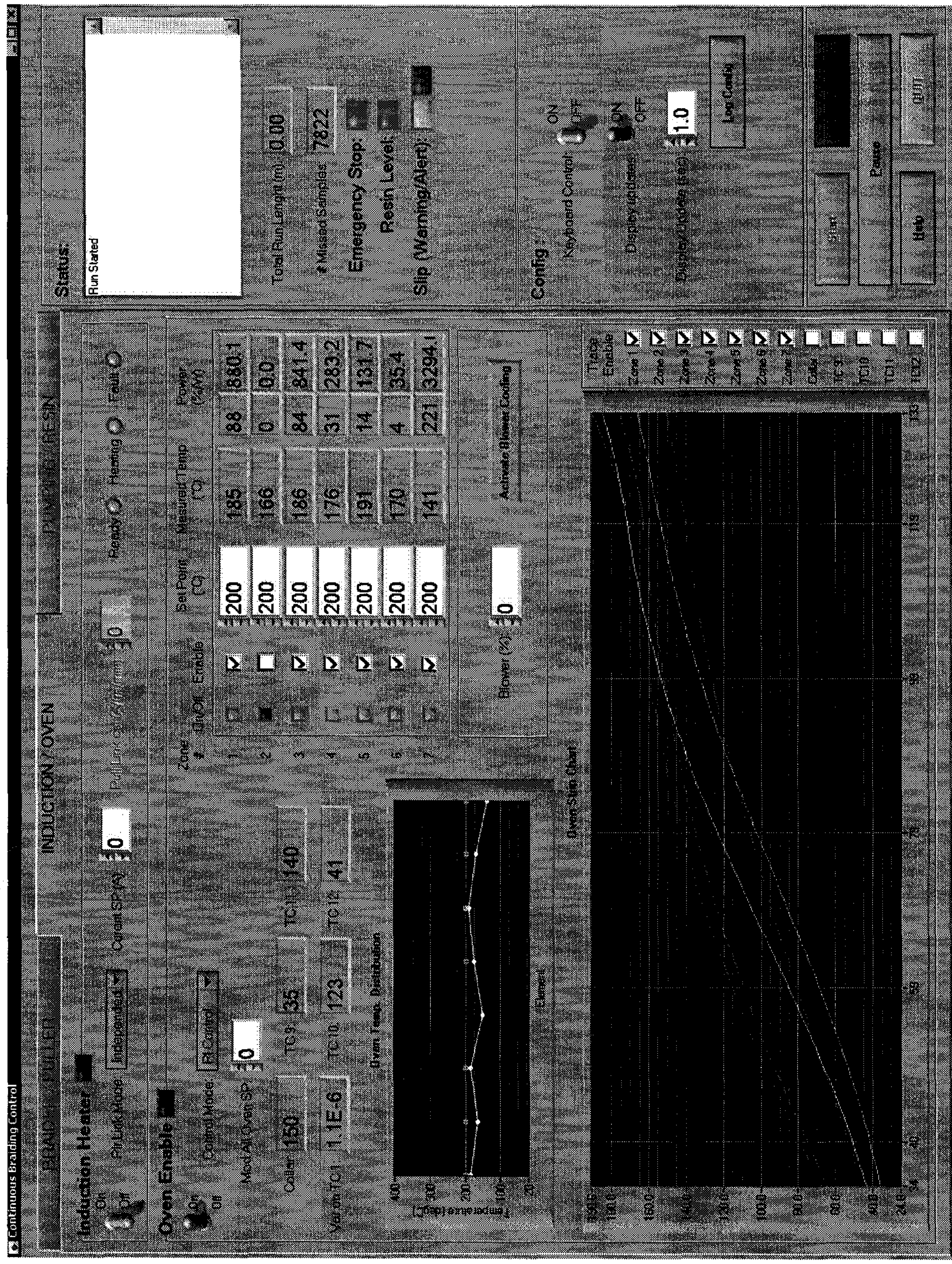

Figure 7.13: Screen shot of the Oven / Induc tab.

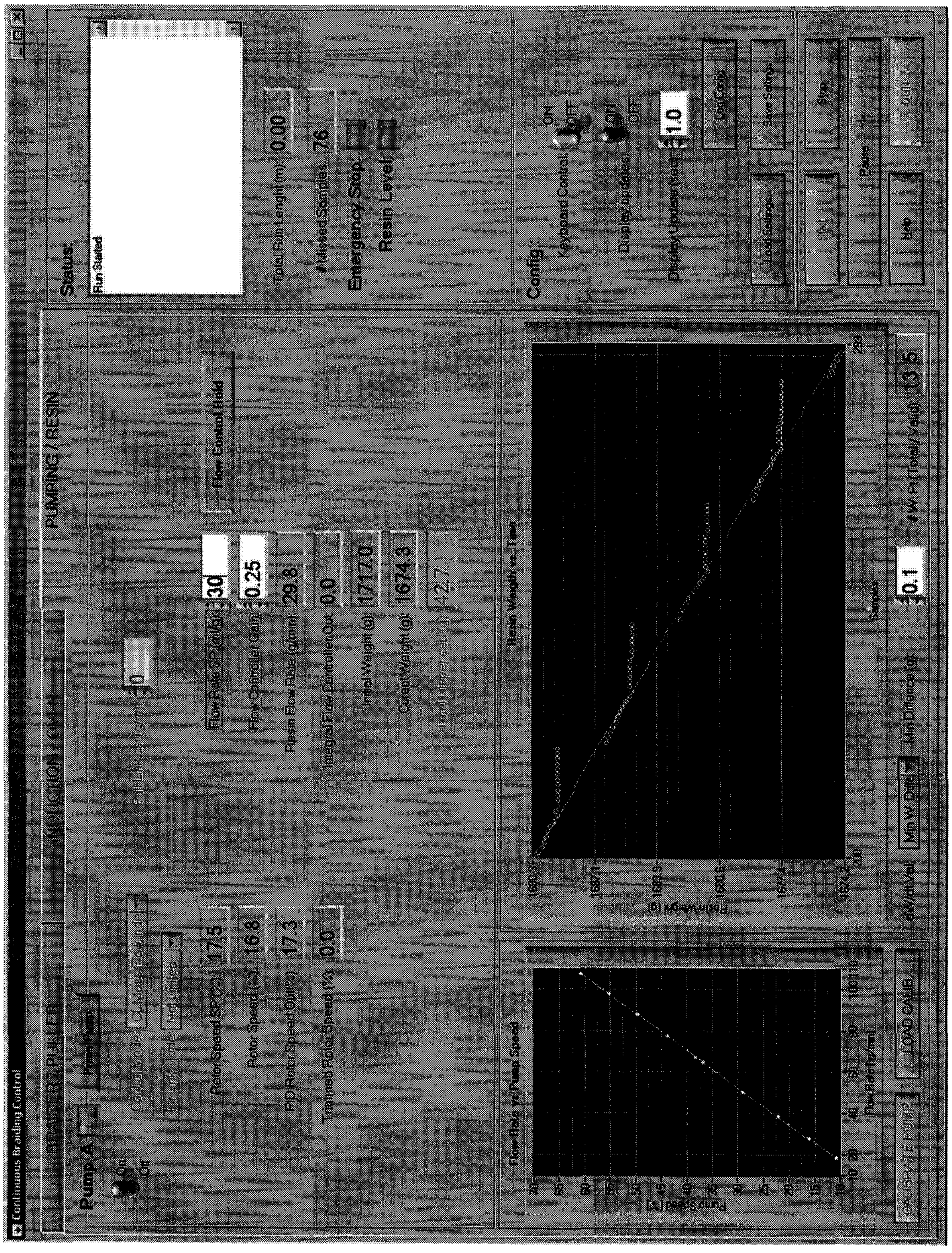

Figure 7.14: Screen shot of the Pumping / Resin tab.

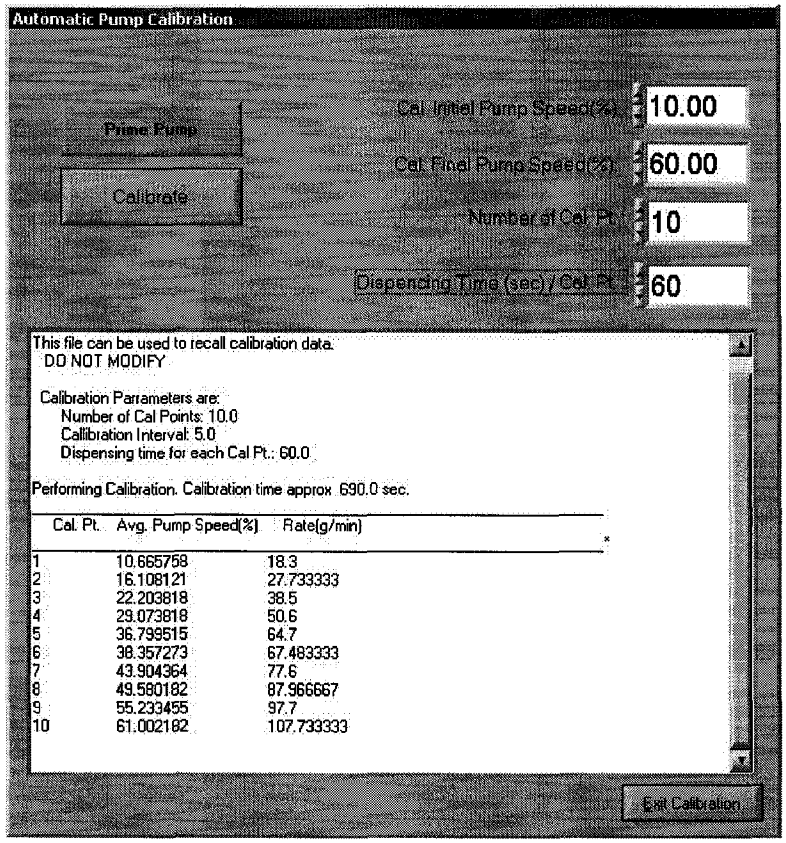

Figure 7.15: Automatic pump calibration utility panel.

7.1.5.2.Summery of Automation Software GUI Controls

Controls for most of the machine operations are very similar. These include the following:

- An enable button or check box to turn machinery on or off.
- A set point field to enter the desired operating set point.
- A control mode selector to change the control algorithm
- A numeric field to display the actual measured variable.

Functionalities of controls located in each part of the GUI, namely the Main Panel, Braider / Puller tab, the Oven / Induc tab and the Pumping / Resin tab are summarized in Tables 7.3 to 7.5, respectively.

During production, small changes in machine set points must often be made. Using the mouse for these changes can be difficult. For this reason, adjustment to several important machine parameters are mapped to specific keyboard keys. To use keyboard control, the functionality must first be enabled through the Keyboard Enable switch located on the Main Panel of the GUI. Specific commands are issued by pressing the appropriate key while activating "Shift" or "Caps Lock". Keypress events are handled through the "Keypress Event Handler" callback of "CBC.c". The callback calls function "keypress" located in "keyboardControl.c"

Table 7.3: Summary of Main Panel GUI controls.

Name	Function
Status	Display textual messages to the user about machine operation and software status important information.
Total Run Length	Display the total length of produces since the start of the run. The measurement is provided by the puller wheel encoder sensor.
Missed Sample	Report the total number of missed sample since the start of the run.
Emergency Stop LED	Display red when the emergency stop is engaged.
Resin Level LED	Display red when the resin level is below the threshold as defined in data.h (presently 200g).
Slip (Warning/Alert) LED (Shown in Figure 7.13 only)	Display green when slip is below Warning/Alert threshold. Display yellow/red when slip above threshold. Threshold values defined in puller/braider tab (Table 7.4).
Keyboard control enable	Enable/Disable Keyboard control.
Display updates (enable)	Enable/Disable display updates.
Display updates (period)	Set the period of display updates.
Log Config(uration)	Open the log configuration dialog.
Load Settings	Load previously save settings.
Save Settings	Save current settings (device set points, control modes...).
Start	Start production.
Stop	Stop production.
Pause	Pause production. Braider, puller, pump, induction heater are turned off. Oven control remains on.
Help	Activate the help dialog.
Quit	Terminate program execution. Disabled when production is started.

Table 7.4: Summary of Braider / Puller tab GUI controls.

Name	Description
Puller	
Puller-Control Mode (P-CM)	1) OL (meter/min). 2) CL PID (meter/min).
Desired Speed	Desired Pulling speed (m/min).
Motor Pull Speed	Pulling speed as estimated by the motor encoder (m/min).
Wheel Pull Speed	Pulling speed as estimated by the wheel sensor encoder (m/min).
Slip Index, Warning, Alarm	Display the slip index, Enter slip warning, Enter slip alarm.
Pull Speed Slip	Slip between the rod and the belt. Displays infinite if no rod in puller (%).
Puller-PID Output (V)	P-CM 1: Output of the puller set point element (V). P-CM 2: Output of puller PID.
Pulling Speed vs. Time (strip chart)	Displays the measured pulling speed from the motor encoder. All acquired samples are shown (60 sample/sec).
Braider Head	
Braider-Control Mode (B-CM)	1) OL Braider under open loop control. 2) CL PID Braider under close loop PID control.
Braider-Plr link Mode (B-PLM)	1) Independent (Spool rotation / min). 2) Link to puller speed. Braid pitch is specified (Spool rot/meter).
Desired Braid Pitch	B-PLM 1:disabled. B-PLM 2:Specify the pitch as set point (rot/m).
Actual Braid Pitch	Braid Pitch calculated from the measured braiding head speed and pulling speed (rot/m).
Desired Braiding Speed	B-PLM 1:Specified braiding speed (rot/min). B-PLM 2: Display the desired braiding speed calculated from desired braid pitch and pulling speed.
Actual Braiding Speed	Estimated braiding speed from motor encoder measurement (rot/m).
Braider-PID output	B-CM 1: Disabled. B-CM 2:Output of the braider PID (V).
Braiding Speed vs. Time (strip chart)	Displays the measured braiding speed. All acquired samples are shown (60 sample/sec).

Table 7.5: Summary of Oven / Induc(tion) tab GUI controls.

Name	Description
Induction Heater	
Plr Link Mode (I-PLM)	1-Independent (Amp.). 2-Linked to pulling speed (Amp/(m/min)).
Current	I-PLM 1: Specify the current set point. I-PLM 2: Display the current set point calculated form link constant and pulling speed.
Link constant	I-PLM1: Disabled. I-PLM 2: Specify the amperage per meters minute.
Ready,Heating, Fault LED	Indicate the induction unit is Ready, Heating, or that a fault has occurred.
Ovens	
Master enable	Enable the oven system.
Control mode	1-PI temperature control. Control oven using gain scheduled PI control. 2-Identification Control. Oven is controlled in open loop about command input when this control mode is first activated. New random command issued every 1h. Used to gather temp response for identification purposes.
Mod(ify) all Oven SP	Change the temperature set point of all oven zones.
Zone set point	Specify the temperature set point of each zone (°C).
Actual zone temperature	Display the measured temperature in each oven zone (°C).
TC 9-12	Display the measured temperature of the spare thermocouples (°C).
Var on TC 1	Variance on the temperature measurement of TC1. Used to evaluate the random noise present on the TC lines.
Blower power	Set the blower power (% of max).
Activate Blower Cooling	Turn on blower cooling. Used to prevent over curing of the rod in case production run must be halted for several minutes.
Temperature distribution(chart)	Display the measured temperature distribution and temperature set points for each zone.
Temperature vs. time (strip chart)	Display the temperature of each zone with respect to time.
Trace enable	Show/Hide the traces on the Temperature vs. time strip chart.

Table 7.6: Summary of Pump / Resin tap GUI controls

Name	Description
Control Mode (CM)	1)Rotor speed OL (% of max). 2)Rotor speed CL PID (% of max). 3)Flow rate OL (g/min) from calibration curve + Rotor speed CL PID. 4)Flow rate CL I(intergal) control + OL cal curve + Rotor speed CL PID.
Plr link Mode (R-PLR)	1)Independent (flow rate independent of puller speed). 2)Linked to pulling (flow rate linked to puller speed).
Dispensing Constant	R-PLR 1: Disabled. R-PLR 2: Specify the dispensing rate per meter of product (g/m).
Pump	
Rotor Speed	CM 1,2: Set the rotor speed. CM 3,4: Display desired rotor speed as calculated by the flow rate controller (% of max speed).
Actual Rotor Speed	Estimated from pump encoder (% of max speed).
PID rotor speed out	Output of the pump rotor PID (% of max speed).
Flow Rate Controller	
Flow rate set point	CM 1,2: Disabled. CM 3,4: Specify the desired flow rate (g/m).
Flow Control Hold	CM 1-3: Disabled. CM 4: Hold the current controller output. Used if more resin must be added on scale.
Flow Controller Gain	CM 1-3: Disabled. CM 4: Specify the flow rate controller integral gain.
Resin Flow Rate	The flow rate estimated from weight measurements (g/min).
Integral Flow controller out	CM 1-3: Disabled. CM 4: Output of the flow rate of the integral controller.
Initial Weight	Weight registered on the resin scale at the beginning of production run (g).
Current Weight	Weight registered on the resin scale after the last sampling time (g).
Total dispensed resin	Total quantity of resin dispensed during the production run (g).

Table 7.5 Summary of Pump / Resin tap GUI controls (Continue)

Name	Description
Pump Calibration	
Pump Speed vs. Flow Rate	Displays the pump speed vs. flow rate calibration points and the fitted polynomial (up to 3rd order) calibration curve.
Calibrate Pump	Launch the pump calibration utility.
Load Calib	Open a file dialog and recall previous pump calibration.
Resin Flow Rate Estimate	
Resin Weight vs. Time (Strip Chart)	Display the weight measurement and the fitted linear function.
Reject Method	Specify the method specified to reject between good and bad weight measurement. 1) Expected value: Use calibration curve to calculate expected value. 2) Minimum difference: Reject based on the difference between to successive points.
Reject Threshold	Value used to reject weight measurements.
Wt (weight) Pt (point) #,Valid	Total number of weight data point,Number of valid points.

Table 7.7: Summery of Automatic Pump calibration GUI controls

Name	Description
Resin Flow Rate Estimate	
Prime Pump	Activate pump to prime tubing.
Calibrate Pump	Start Calibration process.
Cal(ibration) initial speed	Minimum speed for the calibration (% of max).
Cal(ibration) final speed	Maximum speed for the calibration (% of max).
Num of calibration point	Number of calibration point in the calibration interval (as defined by initial and final pump speed).
Dispensing time / cal point	Time to dispense for each calibration points (sec).

7.1.6. Control Algorithms

National Instrument PID packages are used to implement PID controllers for the braider head, puller and resin pump control. This PID package use trapezoid and difference approximations to calculate the integral and derivative control actions, respectively. Although this method is more computational expensive compared to a discretized PID, it allows compensation for non-deterministic sample times of the control loops.

The oven and resin flow controllers use custom-developed code. The integral term is estimated from a trapezoidal integration. Non-deterministic behaviour has less of an effect on the oven and flow control loop since the sampling time is long (10 sec for ovens, 4 sec for flow control).

Default gains for all controllers are defined in data.h as macros.

7.1.7. Data Logging

If desired by the user, logs of machinery operation can be generated by the control software. The log files are recorded in Tab separated text files. All data related to machinery operation is recored. These include machine set point, measured variables, controller outputs, etc. Using the log configuration panel (Figure 7.16) the user can enable logging for individual subsystems, namely, the braiding and pulling, resin dispensing, resin scale and ovens. The logging interval in terms of sampling period can also be specified. For example, if the sampling period for the braiding and pulling subsystem is 0.1 seconds the user may chose to record data every 0.1, 0.2, 0.3... seconds.

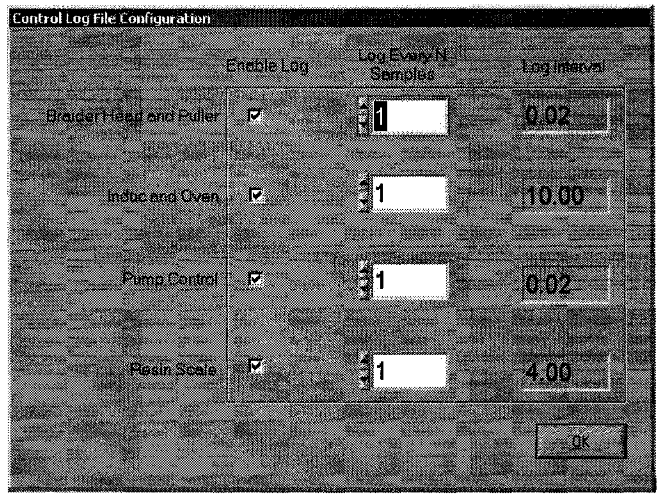

Figure 7.16: Control program log configuration panel.

Logs are created at the start of the run. A unique file name is automatically generated. The file name begins with a prefix corresponding to the type of log file. For example, the braiding log file begins with "CBC_BraidingLog". The current date and time are appended to this prefix. Files are stored in a directory name using the current date. If a directory does not exist, one is automatically created. This task is accomplished using the "CreateFile" function of "util.c"

8 Conclusion and Future Work

This chapter presents concluding remarks on the work presented in this thesis. Recommendations related to manufacturing equipment and future work associated with the continuous braiding process are made.

8.1.Conclusion

The main goal of the work presented in this thesis was to develop a pilot production plant capable of manufacturing a hybrid braided pultruded rod on a continuous basis. To some extent, it was possible to do so prior to this work but the product lacked the quality to provide consistent mechanical properties. Subsequent mechanical testing of the product in concrete beams was therefore not successful. The original production process was done through manual impregnation of the fibres and batch curing in an elevated temperature oven. This method proved time-consuming and lacked the throughput required to evaluate product on a large scale. In section 3.2, a number of key production issues identified following initial production runs were described. Goals aimed to correct these issues where also listed. These goals are recalled here and a summary of how this work has attempted to achieve them is given.

Central fibres must not be damaged. The fibre sorting system was completely redesigned. New spools were constructed to increase the creel capacity. This eliminated the need to double wind spools. Spools are now individually tensioned using a simple spring and friction place mechanism. Fibre damage is also was minimized by using two set of low friction polymeric guide eyes. One set guides the fibre out of the creel, the other into the impregnation ring.

Central fibres must be fully impregnated before the 2D braid is deposited. A previously developed impregnation ring is used for central fibre impregnation. For proper impregnation, each fibre must contact and follow the inner radius of the impregnation ring. This was achieved through the design of the fibre sorting system. The speed of impregnation was increased by decreasing resin viscosity once it had been deposited on the fibre. This is achieved using hot air blown on the wet fibres as they exit the impregnation ring. Lastly, a filter medium is added in the internal ring plenum to increase the back pressure in the ring plenum. This minimized the effect of gravity-induced flow, thus providing uniform flow independent of the vertical position of the feed channels of the ring.

The dispensing rate must be monitored and controlled. Monitoring the dispensing rate is achieved using weight measurements of the resin. The dispensing rate is controlled using a set point element obtained from an automatically generated calibration curve and through pure integral control. The dispensing accuracy is limited by the resin flow rate estimate to approximately ±2 g/min. For the current product, this translates to a maximum error of 2.1% in the fibre volume fraction.

The braiding and pulling speeds must be measurable and controllable. The digital differentiation of optical encoders allows the estimation the of braiding and pulling speeds with an accuracy of 0.118 rpm and 0.014 m/min respectively. Speed control is achieved using a set point profile and an integral trim controller.

The temperatures of the curing ovens must be monitored and controlled. More specifically, the closed loop time constant must be decreased. Monitoring of the oven temperatures is accomplished using wire-supported thermocouples placed directly in the tunnel heating chamber. Control is done using a gaine scheduled PI feedback controller. An air purging system was implemented to increase the oven chamber cooling rate. The system can be used to quickly decrease the oven temperature in the event that the production have to be stop unexpectedly. Conceivably, this prevents over-curing of the product located in the curing oven chamber while production is halted.

Changes in pulling speed must be reflected in appropriate changes in other production quantities such as braiding speed, dispensing rate and curing control parameters. A global controller monitors the pulling speed and adjusts other set points accordingly. The actual pulling speed is measured using a wheel which rests on the pulled product. This sensor allows the automatic detection of slip between the belts and the pulled product which may occur in adverse operation conditions.

Machinery control and monitoring must be centralized such that they may be controlled and monitored by one operator. A computer based control system was implemented to monitor and control all production parameters. A graphical user interface is used to report and modify the operational state of the production parameters. The system also alerts the operator of abnormal operation conditions.

The operator must be able to stop production, if needed, without compromising the quality of the product within the production line. This is greatly simplified by centralizing all machinery control through the control system. A functionality is provided in the control software to pause and resume production using one command. To prevent over-curing of the product located in the curing oven chamber, the oven air purging system may used to quickly decrease the oven temperature when production is halted.

In a recent production run, several meters of 0.5 in carbon rod were produced at line speeds of 0.5 m/min. Visual inspection of the rod indicate that full impregnation and full curing were achieved. The modifications to production equipment and the implementation of a new control system described in this work significantly improved the ability of the pilot production plant to manufacture product with good quality control. Nevertheless, as with all research work of this type, improvements are still possible. Therefore, the next section will give several recommendations regarding possible improvements to the production machinery. Suggestions for future work relating to automation and control of the continuous braiding process are also given.

The changes to the production hardware and automation system are summarized in Table 8.1. In this table, phase 1 refers to the state of the production line prior to this work, while phase 2 refers to the current state of the production line.

Table 8.1: Initial and current state of pilot production plant.

Systems	Phase 1 (2006)	Phase 2 (2008)
Braiding and Pulling	Braiding and pulling (feed rate) speeds are monitored but not automatically controlled.	Incremental encoders monitor the braider and puller motor speeds. A sensor directly monitors the feed rate of the product. The motor speeds is controlled using integral trim controllers
	A 12V DC motor provide power to the pulling station. The Puller is under-powered leading to inconsistent feed rates.	¾ HP synchronous motor and worm gear box provide power to the pulling station.
Fibre Sorting and Impregnation	Carbon strand spool are not individually tensioned leading to entanglement.	Simple tensioning system individually tensions each strand spools.
	Fibre sorting system inadequately handles central strands leading to severe fibre damage and incomplete impregnation of fibre strands.	Improved fibre sorting system eliminates damaged fibres and allows for consistent impregnation of central strands
	Dispensing rate of resin is not monitored and controlled	Automated dispensing system calibration and closed loop control of dispensing rate provide precise dispensing of resin.
Curing	Two tunnel ovens (total length 1.5m). On/Off control. Temperature not monitored in heating chamber leading to inadequate temperature control.	Three tunnel ovens (total length 2.5m). Heater power continuously varied using pulse width modulation. Temperature monitored directly inside the heating chamber and controlled using gain scheduled proportional/integral controllers.
	Cooling of rod relies on natural convection with ambient air. Potential puller damage due to hot rod entering the pulling station.	Forced convection using water cooling. Cool rod enters the pulling station.
	Oven temperature cannot be decrease rapidly.	Blower provided forced cooling inside the heating chamber.
Monitoring and Control	No emergency stop system. In case of emergency all equipment must be shut down manually.	Centralized emergency stop system interrupts machinery power independently of control system. One of six buttons located throughout the production facility can activate the system.
	All machinery is manually controlled from operator observations.	Operation of critical machinery is monitored and automatically controlled
	Machine controls are distributed throughout the production plant	Machine controls are centralized. Operator can adjusts set point through the graphical user interface of the control system.
	Abnormal operating condition must be observed by operators.	Control system automatically reports several abnormal operating condition to the user.
	No data is available about machinery operation following a production run.	Logs files record all machinery data during production.

8.2.Future Work and Recommendations

8.2.1.Braiding and Pulling

Significant advancements have been made in the last decade in the field of machine vision. The increase in available processing power and the decrease in cost of digital cameras have made automated vision systems affordable. From the surveyed literature there are presently no reliable methods to produce 2D braided structure in a completely automated fashion. It is conceivable that machine vision could be used to provide on-line measurements of braiding parameters such as convergence zone geometry, braid angle, coverage factor and mandrel geometry. This would allow control algorithms to regulate the braiding process from measured properties and not solely from model based prediction. This would allow the development of a truly intelligent 2D braiding system.

8.2.2.Fibre Sorting and Impregnation

The impregnation system developed in this work utilizes only one pump. Epoxy and hardener are premixed. The gel time at room temperature of the resin used in the current application is in the order of 20 hours. Using a single pump only creates problems with respect to waste and effort associated with mixing the resin by hand. For some resins the gel time may be much shorter and premixing resin may not be possible. In this case using two pumps and a mixing nozzle would be preferable. With the exception of the resin scale all components have been purchased to provide on-line mixing. The required control system framework should be developed to provide this functionality.

8.2.3.Resin Curing

One aspect of production which has been overlooked in this work is the precise positioning of the induction heating wires within the rod cross-section. Currently it is possible to place one heating wire in the center of the rod. Other wires are typically distributed around the circumference of the impregnation ring. When fibres are grouped to form the rod core no mechanism ensures that the correct radial position of these heating wires is maintained. It was observed from cured rods that all wires tend to move to the center of the rod. A method to achieve more consistent placement of the heating wires is depicted in Figure 8.1. The principal concept of the proposed method is to form a small fibre grouping around the central heating wire. The peripheral heating wires are sandwiched between the small central fibre grouping and the remainder of the central fibres. To form the central fibre grouping a guide ring could be used. Alternatively, if it is found that resin accumulates on the guide ring a secondary, smaller impregnation ring could be used.

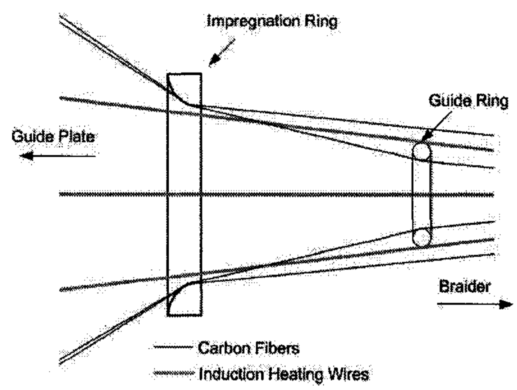

Figure 8.1: Suggested induction heating wire placement method.

Toward the completion period of this work it was observed that a significant time lag is associated with the oven thermocouples. As the oven operates in a steady state regime, it is believed that this does not hinder production. Nevertheless, it is advantageous to have a good knowledge of the curing temperatures for all operating conditions (including transient states). If a disturbance were to occur the true oven temperature would not be known. Although it may be possible compensate for the thermo-couple time lag using an observer, the simplest option is to physically reduce the apparent thermo-couple thermal mass. This may be as simple as replacing the ceramic tube which hold the thermo-couple by a similar fixture made of insulating material. The use of smaller gage thermo-couple wires would also form a junction with a smaller thermal mass .

An air purging system was implemented in an effort to increase the speed of the oven system closed loop response. It was show that with forced cooling the speed of the open loop response could be increased by several folds. This comes at the expense of increased system complexity. It was shown that the current temperature measurement method is not adequate to quantify the oven process with cooling air. It is also believed that temperature measurements of the heating tube are required to regulate the relative heat transfer to the rod. It is believed that both measurements are required, as heat transfer not only occurs by radiation (as in the case without forced cooling) but also through forced convection. In order to truly regulate the oven curing state both heat transfer modes and consequently the temperatures of the air and heating tube must be controlled separatly. The complexity of such a controller is compounded by the non linear nature of both radiation and convection.

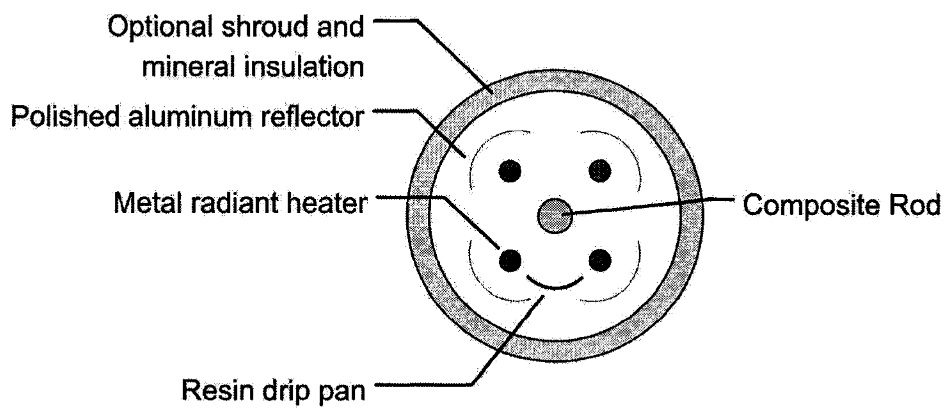

Figure 8.2: Configuration of proposed electric radiant oven.

To a large extent the concept of the air purging system came about to correct a mismatch between the current design of the curing ovens and the production requirements. The ovens which are currently in use are designed to operate at temperatures required in heat treatment of metals, and therefore a large ceramic heating block and high temperature insulation are utilized. These components result in a system with high thermal mass and consequently relatively sluggish behaviour compared to other processes of the production line. The slow behaviour of the ovens are compounded by the addition of the heating tube (to contain resin) which act as a radiation shield between the elements and rod. For polymer processing temperature are typically between 100 and 200°C. For these temperatures the requiered heat flux can readily be achieved using radiant heater without ceramic block. A bank of radiant heaters could be constructed at minimal cost (~2000$) using electric radiant metallic elements (similar to the ones found in household ovens). A proposed configuration is depicted in Figure 8.2. The key to such a system is to utilize electric elements which heat and cool quickly. Polished aluminum reflector direct the radiant energy towards the rod while a drip pan located below the rod collects resin which drips from the rod. A shroud could be used to contain the heat. Alternatively the shroud could be removed such that visual inspection of the curing process is possible. The main advantage of such a system is much faster responses could be achieved using simple control strategies. The size of the chamber could also be increased compared to the current ovens, allowing in-line curing of larger components.

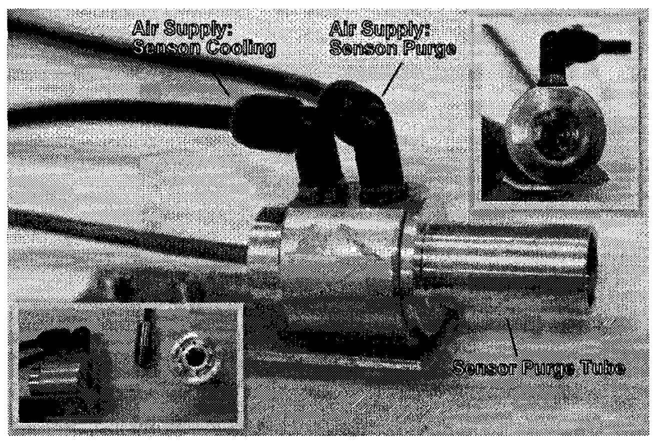

Figure 8.3: Infrared temperature sensor with mounting fixture.

During the initial development of this work an infrared temperature sensor was purchased. As depicted in Figure 8.3, the sensor is mounted in a custom made aluminum fixture. Air lines are provided to cool the sensor and to purge air in front of the sensor lens. It was thought that this device could be used to obtain temperature measurements of the exterior of the rod in the induction or oven stage. Conceivably, the measurements could be used to provide an indication that proper curing was taking place. The information could also provide feedback about the curing process which would in turn allow the development of control strategies to automatically adjust the induction heater power and/or the oven temperatures according to the curing process. It was concluded that this work was outside the scope of this thesis. Further work could address the robustness of the curing process. This would necessarily involve continuing the work on the oven control system. Non contact measurements could be utilized as part of this system.

8.2.4.Process Monitoring and Control System

The current control is developed on a computer running Windows XP. As discussed in Chapter 7, this is not ideal as this is not a real time operating system. It would be preferable to use a real time operating system which would allow true deterministic sampling to be achieved. In response to the deficiency of the Window's family of operating systems National Instrument, the developer of the DAQ card used in this work, has developed a real time operating system compatible with its recent products. The software is available as part of the Mechanical Engineering software subscription. It is believed that after minor modification, the software developed in this work could be adapted to run on this real-time operating system. Once deployed on such a system, sampling of the control loops would be deterministic.

8.2.5.Production

Throughout this thesis, both transient and steady state behaviour of the production machinery was studied. Particular attention was given to factors which could influence the steady state accuracy of controlled variables. In all cases, sub-system behavious where evaluated from physical experiments which simulated production conditions. It would be valuable to evaluated the accuracy of the controlled variable from data obtained during an actual production run. This would ensure that there are no uncontrolled interaction between the various production equipment. Furthermore, for all major sub-systems, (impregnation, braiding and curing) the controlled variables are closely related to product parameters such as the fiber volume fraction, the braid angle and the curing rate. These parameters are not directly controlled and could be influence by unforeseen factors. To evaluate the true abilities of the production plant, a study of the variability in the fiber volume fraction, braid angle and mechanical properties of product should be conducted.

9 References

[1] A. Mazzawi, "The Steady State and Transient Behaviour of 2D Braiding", Unpublished PhD. thesis, University of Ottawa, Dec. 2001.

[2] M. Munro, A. Fahim, J. Gardner, "Ductile CFRP Rebar for Concreate Structures", NSEC I2I Grant Proposal #121PJ313953, 2004.

[3] J, Sandness, "The Optimization of the Curing of Carbon Composite Rebar using a Heat Transfer FEA Model", Unpublished MAs. thesis, University of Ottawa, May 2007.

[4] F. J. Healey, S.R. Sheppeard, "Machine for making and treating braids", US Patent 1,098,257, 1914.

[5] A. Rawal, P. Potluri, C. Steele, "Paths in Three-dimensional Braided Structures",*Journal of Industrial Textiles*, vol. 35, No. 2, pp. 115-135, 2005.

[6] J. F. A. Kessels, R. Akkerman, "Prediction of the yarn trajectory on complex braided preforms", *Composites. Part A, Applied science and manufacturing,* vol. 33, no. 8, pp. 1073-1081, 2002.

[7] F. C. Campbell, "Manufacturing Processes for Advance Composites", New York: Elsevier, 2004, pp. 432-437.

[8] N. Obenshain, "Method of and apparatus for coating paper", US Patent 2,199,228, 1936.

[9] R. A. Tait et al, "Apparatus for resin impregnation of a fibrous substrate", US Patent 5,630,874, 1997.

[10] D. Youngkeit, "Apparatus for coating fiber materials with resin", US Patent 4,561,377, 1985.

[11] J. V. Gauchel, "Apparatus for resin impregnated pultrusion", US Patent 5,747,075", 1998.

[12] G. Gao et al, "Applicator for coating fibrous materials", US Patent 6,383,293, 2002.

[13] H. Kruesi, G. H. Hasko,"Computer Controlled Resin Impregnation for Composite Braiding, US Composite Corp., Troy, NY, MTL TR 87-23, Apr. 1987.

[14] V. Pillai, A. N. Beris, P. Dhurjati, "Intelligent Curing of Thick Composites Using a Knowledge-Based System", *Journal of Composites Materials*, vol. 31, no.1, pp. 22-51, 1997.

[15] S. Parthasarathy, S. C. Mantell, K. A. Stelson, "Estimation, Control and Optimization of Curing in Thick-Section Composite Parts", *ASME Trans., Journal of Dynamic System, Measurement and Control*, vol 126, Dec. 2004.

[16] J.H. Chen, A. Johnston, L. Petrescue, M. Hojjati, P. Richer, "Review of electron beam curing of composites", IAR/NRCC Report, June 2003.

[17] V. Rudnev, D. Loveless, R. Cook, M. Black, "Handbook of Induction Heating", New York: Marcel Dekker, p. 92, 2003

[18] P. Craine, "Resin application using induction heat", *Proc. Electrical Insulation Conference and Electrical Manufacturing & Coil Winding Technology Conference*, issue 23-25, pp. 137-140, Sept. 2003.

[19] Matsen et al., "Method and apparatus for consolidating organic matrix composites using induction heating" US patent 5,591,369, June 1995.

[20] A.D. Murray, "Induction heating method for forming composite articles" US Patent 5338497, Apr. 1994.

[21] G. R. Kodokian, "Method for induction heating of composite material, US Patent 4,340,428", Aug. 1994

[22] J. Sandness, A Fahim, M. Munro, "Rapid curing of 25mm dia. Continuous fiber composite rods", presented at the CSME Conference, Ottawa, Canada, June 6th 2008.

[23] W. Michaelia, U. Rosenbauma and M. Jehrkea, "Processing strategy for braiding next term of complex-shaped parts based on a mathematical process description", *Composite Manufacturing*, vol. 1, issue 4, pp. 243-251, 1990.

[24] P. Potluri, A. Rawal, M. Rivaldi, I. Porat, "Geometrical modeling and control of a triaxial braiding machine for producing 3D preforms", *Composites Part A: Applied Science and Manufacturing*,vol. 34, issue 6, pp. 481-492, 2003.

[25] R. Chiasson, "Computer assisted manufacturing (CAM) and control of composite material braiding", Unpublished Undergraduate Thesis, University of Ottawa, 1993.

[26] B. Lian, L. Jiang, J. J. McGrath, J. Jaranson, "Quantitative determination of morphological features of triaxially braided composites by the use of machine vision", *Composites Science and Technology*, vol. 60, issue 2, pp. 159-166, Feb. 2000.

[27] J. P. Poynton, "Metering pumps selection and application", NewYork: Marcel Dekker, 1983, pp. 75-82.

[28] G. Hillerstrom, J. Sternby, "Application of repetitive control to a peristaltic pump", *Jour. of dynamic systems, measurement, and control*, vol. 116, no. 4, pp. 786-789, Dec. 1994.

[29] E.O. Moralest, M. M. Polycarpout, N. Hemasilpint, J. J. Bissler, "Adaptive control of peristaltic pumps during continuous venovenous hemofiltration", in *Proc. IEEE International Conference on Control Applications*, Aug. 1999, pp. 1306-1311.

[30] D. H. Lee, S. K. Kim, W. L. Lee, S. K. Ha, S. W. Tsai, "Smart cure of thick composite filament wound structures to minimize the development of residual stresses", *Composites Part A: Applied Science and Manufacturing*, vol. 37, issue 4, pp. 530-537, Apr. 2006.

[31] J. Li, S. C Joshi, Y. C. Lam, "Curing optimization for pultruded composite sections", *Composites Science and Technology*, vol. 62, issue 3, pp. 457-467, Feb.-Mar. 2002.

[32] J. G. Ziegler, N. B. Nichols, "Optimum Settings for Automatic Controllers", *ASME,* 1942.

[33] D. E. Rivera, M. Morarim, S. Skogestad, "Internal ,model control, 4. PID controller design", *Industrial and Engineering Chemistry Process Design and Development*, vol. 25 , p.252, 1986.

[34] A. Srinicasa, C. Datur, R. Veillette, B. N. Rosenthal, M. B. Duval , "Projective Control Design for Multi-Zone Crystal Growth Furnace", *IEEE Trans. Control System Technology,* vol. 2, no. 2, pp. 142-147, June 1994.

[35] C. Batur, R. B. Sharpless, W. M. B. Duval, B. N. Rosenthal, "Identification and Control of a multizone crystal growth furnace", *Journal of Crystal Growth,* vol 119, pp. 371-380, 1992.

[36] M. Munro, "Braid formation during the steady state and transient modes in 2d braiding", presented at the CSME Conference, Ottawa, Canada, June 7th 2008.

[37] A. G. Ramm, A. B. Sminoca, "On stable numerical differentiation", *Jour. Mathematics of Computation*, vol 70, no. 235, pp. 1131-1153, 2001.

[38] "HEDS Transmissive Optical Encoder Module", US Digital, Vancover,WA, Product Data Sheet.

[39] "Toho Tenax Besfight G50-300 12K HMA-7C EP01 Continuous Filament Carbon Fiber", [Online]. Available:www.matweb.com

[40] "DuPont Kevlar® 49 Aramid Fibe", [Online]. Available:www.matweb.com

[41] H. Lee, K. Neville, "Handbook of epoxy resins", New York: McGraw-Hill, 1976, pp. 4-14.

[42] D. K. Roach, "Rhythmic muscular activity in the alimentary tract of Arion ater (L.)", *Jour. Comparative Biochemistry and Physiology,* vol. 24, issue 3, pp. 865-878, Mar. 1968.

[43] D. J. Griffihs, "Dynamics of the upper urinary tract: I. Peristaltic flow through a distensible tube of limited length" *Jour. Physics in Medicine and Biology,* vol. 32, pp. 813-822, 1987.

[44] J. C. Misra, S. K. Pandey, "Peristaltic transport of blood in small vessels: study of a mathematical model", *Jour. Computers & Mathematics with Application* , vol. 43, issues 8-9, pp. 1183-1193, Apr.-May 2002.

[45] M. Bu, T. Melvin, T. Ensell, G. Nsell, J. Wilkinson, A Evans, "Design and theoretical evaluation of a novel microfluid device to be used for PCR", *Jour.Micromechanics and Microengineering*, vol. 13, pp. S125-S130, 2003.

[46] "New peristaltic pump finds many applications", *World Pumps*, vol 2001, Issue 417,6,June 2001.

[47] "Introduction to coriolis flowmeter", 2008, [Online]. Available: http://www.efunda.com/designstandards/sensors/flowmeters/flowmeter_cor.cfm

[48]: "Flowmec small capacity flowmeters", Muis Control Ltd., Edmonton, Alberta, Product Data Sheet.

[49]: "Mircro motion LF-series low flow sensor and transmitter", Micro Motion Inc., Boulder, CO, Product data sheet PS-00566, rev. D, March 2007.

[50]: "Positive displacement flowmeters", Flowmec, Sydnew, Australia, Data sheet no. PSLOM-0607.

[51] C. L. Smith, "Digital computer process control ", Scranton, PA: International Textbook,1972.

[52] ,"Peristaltic hose and transfer pumps", PeriFlo, Loveland, OH, [Online]. Available: http://www.periflo.com/engineering.htm

[53] ,"Peristaltic Pump Selection Guide", Wanner Engineering Inc., Minneapolis, MN, [Online]. Available:http://www.vectorpump.com/overview/peristaltic-pumps.html

[54] J. Schaeffer. C. J. Olbricht, and K. M. Koch, "Long term performance of hemofilters in continuous hemofiltration", *Nephron*, vol. 27, no 2, pp. 155-158, 1996.

[55] T. A. Depner, S. Rizwan, and T. A. Stasi, "Pressure effects on roller pump blood flow during hemodialysis", *Trans. American Society for Artificial Internal Organs*, vol. 31, pp. M456-M459, 1990.

[56] P. J. Rousseeuw, A. M.Leroy, "Robust regression and outlier detection", New York: John Wiley & Sons, 2003, pp. 9-12

[57] J. G. Ziegler, N. B. Nichols, "Optimum settings for automatic controllers", *ASME,* 1942.

[58] A.B. Corripio, "Tuning of industrial control systems", Research Triangle Parkm NC: ISA-The Instrumentation, Systems, and Automation Society, 2^d ed., 2001, p. 112.

[59] "Material safety data sheet EPON Resin 828", Hexion Specialty Chemicals Inc, Columbus, OH, May 2008.

[60] S. Zinn, S. L. Semiatin, "Coil design and fabrication: basic design and modifications", 1988, [Online]. Available: http://www.stanleyzinn.com/zone_coils_1.html

[61] "Solid state relay G3NA", Omron Electronic Components, Schaumburg, IL, Product Data Sheet no. JB301-E3-01, March 2005.

[62] F. P. Incropera, D. P. Dewitt, "Fundamentals of heat and mass transfer", NewYork:Wiley, 5th ed., 2002, pp. 366-373.

[63] S. W. Churhill, M. Bernstein, Journal of Heat Transfer, vol. 99, no. 300, 1977.

[64] G. D. Raitnby, K. D. T. Hollands, "A general method of obtaining approximate solutions to laminar and turbulent free convection problems", *Jour. Advance Heat Transfer*, vol. 11,pp. 265-315, 1975.

[65] E. A. Avallone, T. Baumeister III , "Marks' standard handbook for mechanical engineers", NewYork: McGraw-Hill, 10th ed., 1996, pp. 4-63 to 4-64.

[66] "Coiled Nickel-Chromium Alloy Resistance Wire", Omega Inc., Stamford, CT, Product data sheet.

[67] F. P. Incropera, D. P. Dewitt, "Fundamentals of heat and mass transfer", NewYork:Wiley, 5th ed., 2002, pp. 366-373.

[68]: T. Oreilly, " History of Programing Languages", 2004, [Online]. Available: http://oreilly.com/news/graphics/prog_lang_poster.pdf

[71] ,"Programing language – C", American National Standards Institute, Standard no. ISO/IEC 9899:1999, 2007.

10 Bibliography

D. B. Miracle, S. L. Donaldson, "ASM Handbook Volume 21 Composites", Materials Park ,OH: ASM International, 2004, pp.69-77.

W. Douglass, "Braiding and braiding machinery", Phillips Technical Lib, 1964.

F. Ko, C. Pastore, A. Head, 1989, "Atkins and Pearce Handbook of Industrial Braiding", Covington KY: Atkins and Pearce, 1989.

E. G. Freger, V. N. Kestel'man, "Braiding Pultrusion Technology for Advanced Structural Composites", New York: McGraw-Hill Professional, 2004.